Aix-Marseille Université

Ecole Doctorale Sciences de l'Environnement

Thèse

Présenté par

HAMED POURKHORSANDI SOUFIANI

Pour obtenir le grade Doctor en Sciences

De l'Aix-Marseille Université

METEORITES OF IRAN AND HOT DESERTS: CLASSIFICATION AND WEATHERING

Soutenue le 19/02/2018 devant le jury:

Vinciane DEBAILLE	Rapporteur
Bertrand DEVOUARD	Examinateur
Morteza DJAMALI	Invité
Jérôme GATTACCECA	Examinateur
Matthieu GOUNELLE	Examinateur
Hassan MIRNEJAD	Examinateur
Knut METZLER	Rapporteur
Pierre ROCHETTE	Director de Thèse

Left blank intentionally.

RÉSUMÉ:

Les météorites sont parmi les sources d'information les plus importantes sur la structure et l'évolution du système solaire. Elles se sont retrouvées sur les paillasses des laboratoires de recherche soit via une chute connue soit via des trouvailles collectées longtemps (jusqu'à des centaines de milliers d'années) après la chute sur la surface terrestre.

Cette thèse présente une étude des météorites d'Iran, en particulier celles retrouvées dans le désert de Lut et leur comparaison avec celles des autres déserts chauds du monde. Les météorites de Lut sont étudiées en détail en vue de comprendre le potentiel de ce désert dans l'accumulation : sont présentés la classification des météorites, les âges terrestres, l'altération, la distribution spatiale et l'appariement. Nous démontrons la présence de deux champs de dispersion d'une même chute de météorite et mettons en évidence les conditions favorables à la conservation, l'accumulation et la collection des météorites. Les météorites de différents déserts chauds sont étudiées et comparés afin de documenter leur abondance, classification, et l'altération terrestre. Nos données révèlent les différences entre les effets chimiques et minéralogiques de l'altération sur les météorites en provenance de différents déserts.

Parmi les centaines de météorites classifiées des déserts chauds, nous présentons notre étude détaillée sur une chondrite non-groupée (El Médano 301). Cette météorite, pourrait représenter un nouveau sous-groupe des chondrites ordinaire (OCs) avec une composition chimique plus réduite par rapport aux OCs standards. Famenin et Moshampa, deux chutes de météorites de l'été 2015 dans le nord-ouest d'Iran, sont également étudiées en détail.

Famenin est un chondrite ordinaire de type 3 qui présente des caractéristiques intermédiaires entre les chondrites H et L. Nous proposons l'existence d'un nouveau sous-groupe de chondrites ordinaires que nous désignons H^L. Enfin, nous présentons les résultats de notre étude sur la météorite de Moshampa qui est une chondrite bréchifiée de type LL5.

ABSTRACT:

Meteorites are amongst the most important sources of information about the structure, formation, and evolution of the Solar System. They found their ways to the laboratories as samples related either to a known meteorite fall (*falls*), or as "*finds*" being collected up to hundreds of thousands of years after their fall.

This thesis reports studies on the meteorites from Iran, in particular the Lut Desert and their comparison with the meteorites from other hot deserts. Lut Desert meteorites are studied in detail to understand the potential of this desert for hosting meteorites, meteorite classification, terrestrial ages, terrestrial weathering, spatial distribution and pairing. We shows the presence of two main meteorite strewnfields and evidence suitable conditions for preservation, accumulation and finding of meteorites. Meteorites from different hot deserts are studied in order to document meteorite abundances, classification, and their terrestrial alteration. Our data reveal differences between the chemical and mineralogical effects of terrestrial weathering on meteorites from different deserts.

Among the hundreds of classified hot desert meteorites, we present a detailed study on an ungrouped chondrite (El Médano 301). This meteorite might be representative of a new grouplet of ordinary chondrites (OCs) showing more reduced compositions than standard OCs.

Famenin and Moshampa, two meteorites fallen during summer 2015 in NW Iran, are studied in detail. Famenin is a type 3 ordinary chondrite showing characteristics intermediate between H and L chondrites. Together with similar intermediate meteorites, we suggest the existence of a separate ordinary chondrite grouplet for which a different designation (H^L) is proposed. Classification results of Moshampa brecciated LL5 chondrite are reported.

ACKNOWLEDGEMENTS:

Since the arrival day on 12th December 2014, I knew that I'm going to experience a unique adventure in France. And now, after about three years, I know that I was right!

During the last three years, I experienced the craziest scientific works that I could imagine! I could work on objects that had fascinated me since my childhood! I learned A LOT about meteorites and I had the opportunity to do research on them!

This adventure wouldn't be possible without the help of numerous scientists, colleagues, and friends, who I was in touch with.

First of all, I want to say "thank you" to my supervisor Prof. Pierre ROCHETTE. He trusted me to do this project and gave me the freedom to experience different aspects of meteoritics. Thank you for creating an environment without any stress or tension. One major thing that I learned from you, is to be relaxed and to do science this way… This is great! ☺

Dr Jérôme GATTACCECA is the person that I spent the majority of my time in the last three years with (I am so happy about it!). We used to work in the same lab, commuting together to work (everyday), and living in the same building. Our discussions were so precious. They were very helpful for my research, life, etc. Besides being like a supervisor for me, he was a friend of mine and kindly accepted me in his family. I believe without his helps finishing this thesis in this time frame would be almost impossible.

Dr Morteza Djamali is the other person who was always present to help me. Daily talks to him was giving me lots of motivation and energy. I won't forget his helps during this time…

I was happy to be part of a team with kind and bright people. I want to say thank you to Bertrand, Minoru, François, Yvan, Nicolas, Camille, Mighei, and William.

I want to say thank you to my student and postdoc friends who helped me during my studies and would make me laugh all the time. Thank you Aladine, Chloe, Emmeline, Franck, Frida, Jesus, Julie, Maria, Maureen, Riccardo, Ross, and Valenti.

I want to say thank you to Jérôme, Florence, Felix, Livia, and Ondine who accepted me in their family and made me feel at home. I love you all!

Finally, I want to say thank you to my father (Samad), my mother (Najibeh), my brothers, and their families for their support and love since the beginning… I love you all and I am happy for making you happy ☺

Left blank intentionally.

Contents:

Left blank intentionally.

Chapter 1

Introduction and the Thesis Structure

Title: INTRODUCTION AND THE THESIS STRUCTURE

1. METEORITES: THE CELESTIAL STONES

"A meteorite is a natural solid object larger than 10 µm in size, derived from a celestial body, that was transported by natural means from the body on which it formed to a region outside the dominant gravitational influence of that body, and that later collided with a natural or artificial body larger than itself (even if it is the same body from which it was launched)" (Rubin and Grossman 2010). This is one of the most comprehensive and recent definitions of a "meteorite". Although, to reach such a definition, we had to work for more than a century on these unique stones (see McCall et al. 2006 for a review of meteoritics).

Humans have been passionate about "stones falling from the sky" for centuries. There is a great deal of evidences of this. Among them are: (*i*) numerous artifacts made out of meteoritic iron from different civilizations (Comelli et al. 2016; Jambon 2017; Rehren et al. 2013), (*ii*) mythical stories in the folklore and religious literature from different cultures; spanning from the Northern Europe (Haas et al. 2003) to the Middle east (Anonymous 632), and (iii) reports describing meteorite fall events (D'Orazio 2007; Gharib 1999; Nogami 2006).

Now, we know that meteorites are coming from space and they originate from different objects in our Solar System, mainly from the asteroids (e.g., Bowden 2006). Meteorite parent bodies span from the planet Mars, to the Moon, and to the asteroids (and maybe comets) with different sizes. Each of these objects has its own unique formation and evolution history that can be revealed by studying meteorites.

Dating back to ~ 4.6 billion years ago in the Solar Nebula, with the formation of the first solid grains (Ca-Al-rich inclusions, chondrules, etc.), and following their accretion, larger chunks of rocks with a non-volatile composition similar to the Sun's composition formed. With later growing and production of heat resulting from the internal radioisotopes decay and external impacting bodies, some of these objects differentiated. A geological process, which involves layering of a body resulting from the migration of different phases according to their density. Differentiation is mainly controlled by the chemical behavior of the elements. Based on its occurrence and extent, objects in the Solar System can be divided to (*i*) undifferentiated or primitive, and (*ii*) differentiated bodies. A series of reviews on this topic are available in Pater and Lissauer (2015).

Fig. 1 shows a full scheme of meteorite classification using the differentiation history of their parent bodies (Weisberg et al. 2006). Chondrites are meteorites originating from primitive bodies that have never experienced large scale melting and differentiation (undifferentiated). They are physical mixtures of accreted components (Ca-Al-rich inclusions, chondrules, metals, sulfides, dust, etc.) named for the occurrence of chondrules as round shape objects. However, majority of them have experienced degrees of thermal and shock metamorphism and/or aqueous alteration on their parent bodies. Chondrites are the most abundant type of meteorites (86.3% of meteorite falls according to the Meteoritical Society database, http://www.lpi.usra.edu/meteor/metbul.php), which are dominated by ordinary chondrites (93.2% of chondrite falls).

In contrast, differentiated meteorites have experienced high temperatures, melt segregation, and differentiation. Similar to the terrestrial magmatic systems, meteorites from differentiated bodies are divided into two main rocks types: (*i*) primitive achondrites, which are solid residues, left behind melt extraction from the chondritic material, and (*ii*) magmatic meteorites crystallized from the extracted melts or from completely melted and differentiated material. Irons, stony-irons, magmatic achondrites (HED, Lunar, Martian, etc.) are considered as magmatic meteorites.

Considering the vast physicochemical variety in the Solar Nebula and in different bodies in our Solar System, we are expecting much more different meteorite types than shown in Fig. 1. Different meteorite types represent the processes ranging from the pre-Solar, to the accretion periods, and later parent body processes.

Needless to say, meteorites are the key material for obtaining information about the formation and evolution of the Solar System. To access them, we have two opportunities: collecting meteorites related to (*i*) observed or (*ii*) unknown fall events, respectively known as "*falls"* and "*finds"*. *Falls* are fresh samples that have not been affected by the terrestrial altering agents. For this reason, they are the main targets for cosmochemical studies. However, rare occurrence of meteorite falls (~ 10 recorded and collected per year) limits the accesses for a high amount of material. *Finds* have the highest number of meteorites in our collections. They are mostly collected from the cold (e.g., Antarctica) and hot deserts of the planet. There are rare and unique types of meteorites among the *finds*. Some meteorite types have not been recorded among *falls* (e.g., brachinites or lunar meteorites).

Ones of the main differences between *falls* and *finds* is the presence of the terrestrial weathering products in the latter. *Finds* besides offering samples for cosmochemical studies, are also the subjects of works such as: (*i*) studying flux of the extraterrestrial material to the Earth, (*ii*) studying the alteration of extraterrestrial material on terrestrial environment, (*iii*) studying the meteorite fall process by working on ancient meteorite fall strewnfields, (*iv*) working on the climatic history of the meteorite hosting region.

In order to get access to more meteorites, each year different scientific expeditions aiming to collect meteorites take place in hot and cold deserts. Antarctica, the Atacama Desert (Chile), Sahara, and deserts of Oman are the main locations for meteorite searching. Discovering new places suitable for meteorite accumulation is crucial for continuing these activities and brings new information about the aforementioned scientific tasks.

Considering Iran's dry climate and the possibility of a better meteorite preservation in its deserts, the idea of working on this topic came to the author's mind in 2011 and was published in Pourkhorsandi and Mirnejad (2013). New meteorite accumulation sites provide new meteorites that in addition to study the cosmochemical aspects can be used to investigate: (*i*) Weathering and contamination of meteorites (Bland et al. 2006), (*ii*) residence time of meteorites on the Earth (terrestrial age) (Sears 1981), (*iii*) relative frequency of meteorites with different compositions and masses in the site (Gattacceca et al. 2011), (*iv*) effects of climatic, geomorphological, geological properties of the region and meteorite types on preservation and accumulation processes (Schlüter et al. 2002) and (*v*) extracting palaeoclimatic data by studying weathering products (Bland et al. 2002).

Considering these, Lut Desert of Iran was chosen as the focus of the study. To have access to a considerable number of meteorites, tens of amateur meteorite hunters were receiving weekly instructions via social media by the author. In addition, with the help of connections in the Iranian national media (T.V., radio, magazines, and newspapers) the author was giving information for the public about meteorites. This made them ready to collaborate with the scientists. Proof for this, is having fragments of two fall meteorites, Famenin and Moshampa, soon after their fall and hundreds of meteorites from Iranian deserts in our laboratory…

2. SCOPES AND STRUCTURE OF THE THESIS

The main goal of this thesis is studying the meteorites from Iran, in particular the Lut Desert and their comparison with the meteorites from other hot deserts. In this work, we study the hot desert meteorites in order to document meteorite abundances, classification, and their terrestrial alteration. Hundreds of meteorites, with a focus on Lut Desert meteorites were classified. This part of the study is presented in the Parts I and II of the thesis. Part I describes the classification methodology applied in this study along with the detail on the statistics of the classified meteorites. Part II deals with the results of the studies on hot desert meteorites, with a focus on the Lut and Atacama deserts.

Lut Desert meteorites are studied in detail to understand the potential of this desert for hosting meteorites, meteorite classification, terrestrial ages, spatial distribution and pairing. This part of the study is presented in chapters 3-5.

Among the hundreds of meteorites studied from different deserts, we present a detailed study on an ungrouped chondrite (El Médano 301). This meteorite might be representative of a new grouplet of ordinary chondrites and shows unique mineralogical characteristics. Details of this study are presented in the chapter 6.

Being very lucky, two meteorite falls (Famenin and Moshampa) with a time difference of less than 40 days happened in Iran during the first year of this Ph.D.! The two previous meteorites had fallen on 1880 and 1974. Part III (chapters 7-8) presents detailed studies on these meteorites.

References:

Anonymous. 632. Sureh Hud. In *Quran*.

Bland P. a., Berry F. J., Jull a. J. T., Smith T. B., Bevan a. W. R., Cadogan J. M., Sexton a. S., Franchi L. a., and Pillinger C. T. 2002. 57Fe M??ssbauer spectroscopy studies of meteorites: Implications for weathering rates, meteorite flux, and early solar system processes. *Hyperfine Interactions* 142:481–494.

Bland P. A., Zolensky M. E., Benedix G. K., and Sephton M. A. 2006. Weathering of chondritic meteorites. In *Meteorites and the Early Solar System II*. pp. 853–867 http://www.lpi.usra.edu/books/MESSII/9041.pdf.

Bowden A. J. 2006. Meteorite provenance and the asteroid connection. *Geological Society,*

London, Special Publications 256:379–403. https://pubs.geoscienceworld.org/books/book/1632/chapter/107432576/.

Comelli D. et al. 2016. The meteoritic origin of Tutankhamun's iron dagger blade. *Meteoritics & Planetary Science* 51:1301–1309. http://doi.wiley.com/10.1111/maps.12664.

D'Orazio M. 2007. Meteorite records in the ancient Greek and Latin literature: between history and myth. *Geological Society, London, Special Publications* 273:215–225. https://pubs.geoscienceworld.org/books/book/1643/chapter/107453266/.

Gattacceca J. et al. 2011. The densest meteorite collection area in hot deserts: The San Juan meteorite field (Atacama Desert, Chile). *Meteoritics and Planetary Science* 46:1276–1287. http://onlinelibrary.wiley.com/doi/10.1111/j.1945-5100.2011.01229.x/full.

Gharib A. H. 1999. A Fatal Meteorite Shower in 12th Century Iran. *Meteorite* 5:42.

Haas A., Peekna A., and Walker R. E. 2003. Echoes Of Ancient Cataclysms In The Baltic Sea. *Folklore: Electronic Journal of Folklore* 23:49–81. http://www.folklore.ee/folklore/vol23/echoes.pdf.

Jambon A. 2017. Bronze Age iron: Meteoritic or not? A chemical strategy. *Journal of Archaeological Science* 88:47–53. http://linkinghub.elsevier.com/retrieve/pii/S0305440317301322.

McCall G. J. H., Bowden A. J., and Howarth R. J. 2006. *The History of Meteoritics and Key Meteorite Collections: Fireballs, Falls and Finds*, Brassmill Lane, Bath, UK: Geological Society.

Nogami N. 2006. A list of meteorite falls and their impact craters from ancient Chinese records (7th-19th century). In *Proceedings of the International Meteor Conference, Oostmalle, Belgium, 15-18 September, 2005*, edited by Bastiaens L., Verbert J., Wislez J.-M., and Verbeeck C. International Meteor Organisation. pp. 50–52.

Pater I. de, and Lissauer J. J. 2015. *Planetary Sciences*, Cambridge: Cambridge University Press http://ebooks.cambridge.org/ref/id/CBO9781316165270.

Pourkhorsandi H., and Mirnejad H. 2013. Lut Desert (Iran): A High-Potential Area for Finding Meteorites. In *44th Lunar and Planetary Science Conference* http://adsabs.harvard.edu/abs/2013LPI....44.1096P (Accessed July 1, 2015).

Rehren T. et al. 2013. 5,000 years old Egyptian iron beads made from hammered meteoritic iron. *Journal of Archaeological Science* 40:4785–4792. http://linkinghub.elsevier.com/retrieve/pii/S0305440313002057.

Rubin A. E., and Grossman J. N. 2010. Meteorite and meteoroid: New comprehensive definitions. *Meteoritics and Planetary Science* 45:117–125.

Schlüter J., Schultz L., Thiedig F., Al-Mahdi B. O., and Aghreb a. E. a. 2002. The Dar al Gani meteorite field (Libyan Sahara): Geological setting, pairing of meteorites, and recovery density. *Meteoritics* 37:1079–1093.

Sears D. W. G. 1981. Terrestrial ages of meteorites. *Nature* 293:433–433.

Weisberg M. K., McCoy T. J., and Krot A. N. 2006. Systematics and Evaluation of Meteorite Classification. *Meteorites and the Early Solar System II, D. S. Lauretta and H. Y. McSween Jr. (eds.), University of Arizona Press, Tucson, 943 pp., p.19-52* 19–52.

Figure captions:

Fig. 1: Diagram expressing the systematics of meteorite classification and showing the major meteorite divisions, classes, clans, and groups and relationships among meteorite groups. URE - ureilite, ACA - acapulcoite, LOD - lodranite, ANG - angrite, AUB - aubrite, BRA - brachinite, WIN - winonaite, HED - howardite-eucrite-diogenite, MES - mesosiderite, MG PAL – main-group pallasite, ES PAL – Eagle Station pallasite, PP – pyroxene pallasite, SHE – shergottite, NAK – nakhlite, CHA – chassignite, OPX – orthopyroxenite. From: Weisberg et al., (2006).

Figures:

Fig. 1:

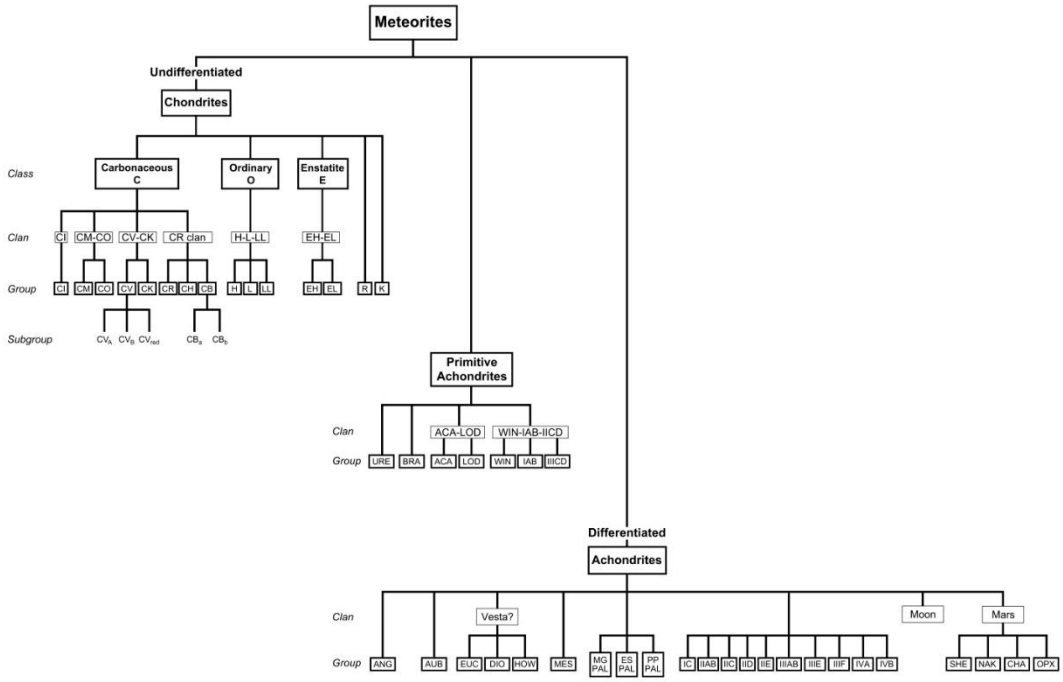

Left blank intentionally.

Part I

Meteorite Classification

Chapter 2

Meteorite Classification at CEREGE

Title: METEORITE CLASSIFICATION AT CEREGE

1. INTRODUCTION

Meteorites are amongst the most important sources of information about the structure, formation, and evolution of the Solar System. They found their ways to the laboratories as samples related either to a known meteorite fall (*falls*), or as "*finds*" being collected up to hundreds of thousands of years after their fall. The majority of the meteorites in our collections are "*finds*" from the hot and cold deserts. Meteorites have different applications in meteoritics such as: (i) cosmochemical studies about the formation and evolution of the Solar System; (ii) physical and chemical structure of the parent bodies; (iii) flux of the extraterrestrial material to the Earth and its variations in time and composition; (iv) alteration of the extraterrestrial material in terrestrial environment; etc.

The main task before doing these studies is the initial recognition and classification of meteorites. This points the high importance of this process. The ultimate goal of meteorite classification is to group all meteorite specimens that share a common origin on a single, identifiable parent body. The most common criteria in meteorite classification comprise physical properties, texture, and mineral chemistry of different phases. Majority of the samples can be classified using these parameters. However, some meteorites require more parameters (such as whole-rock chemical composition and oxygen-isotopic composition) to be classified.

The classification of some samples is not straightforward, and they do not belong to any known meteorite group. In these cases, either the meteorites are called "ungrouped" or "anomalous". As described in the online database of the Meteoritical Bulletin: "the term ungrouped describes meteorites which have been well-enough characterized to determine that they do not fit into any of the established groups."; and, "anomalous designates meteorites that have been determined to be a member of a specific group, but have certain properties that are unusual or distinctive."

In this work, we present the meteorite classification methodology and describe the criteria used to do so. The results comprise the statistics of the meteorites classified and co-classified by the author since January 2015.

2. METHODLOGY

Fig. 1 shows a simplified chart of the meteorite classification methodology being used at CEREGE.

The majority of meteorites contain different proportions of magnetic minerals such as (Fe,Ni) metal. For this reason, magnetic properties such as susceptibility can be used to differentiate meteoritic groups. Magnetic susceptibility is a measure of how magnetizable a substance can become in the presence of a magnetic field and can be used in a general way to describe the various classes of magnetic materials. Fig. 2 shows the ranges of this proxy in different groups of meteorites. Following Rochette et al. (2003) methodology, after weighting the samples, magnetic susceptibility (χ in 10-9 m3/kg) is measured in 2-3 directions using an KLY2 instrument from Agico, with large coil allowing samples up to 300 g. For larger samples the hand held instrument SM30 is used.

Observing the structure and texture of the meteorites after cutting is the next step. Physical characteristics such as the color, the presence or lack of chondrules, Ca-Al-rich inclusions, (Fe,Ni) metal and troilite, impact veins, fusion crust, desert patina, and cracks are reported.

Preparing sections for microscopic observations follows this step. For most of the meteorites, only thick polished sections are prepared. The procedure consists in embedding fragments of meteorites in resin inside cylindrical molds and then polishing using SiC coated papers and diamond spray. The microscopic observations are done using a Leica DM2500P optical microscope and a Hitachi S3000-N scanning electron microscope (SEM). Different textural characteristics related to meteorite type, petrologic type, shock stage, and weathering grade are noted. The main reported characteristics depending on their presence or non-presence are: 1) Chondritic or non-chondritic texture, 2) average chondrule size, 3) average plagioclase size, 4) modal ratio of chondrule/matrix, 6) modal abundance of opaque phases such as (Fe,Ni) metal, troilite, chromite, Fe oxides/oxyhydroxides (both cosmic and terrestrial), and copper, 5) the shape, size, and the relationship between (Fe,Ni) metal and troilite, 6) melt veins and pockets, 7) bandwidth of kamacite in iron meteorites, 8) lineation of primary and secondary components, 9) describing the clasts and their relationship with the host.

In most equilibrated ordinary chondrites (EOCs), classification in possible using only magnetic susceptibility and textural data. However, in weathered meteorites because of their modified magnetic mineralogy, more data are required for classification. Mineral chemistry

503 data obtained using electron micro probe analyses (EMPA) is the main approach. In addition
504 to the EOCs, EMPA was also done on all unequilibrated ordinary chondrites (UOCs) and
505 other meteorite types. These analyses were performed in CAMPARIS facility using a
506 CAMECA SX50 and SX100 instruments.

507 Olivine and low-Ca pyroxene are the most important minerals for classification. In OCs,
508 the most abundant type of meteorites, in a diagram of Fa (%mole) versus Fs (%mole) three
509 main groups are distinguished (Fig. 3). These minerals have more MgO in H chondrites than
510 those in LL chondrites. This behavior is a reflection of their formation in a region more
511 reduced (low fO_2) than that of LL chondrites (e.g., Rubin, 1990). Kamacite and its Co content
512 is the other mineral whose chemistry is useful for the classification of OCs. This is shown in
513 the Fig. 4. In addition to OCs, mineral chemistry is crucial for the classification of
514 achondrites. As shown in Fig. 5, the Mn, Fe, and anorthite contents can be used to
515 differentiated different basaltic material different Solar System.

516 In the case of unequilibrated chondrites and to get a merely representative olivine and low-
517 Ca composition and the chemical distribution, about thirty random analysis points of each
518 mineral are being selected. Meanwhile, for equilibrated meteorites, 2-3 analysis on each
519 mineral are sufficient for a classification purpose.

520

521 **3. RESULTS AND DISCUSSIONS**

522 Table 1 and Fig. 6a lists the finding locations of the meteorites classified in this study (n =
523 706). Detailed descriptions of the classifications are available in the online version of the
524 Meteoritical Bulletin (https://www.lpi.usra.edu/meteor/). The majority of the meteorites are
525 from Chile (n = 373; 53%) and Iran (n = 219; 31%). Following these, meteorites from Oman
526 (n = 76; 11%), Sahara (NWA, Morocco, and Western Sahara) (n = 37; 5%), and France (n =
527 1) come next. Table 2 and Fig 6b shows the statistics of classified meteorites from different
528 types. As it is evident, OCs (n = 95%) and particularly H5 and L6 types constitute the
529 majority of the samples and they are the main types from Iran and Chile, respectively. This is
530 in agreement with the statistics of the meteorites finds and falls (Source: Meteoritical
531 Bulletin). Statistical analyses show that most of the Lut Desert H5 (Kerman series) samples
532 are paired. More details on Lut Desert meteorites are discussed in the next chapters. Rare and
533 less common types of meteorites are dominant among the NWA samples. This is expected as
534 the majority of the EOCs from this region are not being classified by the laboratories.

One of the main application of the produced data is studying the relationship between the weathering grade and magnetic susceptibility of the meteorites. In general, meteorite terrestrial weathering leads to a decrease in the magnetic susceptibility (Rochette et al., 2003). Plotting the weathering grades and magnetic susceptibility data is a good way to depict this. Fig. 7 shows a comparison of data for meteorites from different hot deserts. As it is shown, the curves are not identical. Weathering in different climatic regions causes different secondary mineralogy, which in consequence leads to different magnetic properties. One interesting feature is the increase in logχ in the Lut Desert (Iran) meteorites in weathering grades higher than W3. This is possibly related to the formation of secondary highly magnetic minerals such as magnetite or maghemite in these meteorites, instead of hematite and oxyhydroxides.

4. CONCLUSIONS AND PERSPECTIVES

In this chapter, we reported the meteorite classification methodology conducted in CEREGE. Meteorites from Chile and Iran are the main found locations classified in this work. OCs comprise 95% of the classified meteorites. Comparison of the magnetic susceptibility with weathering grade data shows different weathering behavior in different hot deserts, which is mainly governed by the climate. An increase in the magnetic susceptibility in weathering grades higher than W3 for Lut Desert meteorites is observed which might be related to the formation of magnetite or maghemite during weathering.

Investigation of the terrestrial weathering of Antarctic meteorites using weathering grade and magnetic susceptibility parameters and its comparison with the hot desert samples can give us important information about this process. To do so, measurements on the Belgian Antarctic Meteorite Collection and ANSMET meteorite samples has begun. The results and their interpretations will be published along with the hot desert meteorite data in the near future.

References:

Brearley A. J. and Jones R. H. (1998) Chondritic meteorites. *Rev. Mineral. Geochemistry* **36**.

Folco L., Rochette P., Gattacceca J. and Perchiazzi N. (2006) In situ identification, pairing,

566 and classification of meteorites from Antarctica through magnetic susceptibility
567 measurements. *Meteorit. Planet. Sci.* **41**, 343–353. Available at:
568 http://onlinelibrary.wiley.com/doi/10.1111/j.1945-5100.2006.tb00467.x/abstract [Accessed
569 September 25, 2015].

570 Keil K. and Fredriksson K. (1964) The iron, magnesium, and calcium distribution in
571 coexisting olivines and rhombic pyroxenes of chondrites. *J. Geophys. Res.* **69**, 3487–3515.
572 Available at: http://doi.wiley.com/10.1029/JZ069i016p03487 [Accessed October 19, 2016].

573 Papike J. J., Karner J. M. and Shearer C. K. (2003) Determination of planetary basalt
574 parentage: A simple technique using the electron microprobe. *Am. Mineral.* **88**, 469–472.
575 Available at: http://ammin.geoscienceworld.org/lookup/doi/10.2138/am-2003-2-323.

576 Rochette P., Sagnotti L., Bourot-Denise M., Consolmagno G., Folco L., Gattacceca J.,
577 Osete M. L. and Pesonen L. (2003) Magnetic classification of stony meteorites: 1. Ordinary
578 chondrites. *Meteorit. Planet. Sci.* **38**, 251–268. Available at:
579 http://doi.wiley.com/10.1111/j.1945-5100.2003.tb00263.x [Accessed October 4, 2015].

580 Rubin A. E. (1990) Kamacite and olivine in ordinary chondrites: Intergroup and intragroup
581 relationships. *Geochim. Cosmochim. Acta* **54**, 1217–1232. Available at:
582 http://www.sciencedirect.com/science/article/pii/001670379090148E [Accessed October 4,
583 2015].

584

585 **Table headings:**

586 **Table 1:** Find locations of the studied meteorites.

587 **Table 2:** Classified meteorites based on their type.

588

589 **Figure captions:**

590 **Fig. 1:** The procedure followed in this work for meteorite classification.

591 **Fig. 2:** The decimal logarithm of magnetic susceptibility χ in 10^{-9} m^3 kg^{-1} for different
592 classes of meteorites (mean value and standard deviation), as well as for plutonic, volcanic,
593 metamorphic, and sedimentary rocks from northern Victoria Land, Antarctica (gra, sed, met,

vol). Weathered metal bearing meteorites show lower values than the means above (derived from falls). Source: Folco et al. (2006).

Fig. 3: Fs vs. Fa in >7300 ordinary chondrites, with the symbol color showing the reported classification. Also shown are the recommended ranges for each chondrite group as given Keil and Fredriksson (1964) and Brearley and Jones (1998).

Fig. 4: Kamacite Co concentration vs. olivine Fa content for 113 ordinary chondrites. Data source: (Rubin, 1990).

Fig. 5: Fe/Mn (pyroxene, olivine) vs. %An (plagioclase) for planetary basalts. Source: (Papike et al., 2003).

Fig. 6: Statistics of the classified meteorites.

Fig. 7: A comparison of the relationship between weathering grade and magnetic susceptibility (logχ) in ordinary chondrites from Oman, Atacama Desert (Chile) and Lut Desert (Iran).

Tables:

Table 1.

Place	**n**
Oman	76
Morocco/Western Sahara	8
NWA	29
Iran	219
Chile	373
France	1
Total	706

Table 2.

Type	**n**
Ordinary chondrite	669
Iron	6

Mesosiderite	3
Rumuruti chondrite	1
Carbonaceous chondrite	19
HED	5
Ureilite	2
Ungrouped chondrite	1
Total	706

613

614

615 **Figures:**

616 **Fig. 1:**

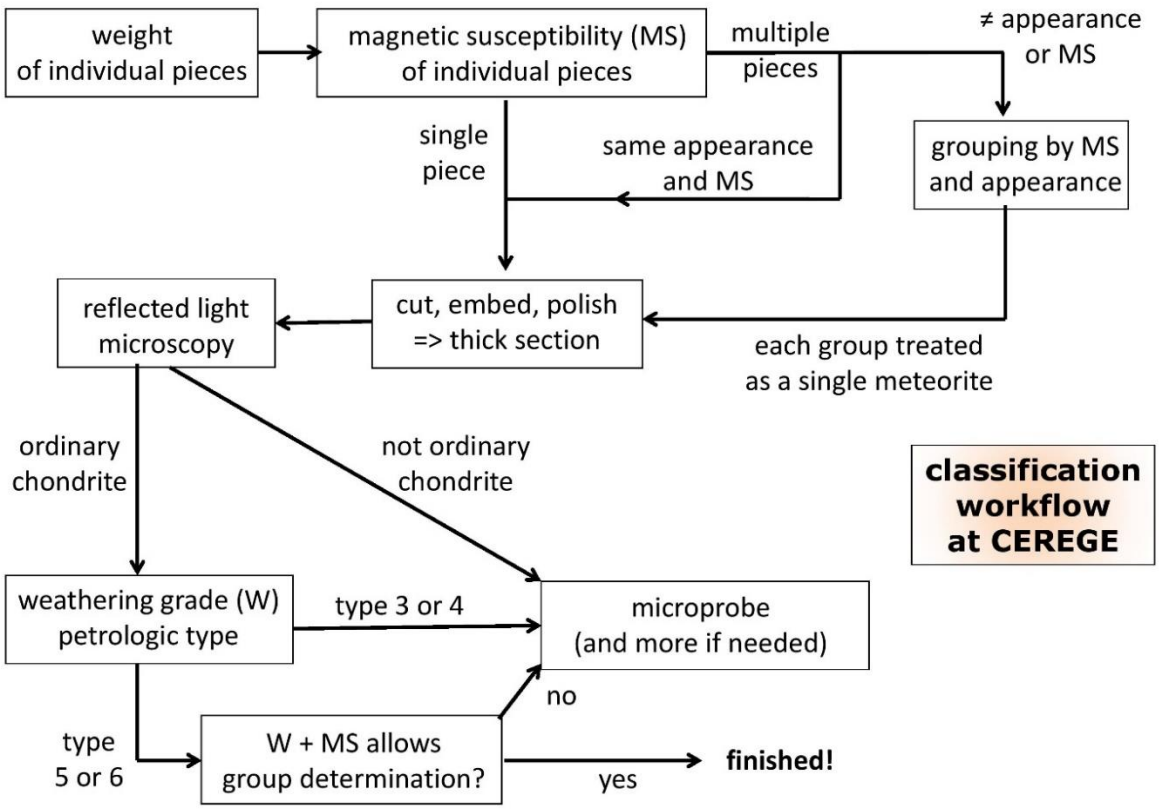

617

618

619

620 **Fig. 2:**

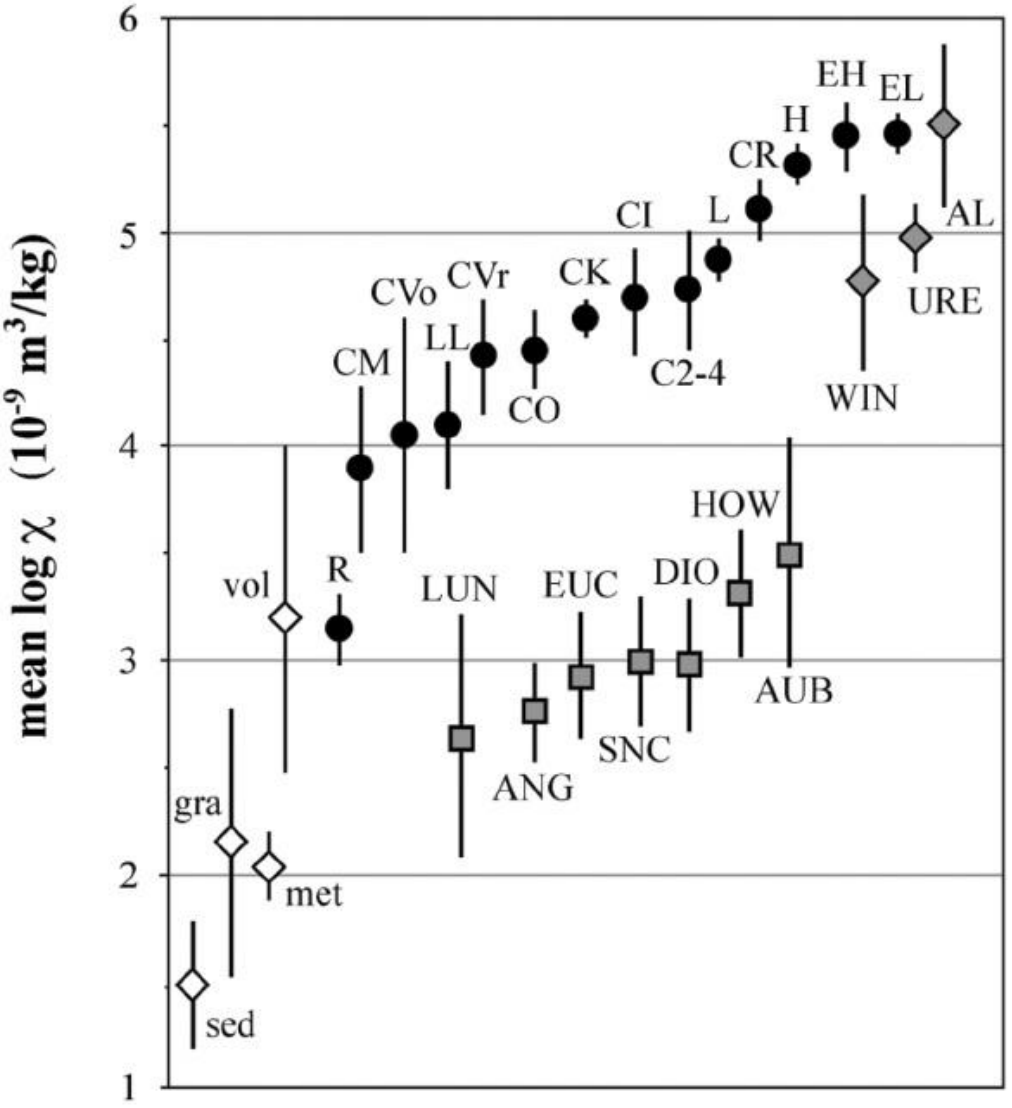

621

622

623

624

625

626

627

628

629

Fig. 3:

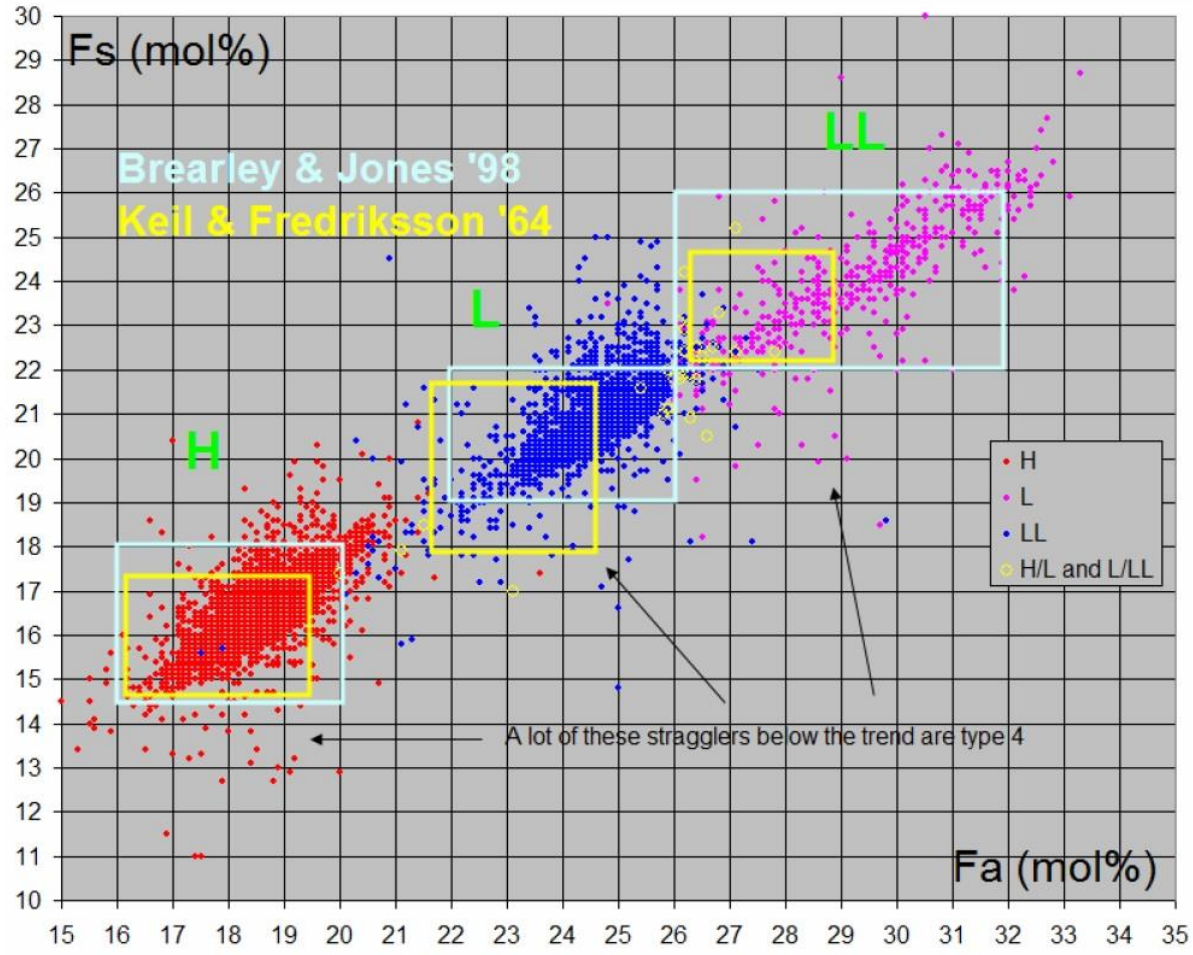
Fs (mol%)
Fa (mol%)
Brearley & Jones '98
Keil & Fredriksson '64
H
L
LL
H
L
LL
H/L and L/LL
A lot of these stragglers below the trend are type 4

642 **Fig. 4:**

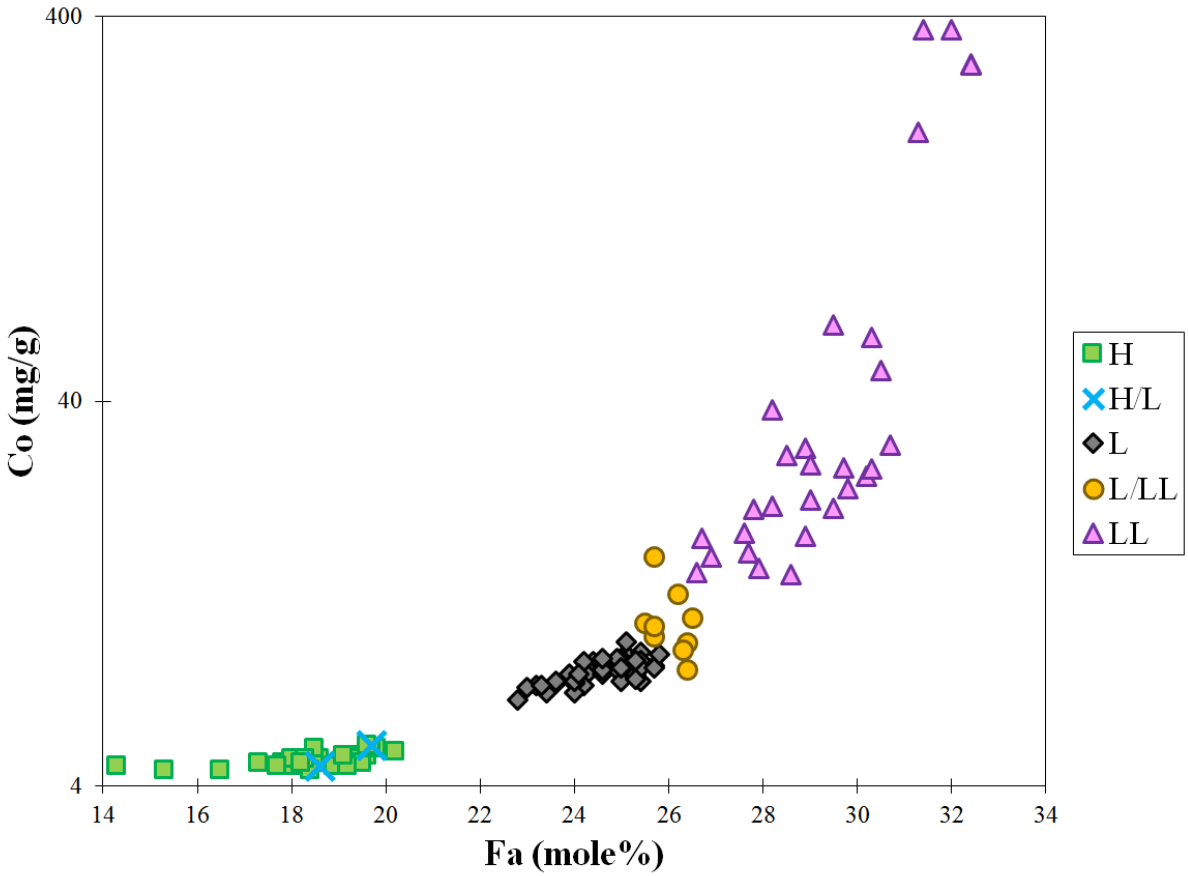

643

644

645 **Fig. 5:**

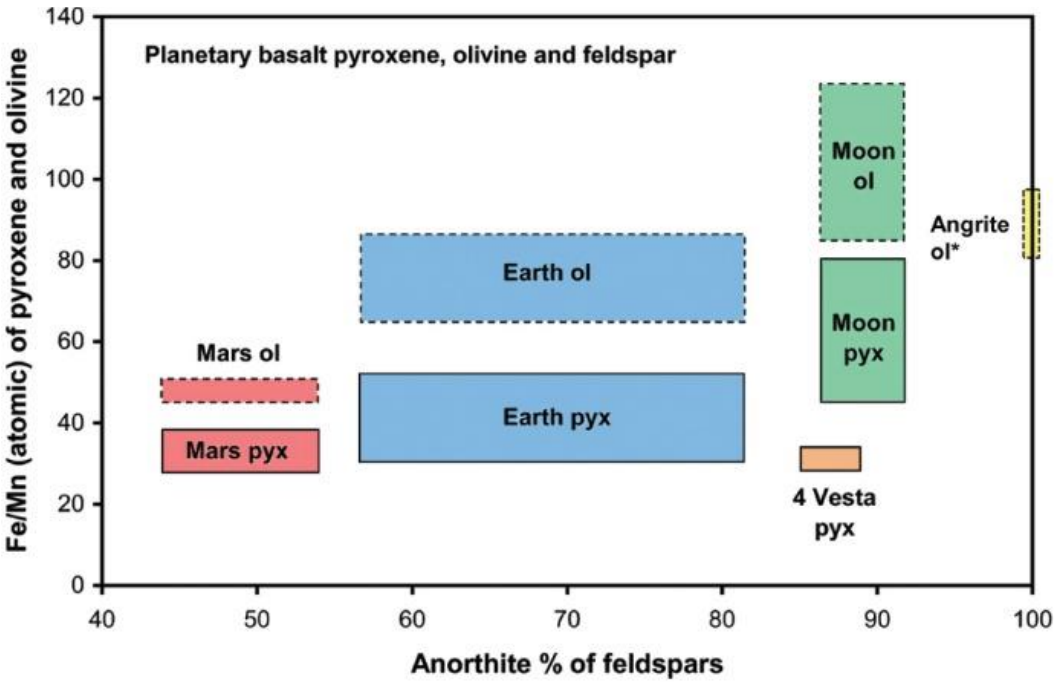

646

647 **Fig. 6:**

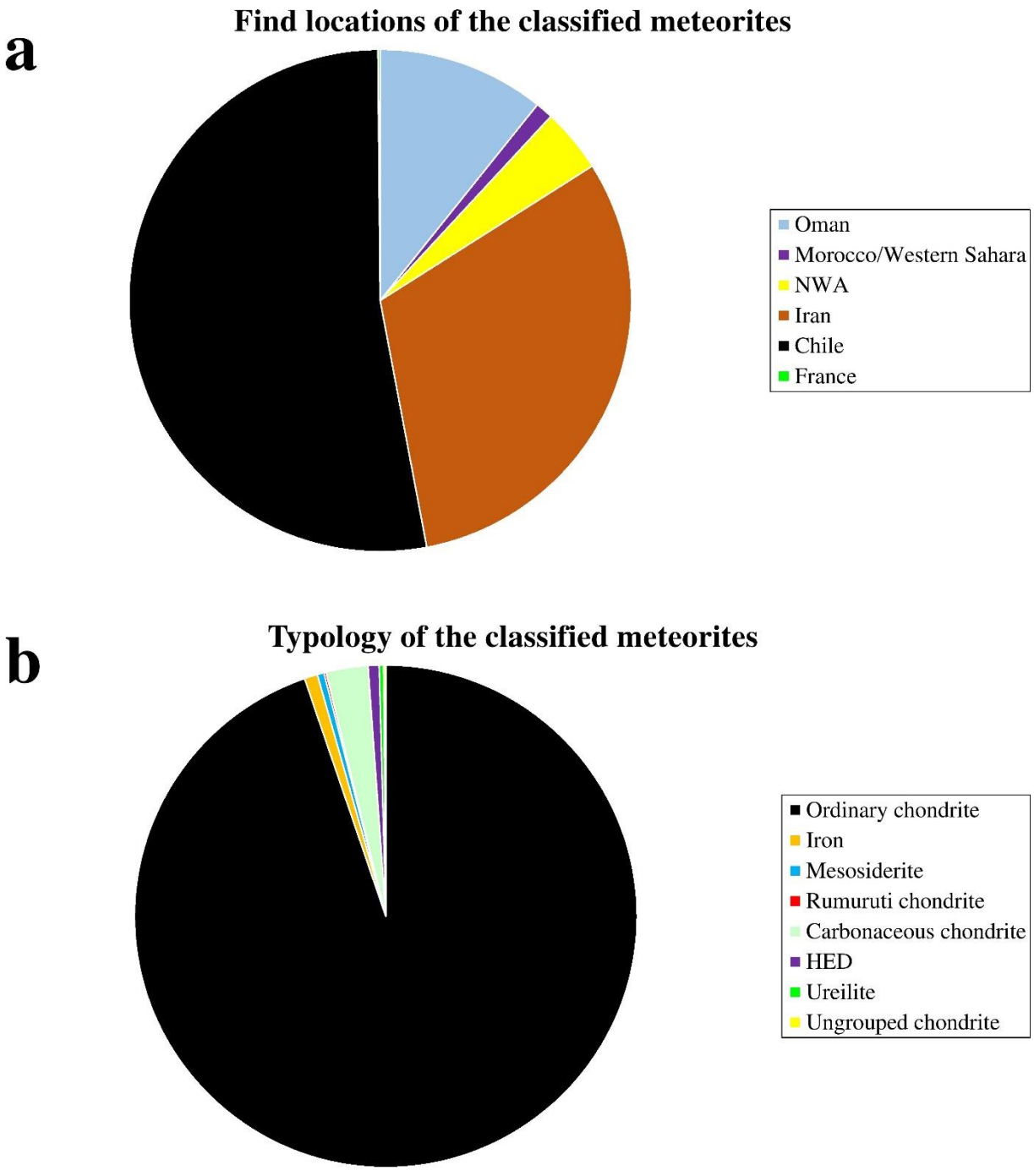

648

649

650

651

652

653

654

Fig. 7:

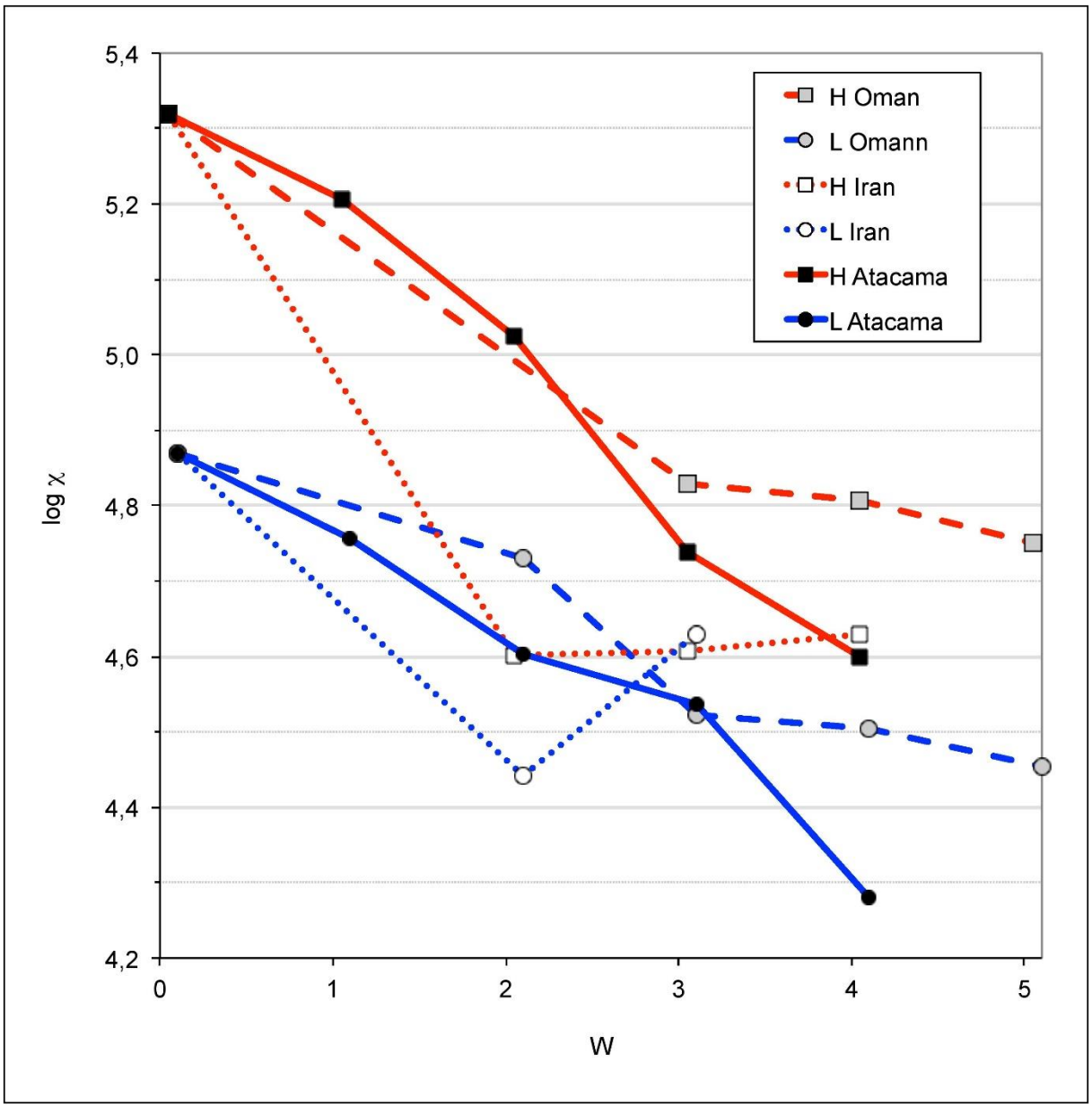
5,4
5,2
5,0
4,8
4,6
4,4
4,2
log χ
0
1
2
3
4
5
W
H Oman
L Omann
H Iran
L Iran
H Atacama
L Atacama

Left blank intentionally.

Part II

Hot Desert Meteorites

Chapter 3

Beginning of Studies on Lut Desert Meteorites: Lut 009 Extended Classification Report

---

Peer-reviewed research paper *Pourkhorsandi et al., Journal of the Earth and Space Physics, 2016*

Journal of the Earth and Space Physics, Vol. 41, No. 4, 2016, PP. 125-130

Lut 009, an H4 (S2, W4) ordinary chondrite meteorite from Lut Desert of Iran

Pourkhorsandi, H.[1*], Mirnejad, H.[2], Rochette, P.[3] and Hassanzadeh, J.[4]

1. Ph.D. Student, Aix-Marseille Université/CNRS/IRD, CEREGE UM34, Aix-en-Provence, France
2. Associate Professor, Department of Geology, Faculty of Sciences, University of Tehran, Iran
3. Professor, Aix-Marseille Université/CNRS/IRD, CEREGE UM34, Aix-en-Provence, France
4. Associate Researcher, Division of Geological and Planetary Sciences, California Institute of Technology, Pasadena, USA

(Received: 20 Apr 2015, Accepted: 06 Oct 2015)

Abstract

Lut 009 meteorite was found during a trip to Lut Desert of Iran in March,2012, at 30°20.38' N, 59°09.04' E. Chemical compositions of equilibrated olivine ($Fa_{19.3 \pm 0.5}$) and orthopyroxene ($Fs_{16.7 \pm 0.6}$) show that the meteorite sample belongs to H group of ordinary chondrites, while the texture (chondrule petrography and plagioclase size) suggests a petrologic type of 4. The Lut 009 has been very weakly shock altered and has a shock stage of S2. Fe-Ni is completely weathered whereas less than 5 percent of troilite is still present. Therefore, the meteorite has a weathering grade of W4. Magnetic susceptibility is $\log \chi = 4.75$ (χ in 10^{-9} m^3/kg) and, thus, consistent with a W4 H ordinary chondrite. Here we report description of Lut 009 in the first extended study on a meteorite from Lut Desert. Along with this sample, in-progress investigations of other meteorites from the desert will open a window into the characteristics of meteorite concentrations in this region.

Keywords: Iran, Lut Desert, Meteorite, Ordinary chondrite.

1. Introduction

Since its early days of formation, the Earth was continuously receiving solid objects derived predominantly from asteroidal, cometary and planetary debris. These fragments are ranged in size from interplanetary and interstellar dust particles to boulder-sized chunks and larger objects. They are also capable of forming impact craters. Natural solid objects, larger than a few mm, that reach the Earth's surface are known as "meteorites" (Hutchison, 2004). They are the oldest material in the solar system and in a large variety of parent bodies. Meteorites are especially valuable samples because they can be investigated in the laboratory with a complete set of sophisticated techniques (e.g., Koeberl and Cassidy, 1991), and their study helps us delineate the origin and evolution of our solar system.

At terrestrial environments, meteorites are subject to oxidation and weathering processes that lead to the formation of secondary alteration minerals and finally destruction of the original rock. The rate of meteorite weathering in continents is governed by the climate. However, hot and cold deserts are the most suitable places for preservation of these objects (Bland et al., 2006). In the recent years, some meteorite has been reported from Lut desert of Iran (http://www.lpi.usra.edu/meteor). A stony meteorite was found by the first author in Lut desert at coordinates of 30°20.38' N, 59°09.04' E on March, 2012, lying on the flank of a sand dune near the margin of Rige-e-Yalan and central hamada (Fig. 1). The official name "Lut 009" was approved by "the Meteorite Nomenclature Committee" in February, 2015. Here we present classification and the results of the textural, magnetic susceptibility and mineral chemistry investigations on Lut 009 meteorite sample, with the purpose for further characterization of the meteorite collection of Lut desert.

2. Lut Desert

According to Pabot (1967), approximately 50 percent of Iran's total surface (~1,625,000 km^2) is covered by desert and semi-desert areas, with precipitation less than 50 mm/yr and 50-100 mm/yr, respectively. Lut Desert, a depression surrounded by mountain ranges, extends over an area of about 80,000 km^2 (between latitudes of 28°21' - 32°N and longitudes of 57°30' - 59°55' E and covers 4.9% of the total surface area of the country).

*Corresponding author: E-mail: pourkhorsandi@cerege.fr

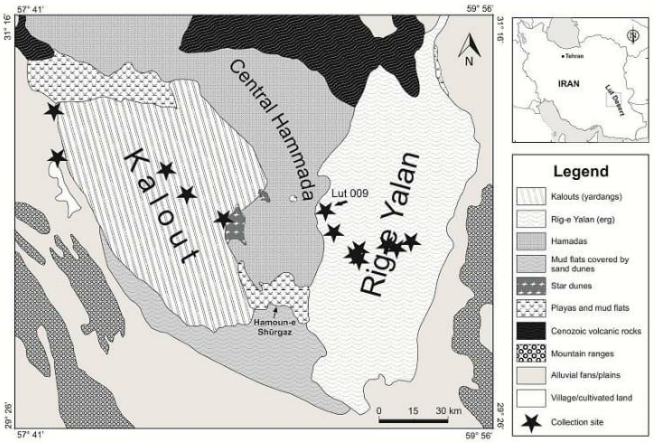

Fig. 1. The map shows central Lut Desert and the location of Lut 009 and other meteorites (from Meteoritical Bulletin)

Based on geographic characteristics, Lut desert is divided into three main units (Mahmoodi, 2002; Ehsani and Quiel, 2008): (1) Northern Lut, characterized by Cenozoic volcanic and sedimentary rocks and vast flat areas, (2) Central Lut, the main unit of Lut characterized by arid to hyperarid conditions, and (3) Southern Lut that is characterized by playas and ravines.

Central Lut comprises three distinct parts: a) the western part occupied by mega-yardangs is known as 'Kalout'; they are some of the world's largest desert landforms separated by large NW-trending wind-swept parallel corridors. These features extend in 140 × 80 km area and were formed by wind and water activities, b) the eastern unit, i.e., Rig-e Yalan (Yalan Erg), is a ~50×100 km sand sea composed of a great massif of dunes and sand rises with heights up to 475 m, and c) the middle part including playas, hamadas and sand sheet type plains.

High temperature, very little precipitation rate (<50 mm/year) and high degrees of evaporation (5000 mm/yr) are some of the main properties of Lut desert. Climate Model Grid (CMG) shows that Lut desert has been the hottest area of the earth in the years 2004, 2005, 2006, 2007 and 2009, with maximum temperatures of 68.0, 70.7, 68.5, 69.0 and 68.6 ^{o}C, respectively (Mildrexler et al., 2011).

According to Pourkhorsandi and Mirnejad (2013), despite vast arid desert areas in Iran (e.g., Dasht-e Kavir, deserts of Yazd and Tabas, Rig-e Jenne desert and Lut), not much attention has been paid to the potential of these Iranian deserts in hosting meteorites. Recent short field surveys to the central Lut Desert by different travel groups have led to the collection of several meteoritic fragments (http://www.lpi.usra.edu/meteor), which points to significant concentrations of meteoritic materials in the area. Climate and surface conditions in Lut desert make it a high-potential region to preserve the meteorites.

3. Methodology

To characterize texture, mineralogy and weathering degree of the meteorite, thin and polished sections were prepared and studied in transmitted and reflected light at the University of Tehran and CEREGE. Using polarizing microscope, mosaic pictures of the meteorite were prepared under transmitted polarized light. Chondrule diameters which are different among different chondrite groups were measured using JMicroVision software based on the mentioned pictures. Reflected polarized light was used to investigate the properties of opaque minerals (primary and terrestrial) and to determine the weathering degree. The chemical composition of ferromagnesian silicates is different among different chondrite groups (Van Schmus and Wood, 1967), and it has been used for the meteorite classification. For this purpose, chemical compositions of olivine and orthopyroxene were determined with JEOL JXA-8200 electron microprobe at California Institute of Technology, using focused electron beam (~1 micrometer in diameter), an accelerating voltage of 15 kV and a beam current of 25 nA. The data were reduced using CITZAF algorithm (Armstrong, 1988). Magnetic susceptibility is another property of meteorites that is different among meteorite

groups (Rochette et al., 2012). Magnetic susceptibility was measured at CEREGE using a KLY2 instrument from Agico equipped with both a large (65cm^3) and a small (10cm^3) coil.

4. Results

Lut 009 is a single stone, ellipsoidal in shape (4×2.5×2 cm) and approximately 41 g in weights (Fig. 2). Its surface is covered by a dark-brown desert patina and no fusion crust, usually formed during the atmospheric entry of the object, is remained on. On the surface, a light colored silicate phase can be seen with the unaided eye that might be a macro-chondrule. In cut surface, light and dark colored chondrules are noticeable (Fig. 2). Two highly and moderately weathered facies are present. One contains metal dissolution pits in an orange colored context and the other one exhibit lesser degree of oxidation grey to light brown parts.

Figure 3 shows the mosaic picture of the studied polished section. Olivine and orthopyroxene are the main mineral phases. Very few troilite (<5%) is present and Fe-Ni metal is completely (>98%) transformed to Fe oxides/ hydroxides (Fig. 4). These secondary products occur as weathering veins and patches that are distributed throughout the meteorite (Fig. 5). Olivine and orthopyroxene are different types of chondrules and porphyritic olivine-pyroxene chondrule type as the most common one (Fig. 6). Some olivine grains show uneven darkening but mostly display sharp and uniform extinctions under polarized light. Chondrules in Lut 009 show sharp boundaries with the matrix and the other components. Average apparent chondrule size is 440±280 µm (n=277). In addition to chondrules, olivine and orthopyroxene occur as chondritic fragments. Plagioclase is usually less than two micrometers.

Electron microprobe analysis of olivine and orthopyroxene are presented in Tables 1 and 2, respectively. Average olivine (n=10) and orthopyroxene (n=2) compositions are $Fa_{19.3 \pm 0.5}$ and $Fs_{16.7 \pm 0.6}$, respectively, and both minerals show homogenous compositions. Measured magnetic susceptibility of the sample is $\log \chi = 4.75$ (χ in 10^{-9} m^3/kg).

Fig. 2. Macroscopic view of Lut 009. Chondrules occur as round dark and light color objects. Metal dissolution pits indicate a high degree of terrestrial alteration.

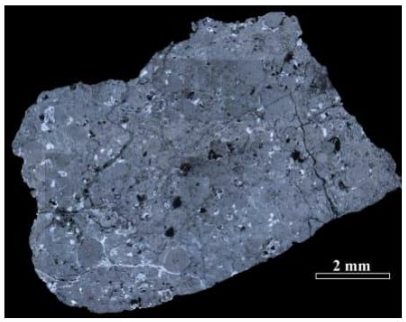

Fig. 3. Mosaic picture of a polished section of Lut 009. Round objects are chondrules and white colored veins and patches are oxidation products of the primary Fe-Ni metal and troilite. Reflected light.

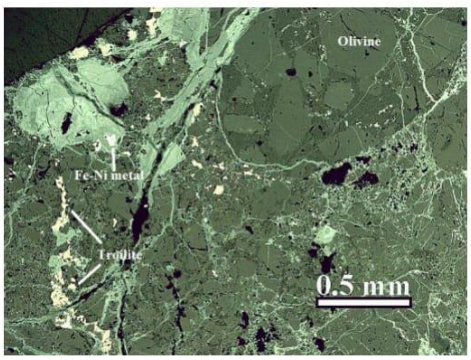

Fig. 4. Troilites (light gray) are less altered than Fe-Ni metal (white) mostly transformed to Fe oxides/hydroxides (dark gray). Reflected light.

Table 1. Representative chemical analyses (wt %) of olivine in Lut 009 ordinary chondrite

Point	SiO_2	TiO_2	Al_2O_3	FeO	MgO	CaO	Na_2O	K_2O	Cr_2O_3	MnO	Total	Fa %
193	41.69	0.02	0.00	17.75	40.51	0.09	0.00	0.00	0.06	0.49	100.61	19.73
194	39.41	0.01	0.01	18.50	41.93	0.03	0.00	0.01	0.03	0.54	100.47	19.84
195	39.34	0.02	0.00	18.18	42.13	0.03	0.00	0.00	0.02	0.51	100.24	19.49
196	39.47	0.01	0.00	18.20	41.98	0.03	0.01	0.01	0.03	0.53	100.26	19.56
197	39.67	0.02	0.00	17.47	43.01	0.02	0.00	0.00	0.00	0.42	100.62	18.56
198	39.58	0.01	0.03	17.85	42.54	0.04	0.01	0.00	0.11	0.50	100.67	19.05
199	39.43	0.01	0.00	17.84	42.56	0.02	0.00	0.00	0.01	0.46	100.33	19.04
200	42.65	0.04	2.56	16.39	36.73	0.25	1.46	0.13	0.35	0.41	100.98	20.02
201	41.65	0.04	1.78	16.31	39.19	0.33	0.84	0.14	0.03	0.38	100.67	18.93
204	39.47	0.09	0.00	17.65	42.52	0.03	0.00	0.00	0.02	0.47	100.26	18.89

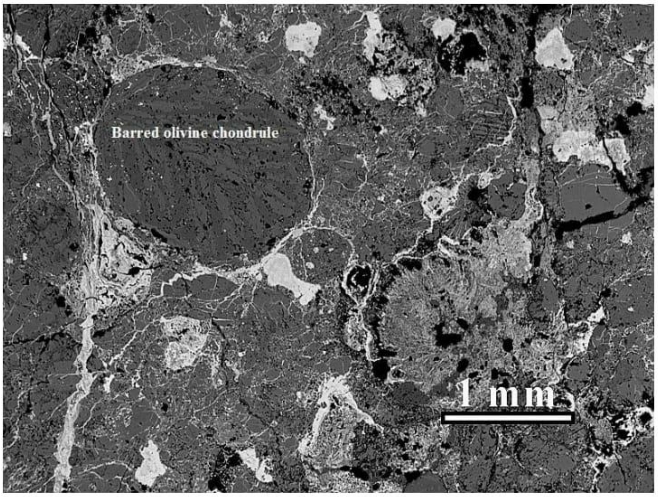

Fig. 5. Terrestrial weathering has affected most of the meteorite. Veins and patches are Feoxides/hydroxides. A barred olivine chondrule can be seen in the view. Reflected light.

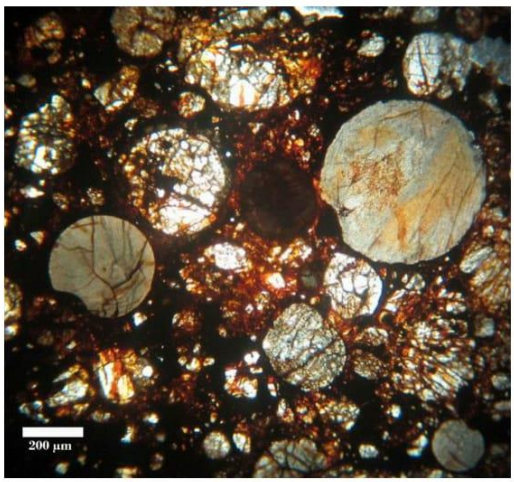

Fig. 6. Different types of chondrules in Lut 009 ordinary chorndrite. Transmitted plain polarized light

Table 2. Representative chemical analyses (wt %) of orthopyroxene in Lut 009 ordinary chondrite

Point	SiO2	TiO2	Al2O3	FeO	MgO	CaO	Na2O	K2O	Cr2O3	MnO	Total	Fs %
202	56.54	0.03	0.19	11.01	30.63	0.80	0.02	0.00	0.27	0.58	100.19	17.27
203	56.58	0.09	0.38	10.18	29.14	2.67	0.19	0.01	0.51	0.49	100.27	16.19

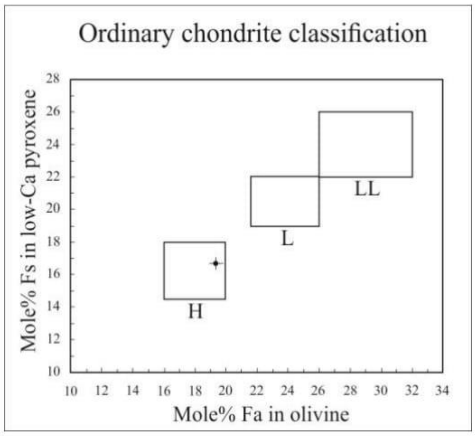

Fig. 7. Average Ca-poor pyroxene versus olivine composition of ordinary chondrites and Lut 009

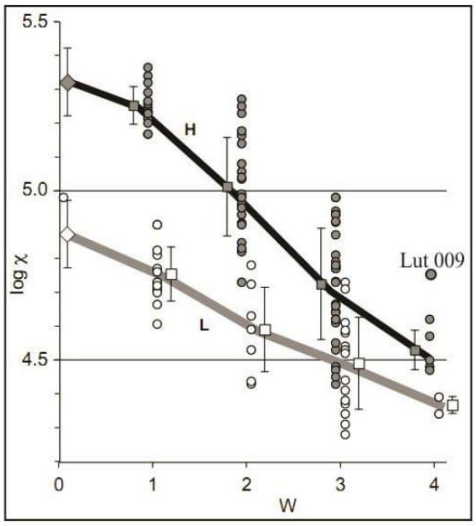

Fig. 8. Log χ as a function of weathering grade for 110 ordinary chondrite finds from the Atacama Desert. Circles are measurements for individual meteorites (solid = H, open = L). Squares are mean values for each weathering grade with associated standard deviation (solid = H, open = L). Diamonds denotes mean values for falls. Lut 009 is in the field of H chondrites. Diagram and description source; Rochette et al. (2012).

5. Conclusions

Lack of fusion crust and severe oxidation of Lut 009 suggest that it has been affected by terrestrial alteration for a long time. Dissolution pits could be the position of former Fe-Ni metal grains, in the most vulnerable phases in terrestrial environments (Buchwald and Clarke Jr., 1989).

The texture and mineralogical components indicate that Lut 009 is an ordinary chondrite. With the homogeneity in olivine composition, chondrule-matrix integrations, size of plagioclase and based on the classification of Van Schmus and Wood (1967), the Lut 009 is a petrologic type of 4. Figure 7 depicts the average olivine and orthopyroxene composition ranges of ordinary chondrites groups and reveals that Lut 009 is an H ordinary chondrite. H ordinary chondrite, in which H stands for "high iron", is the most common type of found meteorites (Hutchison, 2004).

The presence of uneven darkening in olivine and minor fracturing in Lut 009 are consistent with a very weak shock alteration. This indicates a shock stage of S2, based on classification of Stöffler et al. (1991).

The weathering of Fe-Ni metal and troilite as well as unaltered silicate grains suggest that Lut 009 belongs to the weathering grade of W4 (Wlotzka, 1993). Bland et al. (1997) and Lee and Bland (2004) showed that Fe-Ni metal oxidization is faster than troilite and this is the reason for few occurrence of troilite compared to Fe-Ni metal that is completely transformed into Fe oxides/hydroxides. Such a sever oxidation of the Lut 009 and its occurrence on a sand dune field, which can represent its oxidation in a dry region, indicates a high terrestrial age for this meteorite.

For using magnetic susceptibility and weathering grade date to classify Lut 009, the data were plotted in a diagram of log χ versus weathering degree (Fig. 8) (Rochette et al., 2012). The Lut 009 meteorite is consistent with H ordinary chondrites that are also in accordance with mineral chemistry classification.

The meteorite found and classified in this work has been given the official name of Lut 009 (http://www.lpi.usra.edu/meteor) and it

is an H ordinary chondrite with a shock stage of S2 and a weathering grade of W4.

As the number of the reported Iranian meteorites to Meteoritical Bulletin indicated, Lut desert seems to be a suitable place for meteorite preservation in Iran, with a total of 13 meteorites declared to date, most of them in the last 3 years.

Acknowledgments

This work has been supported by Center for International Scientific Studies & Collaboration (CISSC) and French Embassy in Tehran. We thank M. Djamali for providing raw map of Figure 1 and Jérôme Gattacceca for his help during the petrography of the sample. Editorial handling by Prof. Bidokhti and suggestions by two anonymous reviewers are appreciated.

References

Armstrong, J. T., 1988, Quantitative analysis of silicate and oxide minerals, comparison of Monte Carlo, ZAF, and U (qz) procedures, in: Newbury, D. E., (Ed.), Microbeam analysis. Proceedings of the 23rd Annual Conference of the Microbeam Analysis Society, San Francisco Press, San Francisco, 239-246.

Bland, P. A., Kelley, S. P., Berry, F. J., Cadogan, J. M. and Pillinger, C. T., 1997, Artificial weathering of the ordinary chondrite Allegan, Implications for the presence of Cl^- as a structural component in akaganeite, Am. Mineral, 82, 1187-1197.

Bland, P. A., Zolensky, M. E., Benedix, G. K. and Sephton, M. A., 2006, Weathering of chondritic meteorites, in: Lauretta, D. S. and McSween, Jr., H. Y., (Eds.), Meteorites and the Early Solar System II, University of Arizona Press, Arizona, 853-867.

Buchwald, V. F. and Clarke, Jr., R. S., 1989, Corrosion of Fe-Ni alloys by Cl-containing akaganeite (β-FeOOH), the Antarctic meteorite case, Am, Mineral, 74, 657-667.

Ehsani, A. H. and Quiel, F., 2008, Remote sens, Environment, 112, 3284-3294.

Hutchison, R., 2004, Meteorites, a petrologic, chemical and isotopic synthesis, Cambridge University Press, Cambridge.

Koeberl, C. and Cassidy, W. A., 1991, Differences between Antarctic and non-Antarctic meteorites, An assessment, Geochim, Cosmochim, Ac(55), 3-18.

Lee, M. R. and Bland, P. A., 2004, Mechanisms of weathering of meteorites recovered from hot and cold deserts and the formation of phyllosilicates, Geochim, Cosmochim, Ac(68), 893-916.

Mahmoodi, F., 2002, The distribution of erg lands of Iran (in Persian), Forest and Range Protection Research Institute, Tehran.

Mildrexler, D. J., Zhao, M. and Running S. W., 2011, B. Am. Meteorol. Soc., 7, 855-860.

Pabot, H., 1967, Report to government of Iran, pasture development and range improvement through botanical and ecological studies, UNDP, Food and Agricultural Organization of the United Nations, Rome.

Pourkhorsandi, H. and Mirnejad, H., 2013, 44th Lunar and Planetary Science Conference, A1096.

Rochette, P., Gattacceca, J. and Lewandowski, M., 2012, Magnetic classification on meteorites and application to the Soltmany Fall. Meteorites, 2, 67-71.

Stöffler, D., Keil, K. and Scott E. R. D., 1991, Shock metamorphism of ordinary chondrites, Geochim, Cosmochim, Ac(55), 3845-3867.

Van Schmus, W. R. and Wood, J. A., 1967, A chemical-petrologic classification lot the chondritic meteorites, Geochim, Cosmochim, Ac(31), 747-765.

Wlotzka, F., 1993, A weathering scale for the ordinary chondrites, Meteoritics, 28, 460.

Left blank intentionally.

Chapter 4

Meteorites from the Lut Desert: Classification, Spatial Distribution, and Weathering

---

In-preparation for submission to the *Meteoritics & Planetary Science*

Title: METEORITES FROM LUT DESERT (IRAN)

Authors: Hamed Pourkhorsandi[1*], Jérôme Gattacceca[1], Pierre Rochette[1], Massimo D'Orazio[2], Edivaldo dos Santos[x], Roza Scorzelli[x], Hojjatollah Kamali[x], Morteza Djamali[x], Hassan Mirnejad[x], Vinciane Debaille[x], A. J. Timothy Jull[x],

[1] CNRS, Aix-Marseille Univ., IRD, Coll. France, CEREGE, Aix-en-Provence, France

[2]Dipartimento di Scienze della Terra, Università di Pisa, Via S. Maria 53, I-56126 Pisa, Italy

[x]xxx

[x]xxx

[x]Afshin Meteorite Hunting Group, Kerman, Iran

[x]CNRS, IRD, Aix-Marseille Unive., IMBE, Aix-en-Provence, France

[x]Department of Geology, Faculty of Sciences, University of Tehran, Tehran 14155-64155, Iran

[x]Laboratoire G-Time, Université Libre de Bruxelles, CP 160/02, 50, Av. F.D. Roosevelt, 1050 Brussels, Belgium

[x]NSF Arizona AMS Laboratory, University of Arizona, Tucson, AZ 85721, USA

Corresponding author. *E-mail address*: pourkhorsandi@cerege.fr (H. Pourkhorsandi).

To be submitted to the *Meteoritics and Planetary Sciences (MAPS)*

Abstract:

We present for the first time a detailed report on the discovery of a new meteorite collection region in the Lut Desert, eastern-southeastern Iran. We describe the geological, morphological, and climatic setting of this region. Our search campaigns alongside with the activity of meteorite hunters yielded >200 meteorite finds. Here, we report their classification, spatial distribution, and terrestrial weathering.

All the collected meteorites are ordinary chondrites (OCs). The most abundant by far is for the highly weathered paired H5 meteorites distributed in the NW of Kalut area (central Lut).

798 The second are well-preserved paired L5 meteorites found in Kalut too.

799 A detailed study of the geochemistry and mineralogy of selected meteorites reveals
800 significant effects of terrestrial weathering. Fe,Ni metal (simply metal) and troilite are
801 transformed to Fe oxides/oxyhydroxides. A rather unique type of troilite weathering to pyrite
802 and marcasite is observed in most of the Lut meteorites. Magnetic measurements and X-ray
803 diffractrometry show the presence of terrestrial weathering products, with the dominance of
804 maghemite, goethite, and hematite. Mobile elements such as Li, Sr, Mo, Ba, Tl, Th, and U
805 have increased contents with respect to fresh falls. Meanwhile, a decrease in the V, Cr, Co, Rb
806 (and possibly Fe) due to metal oxidation is detectable. The total carbon and $CaCO_3$ is higher
807 than in samples from other hot deserts. The weathering effects, observed in the Lut OCs can
808 be used as distinctive indicators to distinguish them from the meteorites from other regions of
809 the Earth.

810 Three measurements of terrestrial age (^{14}C) show a range of 10-30 ka, which is in the range
811 of ages reported from meteorites from other hot deserts (except the Atacama Desert).

812 Considering the high potential of the Lut in meteorite preservation, systematic works in the
813 future should lead to the discovery of more samples giving access to interesting material of
814 future studies.

815 **Keywords:** Iran, Lut, Desert, Weathering, Chondrite

816

817 ## 1. INTRODUCTION

818 Besides Antarctica cold desert (Harvey 2003), hot deserts are suitable places for
819 preservation, accumulation and the subsequent recovery of meteorites. High numbers of
820 meteorites have been collected and studied from the arid regions of the planet, such as
821 Atacama (Gattacceca et al. 2011; Hutzler et al. 2016; Muñoz et al. 2007), Sahara (Bischoff
822 and Geiger 1995; Ouazaa et al. 2009; Schlüter et al. 2002), Australian deserts (Bevan and
823 Binns, 1989; Bevan, 1992; Benedix et al., 1999), Arabian Peninsula (Al-Kathiri et al., 2005;
824 Gnos et al., 2009; Hezel et al., 2011), and Central and SW USA (Kring et al. 2001; Rubin et
825 al. 2000; Zolensky et al. 1990). Finding new meteorite dense collection areas (DCAs) is
826 important for discovering new and unique meteorite types (e.g., Bischoff, 2001; Kent et al.,
827 2017; Pourkhorsandi et al., 2017), and accessing more samples for statistical works on the
828 flux of extraterrestrial materials (e.g., Bland et al., 1996), studying meteorite fall process by
829 mapping the ancient strewnfields (e.g., Kring et al., 2001; Gnos et al., 2009), studying the
830 alteration of extraterrestrial material on Earth (Bland et al. 2006; Pourkhorsandi et al. 2017b;

831 Saunier et al. 2010; Uehara et al. 2012; Zurfluh et al. 2016) and their relationship with the past
832 climate (Bland et al. 1998; Lee and Bland 2003; Pourkhorsandi et al. 2017b).
833 In this work, we evaluate the potential of Iran for meteorite recovery. Iran is located in SW
834 Asia, in the mid-latitude belt of arid and semi-arid regions of the Earth. These regions cover
835 more than 60% of the country. Despite its surface area and dry climate, few meteorites were
836 recorded until recently. Only two Iranian meteorites, both falls, were cataloged in the
837 Meteoritical Bulletin during 20th century. Veramin a mesosiderite fallen in 1880 (Graham and
838 Hassanzadeh 1990; Ward 1901) and Naragh H6 chondrite fallen in 1974 (Adib and Liou
839 1979; Clarke 1975).
840 Shahdad, the first meteorite find, was collected in 2005 from the western margin of the Lut
841 Desert (Garvie 2012). Lut Desert also known as Dasht-e-Lut is located in east-southeast of the
842 country (Fig. 1a). Considering its climatic, geological and geomorphological characteristics,
843 Pourkhorsandi and Mirnejad (2013) proposed it as a potentially suitable place for meteorite
844 preservation and collection.
845 The first systematic studies on meteorites from Iran and especially Lut, was initiated as a
846 cooperation between CEREGE and the University of Tehran in 2014. The start of the project
847 was concurrent with local media coverage on meteorites by the first author, which lead to the
848 interest of the Iranian public on this topic and the formation of meteorite hunting groups.
849 These groups are active in different regions of the country, especially in the Lut region.
850 Now, less than 5 years after the start of the project, hundreds of meteorites have been
851 collected from Lut. More than 200 meteorites from Lut have been classified and have gotten
852 official names. Many more samples are under classification. Only 8 meteorites were found
853 outside Lut.
854 Most meteorites were collected in two DCAs from central Lut desert, Lut and Kerman (this
855 one encompassing the Kalut geographic region) (Fig. 1b). The DCAs located at the periphery
856 of the Lut desert (Gandom Beryan to the North, Lut-e-Zangi Ahmad to the South) count only
857 8 meteorites.
858 The classification of these meteorites can give insights into the proportion of different
859 groups found in the area to study the flux of meteorites. In addition, pairing the samples
860 evidences on the occurrence of probable meteorite strewnfields. Weathering of these samples
861 and its comparison with those from other hot deserts is another subject of interest, which can
862 be used to study the weathering process and the palaeoclimatic conditions of the desert.
863 Here, we present the data on the classification, weathering and spatial distribution of the
864 Lut meteorites and we report the results of detailed geochemical and mineralogical

865 characteristic of 10 selected meteorites. In addition, we present the terrestrial age data of 3 of
866 selected samples.
867
868 **2. ENVIRONMENT OF THE LUT DESERT**
869 **2.1. Geology and Geomorphology**
870 Lut is a part of the Lut block which itself is a part of the Central Iranian microcontinent.
871 Lut block is bounded to the north by Doruneh, to the east by Nehbandam and to the west by
872 Nayband fault systems. Probably, the South Jazmourian Fault confines the southern part of
873 this block. More details on the geodynamical aspects of Iran and the region are discussed in
874 Aghanabati (2004).
875 Based on the geographic characteristics, Lut is divided into three main units (e.g., Dresch,
876 1968): (*i*) Northern Lut, characterized by Cenozoic volcanic and sedimentary rocks and vast
877 flat surfaces. (*ii*) Central Lut (CL) consists three different parts: (a) Kalut which are
878 megayardangs occupying the western part of CL (Fig. 1 and EA-1) (Ehsani and Quiel 2008;
879 Ghodsi 2017; Mashhadi et al. 2002). There are amongst the largest desert forms of their kind
880 on the planet. Long hills with height around 10 m (and 50 m in some cases) made of clays, silt
881 and sand and also containing evaporites and carbonates, separated by large wind-swept
882 parallel corridors with a NW-SE direction extended in an 140 × 80 km area (Fig. EA-2); (b)
883 Rig-e Yalan (Yalan Erg), the eastern unit of CL is a sand sea composed of a great massif of
884 dunes and sand rises with heights up to 475 m that cover an area of ~ 50 × 100 km; (c) Playas,
885 hammadas and sand sheet type plains form the middle part of CL. (*iii*) Southern Lut is
886 characterized by playas and ravines.
887 Vicinity to the Shahdad-Nehbandan road and more importantly low abundance of
888 terrestrial rocks has made the Kalut to be the main target for meteorite hunting. Except its
889 northern part which is composed of highly saline Rude-e Shur river and the related clay-
890 evaporite rich puffy soils, the rest of the Kalut is dry and is filled by coarse grain sand.
891 **2.2. Climate**
892 High temperature, very low precipitation rate (less than 50 mm/year) and high amounts of
893 evaporation (5000 mm/yr) are the main climatic characteristics of the Lut (Fig. 2a). The De
894 Martonne aridity index (a classic indicator of dryness) which uses temperature and rainfall
895 data of central Lut is less than 1 and is 2-4 for the margins of the desert (e.g., Motamed,
896 1974). Data from *Aqua*/MODIS Climate Model Grid (CMG) shows that Rig-e Yalan of Lut
897 has been the hottest area of the Earth in the years 2004, 2005, 2006, 2007 and 2009 with
898 temperatures of 68.0, 70.7, 68.5, 69.0 and 68.6 ^{o}C, respectively (Mildrexler et al. 2006). Lut

899 is the only area in Iran with a Tropical Hyperdesertic climate, the driest possible bioclimate
900 in the Global Bioclimatic Classification System (Djamali et al. 2011).
901 In order to obtain the first "long-term" in situ climatic data, we placed an automatic
902 thermometer/hygrometer (Lascar EL-USB-2) in Rig-e Yalan and in the location shown to be
903 the hottest spot (30° 2.8' N, 59° 11.9' E) (Mildrexler et al. 2006). The instrument working
904 inside a wooden box 20-30 cm above the ground collected precise data with an interval
905 record time of 60 minutes from April 2014 to February 2016. A brief data analysis shows a
906 range of temperature from 0 to 61 ºC and a humidity range from 3 to 61 %rh. Mean annual
907 temperature and humidity for 2015 are 31.6 ºC and 15.7 %rh, respectively. Fig. 2b shows the
908 plotted data points for the mentioned parameters.
909

910 ## 3. METHODLOGY

911 ### 3.1. Searching Methods

912 As mentioned, the focus of the searches have been on Kalut area (in Kerman DCA).
913 Systematic searches were conducted by both car and foot. Low abundance of terrestrial rocks
914 and the narrow valleys in the Kalut makes searching by car much easier and more efficient
915 than by foot. Contrary to the Kalut, the presence of dark-colored surfaces covered by volcanic
916 rocks in the interdunal areas in Rig-e Yalan and in the Central hammada decreases the chance
917 of finding meteorites. However, we have not done systematic work in these areas yet, but it
918 seems that searching by foot in these two areas is more fruitful (similar to the Atacama
919 Desert). Low abundance of terrestrial rocks in the sheet sand plains of the Rig-e Yalan makes
920 the search by car a better option.

921 ### 3.2. Laboratory Methods

922 Macroscopic observations are done both on the exterior and cut surface of the meteorites.
923 Polished thin and thick sections are prepared and a Leica DM2500P optical microscope is
924 used for petrographic observations.

925 Magnetic susceptibilities are measured on whole samples using KLY2 large coil from
926 Agico and SM150 from ZH instruments. Hysteresis properties for four selected samples were
927 measured with a Princeton Micromag vibrating sample magnetometer (VSM) with a noise
928 level of about 1 nAm^2 and a maximum applied field of 1 T. Hysteresis loops allow the
929 determination of coercivity (BC), saturation magnetization (MS), saturation remanent
930 magnetization (MRS), high-field susceptibility (cHF, including both diamagnetic and

paramagnetic contributions). Coercivity of remanence (BCR) was evaluated through DC back-field demagnetization of the saturation remanence. The magnetic measurements were conducted in CEREGE.

X-ray Diffraction (XRD) powder patterns obtained using the D8 Discover Bruker diffractometer equipped with Cu-Kα tube and nickel filter located at Pontifícia Universidade Católica (PUC), Rio de Janeiro. The data collected from 10 to 90° 2θ with step-size and scan rate of 0.02° and 2.5s/step, respectively. Refinement of the XRD data done using the Bruker TOPAS 4.2© program with the fundamental parameters approach. Up to 18 different phases were considered during the Rietveld modeling. The phases were considered stoichiometric or with constant composition.

Chemical compositions of the mineral phases were determined with CAMECA SXFive and SX100 electron microprobes at the CAMPARIS facility (Paris), using natural and synthetic standards, focused electron beam (~1 µm in diameter), an accelerating voltage of 15 kV and a beam current of 10 nA.

Between 80-100 mg of powdered sample used to measure loss on ignition (LOI) contents on selected meteorites. Samples were heated up to 110 °C, 550 °C, and 850 °C, for 30, 60, and 60 minutes, respectively. Sample weighting followed after a 10 minutes of putting in the desiccator.

The total carbon (TC), total nitrogen, total organic carbon (TOC) measured with a FISONS NA 1500 elemental analyzer (Carlo Erba NA-1500 Elemental Analyser) at CEREGE, as described in Pailler and Bard (2002) and Soulet et al. (2011). Selected meteorite samples were crushed, and homogenized in an agate ball mill. 10-20 mg of the powders loaded in aluminum cups. The TC, nitrogen and the TOC contents of each sample were determined in two separate analyses. We measured TOC after an acid removal of the carbonate fraction. Each TOC measurement was duplicated. In order to calculate the dry weight percentages of calcium carbonate, the following equation was applied: $CaCO_3 = (TC - TOC) \times 8.33$. In the course of the measurements, acetanilide (C_8H_9NO) was used as standard.

For major element analysis, the whole rock powders of selected meteorites digested by alkali fusion method using lithium tetraborate. The analysis carried out using an Ultima-C, Jobin Yvon, Horiba Induced Coupled Plasma–Atomic Emission Spectroscopy (ICP-AES) at CEREGE.

The trace element contents of the selected meteorite samples were determined by Inductively Coupled Plasma-Mass Spectrometry (ICP-MS; Perkin-Elmer NexION® 300x) at the Pisa University's Dipartimento di Scienze della Terra. About 50-100 mg of each whole rock powder dissolved in a mixture of HF and HNO_3 on a hot plate at ~120 °C inside screw-top perfluoroalkoxy (PFA) vessels. Then the sample solutions were spiked with Rh, Re and Bi as internal standards (20 ng ml^{-1} in the final solutions) and diluted to 50 mL in polypropylene flasks. In each step of sample preparation, Mill-Q® purified water (18.2 M cm), ultrapure HF and HNO_3 were used. The correction procedure included (1) blank subtraction, (2) instrumental drift correction using internal standardization and repeated (every 5 samples) analysis of a drift monitor, and (3) oxide-hydroxide interference correction. The geochemical reference samples with basaltic composition WS-E and PM-S, and the Allende chondrite reference sample (USNM 3529, splite 20, position 22) dissolved and analyzed along with the unknown samples to check the accuracy of the results.

Soil samples from three different locations in Kalut collected in order to analyze the trace element contents.

Terrestrial age measurement methodology here.

4. COLLECTED METEORITES

4.1. Classification

Classifications are based on optical microscopic observations, magnetic measurements, and chemical analyses of olivine and low-Ca pyroxene. Magnetic susceptibility (χ) is shown to be a useful proxy to differentiate various types of meteorites and/or to estimate weathering grade (Rochette et al. 2003a, 2008, 2009). It is expressed as the decimal logarithm of χ in 10^{-9} m^3/kg in order to account for the 5 order of magnitude variation in rocks. For strongly magnetic material ($\log \chi > 3$), χ is proportional to the amount of metal, magnetite, maghemite, cohenite, and schreibersite, i.e., minerals with practically equal specific χ. A combination of magnetic susceptibility data with microscopic observations is useful for meteorite classification. It is also applicable to check pairing. After random checking of olivine/pyroxene chemistry for different samples with identical petrographic and magnetic properties and obtaining similar coherent results, we did the classification of the paired samples by only using magnetic susceptibility data and petrographic observations.

The list of studied meteorites along with their classification parameters are reported in Table EA-1. So far, all of the collected and classified meteorites from the Lut are ordinary

chondrites (OCs). Fig. 3 shows the microscopic images of some of the collected meteorites. Here, we discuss two main meteorite types collected from the Lut (Fig. 4).

Amongst the Lut samples with approved names in the Meteoritical Bulletin (n=223), 191 of are H5 (mostly from Kerman DCA). In addition to these 191 samples, hundreds of additional probable H5 fragments have been recovered but not classified officially. These unclassified samples are not discussed here.

Microscopic petrography, magnetic susceptibility, and spatial distribution of the meteorites (section 4.2.) suggest that most of these Kerman H5 fragments are paired, which indicates the presence of an H5 strewnfield, formed by a single meteorite fall event.

Fig. 4a, b show the hand specimen images of the H5 paired samples. Under microscope, they have a chondritic texture with a recrystallized matrix (Fig. 3a,c). Chondrules are readily delineated. Plagioclase average size is less than 20 µm. Most of the H5 fragments contain chromite-plagioclase assemblages. Melt veins and melts pockets are present. Few troilite rim relicts occur around some chondrules. Metal and troilite are well separated from each other. Both metal and troilite are monocrystalline. The H5 fragments have an average $\log\chi = 4.60 \pm 0.12$ (n=187). The relatively narrow ranges of $\log\chi$ and plagioclase average size are strong indicators for pairing the H5 fragments.

The second most abundant meteorite type from Kerman DCA is L5 (Table EA-1; Fig. 3d-f and Fig. 4c,d). Similar to H5, these fragments are also likely paired which suggests another strewnfield. The L5 fragments show a very well-preserved chondritic texture. However, the complete separation of metal from troilite and average plagioclase size (<50 µm) show that they belong to petrologic type 5 (e.g., Van Schmus and Wood, 1967).

4.2. Meteorite Spatial Distribution

Meteorites have been collected in four DCAs defined in the Lut Desert. These DCAs, from highest to lowest number of the classified meteorites, include Kerman (n = 202), Lut (17), Gandom Beryan (n = 6), and Lut-e-Zangi Ahmad (n=2). (Table 1). Kerman DCA covers most of the Kalut, which as mentioned earlier has been the focus of the field work. Rig-e Yalan inside the Lut DCA is the second meteorite-rich region. The reason for the lesser number of meteorites from the central hammada is the dark lithology making it less attractive for meteorite hunting. Gandom Beryan DCA hosts the Gandom Beyran volcanic complex (Yousefi et al. 2017), is a well-known geotourism site which attracts the adventurers and leads to an increase in meteorite finding chance along their route.

Focusing on Kerman DCA and Kalut, Fig. 5a represents the spatial distribution of H5 and the other collected meteorites. H5 strewnfield is located in the northwestern part of the Kalut.

The H5 fragments are not spatially distributed as a function of mass (Fig. 5b). A strewnfield with no sorting indicates either a high angle meteorite fall or a post-impact disturbance caused by floods, which is unlikely in view of the dry climate of the region.

4.3.Terrestrial Ages

The terrestrial ages calculated from the ^{14}C activities measured in three selected samples are reported in Table 2. These samples were collected from Kalut and Rig-e Yalan. Although the number of the analyzed samples is very low, we note that they are in the range of 10-30 kyr. This is in the range of the values reported for meteorites from other hot deserts (Hezel et al. 2011; Jull et al. 2010; Welten et al. 2004) (except the Atacama Desert, Gattacceca et al., 2011).

5. SOIL COMPOSITION

The results of the analysis of the Lut soils samples are reported in Table 3. Normalizing our data and Oman soils samples (Al-Kathiri et al. 2005) to the mean upper continental crust (UCC) composition (Fig. 6) reveals the depletion of the majority of the elements. However, Sr in KS1, KS3, and Oman soils show a positive anomaly. This might be the result of higher carbonate content in soil. In general, Lut soils samples show a homogenous chemical composition. Except few elements such as Ni, Ga, and Rb, Oman and Lut soils are similar. A comparison of the Lut soils and UCC chemical composition with that of mean CI chondrites (Fig. 6) shows very similar geochemical behavior between the soils and UCC without any significant difference.

6. TERRESTRIAL WEATHERING EFFECTS

6.1. Mineralogy and Texture

6.1.1. Petrography

Following our results on the presence of two main meteorite populations (H5 and L5), we focus on their terrestrial weathering.

Lack of fusion crust, presence of a dark-brownish colored desert patina with attached sand grains, orange to brownish color of the broken or cut surfaces, cracks filled by desert sediments, the elevated number of small fragments (< 10 g), and the low number of metal and troilite grains, are common among the majority of the H5 samples (Fig. 3a,c and Fig. 4a,b). This points to the strong effect of terrestrial weathering on the texture and the mineralogy of these samples.

Microscopic survey of the H5 sections shows that in the majority of the meteorites (~80%) more than 60% of the metal/troilite grains are replaced by Fe oxides/oxyhydroxides (Table EA-1). Following the weathering scale of Wlotzka (1993), this corresponds to the weathering grade W3. Weathering products occur as both veins and pockets. W2 and W4 meteorites show similar abundances of 19%. Only one sample (Lut-e-Zangi Ahmad 001) with minor oxidation (W1) was observed which is from the Rig-e Yalan and based on petrographic differences such as the troilite shape and size, is not related to the H5 strewnfield of the Kalut.

The L5 fragments are less weathered than the H5 fragments. Most of them are fully or partly covered by a black fusion crust (Fig. 4c,d). Hygroscopic mineral products formed during the interaction of the meteorite with the water in the desert environment are visible as bulging spots on the exterior of the meteorites. Similar to the "sweating" behavior of Omani OCs described by (Zurfluh et al. 2013), the L5 fragments show crystallization of hygroscopic mineral assemblages in the cut surfaces.

Microscopically, the L5 samples are also less weathered than the H5 fragments, 82% of them being W2 (Table EA-1).

Comparison of the macroscopic and microscopic data of the L5 and H5 fragments, indicate a lower terrestrial weathering and lower terrestrial age for the L5.

6.1.1.1.Troilite weathering

In most samples, troilite has a higher modal abundance than metal, which indicates its higher resistance to weathering. Alteration of troilite to pyrite or marcasite is a ubiquitous and unique characteristics of meteorites from Lut, especially the Kalut H5 fragments. Usually in desert meteorites with progressive weathering, in reaction with water, troilite releases sulfur as sulfuric acid, and the whole rock sulfur budget of the system decreases (Bland et al. 2006; Saunier et al. 2010). Subsequently, Fe oxides/oxyhydroxides replace the troilite grains. Differently, troilite weathering in the Lut occurs in at least in two steps. First troilite turns into pyrite or marcasite, indicating the presence of extra sulfur and sulfuric acid (Hyde et al. 2014; Schoonen and Barnes 1991), and later to Fe oxides/oxyhydroxides. In addition to the Lut meteorites, during the routine classification of meteorites in CEREGE, we have observed rare cases of similar phenomenon in Oman OCs. Al-Kathiri et al. (2005) and Hyde et al. (2014) also mention alteration of troilite to pyrite and marcasite for Omani OCs and NWA 4872 brachinite, respectively.

1093 6.1.2. Magnetic properties

1094 Oxidation of metal in meteorites affects their magnetic properties (Munayco et al. 2013;
1095 Rochette et al. 2003b; Uehara et al. 2012). A decrease in the magnetic susceptibility compared
1096 to the average values for fresh and fall samples of each meteorite group is evident in the Lut
1097 meteorites. With an average logχ of 4.60 ± 0.12 (n=187) compared to the average value of
1098 5.31 ± 0.10 for H falls (Rochette et al., 2003), the paired H5 fragments clearly show the
1099 significant effect of weathering. The same effect also less intense, is observed for the paired
1100 L5 fragments. The average logχ for the L5 fragments is 4.37 ± 0.15 (n=11), which is lower
1101 than the fall L chondrites (4.90 ± 0.09) (Rochette et al., 2003).

1102 The hysteresis properties are presented in Table 4 and Fig. EA-3. Comparison with the data
1103 of Gattacceca et al. (2014) for fall OCs shows the mineralogical modification and the
1104 reshaping of the hysteresis loops, in particular a strong increase of remanence and parameters
1105 typical of fine grained (pseudo-single domain) cubic iron oxide (maghemite or magnetite).

1106 6.1.3. XRD data

1107 The modal mineralogy deduced from XRD analysis of a selection of 10 samples is reported
1108 in Table 5. Besides the usual primary minerals (olivine, pyroxene, anorthite, metal, troilite)
1109 found in OCs, the following weathering products were detected: hematite, maghemite,
1110 goethite, akaganéite, and magnetite. Fig. EA-4 shows the diffractograms of Kerman 003 and
1111 Lut 009 that represent the least and most oxidized meteorites analyzed in this work. The
1112 weathering degree estimated by means of XRD phase analysis reveals that total oxidation
1113 (sum of the modal abundances of the weathering products) for Lut samples ranges from 11 to
1114 27 wt% (or 42 to 78 at% Fe). Comparing the total oxide minerals abundance of the H and L
1115 chondrites from the Lut does not show any correlation between the group and the weathering
1116 of the meteorites. As shown in Fig. 7a, it seems that not only metal and troilite but also all Fe-
1117 bearing minerals including ferromagnesians are affected by weathering. A positive correlation
1118 exist between the abundance of maghemite and total oxides (Fig. 7b). More weathered
1119 samples show higher maghemite contents. A comparison between our data for Lut meteorites
1120 with meteorites from the San Juan DCA in the Atacama Desert (Munayco et al. 2013) shows
1121 differences between their oxidation products. Lut meteorites show higher oxides abundance
1122 and higher terrestrial alteration than those from San Juan. This is in agreement with the much
1123 wetter present day and past climate (over the Holocene) in Lut compared to the the Atacama
1124 Desert. Maghemite, goethite, and hematite are the dominant weathering phases in Lut sample,
1125 however, goethite is the dominant phase in the San Juan samples and hematite is absent. The

dominance of goethite in less weathered San Juan samples might be considered as a lower level of oxidation which is later followed by its transformation to hematite and later to maghemite (e.g., Stanjek 1987).

6.2. Geochemistry

6.2.1. Major and trace element composition

The whole rock major, minor, and trace element chemical composition of the selected samples along with two samples from Atacama (EM 049 and CeC 006) and one sample from Sahara Desert (Aridal 006) are reported in the Table 6. These 3 meteorites from other desert were chosen because of their high weathering grades (see Pourkhorsandi et al. 2017b). Chemical modification of the meteorites compared to the average composition of their corresponding chondrite groups is shown in Fig. 8.

Desert weathering has changed the chemical composition of the meteorites. Elements with higher abundance in the soil and relatively mobile behavior like Li, Sr, Mo, Ba, LREE, Tl, Th, and U are enriched in the meteorites. The higher contents of these elements in hot desert meteorites is reported by various workers (Al-Kathiri et al. 2005; Folco et al. 2007; Hezel et al. 2011; Pourkhorsandi et al. 2017b; Stelzner et al. 1999). A decrease in the contents of V, Cr, Co, Rb due to metal oxidation is detectable. In addition, Fe shows a possible depletion in the H chondrites. Some elements such as Cs and W show various behaviors. Possibly different contents of these elements in the underlying soil might be a reason for this observation.

6.2.2. Loss on ignition contents

Sequential LOI analysis is a common and widely used method to estimate the water content, organic matter, inorganic carbon and mineralogenic residue, in the terrestrial rock and sediment samples. Heating to different temperatures causes various phases to decompose which is usually reflected as the weight deviation from the initial mass (Heiri et al. 2001; Santisteban et al. 2004).

All meteorites (as well as Kilabo LL6 fall) lost 0.8% of their weight after heating up to 110 ºC (Fig. 9, Table EA-3). This temperature marks the removal of free water (moisture) from the samples. Record of the released organic carbon and combined water from hydroxyl iron minerals can be achieved by heating the sample up to 550 ºC. Except Kilabo, in average the hot desert samples loss down to 3.9% of the initial mass. Next step of heating (up to 850 ºC) leads to the decomposition of most carbonates and at the same time oxidation of iron (and troilite) to hematite which causes the weight increase and the color change in the samples. A weight loss is observed for the majority of Lut samples (e.g., Shahdad) which indicates the

presence of carbonates (especially calcite). In contrast, the weight increase after this heating step for samples like Kilabo, EM 049, Kerman 002, and Aridal 006 shows very low concentrations of carbonates in them.

6.2.3. Carbon and nitrogen contents

Decreasing TC content of the OCs resulting from parent body thermal metamorphism has been shown in different works (e.g., Moore and Lewis 1967). Terrestrial weathering is the other process known to be capable of changing TC, in this case as an increasing factor (Ash and Pillinger 1993; Gibson and Bogard 1978).

Indeed Lut meteorites have higher TC compared to falls (Fig. 10a, Table 7). Comparison of the TC, TOC, $CaCO_3$ contents show that the Lut samples are richer than those from the Atacama and Sahara deserts (Fig. 10b). TC shows a good correlation with the $CaCO_3$ content, which shows that $CaCO_3$ is more responsible than TOC for the higher TC content of these meteorites. In other way, it rules out the idea of higher TC in Lut samples because of a possible higher concentration of carbon in the unweathered samples.

Noteworthy is the strongly weathered (W4) Shahdad which shows the highest concentrations of these components as well as a abnormally high (0.104 wt%) nitrogen content. This might be related to the presence terrestrial nitrate minerals in it. Except Shahdad, the other samples show nitrogen abundances which are in the range of the values reported for other OCs (Kung and Clayton 1978).

To conclude, we observe an increase in the carbon contents (TC and TOC) of the Lut meteorites during terrestrial weathering due to formation of $CaCO_3$.

7. SUMMURY

In accordance with previous suggestions (Pourkhorsandi and Mirnejad 2013; Pourkhorsandi et al. 2016), our successful field works demonstrates the suitability of the Lut Desert, at least Kalut, for preservation and accumulation of meteorites.

So far, all of the collected meteorites from the Lut are OCs. Majority of the collected samples belong to two main strewnfields (H5 and L5) located in Kalut. Better preservation of the L5 meteorites compared to the H5 meteorites suggests a younger fall for the former. In the hypothesis that all H5 and L5 from these identified strewnfields represent only two unpaired meteorites and that the other finds are unpaired, the total of unpaired meteorites found in Lut would be 32.

Terrestrial weathering has modified the geochemistry and mineralogy of the Lut meteorites. Mobile elements such as Li, Sr, Mo, Ba, Tl, Th, and U are enriched in the analyzed samples. While a decrease in the V, Cr, Co, Rb (and possibly Fe) due to metal oxidation is detectable. The contents of TC and $CaCO_3$ are higher in these meteorites compared to the fall and find samples from other regions. The same relationship applies for the total abundance of oxides when comparing with San Juan (Atacama Desert) OCs. In comparison, the mineralogy of the weathering products shows differences as the dominance of maghemite, goethite, and hematite in the Lut OCs while goethite having the highest modal abundance in the San Juan (Munayco et al. 2013). The weathering of troilite to marcasite and pyrite is common in the Lut OCs while it is rare in the meteorites from other hot deserts. As suggested by Pourkhorsandi et al. (2016), the abundance of some trace elements such as Ba, Sr, and LREEs in Lut OCs are different from those from other hot deserts. These weathering effects, observed in the Lut OCs can be used as distinctive indicators to distinguish them from the meteorites from other regions of the Earth.

Although this is based on only three meteorites, the terrestrial ages are in the ranges reported for hot desert meteorites (expect for the Atacama Desert).

Our work is a preliminary work, assessing the high potential of the Lut in meteorite preservation, systematic works in the future will lead to the discovery of more samples.

Safety Advices

Drug smugglers are present in the Lut Desert. Beside this, the Iranian police has planted landmines in some regions of the desert to block smuggling ways.

It stands to reason that every field trip in the region, especially for foreign groups, should be done after obtaining proper permissions and guidance from the corresponding authorities.

Acknowledgments

This work has been partly supported by Center for International Scientific Studies & Collaboration (CISSC) and French Embassy in Tehran. First author thanks for a Ph.D. thesis grant devoted by the Cultural Office of the French Embassy in Tehran. We thank all the meteorite hunters who provided their time to collect and provide the samples for study. F. Demory, F. Rostek, H. Miche, and J.P. Lorand are thanked for their helps during the analysis. A. Rubin is thanked for providing Shahdad and Lut 001 thin sections and fragments. H.P.

thanks J. Hassanzadeh for fruitful discussions and guidance and M. Zadsaleh for providing the satellite images.

References

Adib D., and Liou J. G. 1979. The Naragh meteorite - A new olivine-bronzite chondrite fall. *Meteoritics* 14:257–272. http://adsabs.harvard.edu/abs/1979Metic..14..257A.

Aghanabati A. 2004. *Geology of Iran*, Tehran: Geological Survey of Iran.

Al-Kathiri A., Hofmann B. A., Jull A. J. T., and Gnos E. 2005. Weathering of meteorites from Oman : Correlation of chemical and mineralogical weathering proxies with 14 C terrestrial ages and the influence of soil chemistry. *Meteoritics & Planetary Science* 1239:1215–1239. http://onlinelibrary.wiley.com/doi/10.1111/j.1945-5100.2005.tb00185.x/abstract.

Ash R. D., and Pillinger C. T. 1993. Carbon in weathered ordinary chondrites from Roosevelt County. *Lunar and Planetary Science XXIV* 43–44.

Benedix G. K., Keil K., and Murakami J. Y. 1999. Classification of ten new Nullarbor Region meteorites. *Meteoritics & Planetary Science* 34:813–815.

Bevan A. W. R., and Binns R. A. 1989. Meteorites from the Nullarbor Region, Western Australia; I. A review of past recoveries and a procedure of naming new finds. *Meteoritics* 24:127–133.

BEVAN A. W. R. 1992. Australian meteorites. *Records of the Australian Museum, Supplement* 15:1–27.

Bischoff A. 2001. Meteorite classification and the definition of new chondrite classes as a result of successful meteorite search in hot and cold deserts. *Planetary and Space Science* 49:769–776. http://www.sciencedirect.com/science/article/pii/S0032063301000265 (Accessed October 23, 2015).

Biscoff A., and Geiger T. 1995. Meteorites from the Sahara:Find locations, shock classifications, degree of weathering and pairing. *Meteoritics & Planetary Science* 30:113–122. http://onlinelibrary.wiley.com/doi/10.1111/j.1945-5100.1995.tb01219.x/abstract.

1253 Bland P. A., Berry F. J., Smith T. B., Skinner S. J., and Pillinger C. T. 1996. The flux of
1254 meteorites to the earth and weathering in hot desert ordinary chondrite finds. *Geochimica*
1255 *et Cosmochimica Acta* 60:2053–2059.

1256 Bland P. a., Sexton a. S., Jull a. J. T., Bevan a. W. R., Berry F. J., Thornley D. M., Astin T.
1257 R., Britt D. T., and Pillinger C. T. 1998. Climate and rock weathering: A study of
1258 terrestrial age dated ordinary chondritic meteorites from hot desert regions. *Geochimica*
1259 *et Cosmochimica Acta* 62:3169–3184.
1260 http://www.sciencedirect.com/science/article/pii/S0016703798001999.

1261 Bland P. A., Zolensky M. E., Benedix G. K., and Sephton M. A. 2006. Weathering of
1262 chondritic meteorites. In *Meteorites and the Early Solar System II*. pp. 853–867
1263 http://www.lpi.usra.edu/books/MESSII/9041.pdf.

1264 Clarke R. S. 1975. The Meteoritical Bulletin. *Meteoritics* 10:133–158.
1265 http://doi.wiley.com/10.1111/j.1945-5100.1975.tb00018.x.

1266 Djamali M., Akhani H., Khoshravesh R., Ponel P., and Brewer S. 2011. Application of the
1267 Global Bioclimatic Classification to Iran: implications for understanding the modern
1268 vegetation and biogeography. *Ecologia Mediterranea* 37:91–114.

1269 Dresch J. 1968. Reconnaissance dans le Lut (Iran). *Bulletin de l'Association de géographes*
1270 *français* 45:143–153.

1271 Ehsani A. H., and Quiel F. 2008. Application of Self Organizing Map and SRTM data to
1272 characterize yardangs in the Lut desert, Iran. *Remote Sensing of Environment* 112:3284–
1273 3294.

1274 Folco L., D'Orazio M., and Perchiazzi N. 2007. Authenticating the recovery location of
1275 meteorites: The case of Castenaso. *Meteoritics & Planetary Science* 42:321–330.
1276 http://doi.wiley.com/10.1111/j.1945-5100.2007.tb00236.x.

1277 Garvie L. A. J. 2012. The Meteoritical Bulletin, No. 99, April 2012. *Meteoritics & Planetary*
1278 *Science* 47:E1–E52. http://doi.wiley.com/10.1111/maps.12026.

1279 Gattacceca J. et al. 2011. The densest meteorite collection area in hot deserts: The San Juan
1280 meteorite field (Atacama Desert, Chile). *Meteoritics and Planetary Science* 46:1276–
1281 1287. http://onlinelibrary.wiley.com/doi/10.1111/j.1945-5100.2011.01229.x/full.

1282 Gattacceca J., Suavet C., Rochette P., Weiss B. P., Winklhofer M., Uehara M., and Friedrich

J. M. 2014. Metal phases in ordinary chondrites: Magnetic hysteresis properties and implications for thermal history. *Meteoritics & Planetary Science* 49:652–676. http://doi.wiley.com/10.1111/maps.12268 (Accessed October 9, 2015).

Ghodsi M. 2017. Morphometric characteristics of Yardangs in the Lut Desert, Iran. *Desert* 22:21–29.

Gibson E. K. . J., and Bogard D. D. 1978. Chemical alterations of the Holbrook chondrite resulting from terrestrial weathering. *Meteoritics, vol. 13, Sept. 30, 1978, p. 277-289.* 13:277–289.

Gnos E., Lorenzetti S., Eugster O., Jull A. J. T., Hofmann B. A., Al-Khatiri A., and Eggimann M. 2009. The Jiddat al Harasis 073 strewn field, Sultanate of Oman. *Meteoritics & Planetary Science* 44:375–387. http://doi.wiley.com/10.1111/j.1945-5100.2009.tb00739.x.

Graham A. L., and Hassanzadeh J. 1990. The Meteoritical Bulletin. *Meteoritics* 25:59–63. http://doi.wiley.com/10.1111/j.1945-5100.1990.tb00971.x.

Harvey R. 2003. The Origin and Significance of Antarctic Meteorites. *Chemie der Erde - Geochemistry* 63:93–147.

Heiri O., Lotter A. F., and Lemcke G. 2001. Loss on ignition as a method for estimating organic and carbonate content in sediments: reproducibility and comparability of results. *Journal of Paleolimnology* 25:101–110. http://link.springer.com/10.1023/A:1008119611481.

Hezel D. C., Schlüter J., Kallweit H., Jull a. J. T., Al Fakeer O. Y., Al Shamsi M., and Strekopytov S. 2011. Meteorites from the United Arab Emirates: Description, weathering, and terrestrial ages. *Meteoritics and Planetary Science* 46:327–336. http://onlinelibrary.wiley.com/doi/10.1111/j.1945-5100.2010.01165.x/abstract.

Hutzler A. et al. 2016. Description of a very dense meteorite collection area in western Atacama: Insight into the long-term composition of the meteorite flux to Earth. *Meteoritics & Planetary Science* n/a-n/a. http://doi.wiley.com/10.1111/maps.12607.

Hyde B. C., Day J. M. D., Tait K. T., Ash R. D., Holdsworth D. W., and Moser D. E. 2014. Characterization of weathering and heterogeneous mineral phase distribution in brachinite Northwest Africa 4872. *Meteoritics & Planetary Science* 49:1141–1156.

http://doi.wiley.com/10.1111/maps.12320.

Jull a. J. T., Mchargue L. R., Bland P. a., Greenwood R. C., Bevan A. W. R., Kim K. J., Lamotta S. E., and Johnson J. a. 2010. Terrestrial ages of meteorites from the Nullarbor region, Australia, based on 14C and 14C-10Be measurements. *Meteoritics and Planetary Science* 45:1271–1283. http://onlinelibrary.wiley.com/doi/10.1111/j.1945-5100.2010.01289.x/full.

Kemp A. I. S., and Hawkesworth C. J. 2004. Granites and differentiation of the continental crust. *Geochimica et Cosmochimica Acta* 68:A667–A667.

Kent J. J., Brandon A. D., Joy K. H., Peslier A. H., Lapen T. J., Irving A. J., and Coleff D. M. 2017. Mineralogy and petrogenesis of lunar magnesian granulitic meteorite Northwest Africa 5744. *Meteoritics & Planetary Science* 52:1916–1940. http://doi.wiley.com/10.1111/maps.12898.

Kring D., Jull A., McHargue L., Bland P., Hill D., and Berry F. 2001. Gold basin meteorite strewn field, Mojave Desert, northwestern Arizona: Relic of a small late pleistocene impact event. http://oro.open.ac.uk/5771/.

Kung C.-C., and Clayton R. N. 1978. Nitrogen abundances and isotopic compositions in stony meteorites. *Earth and Planetary Science Letters* 38:421–435. http://linkinghub.elsevier.com/retrieve/pii/0012821X78901176.

Lee M. R., and Bland P. a. 2003. Dating climatic change in hot deserts using desert varnish on meteorite finds. *Earth and Planetary Science Letters* 206:187–198.

Mashhadi N., Alavipanah S. K., and Ahmadi H. 2002. Geomorphology studies of Lout yardangs. *Desert (Biaban)* 7:25–43.

Mildrexler D. J., Zhao M., and Running S. W. 2006. Where are the hottest spots on Earth? *Eos, Transactions American Geophysical Union* 87:461–467. http://doi.wiley.com/10.1029/2006EO430002 (Accessed October 21, 2015).

Moore C. B., and Lewis C. F. 1967. Total carbon content of ordinary chondrites. *Journal of Geophysical Research* 72:6289.

Motamed A. 1974. Goegraphy and climate of Lut Iran.pdf. *Geographical Research Quaterley* 11:3–13. http://www.noormags.ir/view/en/articlepage/336794/.

Munayco P., Munayco J., de Avillez R. R., Valenzuela M., Rochette P., Gattacceca J., and Scorzelli R. B. 2013. Weathering of ordinary chondrites from the Atacama Desert, Chile, by Mössbauer spectroscopy and synchrotron radiation X-ray diffraction. *Meteoritics & Planetary Science* 48:457–473. http://doi.wiley.com/10.1111/maps.12067.

Muñoz C., Guerra N., Martínez-Frías J., Lunar R., and Cerda J. 2007. The Atacama Desert: A preferential arid region for the recovery of meteorites-Find location features and strewnfield distribution patterns. *Journal of Arid Environments* 71:188–200.

Ouazaa N. L., Perchiazzi N., Kassaa S., Ghanmi M., and Folco L. 2009. Meteorite finds from southern Tunisia. *Meteoritics & Planetary Science* 44:955–960.

Pailler D., and Bard E. 2002. High frequency palaeoceanographic changes during the past 140 000 yr recorded by the organic matter in sediments of the Iberian Margin. *Palaeogeography, Palaeoclimatology, Palaeoecology* 181:431–452. http://linkinghub.elsevier.com/retrieve/pii/S0031018201004448.

Pourkhorsandi H., and Mirnejad H. 2013. Lut Desert (Iran): A High-Potential Area for Finding Meteorites. In *44th Lunar and Planetary Science Conference* http://adsabs.harvard.edu/abs/2013LPI....44.1096P (Accessed July 1, 2015).

Pourkhorsandi H., Mirnejad H., Rochette P., and Hassanzadeh J. 2016. Lut 009, an H4 (S2, W4) ordinary chondrite meteorite from Lut Desert of Iran. *Journal of the Earth and Space Physics* 41:125–130. https://jesphys.ut.ac.ir/article_55100_7213.html.

Pourkhorsandi H., Gattacceca J., Devouard B., D'Orazio M., Rochette P., Beck P., Sonzogni C., and Valenzuela M. 2017a. The ungrouped chondrite El Médano 301 and its comparison with other reduced ordinary chondrites. *Geochimica et Cosmochimica Acta* 218:98–113. http://linkinghub.elsevier.com/retrieve/pii/S0016703717305689.

Pourkhorsandi H., D'Orazio M., Rochette P., Valenzuela M., Gattacceca J., Mirnejad H., Sutter B., Hutzler A., and Aboulahris M. 2017b. Modification of REE distribution of ordinary chondrites from Atacama (Chile) and Lut (Iran) hot deserts: Insights into the chemical weathering of meteorites. *Meteoritics & Planetary Science*. http://doi.wiley.com/10.1111/maps.12894.

Rochette P., Sagnotti L., Bourot-Denise M., Consolmagno G., Folco L., Gattacceca J., Osete M. L., and Pesonen L. 2003a. Magnetic classification of stony meteorites: 1. Ordinary chondrites. *Meteoritics & Planetary Science* 38:251–268.

1373 http://doi.wiley.com/10.1111/j.1945-5100.2003.tb00263.x.

1374 Rochette P., Sagnotti L., Bourot-Denise M., Consolmagno G., Folco L., Gattacceca J., Osete
1375 M. L., and Pesonen L. 2003b. Magnetic classification of stony meteorites: 1. Ordinary
1376 chondrites. *Meteoritics & Planetary Science* 38:251–268.
1377 http://doi.wiley.com/10.1111/j.1945-5100.2003.tb00263.x (Accessed October 4, 2015).

1378 Rochette P. et al. 2008. Magnetic classification of stony meteorites: 2. Non-ordinary
1379 chondrites. *Meteoritics & Planetary Science* 43:959–980.
1380 http://doi.wiley.com/10.1111/j.1945-5100.2008.tb01092.x.

1381 Rochette P., Gattacceca J., Bourot-Denise M., Consolmagno G., Folco L., Kohout T., Pesonen
1382 L., and Sagnotti L. 2009. Magnetic classification of stony meteorites: 3. Achondrites.
1383 *Meteoritics & Planetary Science* 44:405–427. http://doi.wiley.com/10.1111/j.1945-
1384 5100.2009.tb00741.x.

1385 Rubin A. e., Verish R. s., Moore C. b., and Oriti R. a. 2000. Numerous unpaired meteorites
1386 exposed on a deflating playa lake at Lucerne Valley, California. *Meteoritics & Planetary*
1387 *Science* 35:A181–A183. http://doi.wiley.com/10.1111/j.1945-5100.2000.tb01793.x.

1388 Rudnick R. L., and Gao S. 2003. Composition of the Continental Crust. In *Treatise on*
1389 *Geochemistry*. Elsevier. pp. 1–64
1390 http://linkinghub.elsevier.com/retrieve/pii/B0080437516030164.

1391 Santisteban J. I., Mediavilla R., López-Pamo E., Dabrio C. J., Blanca Ruiz Zapata M., José
1392 Gil García M., Castaño S., and Martínez-Alfaro P. E. 2004. Loss on ignition: a
1393 qualitative or quantitative method for organic matter and carbonate mineral content in
1394 sediments? *Journal of Paleolimnology* 32:287–299.
1395 http://link.springer.com/10.1023/B:JOPL.0000042999.30131.5b.

1396 Saunier G., Poitrasson F., Moine B., Gregoire M., and Seddiki A. 2010. Effect of hot desert
1397 weathering on the bulk-rock iron isotope composition of L6 and H5 ordinary chondrites.
1398 *Meteoritics and Planetary Science* 45:195–209.
1399 onlinelibrary.wiley.com/doi/10.1111/j.1945-5100.2010.01017.x/full.

1400 Schlüter J., Schultz L., Thiedig F., Al-Mahdi B. O., and Aghreb a. E. a. 2002. The Dar al
1401 Gani meteorite field (Libyan Sahara): Geological setting, pairing of meteorites, and
1402 recovery density. *Meteoritics* 37:1079–1093.

1403 Van Schmus W. R., and Wood J. A. 1967. A chemical-petrologic classification for the
1404 chondritic meteorites. *Geochimica et Cosmochimica Acta* 31:747–765.
1405 http://www.sciencedirect.com/science/article/pii/S0016703767800309 (Accessed July 1,
1406 2015).

1407 Schoonen M. a. a., and Barnes H. L. 1991. Reactions forming pyrite and marcasite from
1408 solution: II. Via FeS precursors below 100°C. *Geochimica et Cosmochimica Acta*
1409 55:1505–1514.

1410 Soulet G., Ménot G., Garreta V., Rostek F., Zaragosi S., Lericolais G., and Bard E. 2011.
1411 Black Sea "Lake" reservoir age evolution since the Last Glacial — Hydrologic and
1412 climatic implications. *Earth and Planetary Science Letters* 308:245–258.
1413 http://linkinghub.elsevier.com/retrieve/pii/S0012821X11003505.

1414 Stanjek H. 1987. The formation of maghemite and hematite from lepidocrocite and goethite in
1415 a Cambisol from Corsica, France. *Zeitschrift für Pflanzenernährung und Bodenkunde*
1416 150:314–318. http://doi.wiley.com/10.1002/jpln.19871500509.

1417 Stelzner T. et al. 1999. An interdisciplinary study of weathering effects in ordinary chondrites
1418 from the Acfer region, Algeria. *Meteorit. Planet. Sci.* 34:787–794.

1419 Uehara M., Gattacceca J., Rochette P., Demory F., and Valenzuela E. M. 2012. Magnetic
1420 study of meteorites recovered in the Atacama desert (Chile): Implications for meteorite
1421 paleomagnetism and the stability of hot desert surfaces. *Physics of the Earth and*
1422 *Planetary Interiors* 200–201:113–123. http://dx.doi.org/10.1016/j.pepi.2012.04.007.

1423 Ward H. A. 1901. Veramin Meteorite. *American Journal of Science* s4-12:453–459.
1424 http://www.ajsonline.org/cgi/doi/10.2475/ajs.s4-12.72.453.

1425 Wasson J. T., and Kallemeyn G. W. 1988. Compositions of Chondrites. *Philosophical*
1426 *Transactions of the Royal Society A: Mathematical, Physical and Engineering Sciences*
1427 325:535–544. http://rsta.royalsocietypublishing.org/content/325/1587/535 (Accessed
1428 July 3, 2015).

1429 Welten K. C., Nishiizumi K., Finkel R. C., Hillegonds D. J., Jull A. J. T., Franke L., and
1430 Schultz L. 2004. Exposure history and terrestrial ages of ordinary chondrites from the
1431 Dar al Gani region, Libya. *Meteoritics & Planetary Science* 39:481–498.
1432 http://doi.wiley.com/10.1111/j.1945-5100.2004.tb00106.x.

Wlotzka F. 1993. A weathering scale for the ordinary chondrites. *Meteoritics* 28:460.

Yousefi S. J., Moradian A., and Ahmadipour H. 2017. Petrogenesis of Plio-Quaternary basanites in the Gandom Beryan area, Kerman,Iran: geochemical evidence for the low-degree partial melting of enriched mantle. *Turkish Journal of Earth Sciences* 26:284–301. http://online.journals.tubitak.gov.tr/openDoiPdf.htm?mKodu=yer-1610-22.

Zolensky M. E., Wells G. L., and Rendell H. M. 1990. The accumulation rate of meteorite falls at the earth's surface - The view from Roosevelt County, New Mexico.

Zurfluh F. J., Hofmann B. a., Gnos E., and Eggenberger U. 2013. "Sweating meteorites"-Water-soluble salts and temperature variation in ordinary chondrites and soil from the hot desert of Oman. *Meteoritics and Planetary Science* 48:1958–1980. http://onlinelibrary.wiley.com/doi/10.1111/maps.12211/abstract.

Zurfluh F. J., Hofmann B. A., Gnos E., Eggenberger U., and Jull A. J. T. 2016. Weathering of ordinary chondrites from Oman: Correlation of weathering parameters with ^{14}C terrestrial ages and a refined weathering scale. *Meteoritics & Planetary Science* 51:1685–1700. http://doi.wiley.com/10.1111/maps.12690 (Accessed February 10, 2017).

Figure captions:

Fig. 1: a) Map of the Central Lut Desert; adapted from Pourkhorsandi et al. (2017b). Circles on the Iran map show the location of Yazd, Abarkouh, and Sarvestan meteorites, respectively from north to south. b) Landsat 8 satellite image of the Central Lut Desert and the surrounding areas. Dashed quadrangles show the position of Kerman (west) and Lut (east) DCAs.

Fig. 2: a) Climate diagram of Ziaratgah-Deh-Seyf weather station near Shahdad. Note that the dry season (P<2T) lasts for 12 months. Data from Iran Meteorological Organization. b) One and half a year record of near ground surface variations in temperature and relative humidity. Data collected using a Lascar EL-USB-2 data logger with 1-hour interval records.

Fig. 3: Representative microscopic images of the Lut Desert meteorite in reflected optical light. a) Kerman 046 (H5, W3). b) Lut 010 (LL6, W2-4). c) Kerman 034 (H5, W1-3). d) Kerman 141 (L5, W1/2). e) Kerman 135 (L5, W2). f) Kerman 139 (L5, W2).

Fig. 4: Hand specimen images of the paired H5 (a, b) and L5 fragments (c, d). The longest dimension of the H5 (a) is 12 cm. Scale bar is 1 × 1 cm.

Fig. 5: a) Spatial distribution map of the Kerman DCA meteorites showing the paired H5 and other chondrites. b) Location and the mass of the H5 paired fragments collected from Kalut.

Fig. 6: Bulk geochemistry of Kalut soil samples (KS1-KS3) and soils from Oman (Al-Kathiri et al. 2005) normalized to upper continental crust composition (Kemp and Hawkesworth 2004; Rudnick and Gao 2003). The upper right diagrams shows the Kalut soils (black) and UCC (grey) normalized to mean CI chondrites (Wasson and Kallemeyn 1988).

Fig. 7: a) Comparison of the total oxides (wt%) versus silicates in Lut and San Juan (Atacama Desert) meteorites. b) Total oxides versus maghemite contents in the Lut meteorites. Data obtained by XRD. San Juan data from (Munayco et al. 2013).

Fig. 8: Normalized spider diagrams of (a) H, and (b) L(LL) OCs from the Lut and Atacama Desert. Strontium, Ba, and the REE composition data source: Pourkhorsandi et al. (2017b). The normalization data source: Wasson and Kallemeyn (1988).

Fig. 9: Plotted data of sequential combustion showing mass differences as a function of heat.

Fig. 10: a) Comparison of total carbon contents of find and fall petrologic type >3 OCs with Lut meteorites. Data source of the non-Lut samples: Moore and Lewis (1967). b) Total carbon versus carbonate content of the Lut OCs compared to three samples from the Atacama (CeC 006 and EM 049) and Sahara (Aridal 006) deserts.

Table headings:

Table 1: Statistics of meteorite types and frequency in different DCAs from the Lut Desert.

Table 2: The calculated terrestrial ages of three selected Lut meteorites based on their ^{14}C activities.

Table 3: Trace element chemical composition of three soil samples (KS1-3) from the Kalut region of the Lut Desert and two reference materials (BHVO-1, BHVO-2) analyzed by ICP-MS.

Table 4: Magnetic properties of selected ordinary chondrites from the Lut Desert.

Table 5: Phase modal abundances of selected ordinary chondrites from the Lut Desert obtained by XRD analysis.

Table 6: Whole rock major, minor, and trace element chemical composition of selected Lut Desert OCs along with two from Atacama (EM 049 and CeC 006) and one sample from the Sahara Desert (Aridal 006).

1494 **Table 7:** Total carbon, total nitrogen, total organic carbon, and $CaCO_3$ contents of analyzed
1495 samples.

1496

1497 **Electronic annexes:**

1498 **Fig. EA-1:** Topographic map of Lut and surrounding regions.

1499 **Fig. EA-2:** Aerial photo of Kalut. Credit: xxx.

1500 **Fig. EA-3:** Hysteresis loops of the Lut meteorites.

1501 **Fig. EA-4:** Diffractograms of two Lut meteorites.

1502 **Table EA-1:** List of the classified meteorites in this study.

1503

Tables:

Table 1 (Pourkhorsandi et al.)

	Meteorite Type										
DCA name	H3	H4	H5	H6	L3	L4	L5	L6	LL3	LL6	**Total meteorite number**
Kerman	1	0	183	1	0	0	12	4	0	1	202
Lut	1	4	4	0	1	1	0	2	3	1	17
Gandom Beryan	0	1	5	0	0	0	0	0	0	0	6
Lut-e-Zangi Ahmad	0	0	1	0	1	0	0	0	0	0	2
											Σ = 227

Table 2 (Pourkhorsandi et al.)

Meteorite	**^{14}C total**	**^{14}C (dpm/kg)**	**Terrestrial Age (kyr)**
Kerman 001	3.502E+06	8.16 ± 0.71	14.4 ± 1.5
Lut 006	5.940E+06	5.87 ± 0.30	18.5 ± 1.4
Lut 010	1.523E+06	1.70 ± 0.33	28.8 ± 2.1

1509 Table 3 (Pourkhorsandi et al.)

ppm	**KS1**	**KS2**	**KS3**	**BHVO-1**	**BHVO-2**
Cr	51.2	80.1	60.8	295.2	284.3
Co	7.4	10.2	7.8	46.2	45.1
Ni	19.4	36.3	21.8	125.8	121.8
Cu	14.0	20.6	14.8	129.9	128.4
Zn	44.0	57.8	46.6	96.6	94.1
Ga	9.8	12.5	10.0	21.5	20.4
Ge	1.0	1.0	0.8	1.4	1.4
Rb	56.0	61.0	56.0	8.4	7.9
Sr	687.0	201.3	647.2	360.4	356.1
Y	13.3	16.2	12.5	23.6	23.5
Zr	284.4	152.9	128.5	154.1	153.6
Nb	8.6	8.2	7.8	16.1	16.0
Ba	561.9	331.7	483.0	126.1	126.4
La	18.8	22.4	18.9	15.5	15.6
Ce	35.7	43.5	36.8	37.2	37.6
Pr	4.0	5.0	4.1	5.1	5.2
Nd	15.3	18.2	14.9	23.6	24.0
Sm	3.3	3.8	2.9	5.8	5.9
Eu	0.8	0.8	0.7	2.0	2.0
Gd	2.9	3.6	2.9	6.3	6.4
Tb	0.4	0.5	0.4	0.9	0.9
Dy	2.4	3.1	2.4	5.2	5.3
Ho	0.5	0.6	0.5	1.0	1.0
Er	1.5	1.7	1.4	2.4	2.6
Tm	0.2	0.3	0.2	0.3	0.3
Yb	1.5	1.8	1.4	2.0	1.9
Lu	0.3	0.3	0.2	0.3	0.4
Hf	6.9	4.2	3.5	4.2	4.4
Ta	0.7	0.7	0.7	1.2	1.2
Pb	14.2	11.5	13.2	1.3	1.4
Th	6.2	7.1	7.2	1.2	1.3
U	2.0	2.2	2.0	0.4	0.5

1510

1511 Table 4 (Pourkhorsandi et al.)

Meteorite	**Ms (Am^2/kg)**	**Bc (mT)**	**Bcr (mT)**	**Mrs/Ms**	**Bcr/Bc**
Kerman001	5.528	11.63	24.6	.16	2.12
Kerman002	2.958	10.28	24.47	.12	2.38

Kerman003	2.435	15.77	26.79	2.77E-01	1.70
Lut001	3.613	14.78	27.35	2.38E-01	1.85
Lut003	5.066	13.35	24.33	2.46E-01	1.82

1512

1513 Table 5 (Pourkhorsandi et al.)

Meteorite	Type	Silicates			Opaques		Iron oxides				
		Olivine	Pyroxene	Anorthite	FeNi metal	Troilite	Goethite	Hematite	Maghemite	Magnetite	Akaganéite
Kerman 001	H5	42.36	40.09	1.75	0.00	3.10	5.60	0.00	7.11	0.00	0.00
Kerman 002	L6	49.5	33.75	3.26	0.00	0.94	1.61	2.61	8.33	0.00	0.00
Kerman 003	L5	47.64	33.58	6.1	0.00	1.93	5.07	2.19	3.49	0.00	0.00
Lut 001	H5	37.79	37.82	7.11	0.00	1.31	7.27	0.00	8.71	0.00	0.00
Lut 003	L3	35.11	32.35	6.59	0.00	1.14	8.25	1.66	14.91	0.00	0.00
Lut 006	LL3	55.33	11.45	8.38	0.11	0.08	5.08	1.71	13.21	1.15	3.51
Lut 008	H4	35.82	32.68	5.48	0.00	1.95	6.20	7.05	10.82	0.00	0.00
Lut 009	H4	41.17	21.34	10.04	0.00	0.26	8.35	0.51	18.33	0.00	0.00
Shahdad	H5	37.42	29.86	8.62	0.00	2.48	8.58	1.63	11.41	0.00	0.00

1514

1515 Table 6 (Pourkhorsandi et al.)

	Kerman 001	Kerman 002	Kerman 003	Lut 001	Lut 003	Lut 006	Lut 008	Lut 009	Shahdad	Aridal 006	CeC 006	EM 049	Killabo
SiO_2	32.98	38.90	36.46	37.76	35.77	43.24	34.33	35.22	32.12	36.33	34.94	34.63	40.30
TiO_2	0.11	0.12	0.12	0.11	0.11	0.12	0.11	0.10	0.10	0.11	0.12	0.11	0.12
Al_2O_3	2.00	2.19	2.14	2.12	1.98	2.27	2.02	1.95	1.86	2.05	2.21	2.05	2.36

Fe_2O_3	33.19	29.40	34.35	29.48	37.45	25.14	38.00	32.86	35.35	31.89	32.71	39.06	29.89
MnO	0.30	0.36	0.32	0.34	0.30	0.38	0.30	0.31	0.28	0.34	0.35	0.32	0.38
MgO	23.42	27.19	23.96	25.85	23.87	25.71	20.38	22.65	21.75	25.88	22.85	22.98	30.13
CaO	1.73	1.87	1.86	1.31	1.88	1.83	1.43	1.36	1.50	1.54	1.51	1.56	1.81
Na_2O	0.87	0.92	1.04	0.89	0.91	1.05	0.88	0.85	0.87	0.45	0.62	0.52	0.99
K_2O	0.11	0.10	0.11	0.11	0.13	0.19	0.12	0.10	0.10	0.09	0.14	0.14	0.11
P_2O_5	0.25	0.26	0.24	0.18	0.27	0.21	0.26	0.18	0.22	0.27	0.19	0.28	0.29
Li	4.60	1.99	2.30	4.50	8.80	8.20	2.25	3.90	5.20	1.93	13.00	6.10	n.d.
Be	0.04	0.04	0.03	0.03	0.04	0.04	0.03	0.03	0.03	0.03	0.10	0.08	n.d.
Rb	2.02	2.84	1.52	2.33	1.93	3.10	2.27	1.04	2.31	1.59	5.26	3.32	n.d.
Y	2.14	2.23	2.20	1.68	1.90	2.31	1.95	1.89	1.87	1.60	2.81	2.91	n.d.
Zr	5.4	5.3	5.6	5.6	4.9	7.6	4.8	5.2	5.1	5.2	5.8	5.5	n.d.
Nb	0.46	0.42	0.44	0.46	0.44	0.46	0.39	0.47	0.42	0.47	0.47	0.44	n.d.
Th	0.07	0.07	0.09	0.22	0.07	0.15	0.06	0.10	0.21	0.09	0.19	0.15	n.d.
Pb	0.57	1.08	0.27	0.30	0.55	0.37	0.36	0.36	0.55	0.17	0.43	0.33	n.d.
Ga	4.9	4.7	4.3	5.0	5.2	4.6	4.7	2.9	4.0	4.5	4.8	4.6	n.d.
Zn	40	59	43	41	47	59	42	49	18	37	57	29	n.d.
Cu	88	80	98	92	93	73	112	79	77	76	99	96	n.d.
Ni	14715	10821	11440	14082	14117	5919	14183	11742	14063	11259	10782	13843	n.d.

V	51	55	45	61	55	75	52	59	49	43	114	61	n.d.
Cr	2167	2389	1821	2660	2666	3774	2269	2808	2128	1455	3135	2359	n.d.
Hf	0.16	0.15	0.15	0.16	0.14	0.22	0.13	0.14	0.15	0.16	0.16	0.16	n.d.
Cs	0.29	0.21	0.03	0.04	0.15	0.21	0.39	0.18	0.18	0.04	0.37	0.88	n.d.
Sc	7.7	7.0	8.8	9.4	7.7	9.0	7.8	8.0	8.2	8.3	8.1	9.2	n.d.
Ta	0.02	0.03	0.02	0.03	0.02	0.03	0.02	0.03	0.03	0.03	0.03	0.03	n.d.
Co	600	523	567	455	667	255	628	507	674	396	494	734	n.d.
U	0.10	0.07	0.06	0.07	0.09	0.38	0.04	0.28	0.18	0.04	0.27	0.10	n.d.
W	0.07	0.13	0.19	0.06	0.49	0.02	0.29	0.22	0.16	0.07	0.81	0.19	n.d.
Mo	5.2	4.0	4.2	5.1	9.3	3.5	5.0	5.8	5.3	4.4	4.6	6.7	n.d.
Tl	0.37	< 0.01	< 0.01	0.14	0.18	0.17	0.03	0.14	0.29	< 0.01	0.27	0.13	n.d.

1516 n.d. = not determined.

1517 The units for the major and trace elements is wt% and µg g^{-1}, respectively.

1518 Table 7 (Pourkhorsandi et al.)

Meteorite	Type	Weathering grade	N	TC	TOC	$CaCO_3$
Kerman 001	H4	W4	0.011	0.328	n.d.	n.d.
Kerman 002	L6	W3	0.002	0.072	0.042	0.249
Kerman 003	L5	W2	0.003	0.132	0.066	0.548
Lut 001	H5	W3	b.d.l.	0.187	0.088	0.831
Lut 003	L3	W3	0.002	0.221	0.066	0.548
Lut 006	LL3	W3	0.003	0.124	n.d.	n.d.
Lut 008	H4	W5	b.d.l.	0.126	0.064	0.515
Lut 009	H4	W4	0.009	0.114	0.086	0.233
Shahdad	H5	W4	0.104	0.245	0.074	1.424
Aridal 006	H6	W4	0.006	0.073	0.051	0.181
Caleta el Cobre 006	L6	W3	0.009	0.067	0.051	0.135
El Medano 049	H4	W3	0.014	0.084	0.040	0.367

1519 The unit is wt%. n.d. = not determined. b.d.l. = below detection limit.

1520

1521

1522

1523

1524

1525

1526

1527

1528

1529

Figures:

Fig. 1:

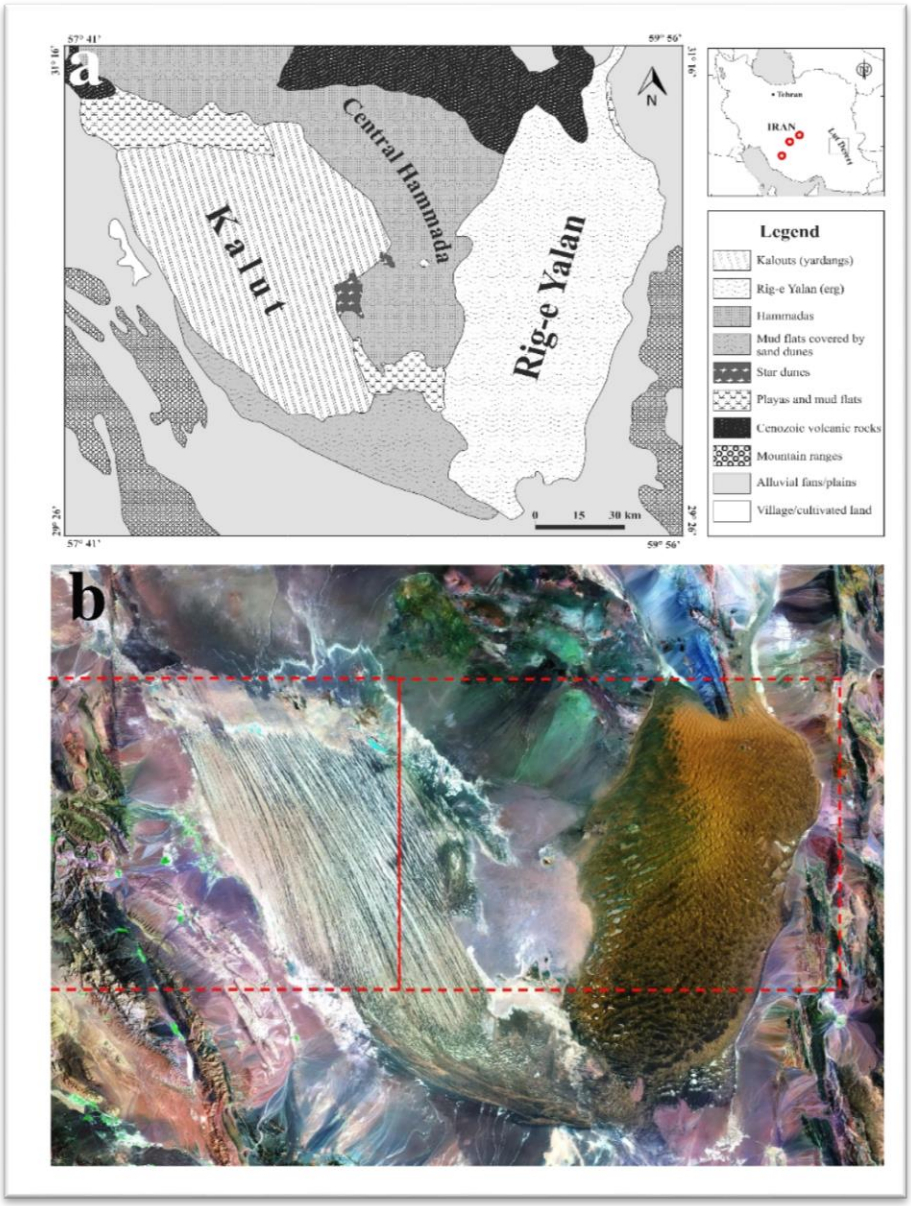

Fig. 2:

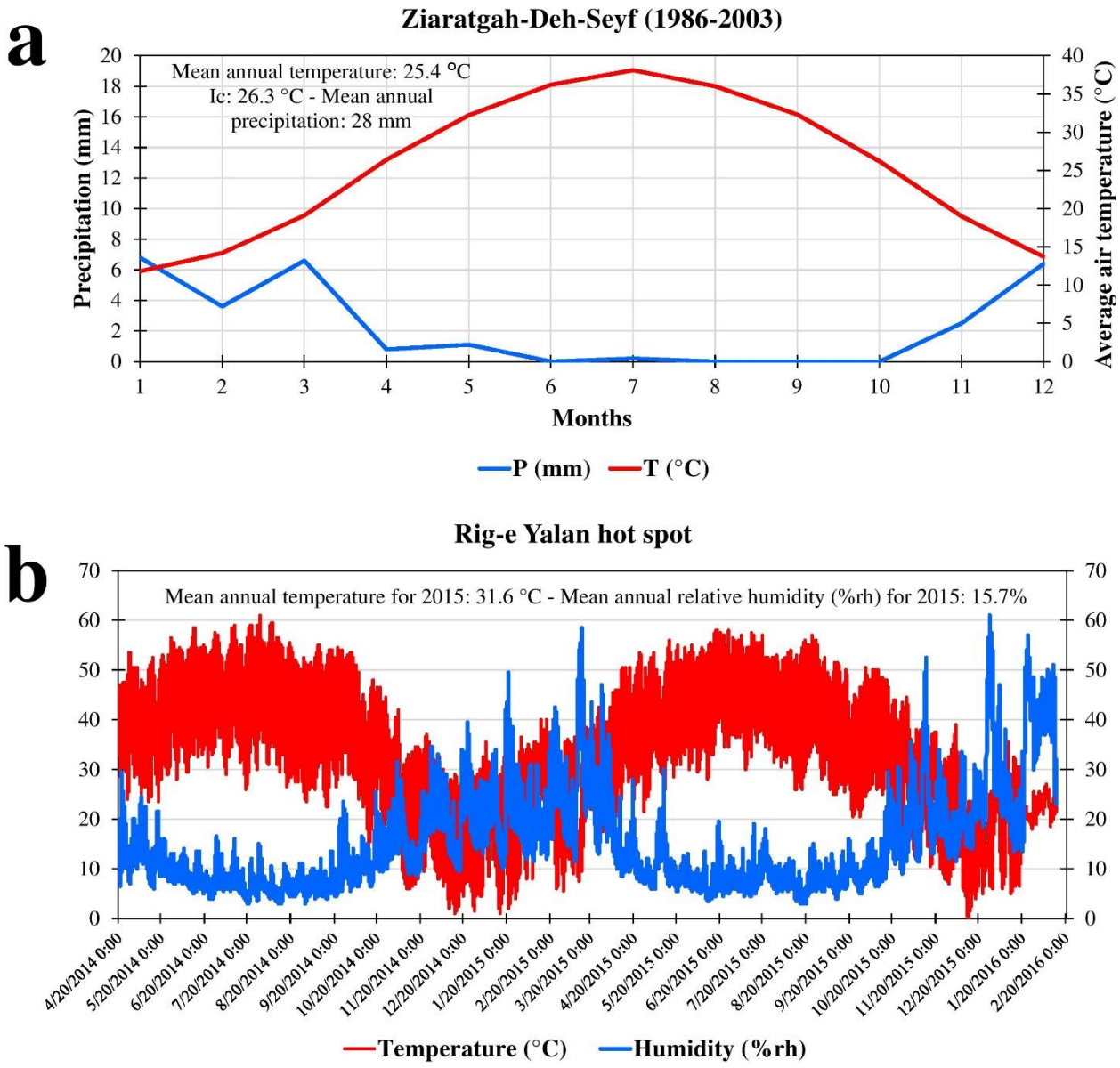
a
Ziaratgah-Deh-Seyf (1986-2003)
Mean annual temperature: 25.4 °C
Ic: 26.3 °C - Mean annual precipitation: 28 mm
Precipitation (mm)
Average air temperature (°C)
Months
P (mm)
T (°C)
b
Rig-e Yalan hot spot
Mean annual temperature for 2015: 31.6 °C - Mean annual relative humidity (%rh) for 2015: 15.7%
Temperature (°C)
Humidity (%rh)

1545 **Fig. 3:**

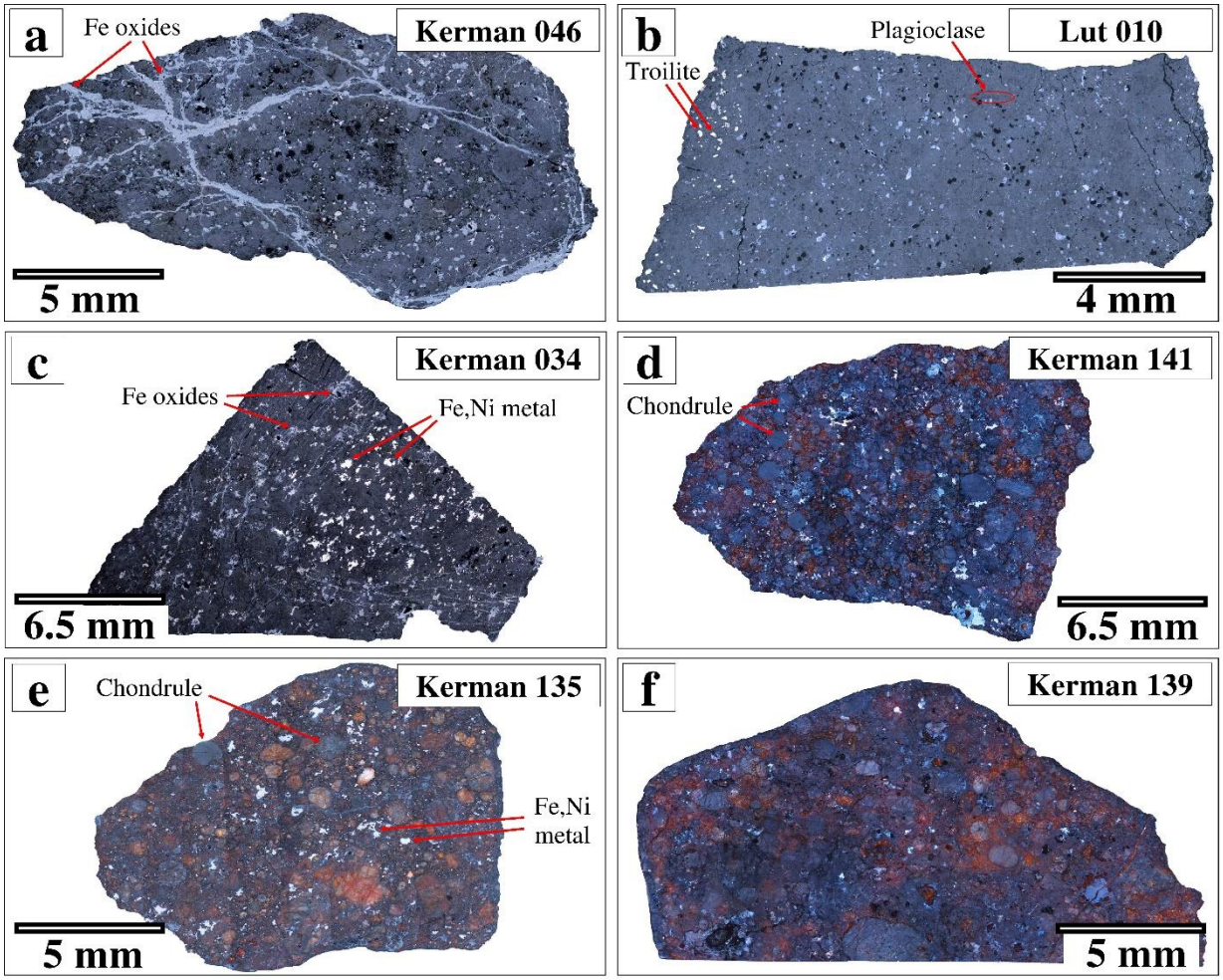

1546

1547

1548

1549

1550

1551

1552

1553

Fig. 4:

Fig. 5:

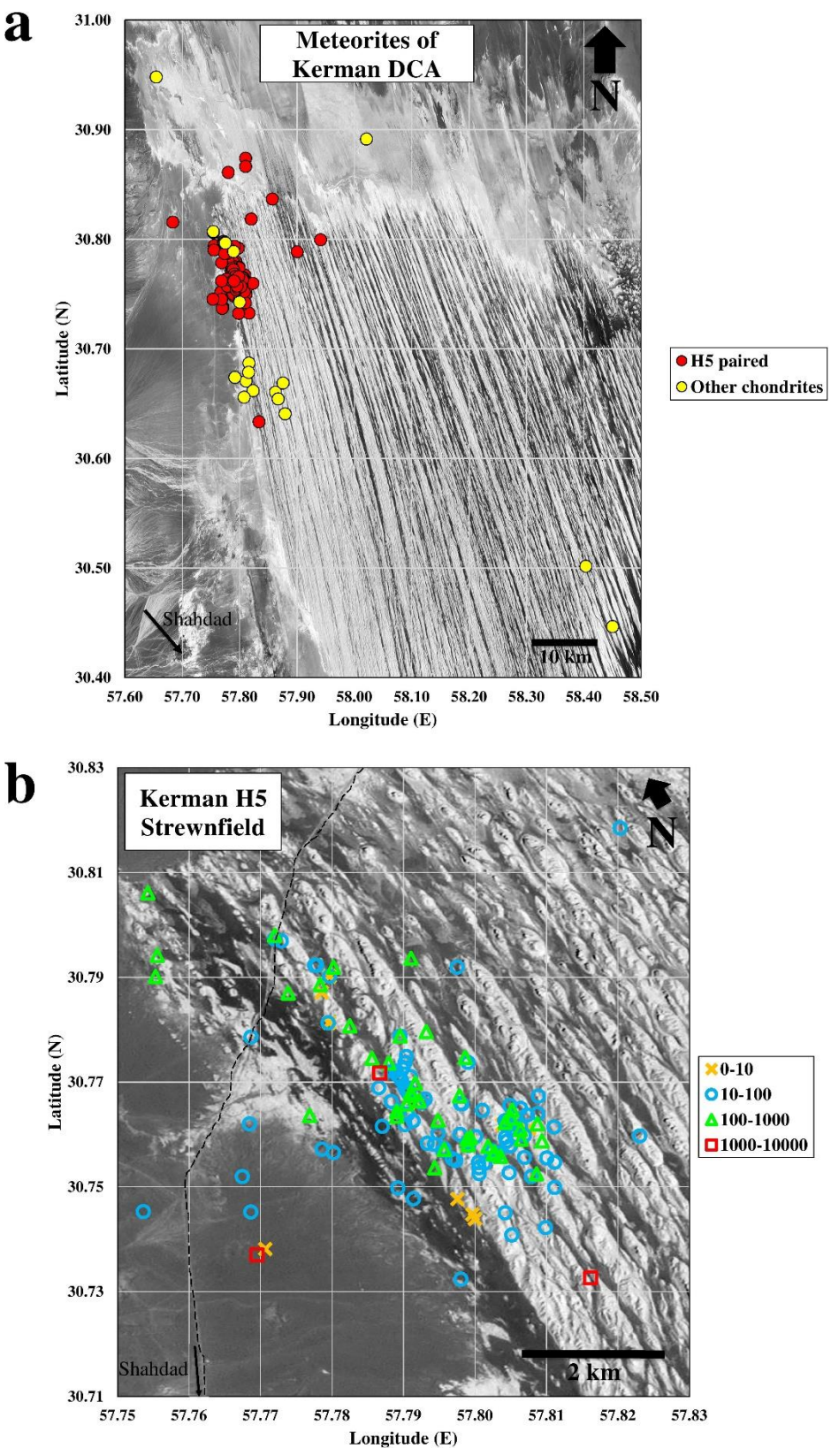
a
Meteorites of Kerman DCA
N
H5 paired
Other chondrites
Shahdad
10 km
Latitude (N)
Longitude (E)
31.00
30.90
30.80
30.70
30.60
30.50
30.40
57.60
57.70
57.80
57.90
58.00
58.10
58.20
58.30
58.40
58.50
b
Kerman H5 Strewnfield
N
0-10
10-100
100-1000
1000-10000
Shahdad
2 km
Latitude (N)
Longitude (E)
30.83
30.81
30.79
30.77
30.75
30.73
30.71
57.75
57.76
57.77
57.78
57.79
57.80
57.81
57.82
57.83

Fig. 6:

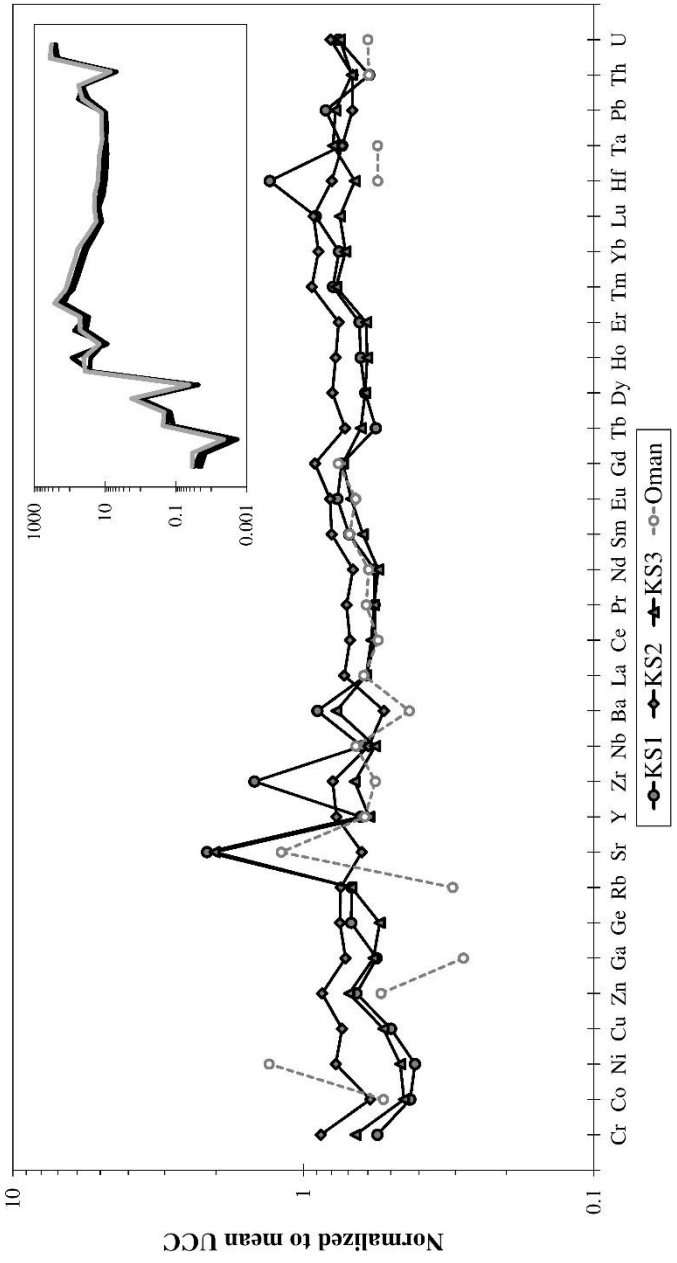
Normalized to mean UCC
10
1
0.1
Cr Co Ni Cu Zn Ga Ge Rb Sr Y Zr Nb Ba La Ce Pr Nd Sm Eu Gd Tb Dy Ho Er Tm Yb Lu Hf Ta Pb Th U
KS1 KS2 KS3 Oman
1000
10
0.1
0.001

1575 **Fig. 7:**

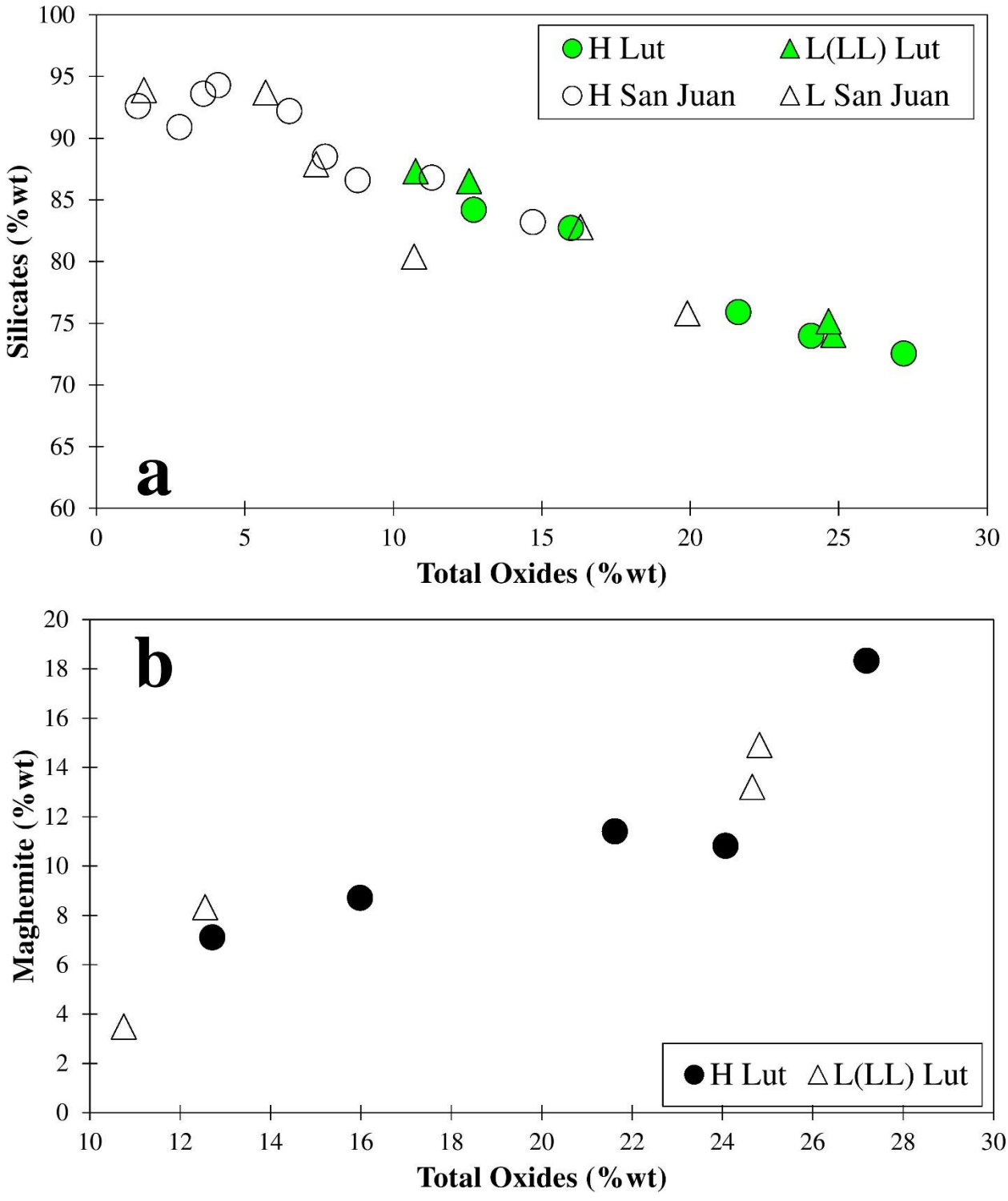

1576

1577

1578

Fig. 8:

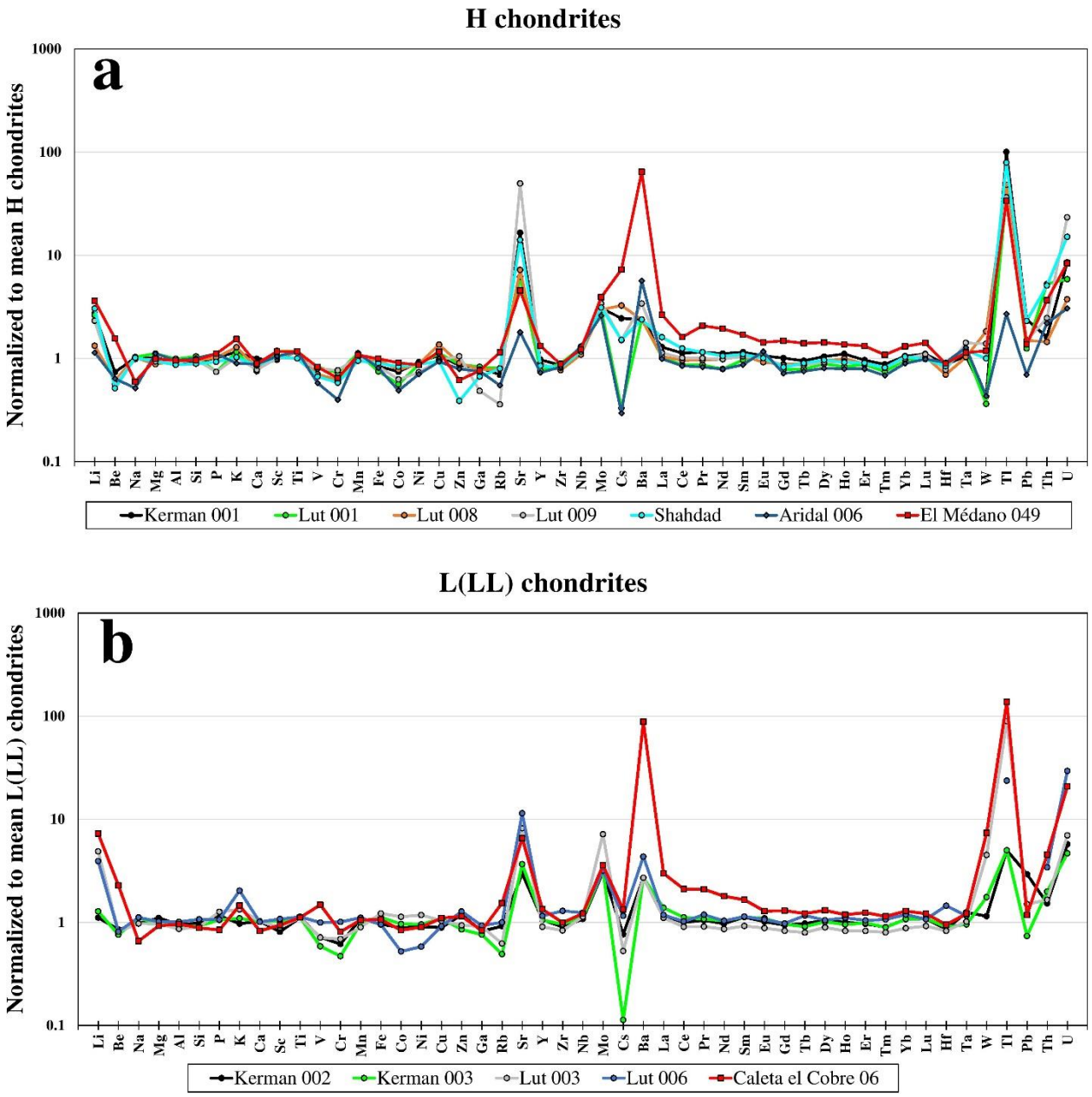
H chondrites
a
Normalized to mean H chondrites
1000
100
10
1
0.1
Li Be Na Mg Al Si P K Ca Sc Ti V Cr Mn Fe Co Ni Cu Zn Ga Rb Sr Y Zr Nb Mo Cs Ba La Ce Pr Nd Sm Eu Gd Tb Dy Ho Er Tm Yb Lu Hf Ta W Tl Pb Th U
Kerman 001
Lut 001
Lut 008
Lut 009
Shahdad
Aridal 006
El Médano 049
L(LL) chondrites
b
Normalized to mean L(LL) chondrites
1000
100
10
1
0.1
Li Be Na Mg Al Si P K Ca Sc Ti V Cr Mn Fe Co Ni Cu Zn Ga Rb Sr Y Zr Nb Mo Cs Ba La Ce Pr Nd Sm Eu Gd Tb Dy Ho Er Tm Yb Lu Hf Ta W Tl Pb Th U
Kerman 002
Kerman 003
Lut 003
Lut 006
Caleta el Cobre 06

Fig. 9:

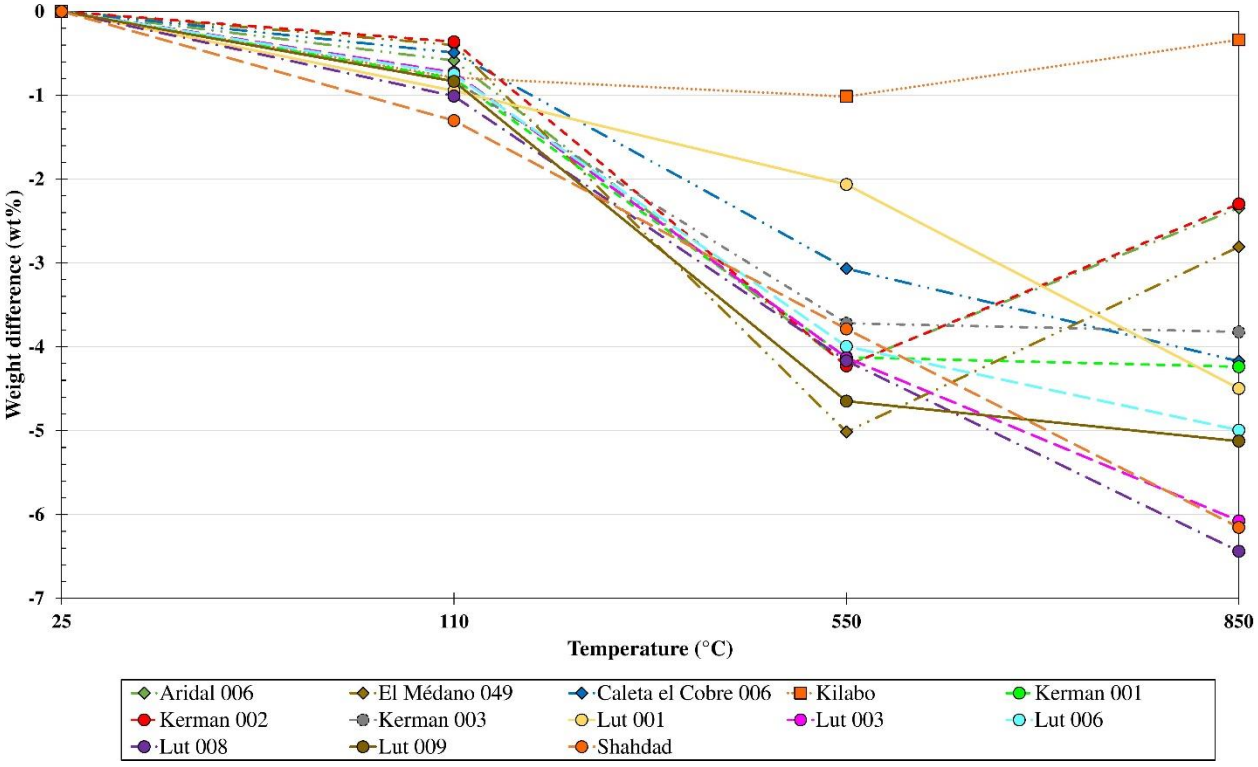
0
-1
-2
-3
-4
-5
-6
-7
Weight difference (wt%)
25
110
550
850
Temperature (°C)
Aridal 006
El Médano 049
Caleta el Cobre 006
Kilabo
Kerman 001
Kerman 002
Kerman 003
Lut 001
Lut 003
Lut 006
Lut 008
Lut 009
Shahdad

1599 **Fig. 10:**

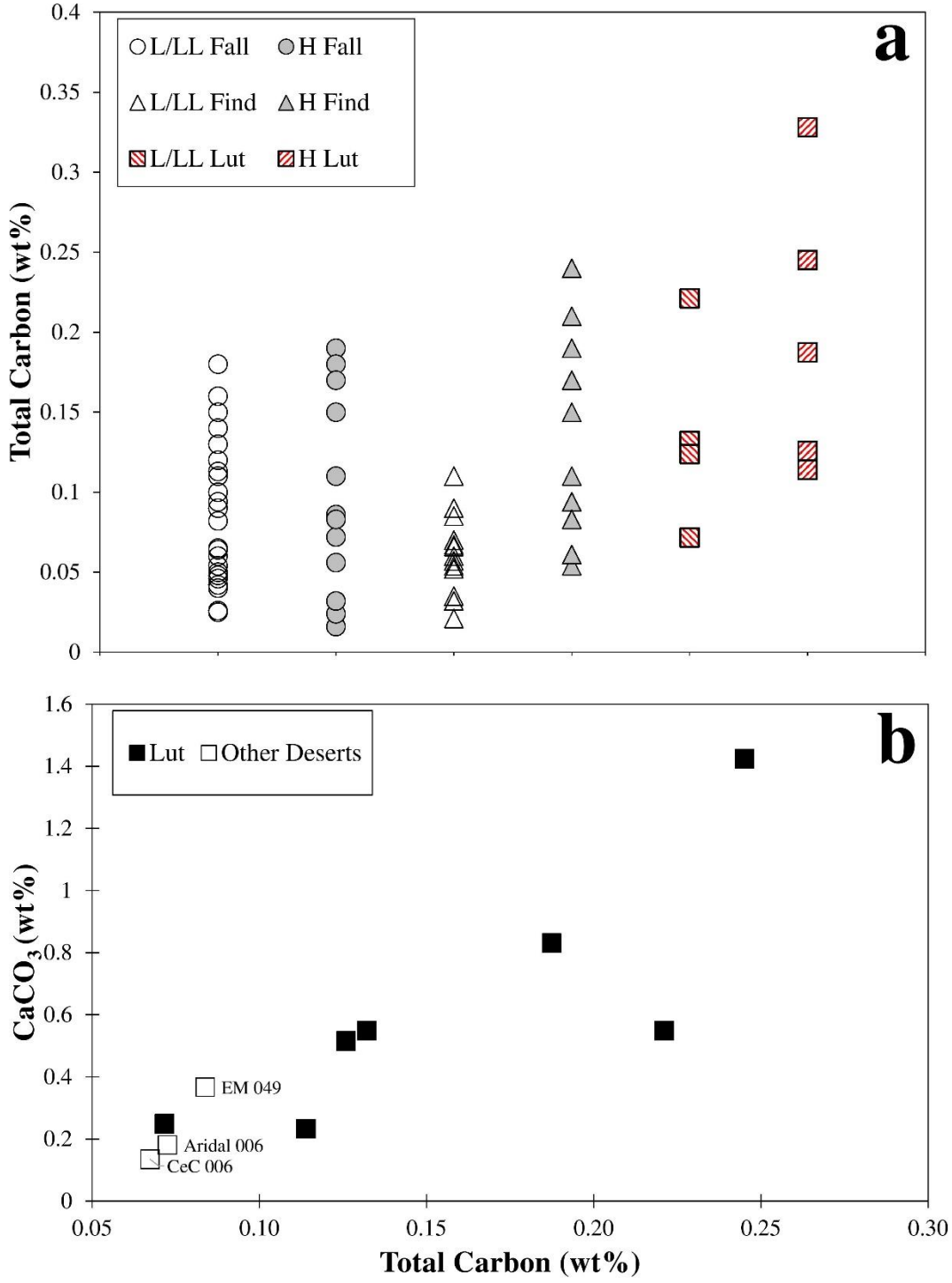

1600

1601

1602

Electronic annexes:

Fig. EA-1:

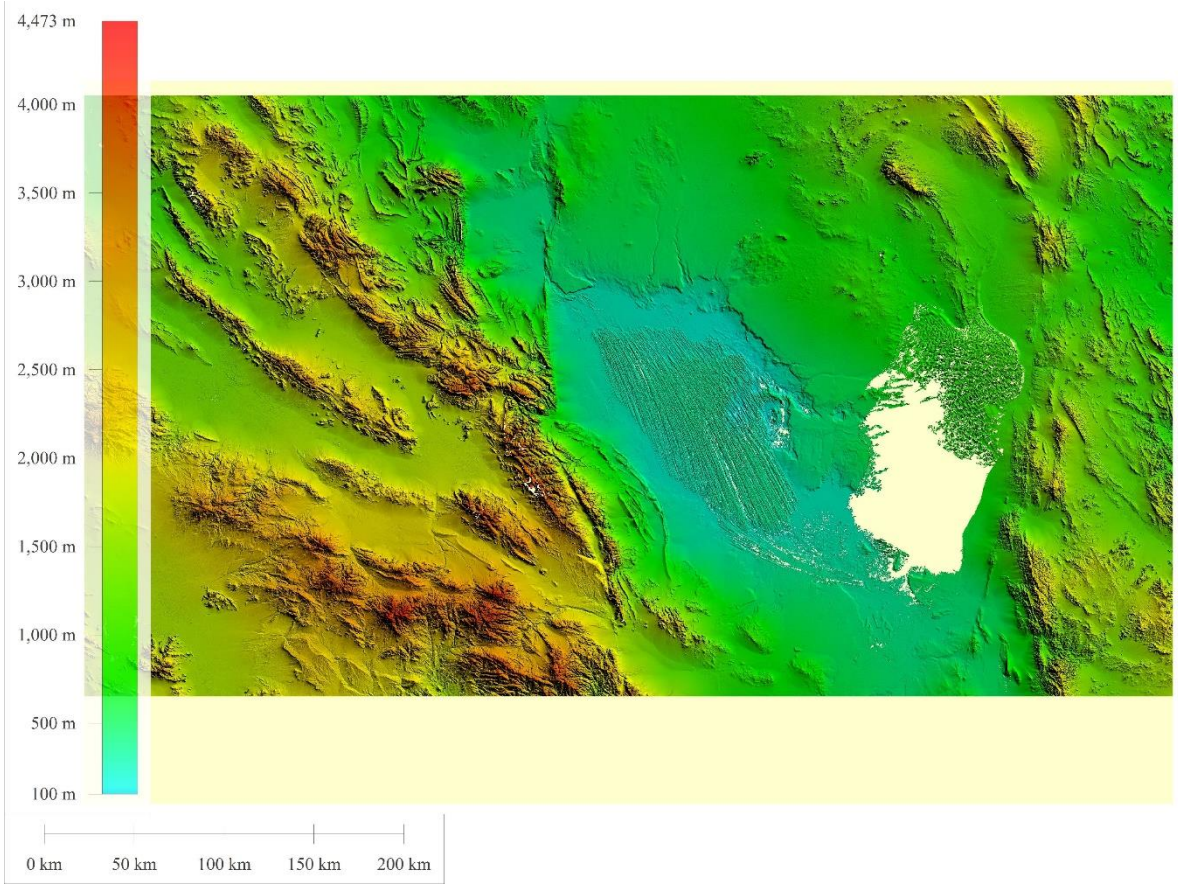

Fig EA-2:

Fig. EA-3:

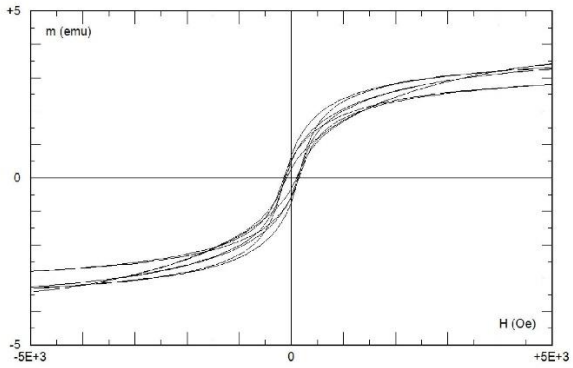

Fig. EA-4:

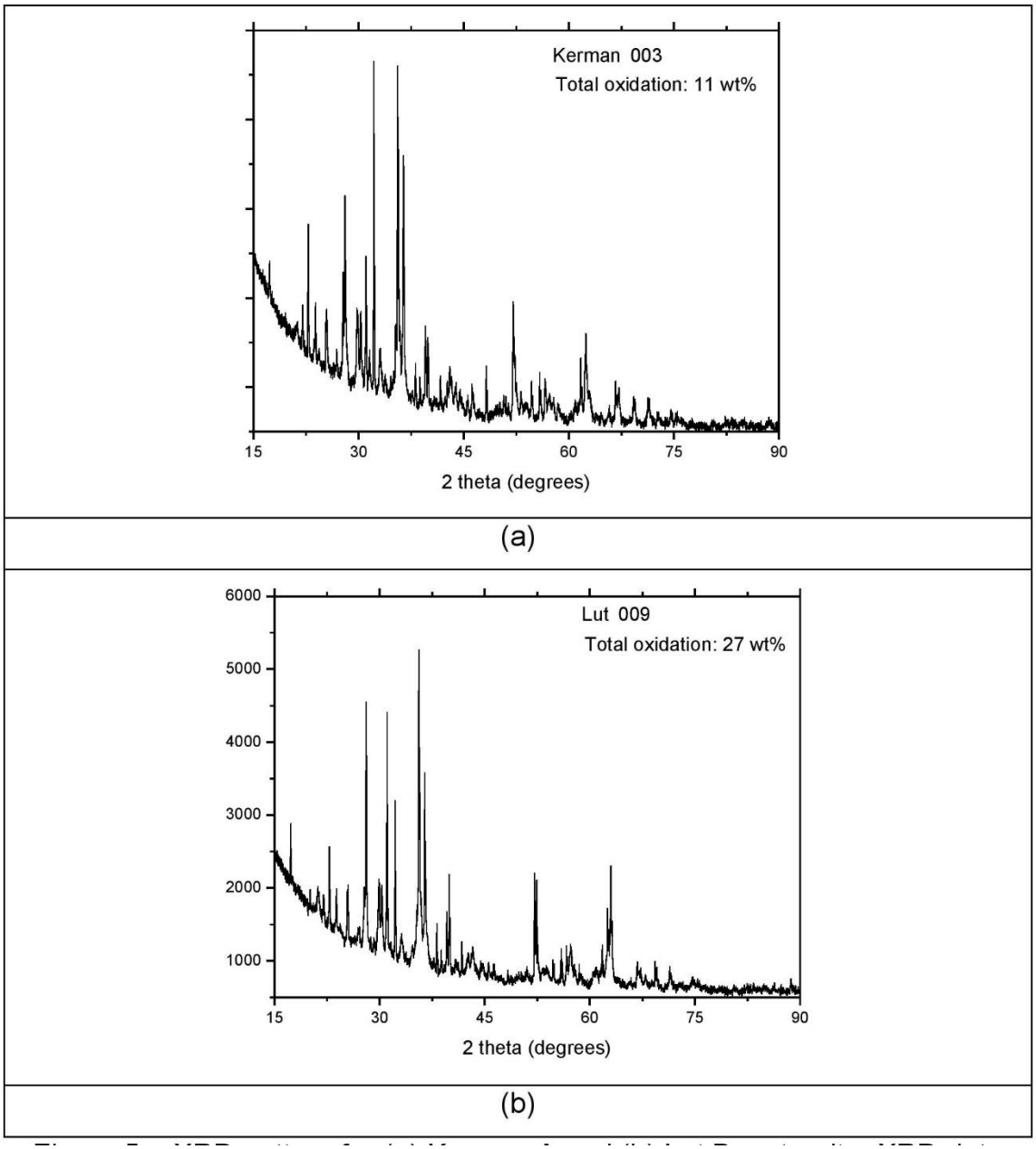
Kerman 003
Total oxidation: 11 wt%
15
30
45
60
75
90
2 theta (degrees)
(a)
Lut 009
Total oxidation: 27 wt%
6000
5000
4000
3000
2000
1000
15
30
45
60
75
90
2 theta (degrees)
(b)

1628 **Table EA-1:**

Name	Latitude	Longitude	Mass (g)	Pieces	Class	Weath	Fa (mol%)	Fs (mol%)	Wo (mol%)	Mag. Sus.
Gandom Beryan 003	31°1.133'N	58°1.367' E	177	1	H5	W2				4.79
Gandom Beryan 004	31°12.567' N	58°8.783' E	6400	1	H5	W3	19.1 (n=1)	17.8 (n=1)	1.5	4.76
Gandom Beryan 005	31° 51.983'N	57° 3.567'E	2510	5	H5	W3	17.9 (n=1)	16.2 (n=1)	1.1	4.67
Gandom Beryan 006	31° 53.650'N	57° 2.833'E	2000	110	H5	W4	18.1 (n=2)	-	-	4.87
Gandom Beryan 007	31° 52.783'N	57° 6.583'E	1430	27	H5	W2	18.6 (n=1)	16.1 (n=1)	1.1	4.91
Kerman 001	30°30.1'N	58°24.2'E	17000	1	H5	W4	18.4±0.2 (n=4)	16.4±0.3 (n=4)	1.1±0.1	4.67
Kerman 002	30°47.33'N	57°47.36' E	211	1	L6	W3	24.8±0.1 (N=2)	21.3 (N=1)	1.6	4.63
Kerman 003	30° 26.80'N	58° 27.00'E	615	1	L5	W2	25.3±0.2 (N=4)	22.0±0.2 (N=4)	1.9±0.8	4.52
Kerman 004	30°45.614' N	57°47.690 'E	70	2	H5	W3	18.9 (N=1)	16.2 (N=1)	1.4	4.6
Kerman 005	30°46.845' N	57°46.949 'E	333	105	H5	W3	18.6 (N=1)	17.2 (N=1)	1.3	4.6
Kerman 006	30°46.047' N	57°47.475 'E	220	10	H5	W3	18.9 (N=1)	16.4 (N=1)	1.4	4.63
Kerman 007	30°46.777' N	57°47.591 'E	176	32	H5	W2	18.9 (N=1)	16.9 (N=1)	2	4.52
Kerman 008	30°45.162' N	57°48.287 'E	20	2	H5	W4	18.7 (N=1)	16.3 (N=1)	1.3	4.61
Kerman 009	30°45.947' N	57°47.424 'E	132	15	H5	W2	18.3 (N=1)	16.5 (N=1)	1.1	4.55

Kerman 010	30°46.726' N	57°47.371 'E	105	5	H5	W3	18.5 (N=1)	16.5 (N=1)	1.3	4.45
Kerman 011	30°45.864' N	57°47.342 'E	155	10	H5	W2	18.7 (N=1)	18.1 (N=1)	1.1	4.5
Kerman 012	30°46.188' N	57°47.498 'E	494	34	H5	W4	19.0 (N=1)	16.4 (N=1)	1.2	4.63
Kerman 013	30°46.041' N	57°47.870 'E	282	15	H5	W3	18.2 (N=1)	16.1 (N=1)	1.2	4.6
Kerman 014	30°45.348' N	57°48.213 'E	604	30	H5	W3/4	18.6 (N=1)	18.3 (N=1)	1.2	4.48
Kerman 015	30°45.379' N	57°48.151 'E	168	2	H5	W3	18.4 (N=1)	16.4 (N=1)	1.4	4.7
Kerman 016	30°46.142' N	57°47.411 'E	33	2	H5	W3	18.4 (N=1)	16.3 (N=1)	1.5	4.61
Kerman 017	30°45.867' N	57°47.363 'E	26	2	H5	W3	18.9 (N=1)	16.3 (N=1)	1.3	4.53
Kerman 018	30°46.879' N	57°46.767 'E	16	1	H5	W3	18.6 (N=1)	18.3 (N=1)	0.6	4.42
Kerman 019	30°45.467' N	57°48.296 'E	92	12	H5	W4	17.0 (N=1)	20.2 (N=1)	0.1	4.58
Kerman 020	30°45.349' N	57°48.214 'E	620	60	H5	W4	19.3 (N=1)	16.4 (N=1)	1.2	4.55
Kerman 021	30°45.300' N	57°47.839 'E	32	6	H5	W4	18.8 (N=1)	16.5 (N=1)	1.2	4.78
Kerman 022	30°45.576' N	57°48.005 'E	98	5	H5	W2/3	18.6 (N=1)	16.2 (N=1)	1.4	4.55
Kerman 023	30°45.464' N	57°48.109 'E	134	9	H5	W3	18.5 (N=1)	16.9 (N=1)	1.3	4.59
Kerman 024	30°48.424' N	57°45.240 'E	16	1	L6	W2	24.3 (N=1)	21.2 (N=1)	1	4.06
Kerman 025	30°46.878' N	57°46.767 'E	13	3	H5	W2/3	16.7 (N=1)	18.0 (N=1)	0	4.74

Kerman 026	30°47.795' N	57°46.500 'E	4	1	L6	W2	24.2 (N=1)	20.8 (N=1)	1.6	4.5
Kerman 027	30°45.985' N	57°47.531 'E	180	8	H5	W4	18.3 (N=1)	16.2 (N=1)	1.3	4.65
Kerman 028	30°38.008' N	57°50.023 'E	7360	22	H5	W2	18.3 (N=1)	17.3 (N=1)	1	4.54
Kerman 029	30°45.149' N	57°48.516 'E	170	12	H3	W2	17.7±4.7 (N=9)	12.9±4.9 (N=10)	0.9±0.4	4.7
Kerman 030	30°45.565' N	57°47.961 'E	200	32	H5	W4	18.5 (N=1)	16.1 (N=1)	0	4.6
Kerman 031	30°45.545' N	57°47.934 'E	150	14	H5		18.5 (N=2)	16.0 (N=2)	1.3	4.82
Kerman 032	30°51.658' N	57°46.802 'E	2900	1	L6	W2	23.8 (N=1)	21.0 (N=1)	1.4	4.49
Kerman 033	30°52.439' N	57°48.621 'E	2630	1	H5	W3	-	15.6 (N=1)	1.2	4.69
Kerman 034	30°51.983' N	57°48.620 'E	720	1	H5	W1/W3	18.4 (N=1)	16.5 (N=1)	1.3	4.97
Kerman 035	30°45.760' N	57°47.689 'E	110	3	H5	W3	18.6 (N=1)	-	-	4.59
Kerman 036	30°45.948' N	57°47.891 'E	65	4	H5	W3	19.5 (N=1)	17.2 (N=1)	1.4	4.53
Kerman 037	30°45.411' N	57°48.149 'E	85	10	H5	W3	18.0 (N=2)	16.1 (N=1)	1.4	4.58
Kerman 038	30°45.482' N	57°47.942 'E	120	10	H5	W2/3	18.5 (N=1)	16.0 (N=1)	1.6	4.63
Kerman 039	30°45.427' N	57°47.740 'E	155	12	H5	W3		17.0 (N=3)	1.7	4.54
Kerman 040	30°45.568' N	57°48.256 'E	40	2	H5	W3/4	19.2 (N=3)	18.7 (N=2)	0.7	4.54
Kerman 041	30°46.302' N	57°47.201 'E	1210	20	H5	W2	18.6 (N=1)	16.5 (N=1)	1.3	4.51

Kerman 042	30°43.956' N	57°48.971 'E	2300	57	H5	W2	18.9 (N=1)	17.1 (N=2)	1.4	4.58
Kerman 043	30°45.150' N	57°48.035 'E	44	1	H5	W2	19.4 (N=1)	-	-	4.58
Kerman 044	30°46.726' N	57°47.371 'E	64	3	H5	W2	19.0 (N=1)	16.6 (N=1)	1.3	4.6
Kerman 045	30°44.561' N	57°47.996 'E	7	1	LL6	W2	28.7 (N=1)	-	-	3.75
Kerman 046	30°48.366' N	57°45.254 'E	819	38	H5	W3	-	-	-	4.53
Kerman 047	30°46.424' N	57°47.413 'E	82	12	H5	W3	-	-	-	4.56
Kerman 048	30°45.806' N	57°47.342 'E	302	47	H5	W3	-	-	-	4.55
Kerman 049	30°46.471' N	57°47.135 'E	172	1	H5	W3	-	-	-	4.56
Kerman 050	30°45.382' N	57°48.193 'E	38	5	H5	W3	-	-	-	4.55
Kerman 051	30°45.787' N	57°48.334 'E	97	5	H5	W3	-	-	-	4.59
Kerman 052	30°45.487' N	57°47.661 'E	73	16	H5	W3	-	-	-	4.57
Kerman 053	30°45.396' N	57°48.163 'E	434	8	H5	W3	-	-	-	4.6
Kerman 054	30°45.874' N	57°48.061 'E	54	7	H5	W4	-	-	-	4.63
Kerman 055	30°45.832' N	57°47.433 'E	60	5	H5	W3	-	-	-	4.5
Kerman 056	30°45.546' N	57°48.387 'E	139	8	H5	W3	-	-	-	4.54
Kerman 057	30°45.933' N	57°48.292 'E	58	11	H5	W3	-	-	-	4.58

Kerman 058	30°46.482' N	57°47.917 'E	133	4	H5	W2	-	16.3 (N=1)	1.4	4.56
Kerman 059	30°45.525' N	57°48.562 'E	303	24	H5	W2	-	17.7 (N=2)	1.2	4.45
Kerman 060	30°44.863' N	57°47.484 'E	50	6	H5	W3	-	-	-	4.51
Kerman 061	30°46.353' N	57°47.393 'E	71	1	H5	W3	-	-	-	4.68
Kerman 062	30°46.078' N	57°47.460 'E	187	7	H5	W3	-	-	-	4.64
Kerman 063	30°45.336' N	57°48.416 'E	30	2	H5	W2	-	-	-	4.78
Kerman 064	30°45.472' N	57°47.946 'E	39	6	H5	W2/3	-	-	-	4.52
Kerman 065	30°46.277' N	57°47.352 'E	45	3	H5	W4	-	-	-	4.65
Kerman 066	30°44.860' N	57°47.852 'E	9	1	H5	W3	-	-	-	4.65
Kerman 067	30°46.254' N	57°47.369 'E	45	5	H5	W3	-	-	-	4.59
Kerman 068	30°47.315' N	57°46.700 'E	362	124	H5	W4	19.0 (N=1)	17.0 (N=1)	1.44	4.7
Kerman 069	30°45.838' N	57°48.527 'E	45	6	H5	W3	-	-	-	4.56
Kerman 070	30°45.218' N	57°48.034 'E	49	16	H5	W3	-	-	-	4.62
Kerman 071	30°46.005' N	57°47.582 'E	50	3	H6	W3	-	-	-	4.63
Kerman 072	30°45.755' N	57°47.480 'E	59	2	H5	W3	-	-	-	4.5
Kerman 073	30°46.325' N	57°47.306 'E	95	2	H5	W4	-	-	-	4.66

Kerman 074	30°45.659' N	57°48.381 'E	240	10	H5	W3	-	-	-	4.53
Kerman 075	30°45.722' N	57°48.524 'E	134	2	H5	W2	-	-	-	4.54
Kerman 076	30°45.590' N	57°48.415 'E	55	3	H5	W3	-	-	-	4.56
Kerman 077	30°44.702' N	57°48.253 'E	50	7	H5	W3	-	-	-	4.56
Kerman 078	30°46.038' N	57°48.533 'E	21	3	H5	W3	-	-	-	4.64
Kerman 079	30°45.737' N	57°48.253 'E	172	7	H5	W3	-	-	-	4.61
Kerman 080	30°45.978' N	57°47.298 'E	70	15	H5	W3	-	-	-	4.53
Kerman 081	30°46.494' N	57°47.423 'E	60	6	H5	W3	-	-	-	4.58
Kerman 082	30°45.600' N	57°47.876 'E	18	1	H5	W3	-	-	-	4.53
Kerman 083	30°45.738' N	57°48.264 'E	43	12	H5	W3	-	-	-	4.61
Kerman 084	30°45.824' N	57°48.438 'E	62	4	H5	W3	-	-	-	4.63
Kerman 085	30°45.748' N	57°48.253 'E	36	1	H5	W2	-	-	-	4.69
Kerman 086	30°47.411' N	57°46.779 'E	15	1	H5	W3	-	-	-	4.49
Kerman 087	30°46.084' N	57°47.444 'E	45	2	H5	W2	-	-	-	4.6
Kerman 088	30°44.992' N	57°48.669 'E	12	1	H5	W2	-	-	-	4.78
Kerman 089	30°45.701' N	57°48.263 'E	33	4	H5	W2	-	-	-	4.76

Kerman 090	30°45.742' N	57°48.270 'E	27	4	H5	W4	-	-	-	4.6
Kerman 091	30°45.667' N	57°48.452 'E	7	1	H5	W2	-	-	-	4.62
Kerman 092	30°47.411' N	57°46.779 'E	8.5	3	H5	W4	19.4 (N=1)	17.0 (N=1)	1.4	4.68
Kerman 093	30°46.135' N	57°47.193 'E	52	2	H5	W3	-	-	-	4.49
Kerman 094	30°46.224' N	57°47.381 'E	22	2	H5	W3	-	-	-	4.52
Kerman 095	30°46.263' N	57°47.459 'E	52	3	H5	W3	-	-	-	4.46
Kerman 096	30°47.538' N	57°46.654 'E	20	24	H5	W4	-	-	-	4.55
Kerman 097	30°47.534' N	57°46.671 'E	82	7	H5	W4	19.3 (N=1)	17.0 (N=1)	1.2	4.75
Kerman 098	30°46.424' N	57°47.942 'E	26	3	H5	W3	-	-	-	4.56
Kerman 099	30°46.878' N	57°46.775 'E	8	5	H5	W3	-	-	-	4.58
Kerman 100	30°45.684' N	57°48.664 'E	31	5	H5	W2/3	-	-	-	4.42
Kerman 101	30°44.448' N	57°48.309 'E	31	6	H5	W4	-	-	-	4.57
Kerman 102	30°45.711' N	57°48.228 'E	7	1	H5	W3	-	-	-	4.59
Kerman 103	30°45.281' N	57°48.029 'E	52	3	H5	W3	-	-	-	4.64
Kerman 104	30°45.899' N	57°48.382 'E	21	3	H5	W3	-	-	-	4.53
Kerman 105	30°46.107' N	57°47.423 'E	34	1	H5	W3	-	-	-	4.65

Kerman 106	30°46.419' N	57°47.276 'E	116	5	H5	W3	-	-	-	4.65
Kerman 107	30°45.692' N	57°48.383 'E	72	6	H5	W3/4	-	-	-	4.47
Kerman 108	30°46.327' N	57°47.338 'E	20	1	H5	W3	17.3 (N=1)	17.4 (N=1)	1	4.72
Kerman 109	30°47.538' N	57°46.654 'E	12	6	H5	W4	-	-	-	4.5
Kerman 110	30°44.631' N	57°47.999 'E	9.3	1	H5	W3	-	-	-	4.63
Kerman 111	30°46.074' N	57°47.439 'E	95	3	H5	W3	-	-	-	4.64
Kerman 112	30°46.094' N	57°47.450 'E	28	5	H5	W3/4	-	-	-	4.49
Kerman 113	30°45.757' N	57°48.251 'E	33	7	H5	W3	-	-	-	4.61
Kerman 114	30°44.986' N	57°47.353 'E	48	2	H5	W4	-	-	-	4.55
Kerman 115	30°45.948' N	57°47.515 'E	6.5	3	H5	W4	-	-	-	4.69
Kerman 116	30°47.228' N	57°46.713 'E	8.3	2	H5	W4	-	-	-	4.68
Kerman 117	30°45.963' N	57°47.551 'E	59	10	H5	W3	-	-	-	4.65
Kerman 118	30°45.331' N	57°48.603 'E	46	3	H5	W3	-	-	-	4.66
Kerman 119	30°45.586' N	57°48.330 'E	29	2	H5	W3	-	-	-	4.45
Kerman 120	30°45.268' N	57°48.081 'E	48	10	H5	W4	-	-	-	4.55
Kerman 121	30°44.686' N	57°47.978 'E	9.2	1	H5	W3	-	-	-	4.68

Kerman 122	30°45.751' N	57°48.262 'E	38	5	H5	W3	-	-	-	4.53
Kerman 123	30°45.667' N	57°48.301 'E	64	7	H5	W4	-	-	-	4.62
Kerman 124	30°44.288' N	57°46.239 'E	8	1	H5	W3	-	-	-	4.52
Kerman 125	30°45.281' N	57°48.668 'E	38	3	H5	W2	-	-	-	4.71
Kerman 126	30°47.516' N	57°47.850 'E	65	2	H5	W2	-	-	-	5.18
Kerman 127	30°56.878' N	57°39.283 'E	181	9	H5	W3	-	-	-	4.52
Kerman 128	30°47.317' N	57°54.017 'E	813	2	H5	W2/3	-	-	-	4.95
Kerman 129	30°47.650' N	57°45.333 'E	191	3	H5	W3	-	-	-	4.47
Kerman 130	30°49.109' N	57°49.218 'E	65	2	H5	W2/3	-	-	-	4.54
Kerman 131	30°50.199' N	57°51.417 'E	136	1	H5	W3	-	-	-	4.58
Kerman 132	30°45.583' N	57°49.383 'E	96	1	H5	W3/4	-	-	-	4.55
Kerman 133	30°45.499' N	57°47.600 'E	79	2	H5	W3	-	-	-	4.57
Kerman 134	30°53.482' N	58°1.250' E	174	11	H5	W3	-	-	-	4.63
Kerman 135	30°48.938' N	57°41.007 'E	5749	1	H5	W2	19.7 (N=1)	16.9 (N=1)	1.1	4.69
Kerman 136	30°45.117' N	57°46.047 'E	28	1	H5	W2	18.5 (N=1)	16.9 (N=1)	1.3	4.75
Kerman 137	30°39.632' N	57°51.754 'E	130	1	L5	W1/2	24.8 (N=1)	20.7 (N=1)	1.6	4.63

Kerman 138	30°39.262' N	57°52.023 'E	1009	2	L5	W2/3	24.8 (N=1)	21.0 (N=1)	1.6	4.4
Kerman 139	30°38.441' N	57°52.750 'E	246	1	L5	W2	25.4 (N=3)	20.9 (N=2)	1.6	4.53
Kerman 140	30°40.136' N	57°52.540 'E	341	1	L5	W2	25.4 (N=2)	21.4 (N=1)	1.4	4.47
Kerman 141	30°40.233' N	57°48.670 'E	1630	2	L5	W1/2	25.4 (N=2)	20.9 (N=1)	1.5	4.2
Kerman 142	30°39.707' N	57°49.403 'E	2498	1	L5	W1/2	25.4 (N=1)	20.5 (N=1)	1.3	4.45
Kerman 143	30°47.836' N	57°46.317 'E	26	1	H5	W3	18.8 (N=1)	17.0 (N=1)	1.2	4.64
Kerman 144	30°47.411' N	57°45.318 'E	152	9	H5	W4	-	-	-	4.75
Kerman 145	30°47.618' N	57°47.463 'E	205	4	H5	W3	-	-	-	4.41
Kerman 146	30°47.516' N	57°46.812 'E	295	5	H5	W3	-	-	-	4.67
Kerman 147	30°46.716' N	57°46.119 'E	25	1	H5	W3	-	-	-	4.65
Kerman 148	30°45.816' N	57°46.611 'E	207	7	H5	W2	-	-	-	4.58
Kerman 149	30°47.219' N	57°46.431 'E	143	3	H5	W2	-	-	-	4.85
Kerman 150	30°45.391' N	57°46.812 'E	20	3	H5	W3	-	-	-	4.65
Kerman 151	30°47.881' N	57°46.319 'E	300	3	H5	W2/3	-	-	-	4.88
Kerman 152	30°45.431' N	57°46.716 'E	20	1	H5	W2/3	-	-	-	4.56
Kerman 153	30°40.439' N	57°47.504 'E	1640	2	L5	W2/3	-	-	-	4.32

Kerman 154	30°39.353' N	57°48.454 'E	1232	2	L5	W2	-	-	-	4.21
Kerman 155	30°41.225' N	57°48.969 'E	200	1	L5	W2	-	-	-	4.16
Kerman 156	30°40.719' N	57°48.941 'E	830	2	L5	W2	25.9 (N=1)	20.7 (N=1)	1.9	4.36
Kerman 157	30°45.486' N	57°47.661 'E	20.6	1	H5	W3	-	-	-	4.57
Kerman 158	30°44.219' N	57°46.171 'E	25.5	1	H5	W3	-	-	-	4.61
Kerman 159	30°47.971' N	57°56.462 'E	20	1	H5	W2	-	-	-	4.64
Kerman 160	30°45.877' N	57°48.312 'E	291	14	H5	W3	-	-	-	4.62
Kerman 161	30°45.417' N	57°47.729 'E	20.6	1	H5	W3	-	-	-	4.59
Kerman 162	30°45.511' N	57°47.936 'E	33.5	1	H5	W3	-	-	-	4.58
Kerman 163	30°45.520' N	57°48.265 'E	15.6	1	H5	W3/4	-	-	-	4.64
Kerman 164	30°44.712' N	57°46.118 'E	23	1	H5	W2	-	-	-	4.81
Kerman 165	30°44.716' N	57°45.216 'E	18	1	H5	W3/4	-	-	-	4.66
Kerman 166	30°45.693' N	57°47.221 'E	13.6	1	H5	W3	-	-	-	4.66
Kerman 167	30°45.788' N	57°48.304 'E	819	37	H5	W2/3	-	-	-	4.58
Kerman 168	30°44.533' N	57°48.593 'E	22	1	H5	W2	-	-	-	4.65
Kerman 169	30°45.952' N	57°47.880 'E	16	2	H5	W3	-	-	-	4.6

Kerman 170	30°45.118' N	57°48.473 'E	68	3	H5	W3	-	-	-	4.69
Kerman 171	30°45.218' N	57°47.661 'E	986	11	H5	W4	-	-	-	4.65
Kerman 172	30°47.816' N	57°46.374 'E	17.5	1	H5	W3	-	-	-	4.61
Kerman 173	30°43.942' N	57°47.882 'E	19.4	1	H5	W2	-	-	-	4.62
Kerman 174	30°45.721' N	57°46.107 'E	23	1	H5	W2/3	-	-	-	4.76
Kerman 175	30°45.321' N	57°47.809 'E	21	1	H5	W4	-	-	-	4.59
Kerman 176	30°45.408' N	57°48.133 'E	13.6	1	H5	W3/4	-	-	-	4.51
Kerman 177	30°45.437' N	57°47.738 'E	18	1	H5	W3	-	-	-	4.54
Kerman 178	30°45.712' N	57°47.413 'E	18.5	1	H5	W3	-	-	-	4.61
Kerman 179	30°48.033' N	57°50.067 'E	61	2	H5	W1-2	-	-	-	4.79
Kerman 180	30°46.900' N	57°50.433 'E	114	2	H5	W3	-	-	-	4.56
Kerman 181	30°47.883' N	57°52.450 'E	1987	1	H5	W2	-	-	-	4.63
Kerman 182	30°41.133' N	57°50.017 'E	265	13	H5	W2	-	-	-	4.66
Kerman 183	30°48.067' N	57°50.050 'E	67	1	H5	W3	-	-	-	4.62
Kerman 184	30°44.283' N	57°50.200 'E	385	17	H5	W3	-	-	-	4.71
Kerman 185	30°46.517' N	57°52.450 'E	935	110	H5	W3	-	-	-	4.63

Kerman 186	30°49.000' N	57°50.467 'E	85	3	H5	W3	-	-	-	4.61
Kerman 187	30°46.467' N	57°52.500 'E	2644	13	H5	W3	-	-	-	4.59
Kerman 188	30°42.067' N	57°48.467 'E	251	4	H5	W3	-	-	-	4.5
Kerman 189	30°48.500' N	57°55.183 'E	117	3	H5	W3	-	-	-	4.56
Kerman 190	30°53.933' N	57°59.250 'E	69	2	H5	W3	-	-	-	4.64
Kerman 191	30°53.817' N	57°58.183 'E	72	1	H5	W3	-	-	-	4.61
Kerman 192	30°51.500' N	57°48.417 'E	120	4	H5	W3	-	-	-	4.59
Kerman 193	30°57.717' N	58°2.133' E	443	60	H5	W5	-	-	-	4.71
Kerman 194	30°59.983' N	58°1.483' E	222	2	H5	W3	-	-	-	4.68
Kerman 195	30°53.333' N	57°58.867 'E	257	9	H5	W2	-	-	-	4.58
Kerman 196	30°53.800' N	57°42.700 'E	40	1	H5	W2/3	-	-	-	4.71
Kerman 197	30°47.067' N	57°47.983 'E	143	6	H5	W3	-	-	-	4.65
Kerman 198	30°45.801' N	57°47.911 'E	43	6	H5	W4	-	-	-	4.54
Kerman 199	30°47.218' N	57°46.923 'E	6.5	1	H5	W4	19.1 (n=1)	17.0 (n=1)	1.2	4.58
Kerman 200	30°39.739' N	57°48.915 'E	1700	2	L5	W2	-	-	-	4.29
Kerman 201	30°54.283' N	58°1.233' E	93	2	H5	W2	-	-	-	4.62

Kerman 202	30°54.917' N	57°59.600 'E	68	2	H5	W2	-	-	-	4.64
Lut-e-Zangi Ahmad 001	29°48.667' N	59°11.667 'E	290	1	H5	W1	19.5 (N=1)	17.3 (N=2)	1.26	5.07
Lut 008	30°23.52'N	58°38.44' E	215	1	H4	W5	18.0±0.2 (N=4)	16.2±0.1 (N=3)	1.0±0.1	4.71
Lut 009	30°20.38' N	59°09.04' E	40.6	1	H4	W4	19.0±0.7 (N=31)	16.0±3.0 (N=31)	0.9	4.75
Lut 010	30°28.038' N	59°23.183 'E	926	10	LL6	W2-4	26.3±0.8 (N=5)	22.3±0.4 (N=3)	1.6±0.2	4.18
Lut 011	30°55.02'N	59°46.07' E	750	2	L4	W2	22.8±1(N=4)	17.7±1.5 (N=4)	0.6±0.8	4.64
Lut 012	30°56.318' N	58°45.421 'E	10311	1	L6	W2	25.3 (N=1)	21.5 (N=1)	1.3	4.42

Left blank intentionally.

Chapter 5

Terrestrial Weathering of Meteorites and Its Effects on Rare Earth Elements

---

Peer-reviewed research paper *Pourkhorsandi et al., Meteoritics & Planetary Science, 2017*

The Meteoritical Society

Meteoritics & Planetary Science 52, Nr 9, 1843–1858 (2017)
doi: 10.1111/maps.12894

Modification of REE distribution of ordinary chondrites from Atacama (Chile) and Lut (Iran) hot deserts: Insights into the chemical weathering of meteorites

Hamed POURKHORSANDI[1*], Massimo D'ORAZIO[2], Pierre ROCHETTE[1], Millarca VALENZUELA[3], Jérôme GATTACCECA[1], Hassan MIRNEJAD[4,5], Brad SUTTER[6], Aurore HUTZLER[7], and Maria ABOULAHRIS[1,8]

[1]CNRS, Aix-Marseille Univ., IRD, Coll. France, CEREGE, Aix-en-Provence, France
[2]Dipartimento di Scienze della Terra, Università di Pisa, Via S. Maria 53, I-56126 Pisa, Italy
[3]Instituto de Astrofísica, Pontificia Universidad Católica de Chile, Vicuña Mackena 4860, Macul, Santiago, Chile
[4]Department of Geology, Faculty of Sciences, University of Tehran, Tehran 14155-64155, Iran
[5]Department of Geology and Environmental Earth Sciences, Miami University, Oxford, Ohio 45056, USA
[6]Jacobs-NASA, Johnson Space Center, Houston, Texas 77058, USA
[7]Natural History Museum, Burgring 7, A-1010 Vienna, Austria
[8]Département de Géologie, Faculté des Sciences, Université Hassan II Casablanca, Casablanca, Morocco
[*]Corresponding author. E-mail: pourkhorsandi@cerege.fr

(Received 04 June 2016; revision accepted 10 April 2017)

Abstract–The behavior of rare earth elements (REEs) during hot desert weathering of meteorites is investigated. Ordinary chondrites (OCs) from Atacama (Chile) and Lut (Iran) deserts show different variations in REE composition during this process. Inductively coupled plasma–mass spectrometry (ICP-MS) data reveal that hot desert OCs tend to show elevated light REE concentrations, relative to OC falls. Chondrites from Atacama are by far the most enriched in REEs and this enrichment is not necessarily related to their degree of weathering. Positive Ce anomaly of fresh chondrites from Atacama and the successive formation of a negative Ce anomaly with the addition of trivalent REEs are similar to the process reported from Antarctic eucrites. In addition to REEs, Sr and Ba also show different concentrations when comparing OCs from different hot deserts. The stability of Atacama surfaces and the associated old terrestrial ages of meteorites from this region give the samples the necessary time to interact with the terrestrial environment and to be chemically modified. Higher REE contents and LREE-enriched composition are evidence of contamination by terrestrial soil. Despite their low degrees of weathering, special care must be taken into account while working on the REE composition of Atacama meteorites for cosmochemistry applications. In contrast, chondrites from the Lut desert show lower degrees of REE modification, despite significant weathering signed by Sr content. This is explained by the relatively rapid weathering rate of the meteorites occurring in the Lut desert, which hampers the penetration of terrestrial material by forming voluminous Fe oxide/oxyhydroxides shortly after the meteorite fall.

INTRODUCTION

As soon as a meteoroid enters the Earth's atmosphere, it is subjected to terrestrial alteration (e.g., Bland et al. 2006). The meteorites which are used for cosmochemical studies are being collected immediately or thousands to several hundred thousands of years after their fall. It has been documented that the mineralogy and chemical compositions of these samples can be affected over a human lifetime (Socki et al. 1991; Bland et al. 1998; Pillinger et al. 2013). Alteration occurs on even shorter time scales of less than decades in the laboratory environment (Velbel 2014) or tens of days in a humid natural environment (Bischoff et al. 2011). Initial investigations on the meteorite weathering processes commenced just after the recognition of a high number of

weathered hot desert samples (e.g., Buddhue 1939; Olsen and Fuchs 1967). Since that time, the discovery of large numbers of meteorites from cold and hot deserts has drawn the attention of researchers to document the effects of weathering on meteorites to avoid any inaccurate interpretation on their geochemical compositions.

The main purposes of meteorite weathering studies are (1) understanding the weathering process occurring within a meteorite and its relationship to the finding place of the meteorite, and (2) identifying the chemical and mineralogical modification during this process, to account for eventual bias in cosmochemical studies (Bland et al. 2006). Several studies have focused on the effect of weathering on the chemical and mineralogical compositions of meteorites from Antarctic and rare hot desert achondrites (White et al. 1967; Gooding 1982; Koeberl and Cassidy 1989; Torigoye-Kita et al. 1995; Swindle et al. 1998; Llorca et al. 2013). Considering their importance and also higher abundance, these studies on the ordinary chondrites (OCs) have high importance, compared to achondrites.

Among the trace elements which are used in geochemical and cosmochemical studies of meteorites, rare earth elements (REEs) have a significant importance. Variations in the abundance of REEs are diagnostic proxies to study evaporation/condensation processes in the nebula (Boynton 1975), parent-body aqueous alteration (Inoue et al. 2009), thermal metamorphism (Murrell and Burnett 1983), magmatic differentiation (Boynton et al. 1976), and terrestrial weathering (Crozaz et al. 2003). Rare earth elements mobilization during terrestrial weathering has been studied by Mittlefehldt and Lindstrom (1991) on Antarctic eucrites and by Crozaz et al. (2003) on hot desert achondrites. Rare earth element sensitivity to weathering may also affect Nd isotopic composition (Crozaz and Wadhwa 2001).

Despite the high number of OCs, limited studies have been conducted on their REE mobilization during terrestrial weathering. Al-Kathiri et al. (2005) suggested a LREE enrichment in OCs from Oman, without presenting HREE concentrations. Saunier et al. (2010) mentioned the high amount of LREE in two highly weathered H5 and L6 OCs.

The goals of this study were to observe the possible differences between the REE contents of meteorites from different hot deserts (in particular Atacama and Lut) and to study the process of REE mobilization during weathering and its relationship to the finding region of the meteorite.

STUDIED METEORITES

In order to investigate the possible effects of meteorite recovery site on the concentrations of REE during weathering, OCs from two hot deserts with markedly different climatic settings were selected. The characteristics of the studied samples are described in the forthcoming subsections.

Ordinary Chondrites from Lut Desert

With an annual precipitation of $\leq$28 mm yr^{-1} (in the marginal regions) and maximum ground temperature of up to 70° C (in the desert) (Djamali et al. 2011; Mildrexler et al. 2011) along with the increasing number of meteorite finds (Pourkhorsandi and Mirnejad 2013; Pourkhorsandi et al. 2016), the Lut desert in Iran has the characteristics of a suitable place for preserving meteorites.

For this study, we selected a set of OCs from different regions of Lut whose characteristics and finding places are presented in Table 1 and Fig. 1a. The analyzed samples comprise meteorites from LL, L, and H groups with petrologic types varying between three and six. Intense oxidation of Fe-Ni metal grains (>95% of them) is the prevalent characteristic of these meteorites (Fig. 2a). According to the method of Wlotzka (1993), weathering degrees of these samples are between W3 and W5. Iron oxides/oxyhydroxides occur as individual patches, veins (along and/or perpendicular to cracks), and lamellar structures occupying former Fe-Ni metal, troilite, and silicate locations. Reflected light optical microscopy reveals the alteration of troilite to pyrite/marcasite—rather than Fe oxides/oxyhydroxides—in some of these samples.

Ordinary Chondrites from Atacama Desert

The central depression of the Atacama, the driest and oldest hot desert on Earth (Hartley et al. 2005), is responsible for the preservation of very old surfaces containing unique meteorite accumulation areas (e.g., San Juan, and El Médano). Other meteorite dense collection areas (DCAs) occur in the domain of the coastal range, known as La Yesera and Pampa de Mejillones DCAs, with a different climatic condition, due to the presence of oceanic aerosols and morning mist coming from the Pacific Ocean. Extreme aridity and the surface stability of the Atacama lower the rate of chemical weathering of meteorites compared to those reported from other hot deserts (Gattacceca et al. 2011) —in this case Lut. Unlike the relatively low number of recovered meteorites from Lut, the Atacama hosts the highest number of meteorites per surface area reported so far (Gattacceca et al. 2011; Hutzler et al. 2016).

In this work, we used samples previously classified and described by Valenzuela (2011) from La Yesera and Pampa de Mejillones DCAs, which are located near to

Table 1. Meteorites studied in this work.

Meteorite	Type	Weathering degree	Terrestrial age (ka)[a]
Ordinary chondrites from Atacama			
La Yesera 01	H6	W3	10.79 ± 1.56
La Yesera 02	LL5	W2	25.44 ± 4.45
La Yesera 03	L4	W4	16.98 ± 2.47
La Yesera 04	L6	W3	34.07 ± 1.92
Pampa (a)	L6	W2	25.08 ± 1.46
Pampa (b)	L4/5	W3	21.29 ± 2.45
Pampa (c)	L4	W4	13.89 ± 2.08
Pampa (d)	L5	W2/3	14.18 ± 1.91
Pampa (g)	L5	W3	14.34 ± 1.62
PdM 02	H5	W3	3.86 ± 1.36
PdM 04	L6	W4/5	23.98 ± 4.40
PdM 07	L6	W4	>27.9
PdM 10	L5	W3	18.06 ± 1.90
PdM 11	L5	W5	4.35 ± 1.34
PdM 12	H4/5	W5	>34.3
PdM 14	L/LL4-6	W2	12.54 ± 1.95
San Juan 01	L5	W2	>28.1
San Juan 02	H6	W2	19.44 ± 1.69
EM 49	H4	W3	1890 ± 80
Estacion Imilac	H5	W1	–
Cobija	H6	W1	19.7 ± 4.20
Rencoret	H6	W3	25.3 ± 6.4
Lutschaunig's Stone	L6	W1	9.2 ± 1.6
CeC 06	L6	W3	2345 ± 80
Paposo	LL6	W2	>49.2
Ordinary chondrites from Lut			
Lut 01	H5	W3	–
Lut 03	L3	W3	–
Lut 06	LL3	W3	–
Lut 08	H4	W5	–
Lut 09	H4	W4	–
Kerman 01	H5	W4	–
Kerman 02	L6	W3	–
Kerman 03	L5	W2	–
Shahdad	H5	W4	–
Ordinary chondrites from Sahara			
Aridal 06	H6	W4	–

[a]Terrestrial age data from Valenzuela (2011) by ^{14}C, and Hutzler (2015) by $^{36}Cl/^{41}Ca$. PdM, Pampa de Mejillones; EM, El Médano; CeC, Caleta el Cobre.

the Pacific coast (Fig. 1b) and are affected by the considerable presence of coastal fog, which means a higher amount of NaCl in the regional soils. Most of these samples were found on sand dunes, in the context of Pleistocene sandstones with paleo-costal lines, with the presence of carbonates in the soils.

To compare the chemical behavior of meteorites from different regions of the same desert, samples from San Juan and El Médano DCAs were chosen. These two regions are different from the coastal regions, as they are situated in much drier climatic conditions. Volcanic rocks cover the surface of these areas, with remarkable presence of gypsum and anhydrite as caliche layers.

Similar to the Lut meteorites, OCs from LL, L, and H groups are included (Table 1). The selected meteorites exhibit weathering degrees between W1 and W5 with a mode at W3. In comparison to meteorites from other hot deserts, Atacama samples have long terrestrial ages. For instance, based on the $^{36}Cl/^{41}Ca$ terrestrial age determinations, Hutzler (2015) presented ages of 1900 ± 80 ka and 2590 ± 100 ka for El Médano 049 and Caleta el Cobre 006 meteorites, respectively. Gattacceca et al. (2011) and Valenzuela (2011) also reported relatively old terrestrial ages (see Table 1 and see the Discussion section).

In addition to these meteorites, an OC from the Sahara (Aridal 006) was selected for analysis and comparison to these measurements.

METHODOLOGY

To prepare the powder used for measuring the abundances of REE in bulk meteorites, samples were examined under a stereomicroscope to check for the presence of any terrestrial material (e.g., cemented or enclosed sand grains inside cracks, fusion crust, desert varnish, and other sedimentary crusts). Each of these materials shows different geochemical behaviors and their contamination can affect the analysis result. For instance, desert varnish tends to show high REE contents (Goldsmith et al. 2014). Thus, care was taken to separate the mentioned products from the exterior and interior of the meteorites. Samples were taken from the interior and from the freshest parts of the meteorites, away from the fusion crust (where present) and the mentioned terrestrial products. To have a representative aliquot of whole rock composition, approximately 1.5–2 g of each meteorite was finely hand-ground in an agate mortar and then carefully homogenized.

Inductively coupled plasma–mass spectrometry (ICP-MS) instruments (VG PQII Plus STE and Perkin-Elmer NexION® 300x) at the Dipartimento di Scienze della Terra of the Università di Pisa were used to determine the trace elements (herein REE, Sr, and Ba) contents of the meteorite samples. About 50–100 mg of each powder was dissolved in a mixture of HF and HNO_3 on a hot plate at ~120° C inside screw-top perfluoroalkoxy (PFA) vessels. It is possible that this dissolution procedure could incompletely dissolve celestine ($SrSO_4$) or barite ($BaSO_4$), which might eventually occur in the samples. However, we always obtained very clear final sample solutions. The sample solutions were then spiked with Rh, Re, and Bi as internal standards (20 ng mL^{-1} in the final solutions) and diluted to 50 mL in polypropylene flasks. In each step of sample preparation, Mill-Q® purified water

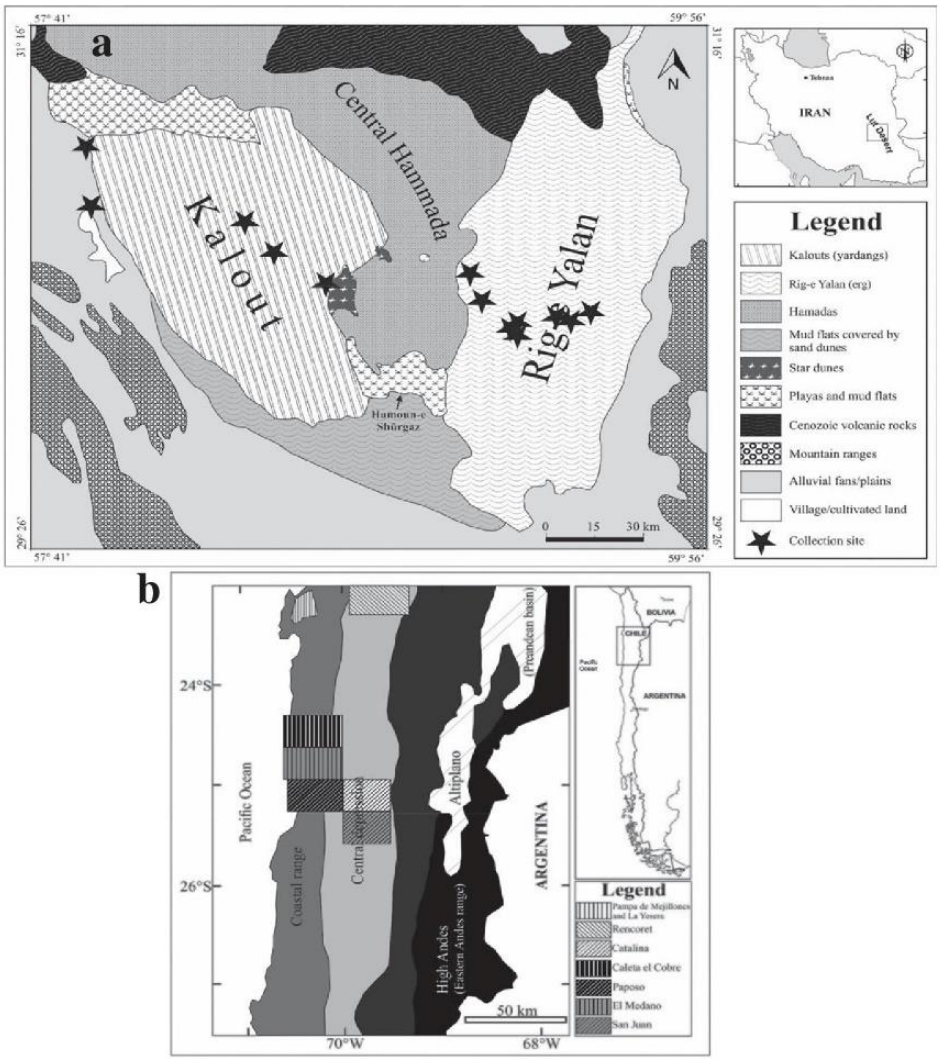

Fig. 1. a) Map of the central Lut Desert and the find locations of the meteorites studied. b) Map of the Atacama Desert and the location of the dense collection areas (DCAs) from which meteorites were used in this study.

(18.2 M cm), and ultrapure HF and HNO_3 were used. The correction procedure included 1) blank subtraction, 2) instrumental drift correction using internal standardization and repeated (every five samples) analysis of a drift monitor, and 3) oxide-hydroxide interference correction. The geochemical reference samples with basaltic composition WS-E, PM-S, and BIR-1, and the Allende chondrite reference sample (USNM 3529, splite 20, and position 22) were dissolved and analyzed along with the unknown samples to check the accuracy of the results. In Table 2, the results are reported for the four analyzed reference sample with literature values, and the detection limits for each analyte were calculated as six times the standard deviation of the blank counts. The analytical precision is between 5 and 10% RSD for elements with concentrations >0.5 μg g^{-1} and between 10 and 20% RSD for elements with concentrations <0.5 μg g^{-1}.

To investigate the effect of surface soil chemical composition and to observe any possible significant anomaly, representative soil samples collected from a hilltop close to Estacion Catalina (25°12.673′S, 69°41.894′W) were used in this study. This region which occurs in the Catalina DCA is composed of igneous rocks with the presence of caliche layers and has very similar lithology to San Juan and El Médano DCAs. Samples containing gravel and soils were collected from depths of 0 to 0.5 cm and 0.5 to 5 cm. The gravels and soils (<2 mm) were then sieved and separated for subsequent analyses. Soil concentrate samples were pulverized to

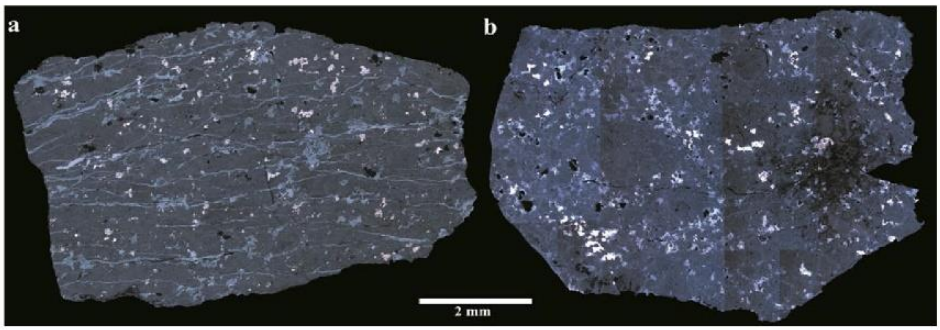

Fig. 2. Mosaic pictures of (a) Kerman 001 and (b) El Médano 049 prepared in reflected polarized light show the different weathering types of the meteorites. Kerman 001 contains clear parallel veins filled with weathering products and represents much stronger weathering than El Médano 049 whose Fe-Ni metal and troilite are not completely altered. (Color figure can be viewed at wileyonlinelibrary.com.)

85% passing 75 μm in tungsten-carbide mill. Total chemistry for major and trace elements was determined using ICP-MS and ICP-AES after a lithium metaborate fusion of each soil sample at the ALS Geochemistry©.

Rare earth elements anomalies represent deviations from neighboring elements based on the expected change in REE abundances as a function of atomic number and ionic radii (Lipin and McKay 1989). To calculate Ce and Eu anomalies, the values were normalized to the corresponding OC group (LL, L, and H) by using the following equations (Dauphas and Pourmand 2015):

$$Ce/Ce^{*} = Ce_N/(La_N^{0.48} \times Pr_N^{0}Pr_N^{0.52}) \quad (1)$$

$$Eu/Eu^{*} = Eu_N/(Sm_N^{0.45} \times Gd_N^{0}Gd_N^{0.55}) \quad (2)$$

where N stands for the normalization of REE to mean OC composition.

The contents of Sr and Ba have been shown to be suitable chemical proxies to evaluate the amount of chemical weathering and differentiate the meteorite collection regions (Al-Kathiri et al. 2005; Folco et al. 2007; Zurfluh et al. 2012).

RESULTS

Meteorite Samples

Rare earth elements, Sr, and Ba concentrations of the meteorites studied are reported in Table 3. The REE data of each group are normalized to the corresponding mean composition of Wasson and Kallemeyn (1988). Masuda–Coryell diagrams of the studied meteorites together with the data of OCs from Oman (Al-Kathiri et al. 2005), UAE (Hezel et al. 2011), Sahara desert (Folco et al. 2007; Saunier et al. 2010), and Europe (Folco et al. 2007) are shown in Fig. 3. Both enrichment and depletion elemental patterns compared to the corresponding OC mean composition can be seen in the diagrams.

ΣREE values in the Atacama and Lut samples have a range of 3.55–5.77 (avg. 4.46; std. 0.79) ppm and 2.98–3.76 (avg. 3.42; std. 0.30) ppm for H, 2.97–6.45 (avg. 3.97; std. 0.88) ppm and 3.26–2.93 (avg. 3.63; std. 0.28) ppm for L, and 3.21–9.82 (avg. 5.95; std. 2.81) ppm (just for Atacama) for LL OCs, respectively (Table 3). These data show a higher amount of REEs in Atacama meteorites than those of Lut.

A closer look at the normalized REE patterns (Fig. 3) reveals an enrichment in La for some samples. This can be up to 2.64 × H in El Médano 049, with an average amount of 1.79 × H (n = 8) and 1.22 × H (n = 5) for Atacama and Lut meteorites, respectively. Likewise, La is enriched up to 2.98 × L in Caleta el Cobre 006, which is an L OC. Average La_N amounts of Atacama and Lut samples are 1.40 × L (n = 14) and 1.15 × L (n = 3), respectively. Among the studied meteorites, Paposo exhibits a remarkable La enrichment (4.05 × LL).

The general shape of the normalized spider diagrams (Fig. 3) indicates the occurrence of a fractionation between light REEs (LREEs) and heavy REEs (HREEs). Figure 4 displays the values of La_N/Lu_N (as an indicative of LREE/HREE fractionation) versus La_N for H and L OCs from different regions. Most of the samples show LREE/HREE ratios of more than 1. The Atacama and Sahara samples tend to represent higher degrees of REE fractionation than Lut and UAE samples. The Gd_N/Yb_N (as an indicator of MREE/HREE fractionation) ratios for the studied samples are mostly less than 1, but as the values are near the error zone, they will not be discussed further.

Cerium and Eu show both negative and positive anomalies (Table 3, Fig. 3). In H OCs, the variation range of Ce/Ce* and Eu/Eu* values for Atacama samples (0.60–1.69 and 0.56–1.08, respectively) is

Table 2. Concentrations (μg g^{-1}) of Sr, Ba, and REE in the four geochemical reference materials analyzed by ICP-MS along with the unknown samples. Literature values for these reference materials are also reported. The last column reports the detection limits (μg g^{-1}) of the used analytical method.

Element	Allende (this work)	Allende (literature)[a]	BIR-1 (this work)	BIR-1 (literature)[b]	WS-E (this work)	WS-E (literature)[c]	PM-S (this work)	PM-S (literature)[c]	Detection limit
Sr	14.5	12 ± 3	122	108	450	410 ± 5	307	280 ± 5	0.5
Ba	4.5	4 ± 1	<10	7	342	338 ± 6	139	148 ± 3.2	0.6–10
La	0.49	0.52 ± 0.04	0.62	0.62	27.6	27 ± 1.1	2.63	2.8 ± 0.17	0.02
Ce	1.24	1.33 ± 0.08	1.90	1.95	60	61 ± 1.4	6.5	6.8 ± 1.25	0.06
Pr	0.21	0.21 ± 0.01	0.39	0.38	8.0	7.8 ± 0.4	1.05	1.08 ± 0.16	0.007
Nd	1.01	0.99 ± 0.03	2.45	2.5	33.3	33 ± 0.7	5.4	5.5 ± 0.25	0.03
Sm	0.33	0.34 ± 0.02	1.10	1.1	8.8	8.8 ± 0.3	1.78	1.75 ± 0.05	0.02
Eu	0.09	0.11 ± 0.01	0.53	0.54	2.31	2.25 ± 0.04	1.04	1.07 ± 0.04	0.05
Gd	0.39	0.42 ± 0.02	1.96	1.85	7.4	7.2 ± 0.23	2.05	2 ± 0.1	0.004
Tb	0.07	0.081 ± 0.010	0.38	0.36	1.10	1.1 ± 0.04	0.35	0.36 ± 0.02	0.002
Dy	0.46	0.42 ± 0.03	2.78	2.5	6.5	6 ± 0.16	2.18	2 ± 0.1	0.005
Ho	0.10	0.10 ± 0.01	0.59	0.57	1.18	1.2 ± 0.06	0.42	0.42 ± 0.03	0.006
Er	0.29	0.29 ± 0.01	1.81	1.7	3.17	3 ± 0.11	1.19	1.1 ± 0.06	0.01
Tm	0.05	0.0572	0.26	0.26	0.42	0.43 ± 0.03	0.16	0.17 ± 0.01	0.003
Yb	0.31	0.30 ± 0.02	1.70	1.65	2.56	2.5 ± 0.1	0.96	1 ± 0.05	0.007
Lu	0.04	0.052 ± 0.006	0.26	0.26	0.36	0.37 ± 0.01	0.14	0.15 ± 0.01	0.002

[a]Jarosewich et al. (1987).
[b]Govindaraju (1994).
[c]Govindaraju (1995).

broader than those of Lut (0.92–0.96 and 0.96–1.29, respectively). In general, no pronounced difference in the amounts of Ce/Ce* and Eu/Eu* between different OC groups exists. A remarkable positive Ce anomaly is evident in Cobija (H6) and Lutschaunig's Stone (L6) (Figs. 3a and 3b). Note that these two meteorites are the least weathered samples (W1) studied so far from the Atacama.

The negative Tm anomaly among the analyzed samples (Fig. 3) is similar to the Tm anomaly in the CI-normalized patterns described from ordinary chondrites (e.g., Dauphas and Pourmand 2015). However, it is not the case here for OC-normalized samples. It should be noted that the seemingly more negative anomalies in H OCs relative to that of L OCs are not real but occurred as the result of the normalization errors.

Logarithmic plot of Sr versus Ba for the OCs from Atacama, Oman, and Sahara is shown in Fig. 5. Different chemical trends are particularly more pronounced among those from the Atacama and Oman.

Atacama Soil Samples

The major and trace element composition of the analyzed soil samples are reported in Table 4. As reflected in their SiO_2 content, the parent rock material is basaltic/andesitic but the soil consists of more acidic (granitic) material than the gravels, which is transported by eolian processes from neighboring lithologies. Both CI-normalized REE patterns of gravels and <2 mm fractions of the soils are fractionated, showing LREE enrichments and a relatively flat HREE (Fig. 6). The LREE enrichment in the <2 mm soil is higher than the parent rock gravels (La_N/Lu_N mean values 9.1 versus 6.7), which is related to the weathering of the parent rock and the higher mobility of LREE into the soils during rock weathering process (Kabata-Pendias and Pendias 2001). The same process explains the negative Eu anomaly of the soils compared to the gravels and more resistance of Eu hosting grains during weathering. However, the chemical differences mentioned between the bedrock and the soil could also affect these patterns.

Comparison of the analyzed samples with the REE composition of upper crust composition (UCC) (Kemp and Hawkesworth 2004) and mean terrestrial soil composition references (Govindaraju 1994; Kabata-Pendias and Pendias 2001) shows their similarity, which implies a well-mixed texture from various bedrocks. In contrast to the Atacama meteorites that generally show higher REE concentrations compared to the other hot desert meteorites, the soils show REE chemical compositions comparable to the UCC and mean soil composition and without any significant compositional difference.

Table 3. Strontium, Ba, and bulk REE composition (μg g^{-1}) and the calculated ratios of the studied meteorites.

Meteorite	Sr	Ba	La	Ce	Pr	Nd	Sm	Eu	Gd	Tb	Dy	Ho	Er	Tm	Yb	Lu	ΣREE	Ce/ Ce*	Eu/ Eu*	Tm/ Tm*	La_N/ Lu_N	La_N/ Sm_N	Gd_N/ Yb_N	Sr/ Ba
La Yesera 01	30.6	38	0.76	1.63	0.22	1.01	0.27	<0.05	0.31	0.05	0.38	0.08	0.23	0.03	0.22	0.03	5.3	0.92	0.56	0.86	2.27	1.73	0.98	0.79
La Yesera 02	26.3	50	0.54	1.54	0.18	0.81	0.23	0.10	0.31	0.05	0.39	0.08	0.25	0.04	0.25	0.03	4.8	1.08	1.28	1.13	1.73	1.52	0.90	0.53
La Yesera 03	37	12.6	0.45	1.12	0.17	0.86	0.26	<0.05	0.29	0.05	0.38	0.09	0.27	0.04	0.25	0.05	4.3	0.90	0.58	0.92	1.04	1.07	0.83	2.99
La Yesera 04	12.4	7.5	0.31	0.81	0.13	0.61	0.20	0.07	0.25	0.05	0.31	0.08	0.21	0.03	0.21	0.03	3.3	0.93	1.03	0.87	0.93	0.97	0.84	1.67
Pampa (a)	18.1	4.1	0.30	0.85	0.12	0.61	0.21	0.10	0.24	0.05	0.33	0.08	0.22	0.03	0.23	0.03	3.4	0.99	1.41	0.88	1.16	0.93	0.75	4.41
Pampa (b)	21.1	5.0	0.29	0.75	0.12	0.52	0.23	0.07	0.23	0.04	0.29	0.07	0.19	0.03	0.20	0.03	3.06	0.91	0.97	0.93	1.14	0.81	0.84	4.21
Pampa (c)	31.8	14.6	0.40	0.94	0.15	0.70	0.23	0.09	0.29	0.05	0.35	0.08	0.26	0.04	0.25	0.04	3.9	0.86	1.06	0.89	1.17	1.10	0.81	2.18
Pampa (d)	21.3	4.8	0.26	0.70	0.11	0.59	0.19	<0.05	0.24	0.04	0.31	0.07	0.21	0.03	0.19	0.03	3.0	0.95	0.75	0.92	0.87	0.84	0.87	4.39
Pampa (g)	38.6	42	0.55	1.08	0.17	0.82	0.26	<0.05	0.32	0.05	0.35	0.09	0.26	0.03	0.23	0.04	4.2	0.81	0.55	0.83	1.39	1.31	0.99	0.92
PdM 02	17.6	5.9	0.43	1.22	0.17	0.73	0.23	0.07	0.25	0.05	0.31	0.08	0.23	0.03	0.23	0.03	4.1	1.05	0.95	0.84	1.45	1.19	0.76	2.96
PdM 04	23.6	8.3	0.39	0.97	0.14	0.68	0.21	0.08	0.25	0.05	0.31	0.07	0.20	0.03	0.21	0.03	3.6	0.92	1.07	0.97	1.24	1.16	0.85	2.82
PdM 07	42	66	0.66	1.13	0.20	0.92	0.25	0.10	0.32	0.06	0.37	0.08	0.25	0.03	0.23	0.03	4.6	0.70	1.13	0.88	1.91	1.65	0.98	0.64
PdM 10	26.1	5.3	0.29	0.88	0.12	0.55	0.21	0.08	0.26	0.05	0.31	0.07	0.19	0.03	0.23	0.03	3.3	1.06	1.10	0.85	0.97	0.90	0.80	4.91
PdM 11	11.3	5.1	0.32	0.82	0.12	0.62	0.22	0.07	0.27	0.05	0.33	0.08	0.24	0.04	0.22	0.03	3.4	0.94	0.94	1.02	1.19	0.90	0.85	2.19
PdM 12	39	21.3	0.43	1.07	0.14	0.68	0.20	0.07	0.25	0.05	0.33	0.07	0.23	0.03	0.21	0.02	3.8	1.00	1.08	0.84	1.69	1.36	0.80	1.85
PdM 14	18.4	12.5	0.27	0.92	0.12	0.59	0.19	<0.05	0.25	0.05	0.30	0.08	0.200	0.03	0.19	0.03	3.2	1.11	0.74	1.08	0.92	0.88	0.94	1.47
San Juan 01	71	52	0.57	1.17	0.18	0.77	0.24	0.11	0.27	0.05	0.34	0.07	0.20	0.03	0.21	0.03	4.3	0.83	1.35	1.00	1.77	1.48	0.89	1.37
San Juan 02	39	9.4	0.38	0.91	0.14	0.69	0.18	<0.05	0.24	0.05	0.32	0.08	0.24	0.03	0.21	0.03	3.5	0.92	0.77	0.75	1.12	1.28	0.80	4.24
EM 49	45	270	0.78	1.34	0.25	1.22	0.31	0.10	0.44	0.07	0.49	0.10	0.30	0.04	0.27	0.04	5.8	0.69	0.91	0.82	1.87	1.56	1.13	0.17
Estacion Imilac	11.8	9.8	0.44	1.03	0.16	0.71	0.21	0.07	0.27	0.05	0.34	0.08	0.24	0.03	0.24	0.03	3.9	0.90	0.97	0.82	1.35	1.29	0.78	1.20
Cobija	15.8	6.2	0.33	1.48	0.12	0.62	0.19	0.07	0.25	0.04	0.33	0.07	0.21	0.03	0.19	0.03	4.0	1.69	1.05	0.85	1.03	1.08	0.89	2.57
Rencoret	26.1	12.9	0.68	1.62	0.22	1.01	0.27	0.09	0.32	0.05	0.35	0.08	0.25	0.04	0.24	0.03	5.2	0.97	0.97	0.81	2.04	1.58	0.89	2.01
Lutschaunig's Stone	10.4	4.2	0.35	1.83	0.14	0.69	0.22	0.07	0.30	0.05	0.38	0.09	0.25	0.03	0.23	0.03	4.7	1.84	0.92	0.89	1.06	0.98	0.92	2.48
CeC 06	72	326	0.92	1.89	0.28	1.22	0.32	0.10	0.40	0.07	0.48	0.10	0.31	0.04	0.28	0.04	6.4	0.85	0.87	0.90	2.46	1.80	1.01	0.22
Paposo	41	70	1.48	3.49	0.50	1.88	0.46	0.10	0.48	0.08	0.52	0.11	0.31	0.05	0.30	0.05	9.8	0.88	0.68	0.99	2.92	2.06	1.15	0.58
Lut 01	62	<10	0.30	0.72	0.11	0.50	0.18	0.08	0.23	0.04	0.30	0.06	0.20	0.03	0.20	0.03	2.98	0.92	1.28	0.82	1.02	1.06	0.80	6.2
Lut 03	91	<10	0.34	0.81	0.12	0.58	0.18	0.07	0.26	0.04	0.33	0.07	0.20	0.03	0.19	0.03	3.26	0.90	1.01	0.94	1.20	1.20	0.94	9.1
Lut 06	126	20.8	0.37	0.92	0.14	0.68	0.23	0.08	0.29	0.06	0.37	0.08	0.24	0.04	0.26	0.03	3.8	0.86	1.01	0.96	1.10	1.04	0.82	6.1
Lut 08	72	<10	0.31	0.79	0.12	0.62	0.20	0.07	0.26	0.05	0.32	0.07	0.20	0.03	0.20	0.03	3.28	0.96	0.96	0.86	1.01	0.99	0.87	7.1
Lut 09	497	14.3	0.33	0.84	0.12	0.62	0.19	0.07	0.25	0.05	0.31	0.07	0.20	0.03	0.20	0.03	3.3	0.95	1.08	0.86	1.03	1.08	0.85	34
Kerman 01	165	<10	0.38	0.93	0.14	0.70	0.21	0.08	0.30	0.05	0.36	0.08	0.22	0.03	0.22	0.03	3.7	0.93	0.99	0.87	1.16	1.12	0.96	16.5
Kerman 02	33	<10	0.35	0.90	0.14	0.66	0.22	0.08	0.29	0.05	0.38	0.08	0.24	0.03	0.23	0.04	3.7	0.91	1.00	0.89	1.07	1.02	0.88	3.3
Kerman 03	41	<10	0.43	1.00	0.14	0.70	0.22	0.08	0.30	0.05	0.37	0.08	0.24	0.03	0.24	0.04	3.9	0.92	1.06	0.87	1.27	1.23	0.89	4.1
Shahdad	141	<10	0.47	1.04	0.14	0.66	0.20	0.07	0.25	0.05	0.33	0.07	0.20	0.03	0.21	0.03	3.8	0.93	1.07	0.85	1.63	1.46	0.79	14.1
Aridal 06	17.9	23.7	0.29	0.70	0.10	0.49	0.16	0.08	0.21	0.04	0.28	0.06	0.18	0.03	0.18	0.03	2.84	0.94	1.49	0.82	1.01	1.14	0.80	0.76

PdM, Pampa de Mejillones; EM, El Médano; CeC, Caleta el Cobre.

DISCUSSION

Our results show that terrestrial weathering may significantly modify the whole rock REE distribution of OCs from hot deserts. However, this modification varies among different deserts. Atacama OCs have higher concentrations of REE and their compositions have been affected to a greater extent than those of Lut.

REE Mobilization During Meteorite Weathering: A Concise Review

Some of the first plausible evidence for REE mobilization during terrestrial weathering of meteorites was reported by Masuda et al. (1977) and Masuda and Tanaka (1978) on samples from Antarctica. These authors, however, considered the differences in the abundance of REE between the internal and external portions of meteorite samples to be intrinsic and primary rather than produced by terrestrial effects. Further studies on Antarctic achondrites attributed the modified REE compositions to cold-desert weathering (Shimizu et al. 1983; Floss and Crozaz 1991; Mittlefehldt and Lindstrom 1991; Shinonaga et al. 1994; Kagi and Takahashi 1998; Swindle et al. 1998). The most prevalent results of weathering effects are LREE-enriched patterns with notable Ce (and in some cases Eu) anomalies produced by aqueous leaching. In a process proposed by Mittlefehldt and Lindstrom (1991) and confirmed by Floss and Crozaz (1991), during the exposure of a meteorite to atmosphere and its heating by the Sun at the surface in Antarctica, surrounding meltwater can penetrate the meteorite through cracks and fractures. In equilibrium with atmospheric CO_2, this fluid becomes a weak carbonic acid solution which could leach the minerals such as Ca-phosphates and causes removal of trivalent REEs. In addition to being in +3 state, Ce and Eu occur as tetravalent and divalent ions, respectively. As Ce^{+4} is less soluble than the +3 REEs and Eu is largely retained in the +2 state in plagioclase (which is relatively unaffected by weathering), these two elements are preferentially retained in the sample and thus show their corresponding anomalies. Another study by Kagi and Takahashi (1998) showed a correlation between Ce anomalies and absorbed water content in Antarctic lunar meteorites that demonstrated the terrestrial origin of these anomalies.

Following the studies on the Antarctic meteorites, attempts were made to investigate the possible weathering effects on hot desert achondrites (both in mineral and whole rocks). In order to monitor the weathering of recently fallen meteorites, Barrat et al. (1999) analyzed fragments of Tatahouine diogenite recovered just 63 yr after its fall. By comparing the REE composition with those of the fragments recovered immediately after the fall, elevated amounts of LREE were found in one of the fragments. This study revealed the disturbance of trace element composition of meteorites in relatively short time spans in a terrestrial environment. Crozaz et al. (2003) evaluated the mineral composition of different achondrite groups by secondary ion mass spectrometry (SIMS) and attributed the elevated levels of LREE in olivine and low-Ca pyroxene to terrestrial contamination. However, Barrat et al. (2003) did not find any significant weathering effects on whole rock REE composition of eucrites from the Sahara desert. A similar conclusion was made during a study of NWA 4872 brachinite by Hyde et al. (2014).

Effects of Weathering on the REE Composition of Atacama and Lut OCs

The aliquots analyzed in our work were from a large mass (about 2 g) of well-mixed powder, so the formation of the observed REE patterns by a nugget effect of REE-rich components is unlikely. Deviations of more than ±10% from the mean composition of the corresponding meteorite groups assure us that the enrichments/depletions are significant.

Unlike the Atacama OCs, those from Lut do not show profound changes in ΣREE (Table 3). Chemical modification of a meteorite during weathering, including changes in REE content, is controlled by several factors such as primary chemical composition, modal composition, degree of recrystallization, shock stage, terrestrial age, and locality (Crozaz et al. 2003). Rare earth elements which are mostly concentrated in Ca-phosphates and silicates (Ebihara and Honda 1984) are released during the weathering of these minerals. This process is facilitated by formation of sulfuric acid inside the meteorite as a result of troilite (FeS) oxidation in contact with meteoric water (e.g., Bland et al. 2006). With the development of primary mineral dissolution, REEs tend to concentrate in veins filled with iron oxides/oxyhydroxides (Thiagarajan and Aeolus Lee 2004).

In contrast to meteorites from Antarctica, which release their REE during weathering on ice, an increase in REE concentration is expected for hot desert meteorites as a consequence of residing on a relatively REE-rich soil surface (Crozaz and Wadhwa 2001). Once a meteorite with its relatively high initial porosity falls on a hot desert surface, soil salts dissolved by water infiltrate into it by capillary forces triggered by temperature fluctuations (Zurfluh 2012). In addition, wind activity, burial in soil, and desert varnish

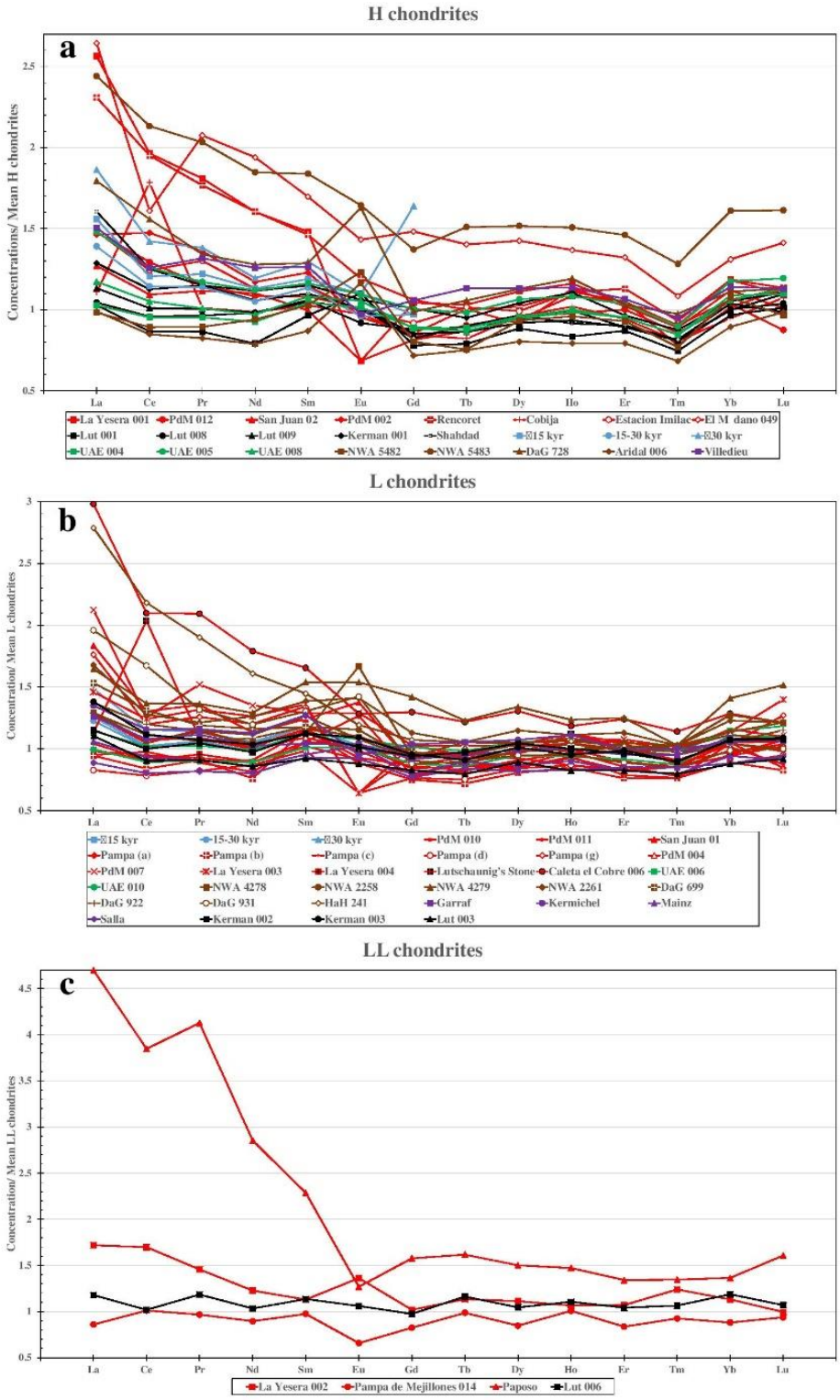

Fig. 3. Normalized REE spider diagrams of (a) H, (b) L, and (c) LL ordinary chondrites. For comparison, the data of OCs from Oman (the average values for different age classes) (Al-Kathiri et al. 2005), UAE (Hezel et al. 2011), Sahara desert (Folco et al. 2007; Saunier et al. 2010), and Europe (Folco et al. 2007) are used along the data of this work. PdM is the abbreviated form of Pampa de Mejillones. (Color figure can be viewed at wileyonlinelibrary.com.)

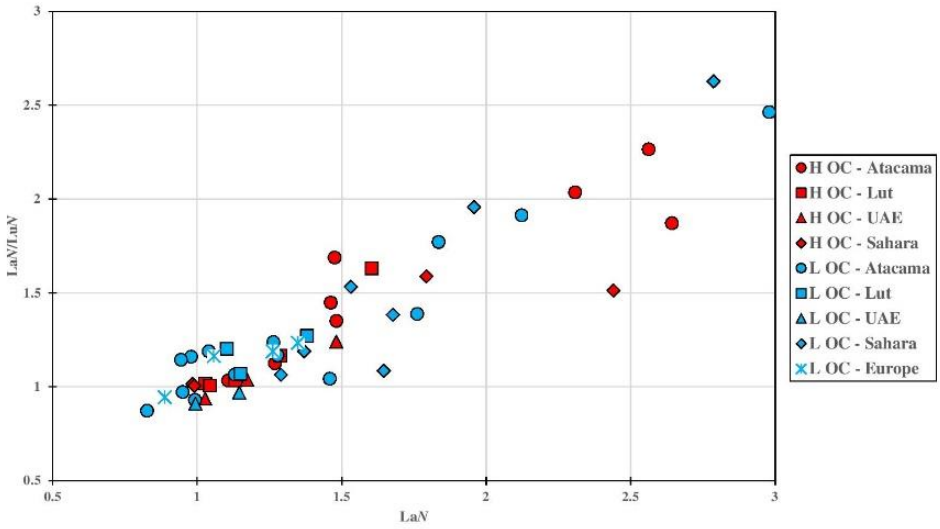

Fig. 4. La_N/Lu_N versus La_N for H and L OCs from different regions. For comparison, the data of OCs from Oman (Al-Kathiri et al. 2005), UAE (Hezel et al. 2011), Sahara desert (Folco et al. 2007; Saunier et al. 2010), and Europe (Folco et al. 2007) are used along the data of this work. (Color figure can be viewed at wileyonlinelibrary.com.)

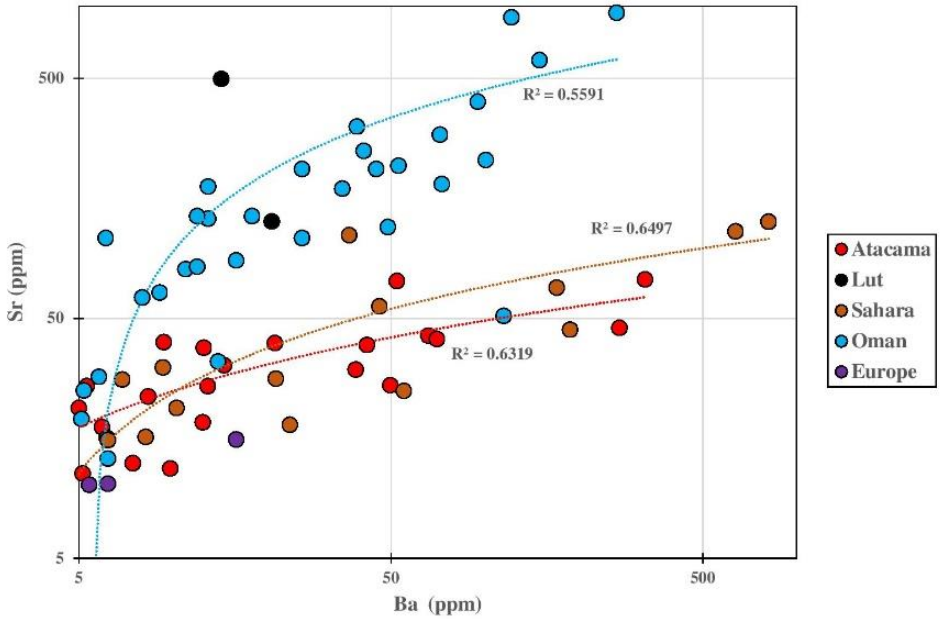

Fig. 5. Sr versus Ba logarithmic plot showing OCs from various areas. The data of OCs from Oman (Al-Kathiri et al. 2005), Sahara desert (Folco et al. 2007; Saunier et al. 2010), and Europe (Folco et al. 2007) are shown along the data of this work. Some samples from Lut with Ba <10 ppm are also included. (Color figure can be viewed at wileyonlinelibrary.com.)

formation introduce terrestrial minerals containing REE, or cause the modification of REE patterns of primary minerals (Crozaz et al. 2003). We suggest that the notable increase in ΣREE contents of the Atacama OCs is caused by these kind of implementations.

Is the modification in REE concentration controlled by the weathering degree of a meteorite? The data of Lut OCs (Tables 1 and 3) show that despite having high degrees of weathering, their ΣREE do not change as much as the Atacama samples. For example, Kerman 001 (W4), which was half-buried in a valley in the Kalout formation with a soil composed of clay, sand, evaporites, and carbonates (Farpoor and Krouse 2008) at the time of recovery

Table 4. Major and trace element chemical composition of soil and gravel sample from Estacion Catalina in the Atacama Desert. Trace element concentration unit is ppm.

	SV2 < 2 mm soil				SV1 gravels			
	CS-Surface-01	CS-Surface-02	CS-1-01	CS-1-02	CS-Surface	CS-1-01	CS-1-02	CS-5
Depth (cm)	0–0.5	0–0.5	0.5–5	0.5–5	0–0.5	0–0.5	0.5–5	>34
SiO_2	59.8	60.4	58	58	53	52.5	57.8	52.5
Al_2O_3	14.65	14.65	14.6	14.65	17.35	17	16.6	17.15
Fe_2O_3	8.09	7.88	7.56	7.62	8.13	8.29	6.99	8.21
CaO	4.42	4.11	3.9	3.97	8.88	8.72	7.46	9.44
MgO	2.11	1.98	2.19	2.23	5.52	5.51	3.82	5.55
Na_2O	2.96	2.84	2.48	2.53	2.94	2.8	2.75	3.04
K_2O	2.42	2.37	2.31	2.31	1.17	1.12	1.3	1.11
Cr_2O_3	0.01	0.01	0.01	0.01	0.01	0.01	0.01	0.01
TiO_2	1.19	1.16	1.08	1.1	1.05	1.06	0.98	1.07
MnO	0.14	0.16	0.12	0.13	0.13	0.14	0.15	0.13
P_2O_5	0.19	0.2	0.21	0.23	0.27	0.23	0.23	0.23
Total %	96.14	95.92	92.6	92.92	98.6	97.53	98.27	98.58
Rb	84.1	85.4	95	91.6	30.5	25.4	35.6	19.2
Sr	525	483	423	421	931	865	878	921
Ba	931	954	789	782	412	384	779	360
La	25.8	26.1	26.1	25.8	19.6	18.8	20.1	17.9
Ce	52	53	52.6	52.4	42.2	40.4	45.6	38.7
Pr	6.3	6.4	6.4	6.4	5.3	5.1	5.3	4.9
Nd	24.3	24.3	25	24.4	21.8	21.1	21.5	20.5
Sm	4.9	4.6	4.9	4.8	4.3	4.3	4.3	4.1
Eu	1.2	1.3	1.2	1.2	1.4	1.4	1.4	1.4
Gd	5	4.7	5	4.7	4.8	4.4	4.8	4.4
Tb	0.7	0.7	0.7	0.6	0.7	0.6	0.7	0.6
Dy	3.7	3.7	3.8	3.8	3.8	3.8	3.9	3.6
Ho	0.7	0.7	0.7	0.7	0.7	0.7	0.7	0.7
Er	2.3	2.2	2.3	2.2	2.2	2.2	2.3	2.1
Tm	0.3	0.3	0.3	0.3	0.3	0.2	0.3	0.3
Yb	2.1	2.1	2.1	2	2	1.9	2.1	1.9
Lu	0.3	0.3	0.3	0.3	0.3	0.3	0.3	0.3
La_N/Lu_N	9.1	9.2	9.2	9.1	6.9	6.6	7.1	6.3

and exhibits well-developed parallel weathering veins (Fig. 2a), does not show any noticeable deviation from the mean composition. In comparison, the Atacama samples that are generally less weathered show higher ΣREE. For example, El Médano 049, which contains the highest ΣREE among the studied H OCs and was recovered from a deflated soil surface on granitoids, is also highly weathered (W3, Fig. 2b), although less than Kerman 001. Compared to samples from other regions, we see that three highly weathered H OCs from UAE (Hezel et al. 2011) and even weathered samples from Europe (Folco et al. 2007) show ΣREE contents similar to Lut samples. However, ΣREE is elevated in highly weathered Saharan OCs (analyzed by Saunier et al. 2010) and Aridal 006 (W4). Therefore, the meteorite weathering as shown by weathering degree (Wlotzka 1993) and veins filled with secondary products is not the only factor responsible for the ΣREE increase.

As for REEs, different chemical trends in Sr and Ba are also evident in meteorites from different regions (Figs. 5 and 7). Al-Kathiri et al. (2005) and Folco et al. (2007) showed that the weathering of meteorites in Oman and Sahara deserts (respectively) increases the Sr and Ba contents of meteorites. The carbonate basement and the Sr- and Ba-rich soils in Oman deserts are responsible for the further enrichments of these elements in the recovered meteorites from the region. In some cases from Oman, high concentrations of Sr and Ba in the soil lead to the formation of secondary celestine and barite inside the meteorites (Al-Kathiri et al. 2005). Meteorites from Atacama exhibit a different trend compared to Oman meteorites (Fig. 5). The majority of collecting site of the meteorites from Atacama is mostly made of volcanics and evaporites (Valenzuela 2011), which usually have lower concentrations of Sr and Ba than carbonates. The difference in the soil type can explain different trends in the Sr budget. Compared to

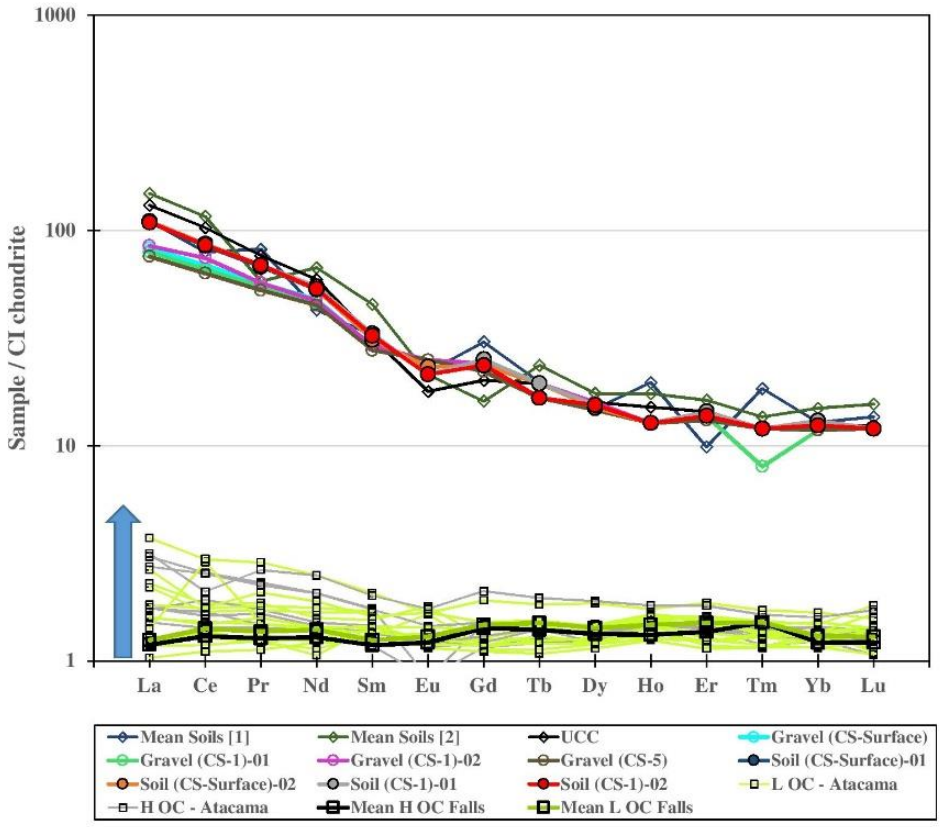

Fig. 6. REE chemical composition of Estacion Catalina soil composition compared to the mean terrestrial soil compositions (Govindaraju 1994; Kabata-Pendias and Pendias 2001). The Atacama H and L OCs show LREE enrichment in relation to falls in an attempt to reach equilibrium during the hot desert terrestrial weathering. (Color figure can be viewed at wileyonlinclibrary.com.)

the Omani and Atacama OCs, the samples from Lut desert have very low Ba contents (<10 ppm). On the other hand, Sr concentrations of Lut OCs are in the range of Omani meteorites. Considering Sr and La contents (Fig. 7), again we see difference in the chemical composition of meteorites from different regions. These differences can be used as proxies which allow distinguishing between Atacama meteorites from Oman and Lut. Al-Kathiri et al. (2005) reported a positive correlation between weathering degree and Sr, Ba concentration for Omani OCs; however, we do not see any correlation between these parameters for the meteorites from Atacama and Lut samples.

The Atacama Desert has exceptionally high meteorite concentrations compared to other hot deserts. In a study of 22 meteorites, Gattacceca et al. (2011) found half of the meteorites with terrestrial ages older than 20 ka, which is much older than the age ranges reported from other hot deserts. We may hypothesize that the generally high terrestrial age of the Atacama meteorites is the main reason for their high ΣREE amounts. A similar effect of terrestrial age on REE content can be seen in higher amounts of La in very old meteorites from Atacama and in samples with terrestrial ages of more than >30 kyr from Oman (Al-Kathiri et al. 2005) (Fig. 3a).

Most of the Atacama and some highly weathered Saharan OCs show differentiated REE patterns (Figs. 3 and 4). As the soil and sedimentary materials typically exhibit higher LREE contents (Aide and Aide 2012), as observed in our analyzed samples from the Atacama, the residence of a meteorite on a soil surface increases the LREE content of the meteorite (Dreibus et al. 2001; Crozaz et al. 2003; Al-Kathiri et al. 2005). The studied meteorites and their REE patterns, which tend to converge toward that of the surface material, are consistent with the assumption that soil has affected their chemical composition (Fig. 6). Taking into account the different soil types of the meteorite collecting sites (carbonate in Oman versus volcanic/evaporitic in Atacama and clay/sand in Lut), it can be deduced that nearly all of the meteorites represent approximately similar LREE-enriched patterns which form as a result of both (1) higher abundance of LREE

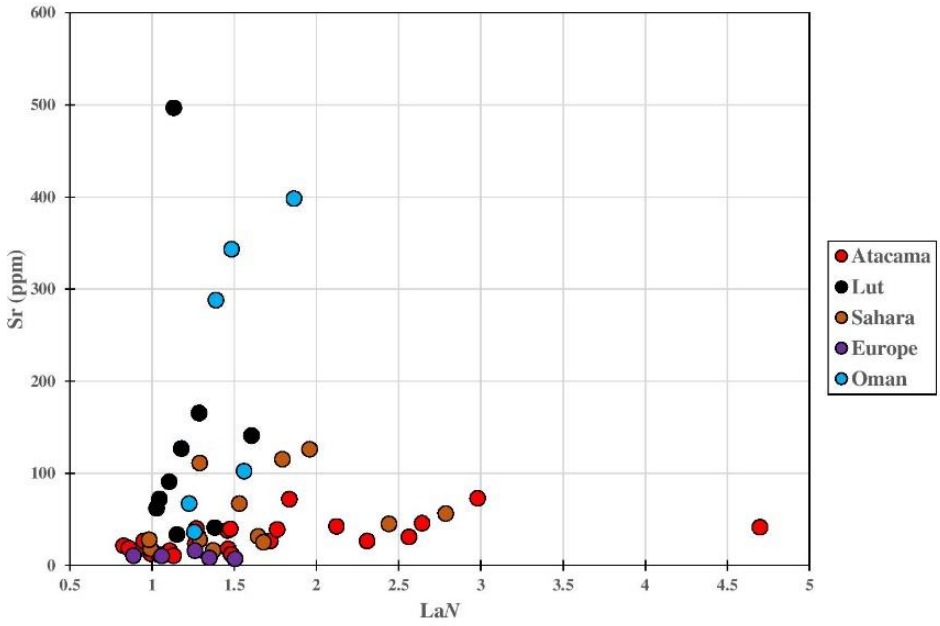

Fig. 7. Different chemical trends of OCs from different regions can be seen in the Sr versus La_N plot. The data of L and H OCs from Oman, in different age classes (Al-Kathiri et al. 2005), Sahara desert (Saunier et al. 2010; Folco et al. 2007), and Europe (Folco et al. 2007) are shown along the data of this work. (Color figure can be viewed at wileyonlinelibrary.com.)

in soils and (2) higher solubility of LREE (Aide and Aide [2012] and references therein).

Different clay and iron oxide/oxyhydroxide minerals display specific Ce and Eu anomalies. These minerals, which are the main components of soils, occur in different proportions based on the soil type; as a result, different Ce and Eu anomalies are exhibited in different soils (Laveuf and Cornu 2009). Although most of the Ce anomalies in our data are small and hardly significant, two slightly weathered (W1) meteorites (Cobija and Lutschaunig's Stone) display notable positive Ce anomalies (Figs. 3a and 3b) that might reveal the incipient phase of REE modification during weathering. Cerium is the most abundant REE in the average soil composition (Aide and Aide 2012). Once the meteorite falls, the initial physical soil contamination through cracks and fractures gives it a positive Ce anomaly. By developing the chemical weathering, trivalent REEs of the soil with higher solubility rates than Ce^{+4} infiltrate the meteorite, and most of the Ce oxides to Ce^{+4} and is preferentially retained in the soil. Progressive alteration of the meteorite and the addition of trivalent REEs remove the initial positive Ce anomaly. At higher residence times and more interaction of terrestrial contaminants with meteorite, the amount of La and Pr exceeds the Ce concentration and creates a negative Ce anomaly that is evident in the REE patterns of some meteorites with high terrestrial ages such as La Yesera 003, Caleta el Cobre 006, Paposo, and El Médano 049 (Fig. 3). Variation in Eu anomalies among studied meteorites can result from contamination by different soil components, although the presence of possible primary plagioclase should not be excluded as an explanation.

Putting these data together, we hypothesize that terrestrial age rather than weathering degree is the main governing factor of REE content and its modification in hot desert OCs, even though degree of weathering and terrestrial age at a given recovery site show a positive correlation (e.g., Bland et al. 2006). Indeed, the formation of secondary oxidation products decreases the porosity of the meteorite by filling the fractures and cracks which are the pathways for REE containing terrestrial fluid to circulate and solid materials to penetrate (Bland et al. 2006). The earlier this process initiates, the lower the possibility that a terrestrial material is able to affect the REE composition of the meteorite. However, in areas with low weathering rates (like Atacama), greater amounts of soil and fluid penetrate the meteorite and modify the composition readily.

We observe that as the meteorites from Atacama are older than those from Lut and other regions (Sahara, Oman), and also owing to low weathering rates in the former, more time has been available for the terrestrial environment to affect the chemistry of Atacama OCs by means of different interactions. The

terrestrial ages of Saharan meteorites used in this study are not determined; however, by comparing their weathering degree with terrestrial age of other meteorites collected from this desert (e.g., Welten et al. 2004), their terrestrial ages are expected to be high. The prevailing humid environment for UAE and Europe and thus higher weathering rates (Folco et al. 2007; Hezel et al. 2011) might have prevented the formation of a pronounced ΣREE increase in meteorites from these area. We believe that the terrestrial age range of highly weathered Lut meteorites shall be in the range of UAE meteorites. The occurrence of archaeological sites in the surroundings of Lut (e.g., Muscarella 2001) points to wetter climatic conditions, at least periodically over the last 10 kyr compared to today. This is in agreement with the high weathering degree and the lack of a pronounced ΣREE change in the chemical composition of Lut OCs.

A large number of meteorites from Atacama are expected to be recovered in the future (Gattacceca et al. 2011; Hutzler et al. 2016). Hence, care must be taken into account while working on the REE composition of even "fresh-looking" Atacama meteorites.

CONCLUSIONS

The chemical compositions of OCs from Atacama and Lut along with the published data from other hot desert areas reveal a difference in the effects of terrestrial weathering on REE distribution between these populations. Optimal conditions for meteorite preservation in the Atacama Desert (i.e., high stability of the surface and low meteorite weathering rates) provide enough time for the meteorites to interact efficiently with terrestrial materials. In contrast, higher weathering rates of the meteorites from other hot deserts (specifically Lut) prevent such interactions. As a consequence, the highly weathered meteorites from Lut desert have lower ΣREE contents than those of the moderately weathered meteorite from Atacama. In some cases, even the OCs with minor weathering from Atacama show modified REE patterns with notable positive Ce anomaly. These anomalies may have been created by the initial physical contamination (the addition of soil or dust directly into the fractures, rather than more time-consuming chemical weathering) and then by the addition of trivalent REEs. Notwithstanding the lack of terrestrial age data for Lut meteorites, it is envisaged on the basis of almost unaffected REE compositions and high weathering degrees that this area was wetter than today over the last tens of thousands of years and generally had a climate similar to the UAE and Oman deserts.

Future investigations on the mobilization of REE isotopes, which are being used frequently in cosmochemistry, are needed to estimate their behavior during weathering.

Acknowledgments—We thank the staff of the Cultural Office of the French Embassy in Tehran who supported the field trips in Iran and a Ph.D. thesis grant for the first author. Providing samples by Rodrigo Martínez, Edmundo Martínez, Enrique Stucken, and the Natural History Museum of London is appreciated. M.V. thanks the support by CONICYT-FONDECYT project No 3140562. H. P. thanks Morteza Djamali for his suggestions during preparation of the manuscript. We thank A. J. T. Jull for editorial handling, and P. Bland and an anonymous referee for their constructive reviews.

Editorial Handling—Dr. A. J. Timothy Jull

REFERENCES

Aide M. T. and Aide C. 2012. Rare earth elements: Their importance in understanding soil genesis. *ISRN Soil Science* 2012:1–11.

Al-Kathiri A., Hofmann B. A., Jull A. J. T., and Gnos E. 2005. Weathering of meteorites from Oman: Correlation of chemical and mineralogical weathering proxies with 14 C terrestrial ages and the influence of soil chemistry. *Meteoritics & Planetary Science* 1239:1215–1239.

Barrat J. A., Gillet P., Lesourd M., Blichert-Toft J., and Poupeau G. R. 1999. The Tatahouine diogenite: Mineralogical and chemical effects of sixty-three years of terrestrial residence. *Meteoritics & Planetary Science* 34:91–97.

Barrat J. A., Jambon A., Bohn M., Blichert-Toft J., Sautter V., Göpel C., Gillet P., Boudouma O., and Keller F. 2003. Petrology and geochemistry of the unbrecciated achondrite Northwest Africa 1240 (NWA 1240): An HED parent body impact melt. *Geochimica et Cosmochimica Acta* 67:3959–3970.

Bischoff A., Jersek M., Grau T., Mirtic B., Ott U., Kučera J., Horstmann A., Laubenstein M., Herrmann S., Řanda Z., Weber M., and Heusser G. 2011. Jesenice-A new meteorite fall from Slovenia. *Meteoritics & Planetary Science* 46:793–804.

Bland P. A., Berry F. J., and Pillinger C. T. 1998. Rapid weathering in Holbrook; an iron-57 Mossbauer spectroscopy study. *Meteoritics & Planetary Science* 33:127–129.

Bland P. A., Zolensky M. E., Benedix G. K., and Sephton M. A. 2006. Weathering of chondritic meteorites. In *Meteorites and the early solar system II*, edited by Lauretta D. and McSween H. Y. Tucson, Arizona: University of Arizona Press. pp. 853–867. http://www.lpi.usra.edu/books/MESSII/9041.pdf.

Boynton W. V. 1975. Fractionation in the solar nebula: Condensation of yttrium and the rare earth elements. *Geochimica et Cosmochimica Acta* 39:569–584.

Boynton W., Starzyk P., and Schmitt R. 1976. Chemical evidence for the genesis of the ureilites, the achondrite

Chassigny and the nakhlites. *Geochimica et Cosmochimica Acta* 40:1439–1447.

Buddhue J. D. 1939. The oxidation of meteorites. *Contributions of the Society for Research on Meteorites* 2:75–79.

Crozaz G. and Wadhwa M. 2001. The terrestrial alteration of saharan shergottites Dar al Ganid 476 and 489: A case study of weathering in a hot desert environment. *Geochimica et Cosmochimica Acta* 65:971–978.

Crozaz G., Floss C., and Wadhwa M. 2003. Chemical alteration and REE mobilization in meteorites from hot and cold deserts. *Geochimica et Cosmochimica Acta* 67:4727–4741.

Dauphas N. and Pourmand A. 2015. Thulium anomalies and rare earth element patterns in meteorites and Earth: Nebular fractionation and the nugget effect. *Geochimica et Cosmochimica Acta* 163:234–261.

Djamali M., Akhani H., Khoshravesh R., Ponel P., and Brewer S. 2011. Application of the global bioclimatic classification to Iran: Implications for understanding the modern vegetation and biogeography. *Ecologia Mediterranea* 37:91–114.

Dreibus G., Huisl W., Haubold R., and Jagoutz E. 2001. Influence of terrestrial desert weathering in Martian meteorites (abstract 50). *Meteoritics & Planetary Science* 36.

Ebihara M. and Honda M. 1984. Distribution of rare earth elements and uranium in various components of ordinary chondrites. *Meteoritics* 19:69–77.

Farpoor M. H. and Krouse H. R. 2008. Stable isotope geochemistry of sulfur bearing minerals and clay mineralogy of some soils and sediments in Loot Desert, central Iran. *Geoderma* 146:283–290.

Floss C. and Crozaz G. 1991. Ce anomalies in the LEW85300 eucrite: Evidence for REE mobilization during Antarctic weathering. *Earth and Planetary Science Letters* 107:13–24.

Folco L., D'Orazio M., and Perchiazzi N. 2007. Authenticating the recovery location of meteorites: The case of Castenaso. *Meteoritics & Planetary Science* 42:321–330.

Gattacceca J., Valenzuela M., Uehara M., Jull A. J. T., Giscard M., Rochette P., Braucher R., Suavet C., Gounelle M., Morata D., Munayco P., Bourot-Denis M., Bourles D., and Demory F. 2011. The densest meteorite collection area in hot deserts: The San Juan meteorite field (Atacama Desert, Chile). *Meteoritics & Planetary Science* 46:1276–1287.

Goldsmith Y., Stein M., and Enzel Y. 2014. From dust to varnish: Geochemical constraints on rock varnish formation in the Negev Desert, Israel. *Geochimica et Cosmochimica Acta* 126:97–111.

Gooding J. L. 1982. Mineralogical aspects of terrestrial weathering effects in chondrites from Allan Hills, Antarctica. *Lunar and Planetary Science* 12B:1105–1122.

Govindaraju K. 1994. 1994 compilation of working values and sample description for 383 geostandards. *Geostandards and Geoanalytical Research* 18:1–158.

Govindaraju K. 1995. 1995 working values with confidence limits for twenty-six CRPG, ANRT and IWG-GIT geostandards. *Geostandards and Geoanalytical Research* 19:1–32.

Hartley A. J., Chong G., Houston J., and Mather A. E. 2005. 150 million years of climatic stability: Evidence from the Atacama Desert, northern Chile. *Journal of the Geological Society* 162:421–424.

Hezel D. C., Schlüter J., Kallweit H., Jull A. J. T., Al Fakeer O. Y., Al Shamsi M., and Strekopytov S. 2011. Meteorites from the United Arab Emirates: Description, weathering, and terrestrial ages. *Meteoritics & Planetary Science* 46:327–336.

Hutzler A. 2015. The flux of meteorites on Earth: Contribution of measuring the concentration of multiple cosmogenic nuclides, and collections in arid areas. Aix-Marseille Université, Marseille, France.

Hutzler A., Gattacceca J., Rochette P., Braucher R., Carro B., Christensen E.J., Cournede C., Gounelle M., Laridhi Ouazaa N., Martinez R., Valenzuela M., Warner M., and Bourles D. 2016. Description of a very dense meteorite collection area in western Atacama: Insight into the long-term composition of the meteorite flux to Earth. *Meteoritics & Planetary Science* 51:468–482.

Hyde B. C., Day J. M. D., Tait K. T., Ash R. D., Holdsworth D. W., and Moser D. E. 2014. Characterization of weathering and heterogeneous mineral phase distribution in brachinite Northwest Africa 4872. *Meteoritics & Planetary Science* 49:1141–1156.

Inoue M., Nakamura N., and Kimura M. 2009. Tetrad effects in REE abundance patterns of chondrules from CM meteorites: Implications for aqueous alteration on the CM parent asteroid. *Geochimica et Cosmochimica Acta* 73:5224–5239.

Jarosewich E., Clarke C. R. S., and Barrows J. N. 1987. Allende meteorite reference sample. *Smithsonian Contributions to the Earth Sciences* 27:1–49.

Kabata-Pendias A. and Pendias H. 2001. Trace elements in soils and plants. Boca Raton, Florida: CRC Press. 23 p.

Kagi H. and Takahashi K. 1998. Relationship between positive cerium anomaly and adsorbed water in Antarctic lunar meteorites. *Meteoritics & Planetary Science* 33:1033–1040.

Kemp A. I. S. and Hawkesworth C. J. 2004. Granites and differentiation of the continental crust. *Geochimica et Cosmochimica Acta* 68:A667.

Koeberl C. and Cassidy W. A. 1989. Differences between Antarctic and non-Antarctic meteorites. *An assessment. Geochimica et Cosmochimica Acta.* 55:3–18.

Laveuf C. and Cornu S. 2009. A review on the potentiality of rare earth elements to trace pedogenetic processes. *Geoderma* 154:1–12.

Lipin B. R. and McKay G. A. 1989. Geochemistry and mineralogy of rare earth elements. In *rare earth element chemistry*, edited by Lipin B. R. and McKay G. A. Chantilly, Virginia: Mineralogical Society of America. pp. 345–373.

Llorca J., Roszjar J., Cartwright J. A., Bischoff A., Ott U., Pack A., Merchel S., Rugel G., Fimiani L., Ludwig P., Casado J. V., and Allepuz D. 2013. The Ksar Ghilane 002 shergottite—The 100th registered Martian meteorite fragment. *Meteoritics & Planetary Science* 48:493–513.

Masuda A. and Tanaka T. 1978. REE, Ba, Sr and Rb in the Yamato meteorites, with special reference to Yamato-691 (a), -692(b) and -693(c). *Memoirs of National Institute of Polar Research.* Special issue8:229–232.

Masuda A., Tanaka T., Asakura J., and Shimizu H. 1977. REE, Rb, Sr and Ba abundances in Yamato (j),(k) and (m) meteorites *Antarctic Record* 58:197–203.

Mildrexler D. J., Zhao M., and Running S. W. 2011. Satellite finds highest land skin temperatures on Earth. *Bulletin of the American Meteorological Society* 92:855–860.

Mittlefehldt D. W. and Lindstrom M. M. 1991. Generation of abnormal trace element abundances in Antarctic eucrites

by weathering processes. *Geochimica et Cosmochimica Acta* 55:77–87.

Murrell M. and Burnett D. 1983. The behavior of actinides, phosphorus, and rare earth elements during chondrite metamorphism. *Geochimica et Cosmochimica Acta* 47:1999–2014.

Muscarella O. W. 2001. Jiroft and "Jiroft-Aratta": A review article of Yousef Madjidzadeh, "Jiroft: The Earliest Oriental Civilization." *Bulletin of the Asia Institute* 15:173–198.

Olsen E. and Fuchs L. H. 1967. The state of oxidation of some iron meteorites. *Icarus* 6:242–253.

Pillinger C. T., Greenwood R. C., Gibson J. M., Pillinger J. M., and Gibson E. K. 2013. The Holbrook Meteorite—99 years out in the weather. 44th Lunar and Planetary Science Conference. LPI Contribution No. 1719. Houston, Texas: Lunar and Planetary Institute. 2883 p.

Pourkhorsandi H. and Mirnejad H. 2013. Lut Desert (Iran): A high-potential area for finding meteorites. 44th Lunar and Planetary Science Conference. CD-ROM.

Pourkhorsandi H., Mirnejad H., Rochette P., and Hassanzadeh J. 2016. Lut 009, an H4 (S2, W4) ordinary chondrite meteorite from Lut Desert of Iran. *Journal of the Earth and Space Physics* 41:125–130.

Saunier G., Poitrasson F., Moine B., Gregoire M., and Seddiki A. 2010. Effect of hot desert weathering on the bulk-rock iron isotope composition of L6 and H5 ordinary chondrites. *Meteoritics & Planetary Science* 45:195–209.

Shimizu H., Masuda A., and Tanaka T. 1983. Cerium anomaly in REE pattern of Antarctic eucrite. Memoirs of National Institute of Polar Research. Special issue 30:341–348.

Shinonaga T., Endo K., Ebihara M., Heumann K. G., and Nakahara H. 1994. Weathering of Antarctic meteorites investigated from contents of Fe^{3+}, chlorine, and iodine. *Geochimica et Cosmochimica Acta* 58:3735–3740.

Socki R. A., Gibson E. K., Jull A. J. T., and Karlsson H. R. 1991. Carbon and oxygen isotope composition of carbonates from an L6 chondrite: Evidence for terrestrial weathering from the Holbrook meteorite. *Meteoritics* 26:396.

Swindle T. D., Kring D. A., Burkland M. K., Hill D. H., and Boynton W. V. 1998. Noble gases, bulk chemistry, and petrography of olivine-rich achondrites Eagles Nest and Lewis Cliff 88763: Comparison to brachinites. *Meteoritics & Planetary Science* 33:31–48.

Thiagarajan N. and Aeolus Lee C.-T. 2004. Trace-element evidence for the origin of desert varnish by direct aqueous atmospheric deposition. *Earth and Planetary Science Letters* 224:131–141.

Torigoye-Kita N., Misawa K., and Tatsumoto M. 1995. U-Th-Pb and Sm-Nd isotopic systematics of the Goalpara ureilite: Resolution of terrestrial contamination. *Geochimica et Cosmochimica Acta* 59:381–390.

Valenzuela E. M. 2011. Procesos de Meteorización en Condritos Ordinarios del Desierto de Atacama, Norte de Chile: Nuevos Antecedentes sobre Meteorización de Material Extraterrestre en Ambientes Desérticos. Universidad de Chile.

Velbel M. A. 2014. Terrestrial weathering of ordinary chondrites in nature and continuing during laboratory storage and processing: Review and implications for Hayabusa sample integrity. *Meteoritics & Planetary Science* 49:154–171.

Wasson J. T. and Kallemeyn G. W. 1988. Compositions of chondrites. *Philosophical Transactions of the Royal Society A: Mathematical, Physical and Engineering Sciences* 325:535–544.

Welten K. C., Nishiizumi K., Finkel R. C., Hillegonds D. J., Jull A. J. T., Franke L., and Schultz L. 2004. Exposure history and terrestrial ages of ordinary chondrites from the Dar al Gani region, Libya. *Meteoritics & Planetary Science* 39:481–498.

White J. S., Henderson E. P., and Mason B. 1967. Secondary minerals produced by weathering of Wolf Creek meteorite. *The American Mineralogist* 52:1190–1197.

Wlotzka F. 1993. A weathering scale for the ordinary chondrites. *Meteoritics* 28:460.

Zurfluh F. J. 2012. Quantification of terrestrial weathering and contamination in meteorites recovered in the Sultanate of Oman. Universität Bern.

Zurfluh F. J., Hofmann B. A., Gnos E., Eggenberger U., Greber N. D., and Villa I. M. 2012. Weathering and strontium contamination of meteorites recovered in the sultanate of Oman. *Meteorite* 2000:34–38.

Left blank intentionally.

Chapter 6

“Unique” Meteorites from Hot Deserts: the Case of EM 301

Peer-reviewed research paper *Pourkhorsandi et al., Geochimica et Cosmochimica Acta, 2017*

Available online at www.sciencedirect.com

ScienceDirect

Geochimica et Cosmochimica Acta 218 (2017) 98–113

Geochimica et Cosmochimica Acta

www.elsevier.com/locate/gca

The ungrouped chondrite El Médano 301 and its comparison with other reduced ordinary chondrites

Hamed Pourkhorsandi [a,*], Jérôme Gattacceca [a], Bertrand Devouard [a], Massimo D'Orazio [b], Pierre Rochette [a], Pierre Beck [c], Corinne Sonzogni [a], Millarca Valenzuela [d,e]

[a] CNRS, Aix-Marseille Univ., IRD, Coll. France, CEREGE, Aix-en-Provence, France
[b] Dipartimento di Scienze della Terra, Università di Pisa, Pisa, Italy
[c] Institut de Planétologie et d'Astrophysique de Grenoble, Grenoble, France
[d] Millennium Institute of Astrophysics (MAS), Pontificia Universidad Católica de Chile, Santiago, Chile
[e] Instituto de Astrofísica, Pontificia Universidad Católica de Chile, Santiago, Chile

Received 27 January 2017; accepted in revised form 2 September 2017; Available online 12 September 2017

Abstract

El Médano 301 (EM 301) is an ungrouped chondrite with overall texture and trace-element distribution similar to those of ordinary chondrites (OCs), but with silicate (olivine and low-Ca pyroxene) compositions that are more reduced than those in OCs, with average olivine and low-Ca pyroxene of $Fa_{3.9\pm0.3}$ and $Fs_{12.8\pm4.9}$, respectively. These values are far lower than the values for OCs and even for chondrites designed as "reduced" chondrites. Low-Ca pyroxene is the dominant mineral phase and shows zoning with higher MgO contents along the crystal rims and cracks (reverse zoning). The Co content of kamacite is also much lower than the concentrations observed in OCs (below detection limit of 0.18 wt% versus 0.44–37 wt%). Oxygen isotopic composition is $\Delta^{17}O = +0.79,+0.78‰$ and slightly different from that of OCs. The lower modal olivine/pyroxene ratio, different Infrared (IR) spectra, lower Co content of kamacite, lower mean FeO contents of olivine and pyroxene, different kamacite texture, and different oxygen-isotopic composition show that EM 301 does not belong to a known OC group. EM 301 shows similarities with chondritic clasts in Cumberland Falls aubrite, and with Northwest Africa 7135 (NWA 7135) and Acfer 370 ungrouped chondrites. However, dissimilar to NWA 7135 and the clasts, it does not contain highly reduced mineral phases like daubréelite.

Our observations suggest the formation of EM 301 in a nebular region compositionally similar to OCs but with a different redox state, with oxygen fugacity (fO_2) in this region lower than that of OCs and higher than that of enstatite chondrites condensation region. A second, possibly nebular, phase of reduction by the production of reducing gas phases (e.g., C-rich) could be responsible for the subsequent reduction of the primary material and the occurrence of reverse zoning in the low-Ca pyroxene and lower average Fa/Fs ratio. Based on the IR spectra of EM 301 we suggest the possibility that the parent body of this chondrite was a V-type asteroid.

Keywords: Ordinary chondrite; Enstatite chondrite; Reduced chondrite; Solar nebula; Reduction

1. INTRODUCTION

Chondrites account for the vast majority of meteorites in our collections. Ordinary chondrites (OCs) are the most

* Corresponding author.
E-mail address: pourkhorsandi@cerege.fr (H. Pourkhorsandi).

https://doi.org/10.1016/j.gca.2017.09.013
0016-7037/

abundant and form a class divided into H, L, and LL groups. This division chiefly corresponds to variable oxidation state among the groups, as reflected in their mineralogy, whole-rock chemistry and oxygen-isotopic compositions. The fO_2 increases from H to LL chondrites (Rubin, 1990; Osadchii et al., 2017). Much more reduced than OCs, enstatite chondrites (ECs) show different whole-rock chemistry, mineral abundances, mineral chemistry, and oxygen-isotopic composition (e.g., Keil, 1989; Weisberg and Kimura, 2012; El Goresy et al., 2017). A significant compositional hiatus exists between the H and E chondrites, which may be an artefact due to incomplete sampling of an originally more continuous spectrum of chondritic material (Bild and Wasson, 1977). Considering average olivine and low-Ca pyroxene compositions, primitive achondrites such as winonaites, acapulcoites, and lodranites as well as chondritic clasts in the iron meteorites occur inside such a gap (e.g., Schrader et al., 2017). Moreover, a few ungrouped chondrites show intermediate compositions between H and E chondrites (Kallemeyn and Wasson, 1985). Their study may shed light on the condensation/accretion processes occurring in the nebula, and provide information, about their otherwise unsampled parent bodies.

Among these rare samples are dark chondritic clasts in the Cumberland Falls aubrite (CFC). These clasts have whole-rock chemical compositions similar to those of OCs, but have Mg-rich olivine ($Fa_{0.08–3.66}$) and pyroxene ($Fs_{0.07–14.5}$) compositions (e.g., Neal and Lipschutz, 1981). It was suggested that these clasts are the fragments of an otherwise unsampled "F chondrite" (F for "Forsterite") parent body which upon a collision with the aubrite parent body led to the formation of Cumberland Falls polymict breccia (Neal and Lipschutz, 1981). Another interpretation suggests that these clasts could have resulted from the reduction of a LL chondrite clasts in the presence of the highly reduced aubrite host (Kallemeyn and Wasson, 1985). Acfer 370, an ungrouped chondrite of petrologic type 3 (Moggi-Cecchi et al., 2009) and NWA 7135, an ungrouped chondrite of petrologic type 3/4 (Irving et al., 2015), are two other chondrites that show affinities with CFC. Other chondrites, defined as low-FeO ordinary chondrites, have OC whole-rock chemical composition but olivine and pyroxene richer in Mg than OCs (Wasson et al., 1993). Chondritic clasts inside IIE iron meteorites, defined as HH chondrites, with reduced olivine and pyroxene compositions and higher concentration of siderophile elements than OCs, are thought to be fragments of a different parent body than H chondrites (Bild and Wasson, 1977; Bogard et al., 2000; Schrader et al., 2017).

Here we report on the petrography, mineral chemistry, whole-rock trace-element composition, oxygen-isotopic composition, and IR-spectroscopy of EM 301, an ungrouped chondrite that shows similarities with NWA 7135, Acfer 370 and the CFC. NWA 7135 and CFC were also studied during this work for comparison.

2. SAMPLES AND METHODS

EM 301 was found in 2013 during a systematic search for meteorites in the Atacama Desert (Chile). It is composed of two stones found less than 1 m apart, and totaling 17.9 g. Both petrography and mineral chemistry analysis confirmed pairing of the two fragments. The whole meteorite is deposited at CEREGE. Magnetic susceptibility was measured on the two pieces using a KLY2 instrument from Agico (Rochette et al., 2003). Thick and thin polished sections were prepared from the two pieces. For comparison, thick polished sections of NWA 7135 (from CEREGE collection) and Cumberland Falls aubrite (section #2840-2 from Muséum National d'Histoire Naturelle-Paris) were examined. Mineralogical and petrological studies were conducted with a Leica DM2500P optical microscope and a Hitachi S3000-N Scanning Electron Microscope (SEM) equipped with a Bruker X-ray Energy Dispersive Spectrometer (EDS) at CEREGE (Aix-en-Provence). In addition, a Zeiss Gemini 500 SEM at CP2M (Marseille) was used for further imaging and elemental mapping. Chemical compositions of the mineral phases were determined with CAMECA SX100 electron microprobe at the CAMPARIS facility (Paris), using natural and synthetic standards, focused electron beam (~1 μm in diameter), an accelerating voltage of 15 kV and a beam current of 25 nA. To correct the deviation of Co content produced by the occurrence of an interference between Co and Fe of the metal grains (Afiattalab and Wasson, 1980), a correction for the Co content of by a factor equal to 0.0012 (Fe concentration) was applied.

The whole-rock trace-element content of EM 301 was determined by Inductively Coupled Plasma - Mass Spectrometry (ICP-MS) using a Perkin-Elmer NexION® 300x spectrometer at the Pisa University's Dipartimento di Scienze della Terra. The geochemical reference samples with basaltic composition WS-E and PM-S, and the Allende carbonaceous chondrite reference sample (USNM 3529, splite 20, position 22) were dissolved and analyzed along with EM 301 to check the accuracy of the results. About 50–100 mg of each powder were dissolved in a mixture of HF and HNO_3 on a hot plate at ~120 °C inside screw-top perfluoroalkoxy (PFA) vessels. Then the sample solutions were diluted to 50 mL in polypropylene vials. In each step of sample preparation, Mill-Q® purified water (18.2 M cm), ultrapure HF and HNO_3 were used. The sample solutions were introduced into the plasma after online mixing with a solution containing 20 ng/mL each of Rh, Re and Bi as internal standards. The elements Li, Be, Ga, Rb, Sr, Y, Zr, Nb, Mo, Cs, Ba, REE, Hf, Ta, W, Pb, Th, U were determined in "standard mode", whereas the elements Sc, V, Cu were determined in "kinetic energy discrimination mode, KED" using a He flow of 3.7 mL/min. Analyses were done using an external calibration performed with a solution of the BE-N (alkaline basalt) geochemical reference sample. In Table 1 the results of the ICP-MS analyses of Allende (two separate dissolutions), PM-S and WS-E, along with their reference values are reported. In the same table are reported the detection limits for each analyte calculated as three times the standard deviation of the procedural blank concentrations. The analytical precision is between 5% and 10% RSD for elements with concentrations >0.5 μg/g and between 10% and 20% RSD for elements with concentrations <0.5 μg/g.

Table 1
Trace-element concentrations (μg/g) determined by ICP-MS for EM 301 and for three geochemical reference samples. The last column reports the detection limit in the solid sample (μg/g) for each element.

	El Médano 301	Allende A this work	Allende B this work	PM-S this work	WS-E this work	Allende[a]	PM-S[b]	WS-E[b]	Detection Limit
Li	2.65	1.70	1.58	7.5	13.9	1.5	7.55	13.5	0.2
Be	0.04	0.04	0.04	0.30	1.10	n.d.	0.418	1.1	0.005
Sc	5.5	10.3	11.2	32.4	26.9	11.0	34	27.6	0.03
V	41	87	95	179	313	92	186.4	336	0.1
Cu	72	91	104	53	61	119	57.2	66.2	2
Ga	5.9	5.5	5.5	14.1	22.6	6.15	15.6	21.6	0.04
Rb	2.71	1.16	1.17	0.82	25.9	1.10	0.978	25.77	0.03
Sr	23.1	14.6	16.5	256	409	12	279.2	407.5	2
Y	2.04	2.72	2.81	10.8	32.6	3.10	11.31	31.8	0.01
Zr	5.9	7.0	7.1	35	202	9.0	38.2	203.6	0.05
Nb	0.37	0.58	0.58	2.21	17.9	0.62	2.44	17.89	0.06
Mo	4.1	4.0	n.d.	1.65	3.6	2.5	1.7	3.54	0.1
Cs	0.516	0.086	0.086	0.331	0.466	0.0857	0.372	0.482	0.01
Ba	105	4.4	4.8	145	340	4.00	148.1	335	0.6
La	0.609	0.487	0.508	2.43	26.4	0.52	2.683	26.61	0.02
Ce	1.56	1.27	1.30	6.5	61	1.33	6.87	59.8	0.06
Pr	0.188	0.191	0.198	1.01	7.8	0.210	1.069	7.74	0.006
Nd	0.828	0.951	1.026	5.3	32.9	0.990	5.52	32.77	0.03
Sm	0.229	0.304	0.315	1.70	8.6	0.340	1.784	8.7	0.006
Eu	0.087	0.104	0.112	1.05	2.23	0.110	1.069	2.206	0.001
Gd	0.311	0.421	0.396	2.15	7.3	0.420	2.04	7.24	0.005
Tb	0.054	0.074	0.072	0.342	1.10	0.081	0.338	1.082	0.001
Dy	0.341	0.486	0.479	2.11	6.3	0.420	2.095	6.131	0.004
Ho	0.074	0.102	0.104	0.426	1.19	0.100	0.428	1.176	0.001
Er	0.222	0.309	0.301	1.18	3.15	0.290	1.14	3.069	0.001
Tm	0.033	0.053	0.046	0.159	0.431	0.0572	0.169	0.422	0.001
Yb	0.208	0.303	0.301	0.968	2.53	0.300	0.997	2.513	0.001
Lu	0.033	0.046	0.046	0.148	0.377	0.052	0.151	0.357	0.001
Hf	0.170	0.195	0.202	1.06	5.3	0.210	1.1	5.2	0.001
Ta	0.025	0.042	0.040	0.17	1.15	n.d.	0.19	1.116	0.002
W	0.27	0.17	0.17	0.19	0.42	0.167	0.3	0.5	0.1
Pb	0.97	1.23	1.27	2.52	14.1	1.39	2.47	12.33	0.3
Th	0.115	0.082	n.d.	0.056	3.10	0.065	0.053	2.992	0.004
U	0.061	0.018	0.017	0.016	0.653	0.016	0.019	0.624	0.003

The unit is μg/g.
n.d. = not determined.
[a] Jarosewich et al. (1987) and Friedrich et al. (2003).
[b] GeoReM (Geological and Environmental Reference Materials) website (http://georem.mpch-mainz.gwdg.de.

Reflectance spectra of powders of EM 301 and NWA 7135 were obtained using the spectro-gonio-radiometer at the Institut de Planétologie de Grenoble (Brissaud et al., 2004; Beck et al., 2011).

Measurements of $\delta^{18}O$ and $\delta^{17}O$ of two 1.5 mg aliquot of silicates hand-picked from a powdered and acid-washed 200 mg bulk sample were carried out at the Stable Isotopes Laboratory of CEREGE, by laser fluorination coupled with isotope ratio mass spectrometry (IRMS) (Alexandre et al., 2006; Crespin et al., 2008) adapted for measurement of extraterrestrial materials (Suavet et al., 2010). The three oxygen isotopic compositions were measured with a dual-inlet mass spectrometer Thermo-Finnigan Delta Plus. The oxygen isotope results are expressed in ‰ versus the international reference standard V-SMOW: $\delta^{18}O = (((^{18}O/^{16}O)_{sample}/(^{18}O/^{16}O)_{V\text{-}SMOW} - 1) \times 1000$ and $\delta^{17}O = (((^{17}O/^{16}O)_{sample}/(^{17}O/^{16}O)_{V\text{-}SMOW} - 1) \times 1000$. The $\delta^{18}O$ and $\delta^{17}O$ values of the reference gas were calibrated with measurements of NBS28 standard ($\delta^{18}O = 9.60‰$, Gröning, 2004). $\Delta^{17}O$ is computed as $\Delta^{17}O = \ln(1 + \delta^{17}O) - \lambda \ln(1 + \delta^{18}O)$ with $\lambda = 0.5247$ (Miller, 2002). The $\delta^{17}O$ value of the NBS28 standard ($\delta^{17}O = 5.026‰$) was computed so as to give $\Delta^{17}O = 0‰$. The measurements were corrected on a daily basis using 1.5 mg quartz internal laboratory standard "Boulangé" (Alexandre et al., 2006; Suavet et al., 2010). During the analyzing period, the analytical uncertainties derived from repeated measurement (n = 29) of this internal laboratory standard are 0.09‰, 0.17‰, 0.05‰ for $\delta^{17}O$, $\delta^{18}O$ and $\Delta^{17}O$, respectively.

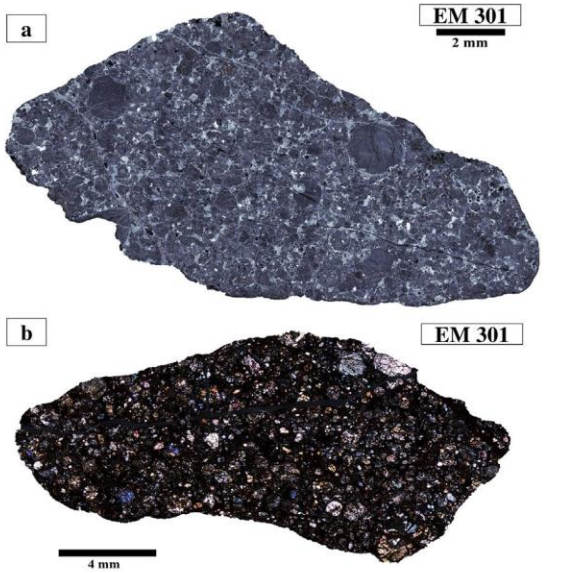

Fig. 1. Full section optical mosaic images of EM 301. (a) Thick polished section in reflected light showing the terrestrial weathering products as light grey patches and veinlets. Dark grey portions are silicates and white spots are the (Fe,Ni) metal grains. (b) Thin section in cross polarized light showing the chondritic textures. Porphyritic chondrules with higher abundance of pyroxene (low birefringence colors) are the dominant chondrule types. The other chondrule types based on their abundance are radial pyroxene, granular, cryptocrystalline, and barred olivine.

3. RESULTS

3.1. Petrography

3.1.1. El Médano 301

Due to wind abrasion in the desert environment, both stones are devoid of fusion crust. Cut surfaces of both pieces show a dark brown interior with visible chondrules and metal grains. Optical and electron microscope observations reveal well-preserved and closely packed chondrules and chondrule fragments (Fig. 1a). Modal abundances of chondrules and matrix measured by point counting (n = 720) are 80 vol% and 20 vol%, respectively. Porphyritic (POP, PO and PP), cryptocrystalline, radial pyroxene, barred olivine, barred pyroxene, and granular olivine-pyroxene chondrules are present (Fig. 1b). The porphyritic chondrules contain much higher pyroxene abundance than olivine and the PP chondrules are dominant. In addition, radial pyroxene chondrules are much more abundant than barred olivine chondrules, which are present only as two chondrules in a full thin section.

Average apparent chondrule diameter is 502 ± 319 μm (n = 99), with a median, mode, and maximum diameters of 400, 300, and ~ 2000 μm, respectively (Fig. 2). Low-Ca pyroxene is the main mineral and Mg-rich olivine, Ca-rich pyroxene, chlorapatite, albitic feldspar, chromite, troilite, (Fe,Ni) metal are the minor and accessory phases. Observation of a full section (~ 115 mm^2) shows that primary (Fe,Ni) metal and sulfides have been extensively (>95%) replaced by Fe oxides/hydroxides during terrestrial weathering, which corresponds to a weathering degree W4 using the ordinary chondrite scheme of Wlotzka (1993). Magnetic susceptibility is log χ = 4.62 (χ in 10^{-9} m^3/kg), but because of the extensive weathering, this value is not a direct proxy to the initial metal content. Point counting (n = 597) under reflected light optical microscopy, with a magnification of X500, yields the following proportions: 66 vol% silicates, 31 vol% weathering products, 2 vol% troilite, 0.7 vol% (Fe,Ni) metal and 0.5 vol% chromite. Using an average density of 4.5 g/cm^3 for the weathering products (intermediate value between goethite and magnetite), assuming that metallic, troilite and weathering products form a closed system in which total iron content is constant, and using the average abundance of troilite in OCs (5.3 wt %; Keil, 1962) as the initial troilite content, the initial metal content can be estimated to about 13 wt%. This value is near the lower limit of the values reported for H chondrites (14.2–19.8 wt%; Keil, 1962). Point counting survey on a ~500 × 500 μm backscattered electron (BSE) image (Fig. EA-1) gives the following modal abundances: 42 vol % low-Ca pyroxene, 6 vol% high-Ca pyroxene, 8 vol% olivine, 9 vol% feldspar and/or glass, and 32 vol% weathering products and opaque minerals. Olivine grains show sharp optical extinction and no strong fracturing, indicating a shock stage S1 (unshocked) using the classification of Stöffler et al. (1991), originally designed for ordinary chondrites. SEM-EDS analysis reveals that pyroxenes are Mg-rich and the abundant presence of type I chondrules

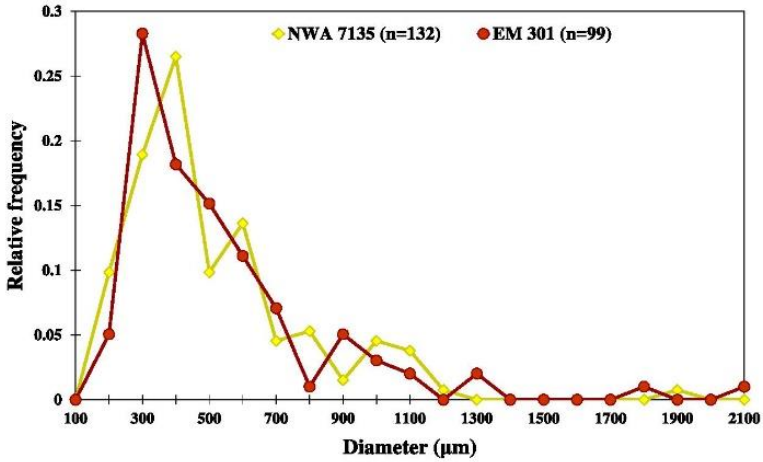

Fig. 2. Size frequency distribution of the chondrule diameters in EM 301 and NWA 7135. Horizontal axis values mark the upper limits of the size bins.

(Fig. 3a). Olivine is homogeneous in MgO content, whereas the majority of the low-Ca pyroxene grains show a reverse zoning with higher amount of MgO in the crystal rims and along cracks (Fig. 3b and c). Chondrule rims contain smaller grains of euhedral crystals (Fig. 3a and d). A pyroxene-dominated chondrule (Fig. 3a and d) shows aligned silica grains, (Fe,Ni) metal and regions differing in the MgO contents. Feldspar (plagioclase) is rare, but reaches up to 10 μm.

Troilite is monocrystalline, anhedral to subhedral in shape, and most often well separated from the (Fe,Ni) metal (Fig. 3e and f). Silicates with absorbed and rounded margins (and in some cases laths) occur inside some of the troilite grains (Fig. 3f). As mentioned, most of the metal grains are replaced by terrestrial weathering products, but those preserved show unusual textures like inclusions of Ni-rich (taenite) euhedral crystals in kamacite (Fig. 3e and g). This special (Fe,Ni) metal texture show similarities, though at a larger scale, with some metal spherules containing fine-grained plessitic intergrowth with submicrometers Ni-rich grains found in most chondrules of Semarkona LL3.0 chondrite (Kimura et al., 2008). Taenite grains are smaller than 20 μm and show preferential orientations along three directions. Terrestrial alteration of (Fe,Ni) metal grains initiates from the kamacite/taenite contact zone and develops until complete replacement of the kamacite (Fig. 3e). Beside (Fe,Ni) metal grains in the matrix, some low-Ca pyroxene dominated chondrules contain frequent (Fe,Ni) metal blebs which are less weathered and show a homogeneous texture (Fig. 3d). Chromite is present as euhedral to subhedral grains (Fig. 3f). Calcium and sulfur rich grains that may represent weathered oldhamite occur adjacent to some weathering patches but there is no unambiguous evidence for the presence of this mineral.

3.1.2. Northwest Africa 7135

NWA 7135, also described by Irving et al. (2015), shows a texture similar to EM 301 (Fig. 4). Well-defined chondrules are set within a matrix of enstatite laths set in a background of Fe oxide/oxyhydroxides (Fig. 5a). The average apparent chondrule diameter is 476 ± 271 μm ($n = 132$) (Fig. 2). Maximum chondrule size is 1880 μm. Median and mode values for chondrule diameters are 400 and 280 μm, respectively. Low-Ca pyroxene is the dominant phase. It does not show the zoning observed in EM 301 where grain rims are enriched in MgO. However, some chondrules show zones with different Mg-content and (Fe, Ni) metal blebs, identical to those in EM 301 (Fig. 5b). Except for chromite, the majority of the other opaque phases outside of the chondrules have been altered in the terrestrial environment. As reported by Irving et al. (2015), we observed a few preserved grains of oldhamite and daubréelite.

3.1.3. Chondritic clasts in Cumberland Falls Aubrite

The studied section of Cumberland Falls consists of white enstatite-rich aubrite host and a dark colored chondritic clast (Fig. 6). The highly shocked nature of the clast is evidenced by the presence of troilite melt veins and droplets, and by shock darkening. The texture of the clast and the visual structure of the silicates show no similarities with the textures of EM 301 or NWA 7135. With a chondrule size ranging from 500 to 2000 μm (Rubin, 2010a), CFC generally have larger chondrule sizes than EM 301 and NWA 7135, an observation that cannot be attributed to thermal metamorphism (e.g., Schrader et al., 2017) as most of the studied CFC clasts are only very slightly metamorphosed (type 3) (Binns, 1969; Neal and Lipschutz, 1981).

3.2. Mineral Chemistry

Tables 2–4 report the chemical compositions of olivine, low-Ca pyroxene and (Fe,Ni) metal of EM 301, respectively. Low-Ca pyroxene shows a range of chemical compositions, whereas olivine has a relatively narrow chemical distribution (Fig. 7). Average olivine ($n = 15$) and orthopyroxene ($n = 13$) compositions are $Fa_{3.9\pm0.3}$ and $Fs_{12.8\pm4.9}$, respectively. As shown in Fig. 8, these values are far from

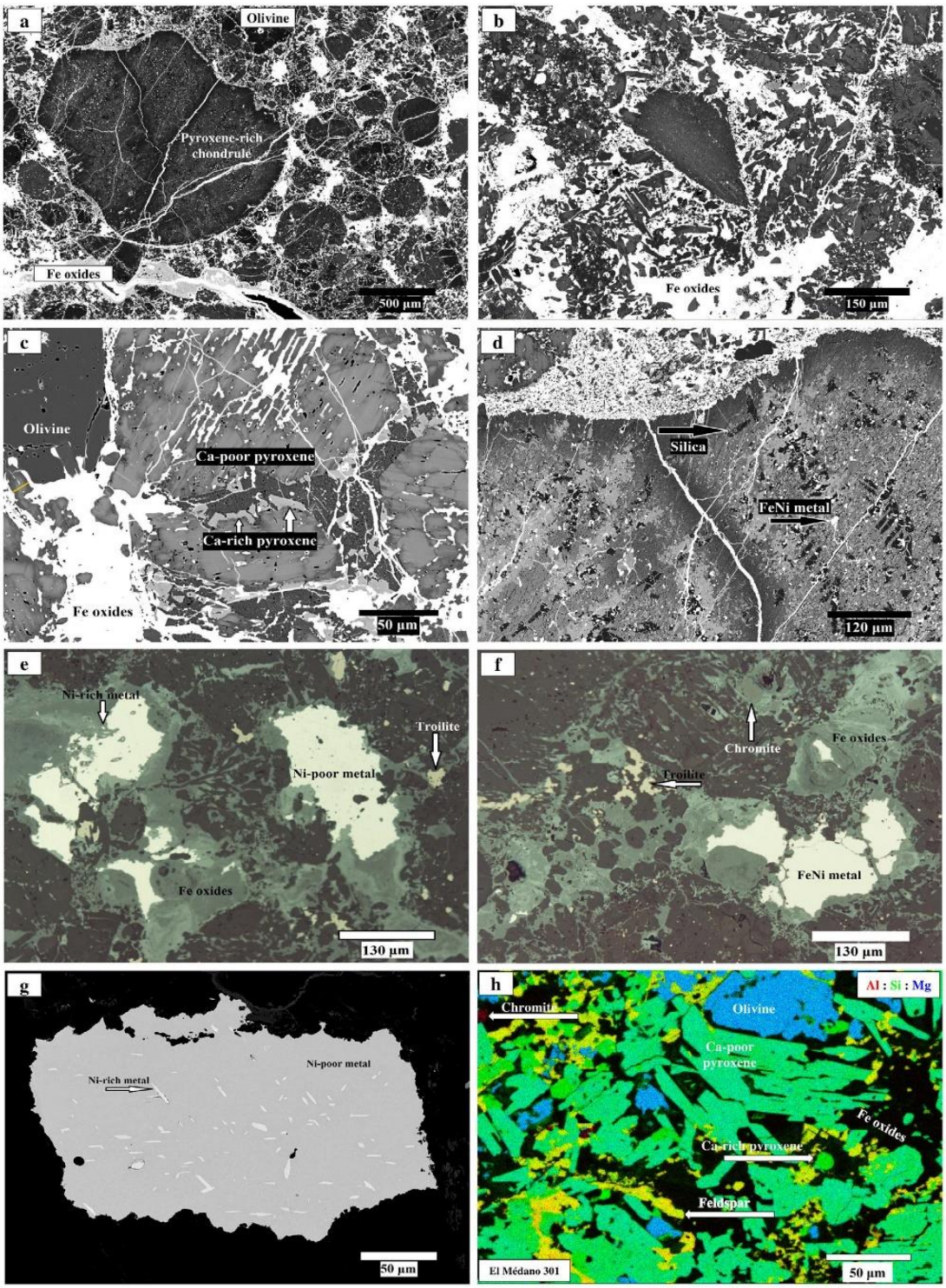

Fig. 3. Electron and optical microscope images of EM 301. (a) BSE image showing the high abundance of low-Ca pyroxene in the chondrules and matrix. Few olivine grains (darker grains) are visible. Note the occurrence of chondrule with different MgO and FeO concentration contents. (b) BSE image showing mostly elongated enstatite with Mg-rich rims in. (c) BSE image showing reverse zoning in low-Ca pyroxene. Yellow bar shows the location of the chemical profiles shown in Fig. 13. (d) BSE image of a pyroxene dominated chondrule, showing region with different MgO contents and silica and (Fe,Ni) metal blebs. Note the MgO regions along the rim and a major crack. (e) Reflected light image showing that Ni-rich metal is more resistant than Ni-poor metal to the terrestrial weathering. (f) Troilite, (Fe,Ni) metal and chromite constitute the main opaque phases in EM 301. Majority of the (Fe,Ni) metal is weathered to Fe oxides (reflected light image). (g) Some (Fe,Ni) metal grains in EM 301, show the exsolution of two Ni-rich and Ni-poor metal phases (BSE image). (h) An RGB image of EM 301 with Al in red, Si in green, and Mg in blue channels, respectively. The dominance of low-Ca pyroxene is clear in this image.

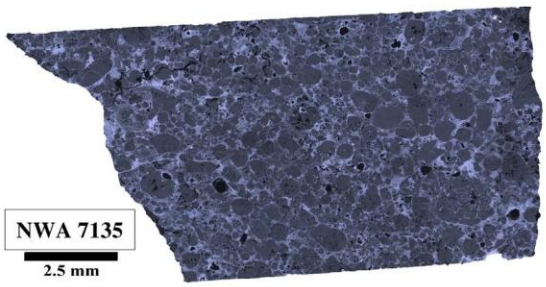

Fig. 4. Full thick section optical mosaic image of NWA 7135 in reflected light showing the chondritic textures and severe terrestrial weathering as evidenced by Fe oxides/oxyhydroxides mineral assemblages shown as (light grey patches and veinlets). Dark grey portions are silicates and rare white to yellowish spots (right up side for example) are the (Fe,Ni) metal and troilite grains.

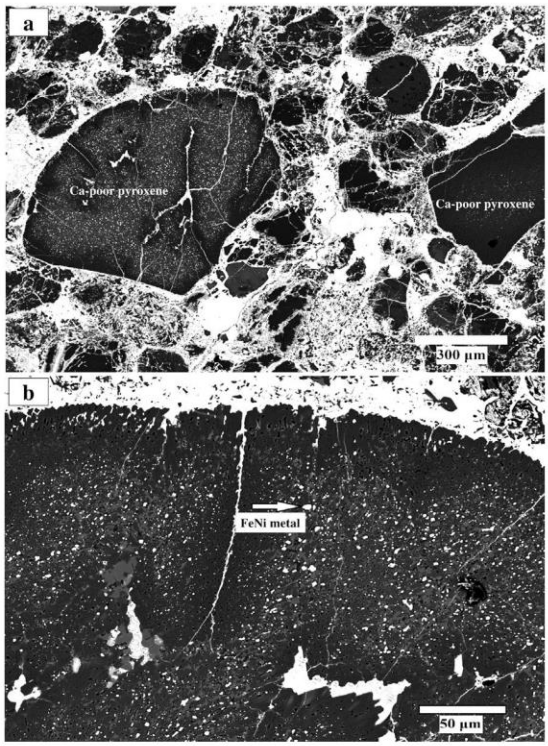

Fig. 5. BSE images of NWA 7135 showing (a) the dominance of Mg-rich pyroxene; (b) a pyroxene dominated chondrule showing regions with different MgO contents and silica and (Fe,Ni) metal blebs. Note the MgO-rich regions along the rim and a major crack. The white regions in the matrix and along the cracks are terrestrial weathering products. Metal grains occur as white spots inside the silicate grains.

the compositions of olivine and low-Ca pyroxene of equilibrated ordinary chondrites, and from those reported in chondrites and chondritic clasts described as HH, low-FeO, and reduced ordinary chondrites. Together with CFCs, NWA 7135 and Acfer 370, EM 301 forms a well-separated cluster. Compared to Acfer 370 and NWA 7135, EM 301 shows more reduced ferromagnesian silicate compositions. Olivine and low-Ca pyroxene show percent

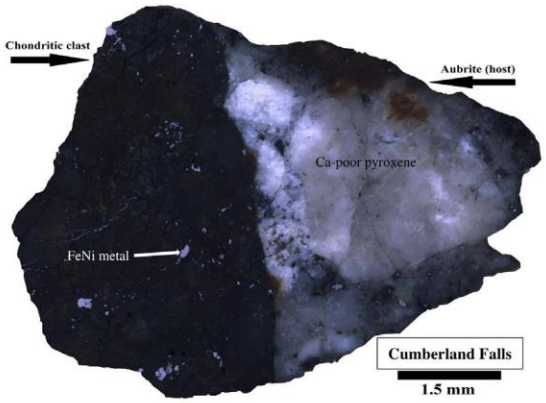

Fig. 6. Full thick section reflected light image of Cumberland Falls (section #2840-2 from MNHNP). Low-Ca pyroxene is the main component of the aubrite host. The darker chondritic region constitutes chondrules, (Fe,Ni) metal, and troilite grains that in most cases form shock assemblages indicative of an impact event.

mean deviations (PMD) of 5.0% and 34%, respectively, which indicate a petrologic type 4. The Co concentration of kamacite (Table 4) is below detection limit (0.18 wt%). This is way below the observed concentrations for H (0.44–0.51 wt%), L (0.70–0.95 wt%) and LL (0.42–37 wt %) chondrites (Rubin, 1990). The Si content of the analyzed kamacite grains was also lower than the detection limit (0.04 wt%).

3.3. IR-Spectroscopy

The infrared reflectance spectrum of EM 301 and NWA 7135 were obtained on powdered samples leached with HCl to remove weathering products (oxyhydroxides) that otherwise would dominate the spectrum. The spectrum reveals the presence of two strong absorptions around 0.92 µm (Band I) and 1.9 µm (Band II) (Fig. 9). The presence and position of these two bands are typical of a pyroxene signature (Cloutis and Gaffey, 1991). Addition of olivine, would tend to decrease the area of the 1.9 µm feature and to shift the band center of Band I toward higher wavelength, as is observed for ordinary chondrites.

3.4. Trace-element bulk chemistry

The whole-rock trace-element composition of EM 301 is reported in Table 1. The CI-normalized trace-element pattern shows enrichments of Ba (×43.6), Sr (×3.2) and LREE (up to ×2.4 for La), which are indicative of terrestrial weathering (Pourkhorsandi et al., 2017). Keeping in mind these effects, the trace-element contents are in the range of ordinary chondrites (Fig. 10; Wasson and Kallemeyn, 1988).

3.5. Oxygen-isotopic composition

Oxygen-isotopic composition analysis yielded the following results: $\delta^{17}O = +3.61$, $+3.78‰$, $\delta^{18}O = +5.38$, $+5.71‰$, $\Delta^{17}O = +0.79$, $+0.78‰$. Fig. 11 depicts the

Table 2
Representative olivine compositions (in wt%) from EM 301.

SiO_2	41.50	42.48	41.73	42.06	42.47	43.29	42.77	41.80	42.68	41.79	42.45	42.40	41.21	43.50	43.20	43.49	42.74	41.95	41.93
FeO	3.65	3.60	3.75	3.76	3.67	3.70	3.76	3.91	3.79	4.05	3.98	4.08	4.02	3.88	3.93	3.94	3.91	4.92	4.28
MnO	0.52	0.58	0.50	0.54	0.57	0.47	0.45	0.57	0.50	0.55	0.56	0.45	0.46	0.53	0.51	0.44	0.43	0.46	0.56
MgO	55.78	53.70	55.68	55.38	53.52	53.31	54.14	56.06	53.64	56.46	54.92	56.14	55.46	53.42	54.01	53.60	53.01	52.76	55.58
Total	101.45	100.36	101.66	101.74	100.23	100.77	101.12	102.34	100.61	102.85	101.91	103.07	101.15	101.33	101.65	101.47	100.09	100.09	102.35
Fa (mol%)	3.54	3.63	3.64	3.67	3.71	3.75	3.75	3.77	3.81	3.87	3.90	3.91	3.91	3.92	3.92	3.96	3.97	4.97	4.14

Detection limits (wt%) = Si (0.07), Al (0.06), Ti (0.13), Fe (0.16), Cr (0.07), Mn (0.14), Mg (0.07), Ca (0.05), Ni (0.18).
The concentrations of Al_2O_3, TiO_2, Cr_2O_3, CaO, are below detection limit.

$\Delta^{17}O$ versus $\delta^{18}O$ values of EM 301 along with literature data for H, L, and LL chondrites, and the chondrites/clasts with more reduced compositions than the ordinary chondrites. EM 301 shows higher $\delta^{18}O$ values than those of H chondrites and together with NWA 7135, Burnwell, Suwahib (Buwah) and the CFCs forms a different cluster. Since the samples were acid washed and clean hand-picked silicate crystals were used for the analyses, we believe that the effect of the terrestrial alteration on the heavier oxygen-isotopic composition of EM 301 is insignificant.

4. DISCUSSION

4.1. Classification

Whole-rock trace-element composition of EM 301 shows an affinity to OCs. The average apparent chondrule size of EM 301 is intermediate between values for H (Weisberg et al., 2006) and L (Rubin, 2010b) chondrites. However, a higher pyroxene/olivine ratio (~6), higher MgO contents of olivine and pyroxene, lower Co contents of kamacite, and different oxygen-isotopic composition, hinders its classification as a member of one of the typical OC groups (H, L, LL). In fact, the chemical range of the ferromagnesian minerals (olivine and pyroxene) in EM 301 is much closer to ECs than to OCs. From a spectral point of view, it does not show similarities with ordinary chondrites and its spectra resemble that of howardites, i.e. V-type related material (Fig. 12).

Whole-rock trace-element composition, oxygen-isotopic composition, and chemistry of olivine, pyroxene, and kamacite in EM 301 show similarities with CFC, Acfer 370, and NWA 7135. However, its general texture (e.g., chondrule size) is different from CFC and the highly reduced opaque minerals observed in NWA 7135 are absent (or weathered) in EM 301.

Chondrites with affinities to OCs but with higher contents of MgO in their ferromagnesian minerals have been reported with different terms such as, "HH" (Bild and Wasson, 1977), "reduced OCs" (Wasson et al., 1993), and "low-FeO" (Russel et al., 1998; Troiano et al., 2011). Hereafter we will use "reduced chondrites" collectively for these three groups. The term "forsterite chondrites" has been used to designate samples such as CFC (Graham et al., 1977) and NWA 7135 (Kuehner et al., 2015) whose ferromagnesian minerals have even higher MgO contents (similar to the ones in EM 301). Because EM 301 has different texture and/or opaque mineralogy than the CFC and NWA 7135, and also because of the poorly discriminant character of this term (forsterite being abundant in many chondrite groups), we use the denomination "highly reduced ordinary chondrite" for EM 301 in the following.

4.2. Origin of El Médano 301 chondrite

4.2.1. Introduction

To investigate the origin of EM 301, we compare it with OCs, ECs, and the reduced chondrites. Based on the mean Fa (mole%) and Fs (mole%) contents, OCs are divided into H ($Fa_{16.0–20.0}$; $Fs_{14.5–18.0}$), L ($Fa_{22.0–26.0}$; $Fs_{19.0–22.0}$) and LL

Table 3
Representative and low-Ca pyroxene compositions (in wt%) from EM 301.

SiO_2	59.34	59.77	57.61	57.19	54.31	59.13	58.86	57.13	55.22	56.88	58.32	56.41	56.53
Al_2O_3	0.90	0.10	0.14	b.d.l.	0.33	0.12	0.45	0.22	0.26	0.57	b.d.l.	0.53	0.21
TiO_2	0.13	0.14	0.22	0.13	b.d.l.	0.12	b.d.l.	b.d.l.	b.d.l.	b.d.l.	b.d.l.	b.d.l.	b.d.l.
FeO	3.71	4.69	5.48	5.44	7.54	7.60	9.47	11.08	11.12	10.96	11.27	11.87	13.36
Cr_2O_3	0.42	b.d.l.	0.50	0.08	0.49	0.18	0.27	0.36	0.19	0.40	0.21	0.51	0.41
MnO	0.71	0.59	0.46	0.68	0.70	0.58	0.51	0.27	0.55	0.39	0.49	0.61	0.51
MgO	35.49	36.21	36.73	36.19	37.99	33.39	31.54	32.47	32.09	30.48	31.06	29.69	28.87
CaO	0.61	0.30	0.43	0.44	0.38	0.47	0.46	0.47	1.01	0.65	0.24	0.75	0.73
Total	101.31	101.8	101.57	100.15	101.74	101.59	101.56	102	100.44	100.33	101.59	100.37	100.62
Fs (mol%)	5.47	6.74	7.67	7.72	9.95	11.23	14.29	15.94	15.97	16.57	16.83	18.05	20.32

b.d.l. = below detection limit.
Detection limits (wt%) = Si (0.07), Al (0.06), Ti (0.13), Fe (0.16), Cr (0.07), Mn (0.14), Mg (0.07), Ca (0.05), Ni (0.18).
The concentrations of Na_2O, K_2O, P_2O_5, Ni, and S are below detection limit.

Table 4
(Fe,Ni) metal compositions (in wt%) from EM 301.

	Kamacite	Kamacite	Kamacite	Kamacite	Kamacite	Kamacite	Kamacite	Kamacite	Taenite	Taenite	Taenite
Si	b.d.l.	b.d.l.	b.d.l.	b.d.l.	b.d.l.	b.d.l.	b.d.l.	b.d.l.	b.d.l.	0.04	b.d.l.
Cr	b.d.l.	b.d.l.	b.d.l.	b.d.l.	b.d.l.	b.d.l.	b.d.l.	b.d.l.	b.d.l.	0.08	0.07
Fe	92.74	90.85	92.93	91	91.9	91.49	90.48	91.3	71.81	45.33	44.36
Ni	5.71	5.79	5.99	6.15	6.17	6.5	6.55	6.7	25.19	52.25	52.94
Total	98.51	96.71	99.01	97.25	98.06	98.02	97.05	98.09	97	97.65	97.36

b.d.l. = below detection limit.
Detection limits (wt%) = Si (0.04), S (0.04), Cr (0.07), Fe (0.21), Co (0.18), Ni (0.18).
The concentrations of S, Co in the analyzed points are below detection limit.

($Fa_{26.0–32.0}$; $Fs_{22.0–26.0}$) groups (Brearley and Jones, 1998). Olivine is the dominant mineral in OCs and its chemical composition along with the Co concentration of kamacite is an accepted proxy of the oxidation–reduction state of the sample (Rubin, 1990). By formation of (Fe,Ni) metal (kamacite/taenite) in a reducing environment (low-fO_2), and incorporation of iron to these phases, FeO content of the silicate phases decreases and in contrast, in a more oxidizing environment (high-fO_2), more iron is incorporated in silicates. As a result, in low-fO_2 conditions, ferromagnesian silicates are richer in MgO and the concentration of Co (and Ni) is lower in kamacite grains (Rubin, 1990). The FeO content of olivine and Co concentration in kamacite, with increasing oxidation, increase from H to L, and LL chondrites. The extreme effect of formation in an environment with low-fO_2 is observed in ECs, in which almost pure enstatite is the dominant silicate phase and the majority of the Fe forms kamacite grains, as well as a variety of reduced minerals (e.g., carbides, phosphides, Ca or Mg sulfides; Keil, 1989).

4.2.2. The reduced chondrites

As mentioned in Section 4.1., beside typical OCs and ECs, some chondrites show intermediate characteristics, still with stronger affinities with OCs. Such reduced chondrites (relative to OCs), occur in at least three distinct "clusters": (1) low-FeO, (2) HH, and (3) CFC.

Based on the MgO-rich olivine/pyroxene and oxygen-isotopic compositions of Willaroy ($Fa_{14.1}$; $Fs_{13.3}$) and Suwahib (Buwah) ($Fa_{13.5}$; $Fs_{13.2}$), Scott et al. (1985) interpreted these meteorites as representatives of a distinct chondritic group. Cerro los Calvos with similar characteristics ($Fa_{12.5}$; $Fs_{11.7}$), was classified as an H chondrite defining the extreme limit of H compositional field (Whitlock et al., 1991). Reduction of normal H and L chondritic material during thermal metamorphism within the parent body in the presence of a reducing agent (e.g., graphite) was suggested by Wasson et al. (1993) to account for the formation of these chondrites as well as of Moorabie ($Fa_{15.9}$; $Fs_{15.3}$). In contrast, based on evidences such as the low Co content of kamacite, and the lack of a reducing agent, McCoy et al. (1994) proposed their formation in nebular rather than asteroidal setting. The lack of clasts with characteristics similar to low-FeO chondrites in H chondrites made them to consider these samples originating from different objects than the H chondrites parent body(ies). Burnwell anomalous H4 chondrite ($Fa_{15.8}$; $Fs_{13.4}$), is a relatively large reduced chondrite (measuring $15.5 \times 7 \times 5$ cm), much larger than the size of the reduced clasts in aubrites and IIE irons. Russel et al. (1998) suggest the necessity of a period of intense parent body thermal activity to reduce a volume of rock with the size of Burnwell with a reducing process similar to that proposed by Wasson et al. (1993). However, the occurrence of such high temperature period is in conflict with the low petrologic degree of Burnwell. Therefore, they consider a nebular origin to explain the reduced nature of Burnwell. Other studies of low-FeO chondrites, also propose either nebular or parent body origins (Troiano et al., 2011; Yamaguchi et al., 2015).

IIE irons (such as Netschaëvo, Techado, Garhi Yasin) host chondritic clasts with lower Fa and Fs ($Fa_{14.3}$, $Fs_{14.0}$; in Netschaëvo), distinct chromite composition, lower Co

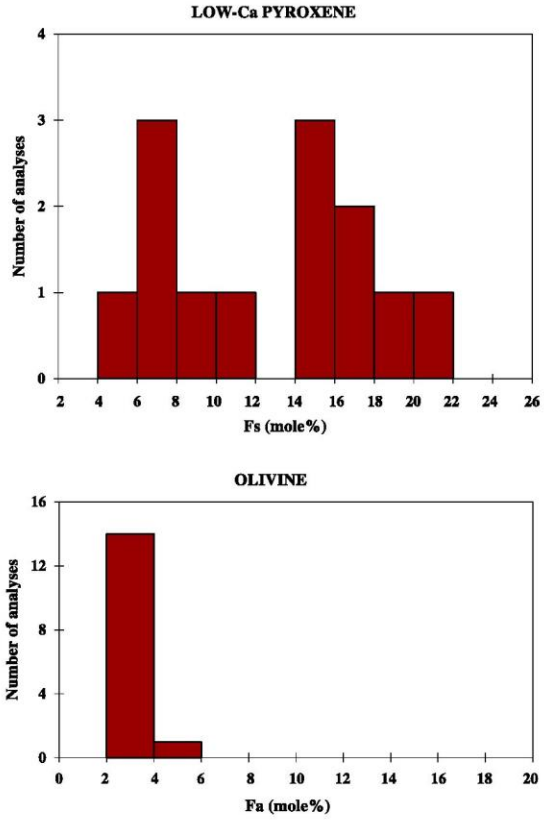

Fig. 7. Histograms showing the compositional distributions of randomly chosen (a) low-Ca pyroxene (n = 14) and (b) olivine (n = 19) grains in EM 301.

content in kamacite, and different oxygen-isotopic composition compared to H chondrites (Bild and Wasson, 1977; McDermott et al., 2016; Schrader et al., 2017). Based on these properties and the higher concentration of siderophile elements in whole-rock chemical composition, Bild and Wasson (1977) named them HH chondrites and proposed an origin from a distinct parent body.

The chondritic clasts of Cumberland Falls are mostly of petrologic type 3 or 4 (Binns, 1969), but type 6 clasts and impact melt clasts have also been reported (Rubin, 2010a; Kuehner et al., 2016). The whole-rock chemistry of CFC is in the range of LL chondrites (Kallemeyn and Wasson, 1985). However, unlike in OCs, pyroxene is the dominant silicate phase in CFC and their olivine/pyroxene and kamacite chemistry is different from OCs. In addition, their oxygen-isotopic composition are different from OCs and ECs. Two different alternatives have been given for their formation: (i) formation in a nebular region more reduced than the OCs formation region and thus provenance from a distinct parent body (Graham et al., 1977; Neal and Lipschutz, 1981; Verkouteren and Lipschutz, 1983; Grady and Pillinger, 1986; Lipschutz et al., 1988; Keil, 2010; Kuehner et al., 2016), (ii) reduction of LL chondritic material in the presence of the reducing aubrite host after an impact event and the later modification of mineral and oxygen isotopic compositions (Wasson and Kallemeyn, 1984; Kallemeyn and Wasson, 1985; Rubin, 2010a).

4.2.3. El Médano 301

Chemical and oxygen-isotopic composition, and general texture of EM 301 indicate its affinity with OCs. Still, there are significant differences between EM 301 and OCs. These include: (1) lower modal olivine/pyroxene ratio, (2) lower Co content of kamacite, (3) higher mean MgO contents of olivine and pyroxene, (4) different kamacite texture, and (5) different oxygen-isotopic composition.

EM 301, NWA 7135, CFC, and Acfer 370 share similar oxygen isotopic composition and ferromagnesian minerals compositions. However, there are differences among these samples. The occurrence of daubréelite, oldhamite, schreibersite, and djerfisherite in NWA 7135 (Irving et al., 2015) indicates its formation in very reduced conditions. Similar minerals are reported from CFC (Rubin, 2010a). In contrast, despite a low weathering degree (W1) in parts of the meteorite, none of these minerals are reported in Acfer 370 (Moggi-Cecchi et al., 2009). During SEM survey of EM 301, except possible weathering products of oldhamite, we did not find any evidence for these very reduced minerals, although we admit that owing to the strong weathering, their preservation (if they ever existed) may not have been granted.

The texture and silicate mineralogy of EM 301 and NWA 7135 show similarities with that of ECs. The matrix is composed of enstatite laths set in an iron oxide/oxyhydroxide mélange of weathering products. This texture is somehow similar to a "remnant" of the "metal/sulfide-silicate intergrowths" observed in some ECs, which are interpreted as the result of impact melting in a reduced lithology (Lin and Kimura, 1998; van Niekerk and Keil, 2006; Rubin and Wasson, 2011; Horstmann et al., 2014). However, the preserved kamacite grains in EM 301 do not host such enstatite laths, which does not support a similar impact melting process. Kamacite is Si-poor (below detection limit of 0.04 wt%) in EM 301, and also in CFC (Rubin, 2010a), and NWA 7135 (Irving et al., 2015), which is in contrast to their Si-rich nature in ECs (up to about 3.0 wt% Si in the metal of EH3s and up to about 1.4 wt% in EL3s) (Weisberg et al., 1995). In addition, olivine is a rare silicate in ECs (e.g., Keil, 1989), but it is relatively abundant in the aforementioned chondrites. The olivine and pyroxene composition of EM 301 is close to the reported values for the Kakangari chondrites (Graham et al., 1977; Weisberg et al., 1996), but the matrix/chondrule ratio, oxygen-isotopic composition and whole-rock chemistry are different. Putting all the data together, we observe the effects of low-fO_2 conditions (compared to OCs) during formation and/or evolution of EM 301. These conditions could have prevailed in the nebula and/or the parent body (asteroidal processes).

The solar nebula contained regions with different level of fO_2 (Larimer and Bartholomay, 1979; Rubin and Wasson, 1995; Grossman et al., 2008). It is believed that the formation region of ECs had a C/O ratio higher than the solar value (Larimer and Bartholomay, 1979). The presence of reducing C-rich phases, such as organic matter and graphite, resulted in the formation of the observed EC mineralogy (high modal pyroxene/olivine ratio, Mg-rich nature of the mafic minerals, etc.).

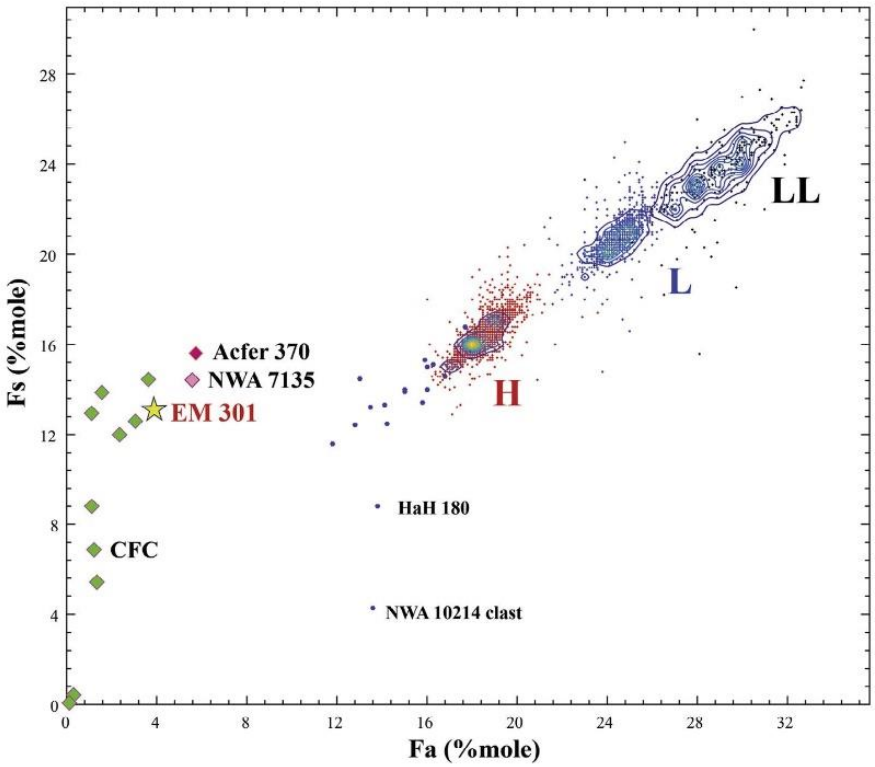

Fig. 8. Scatter diagram showing the average Fa content of olivine (mol%) in EM 301, CFC, reduced, and OCs. Density contour plots drawn using petrologic type ≥3.9, H (n = 4696), L (n = 2040) and LL (n = 360) chondrites. For Cumberland Falls, average values for different clasts are shown (data from Neal and Lipschutz, 1981). The mean compositional values of OCs from MetBase (Koblitz, 2005), and reduced chondrites and chondritic clasts (both shown as dots) are plotted for comparison. The plotted reduced chondritic meteorites and clasts are LaPaz Icefield (LAP) 04757 and 04773 (Connolly et al., 2007), Suwahib (Buwah) and Willaroy (Scott et al., 1985), Cerro los Calvos and Moorabie (Wasson et al., 1993), Burnwell (Russel et al., 1998), Allan Hills A77221 (Grossman, 1994), Elephant Moraine (EET) 96031 (Grossman, 1998), Beni Semguine (Grossman, 1999), Miller Range (MIL) 07273 (Weisberg et al., 2010), Yamato 982717 (Ruzicka et al., 2015), Garhi Yasin clast (McDermott et al., 2016), Techado and Netschaëvo clasts (Van Roosbroek et al., 2015), NWA 10214 unique clast (Rubin et al., 2016), Hammadah al Hamra (HaH) 180 (Grossman, 1997), Acfer 370 (Moggi-Cecchi et al., 2009) and NWA 7135 (Irving et al., 2015).

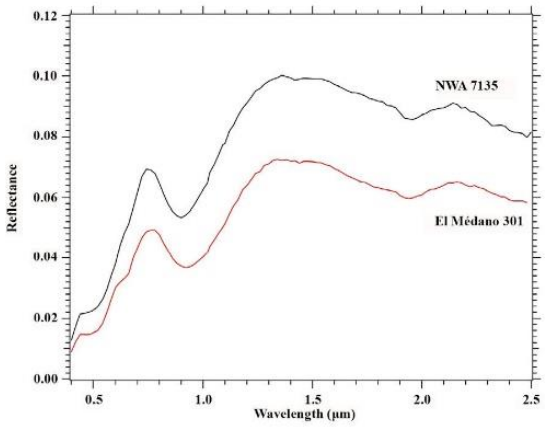

Fig. 9. IR spectra of EM 301 and NWA 7135.

However, some parent body processes can also lead to reduction. Among these are: impact melting (Horstmann et al., 2014), impact and reduction in the presence of reduced material in the host (Rubin, 2010a), and the reducing effect of C-rich gases during parent body degassing (Sugiura et al., 1985). As proposed for the formation of CFC (Kallemeyn and Wasson, 1985), and low-FeO chondrites (Wasson et al., 1993), parent body reduction can change the oxidation state of the minerals by forming Mg-rich ferromagnesian silicates and Co-poor kamacite (Wasson et al., 1993). An inverse process (parent body oxidation), is proposed to describe the occurrence of EH clasts in Galim LL-EH polymict breccia (Rubin, 1997), which show a composition similar to CFC.

We suggest that EM 301 formed in a nebular location with fO_2 intermediate between OCs and ECs. Indeed, EM 301 is devoid of shock metamorphic features (sharp olivine optical extinction, no shock veins, no polycrystalline troilite, no metallic copper, no fractures in ferromagnesian minerals) and of traces of melting or annealing (low metamorphic grade) to transform the olivine to pyroxene during a high temperature event. This points to a nebular rather than asteroidal origin for the primary characteristics of EM 301.

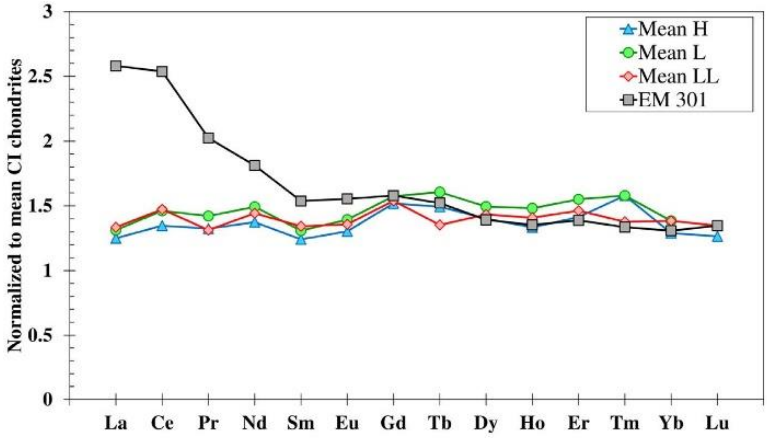

Fig. 10. CI-normalized REE chemical composition of EM 301 is identical to the mean composition of OCs. Mean OCs data from (Wasson and Kallemeyn, 1988). Note the higher abundance of LREEs in EM 301 which is the result of terrestrial weathering.

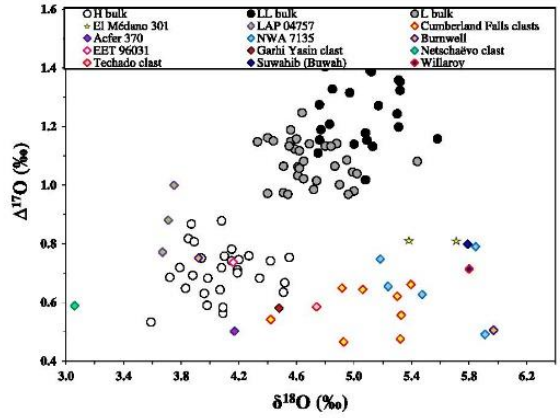

Fig. 11. $\Delta^{17}O$ versus $\delta^{18}O$ values of EM 301 compared to type 4–6 OCs and the reduced chondrites. Data list and references are: OCs (Clayton and Mayeda, 1991), CFC (Kuehner et al., 2016), NWA 7135 (Kuehner et al., 2015), Acfer 370 (Moggi-Cecchi et al., 2009), Burnwell (Russel et al., 1998; Troiano et al., 2011), LAP 04757 (Connolly et al., 2007; Troiano et al., 2011), EET 96031 (Troiano et al., 2011) Suwahib (Buwah) and Willaroy (Scott et al., 1985), Garhi Yasin, Techado and Netschaëvo chondritic clasts (McDermott et al., 2016). Different data points for NWA 7135 and LAP 04757 represent different aliquots analyzed. $\Delta^{17}O$ values are calculated using a slope of 0.52.

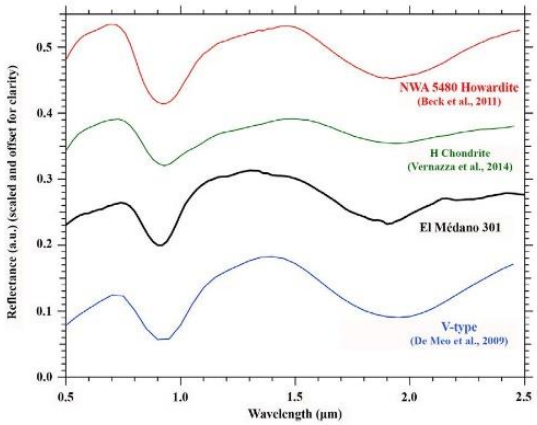

Fig. 12. A comparison of the IR spectra of IR spectra of EM 301 with V-type asteroids, H chondrites and an howardite.

Olivine and pyroxene can record secondary reduction events as "reverse" zoning (Mg-rich rims) (Weisberg et al., 1994; Goodrich et al., 2006; Rubin, 2010a) and higher mean Fs to Fa ratio (Wasson et al., 1993; Keil, 2007; Rubin, 2010a). The outer rims and crack walls in pyroxene grains in EM 301 are Mg-rich (Fig. 3b and c). Such zoning along a low-Ca pyroxene is shown in Fig. 13. This can be an evidence of a secondary reduction event. Olivine coexisting in equilibrium with pyroxene has a higher content of FeO than pyroxene (e.g., Keil and Fredriksson, 1964). With increasing reduction, Fe forms metallic phases and Fa and Fs contents become lower than the original precursor. Because diffusion in olivine is faster than pyroxene (e.g., Freer, 1981), during a subsequent reduction event, it equilibrates faster than pyroxene. If the equilibrium does not reach completion, the pyroxene grains show wider compositional range and retain more ferrous compositions than olivine. This is what is observed in EM 301 and a secondary reduction event can be responsible for that. The same explanation is suggested for CFC (Wasson et al., 1993; Rubin, 2010a), and could also apply to NWA 7135 and Acfer 370.

The origin of such secondary reduction events can be: (ii) nebular material mixing and injection of reducing components in the formation region of the grains (e.g., Fegley, 2000; Bockelée-Morvan et al., 2002; Zanda et al., 2006) (ii) reduction in the parent body. The latter process can occur during release and circulation of reducing gases (especially C-rich gases) through high permeability zones and along cracks during the degassing of a parent body (Sugiura et al., 1984; Sugiura et al., 1985; Sugiura et al., 1986; Krot, 1994; Hashizume and Sugiura, 1998). It is noteworthy that formation of EM 301 in a region more reduced than the one of the OCs means a higher abundance of

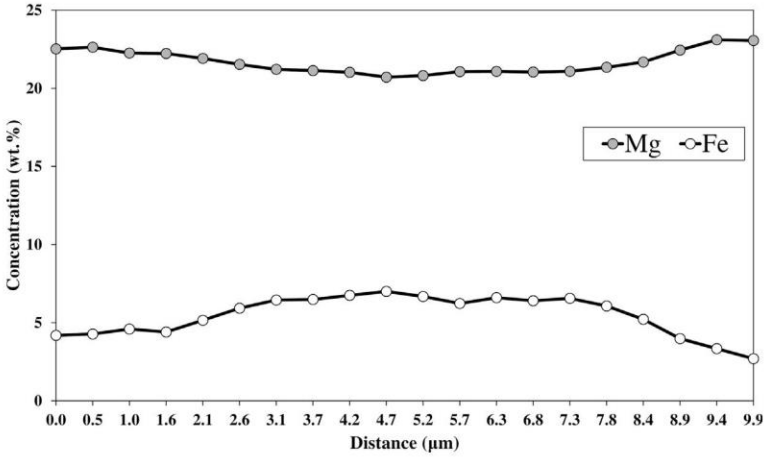

Fig. 13. Higher Mg (wt%) and lower Fe (wt%) contents in a representative low-Ca pyroxene (shown in Fig. 3c) in EM 301 are the representatives of a reverse zoning.

C-rich material in the resulting parent body and higher amount of reducing gasses during asteroidal processes (such as metamorphism). However, considering EM 301's relatively unequilibrated character and low petrologic type, and the necessity for high degrees of thermal metamorphism for parent body reduction (e.g., Russel et al., 1998; Schrader et al., 2017), a secondary nebular reduction event is more likely than a one occurring in the parent body (Rubin, 2017; Schrader et al., 2017).

Shifting of oxygen isotopic composition by impact and associated reduction like in CFCs (Wasson and Kallemeyn, 1984), or by intense thermal metamorphism and associated mass dependent fractionation like in Watson 012 H7 chondrite (Tait et al., 2014) are not applicable to EM 301 that lacks evidence for shock or intense thermal metamorphism.

We suggest that EM 301 formation region in the nebula had a trace-element composition pattern similar to OCs, but fO_2 intermediate between OCs and ECs. These reducing conditions (in comparison with OCs) have resulted in the formation of a higher modal pyroxene/olivine ratio, Mg-rich olivine and pyroxene, different oxygen-isotopic composition, and, for NWA 7135, formation of highly reduced opaque phases. During a secondary reduction event which might have happened in the nebula, Mg-rich rims have formed in EM 301 and also the mean Fs has become higher than the mean Fa, which is also observed in NWA 7135, CFC, and Acfer 370. A reason for the lack of reverse zoning in pyroxene of NWA 7135 may be more intense reduction and associated diffusion of Fe-Mg.

4.2.4. Possible parent body

The reflectance spectrum of EM 301 is quite different from those of ordinary chondrites. This difference is explained by a higher pyroxene/olivine ratio, but also by the low Fe content of olivine ($Fa_{3.9\pm0.3}$), which makes it almost spectrally neutral. The reflectance spectrum of EM 301 is similar to that of material typically interpreted as differentiated: it resembles typical spectra of Howardites-Eucrites-Diogenites (HED) meteorites (Fig. 12). The position of Band I and Band II of EM 301 (0.92 and 1.92 μm) are typical of Fe-poor pyroxene. They are reminiscent of, but not identical to values found for 4-Vesta (on average 0.93 μm and 1.96 μm; De Sanctis et al., 2012).

While the surface of 4-Vesta is not a perfect spectral match to EM 301 spectrum (and while we now have the confirmation from the DAWN mission that 4-Vesta is related to HED meteorites) there are a number of V-type asteroids (with spectra similar to 4-Vesta) that do not have a dynamical affinity with 4-Vesta and could be sampling a different parent body (Nesvorný et al., 2008). The spectra of V-type asteroids shows the presence of both Band I and II, with a high Band II to Band I ratio, (i.e. a spectra dominated by pyroxene). Several V-type families have been distinguished: (i) vestoids (with dynamical affinities with Vesta) (ii) fugitives (with $a < 2.3$ (Astronomical Unit) a.u. but inclination and eccentricity similar to vestoids, Nesvorný et al., 2008) (iii) low-inclination V-types (with 2.3 a.u. $< a < 2.5$ a.u, and $i < 6°$, according to Nesvorný et al., 2008)) (iv) Near-Earth Asteroid with V-type spectra and last (v) Middle or Outer Belt V-type, MOV (Ieva et al., 2016). Among all these V-types, an important variability is present in the Band I and Band II positions (from 0.90 to 0.95 μm for Band I and from 1.89 to 2.05 μm for Band II). This variability includes objects with band positions similar to those measured for EM 301. While vestoids and fugitives are most likely related to HED meteorites, a number of V-types might in fact be related to chondritic material similar to EM 301.

5. CONCLUSION

EM 301 is a type 4 chondrite containing Mg-rich olivine and pyroxene with average compositions of $Fa_{3.9\pm0.3}$ and $Fs_{12.8\pm4.9}$, respectively, which are intermediate between ordinary and enstatite chondrites. Its oxygen-isotopic composition ($\Delta^{17}O = +0.79,+0.78‰$) is different from other ordinary chondrites. It shows a whole-rock trace element composition similar to OCs. However, its olivine/pyroxene modal abundance, and olivine/pyroxene/kamacite chemical

composition suggest its formation in nebular region with lower fO_2 than OCs. The general similarities between EM 301 and NWA 7135 and probably CFC and Acfer 370, suggests that these meteorites may have formed in region with relatively similar physico-chemical conditions. In EM 301, the Mg-rich rims in pyroxene and higher mean Fs/mean Fa ratio suggesting a secondary reduction event, which probably has occurred in the nebula.

The IR spectrum of EM 301 dominated by a pyroxene signature is markedly different from those of typical ordinary chondrites. Similar spectra when observed among main-belt asteroids are usually interpreted as "basaltic", as is the case of V-type asteroids. The presence of chondritic material with pyroxene-like reflectance spectra suggests that a number of V-type, in particular those that are not dynamically related to Vesta, might in fact be chondritic.

ACKNOWLEDGMENTS

Fabien Kuntz and the National History Museum in Paris (MNHNP) are acknowledged for the loan of NWA 7135 and Cumberland Falls, respectively. This work was partly funded by the Agence Nationale de la Recherche (grant ANR-13-BS05-0009). Cultural Office of the French Embassy in Tehran is acknowledged for providing Ph.D. grant for the first author. Minoru Uehara is thanked for useful discussions. M.V. thanks the support by CONICYT-FONDECYT project N° 3140562. We thank Alexander N. Krot for editorial handling and very useful suggestions, and Devin Schrader, Anthony Irving and an anonymous referee for their constructive reviews.

APPENDIX A. SUPPLEMENTARY MATERIAL

Supplementary data associated with this article can be found, in the online version, at http://dx.doi.org/10.1016/j.gca.2017.09.013.

REFERENCES

Afiattalab F. and Wasson J. T. (1980) Composition of the metal phases in ordinary chondrites: implications regarding classification and metamorphism. *Geochim. Cosmochim. Acta* **44**, 431–446.

Alexandre A., Basile-Doelsch I., Sonzogni C., Sylvestre F., Parron C., Meunier J.-D. and Colin F. (2006) Oxygen isotope analyses of fine silica grains using laser-extraction technique: comparison with oxygen isotope data obtained from ion microprobe analyses and application to quartzite and silcrete cement investigation. *Geochim. Cosmochim. Acta* **70**, 2827–2835.

Beck P., Barrat J.-A., Grisolle F., Quirico E., Schmitt B., Moynier F., Gillet P. and Beck C. (2011) NIR spectral trends of HED meteorites: can we discriminate between the magmatic evolution, mechanical mixing and observation geometry effects? *Icarus* **216**, 560–571.

Bild R. W. and Wasson J. T. (1977) Netschaëvo: a new class of chondritic meteorite. *Science* **197**, 58–61.

Binns R.A. (1969). A Chondritic inclusion of unique type in the Cumberland Falls meteorite. Meteorite Res., pp. 696–704.

Bockelée-Morvan D., Gautier D., Hersant F., Huré J.-M. and Robert F. (2002) Turbulent radial mixing in the solar nebula as the source of crystalline silicates in comets. *Astron. Astrophys.* **384**, 1107–1118.

Bogard D. D., Garrison D. H. and McCoy T. J. (2000) Chronology and petrology of silicates from IIE iron meteorites: evidence of a complex parent body evolution. *Geochim. Cosmochim. Acta* **64**, 2133–2154.

Brearley A. J. and Jones R. H. (1998) Chondritic meteorites. J.J. Papike (Ed.), Planetary Materials, Reviews in Mineralogy, vol. 36, Mineralogical Society of America, Washington, D.C. (1998).

Brissaud O., Schmitt B., Bonnefoy N., Douté S., Rabou P., Grundy W. and Fily M. (2004) Spectrogonio radiometer for the study of the bidirectional reflectance and polarization functions of planetary surfaces 1 Design and tests. *Appl. Opt.* **43**, 1926–1937.

Clayton R. and Mayeda T. (1991) Oxygen isotope studies of ordinary chondrites. *Geochim. Cosmochim. Acta* **55**, 2317–2337.

Cloutis E. A. and Gaffey M. J. (1991) Pyroxene spectroscopy revisited: spectral-compositional correlations and relationship to geothermometry. *J. Geophys. Res.* **96**, 22809–22826.

Connolly H. C., Smith C., Benedix G., Folco L., Righter K., Zipfel J., Yamaguchi A. and Aoudjehane H. C. (2007) The Meteoritical Bulletin, No. 92, 2007 September. *Meteorit. Planet. Sci.* **42**, 1647–1694.

Crespin J., Alexandre A., Sylvestre F., Sonzogni C., Paillès C. and Garreta V. (2008) IR laser extraction technique applied to oxygen isotope analysis of small biogenic silica samples. *Anal. Chem.* **80**, 2372–2378.

Fegley, Jr., B. (2000) Kinetics of gas-grain reactions in the Solar Nebula. *Space Sci. Rev.* **92**, 177–200.

Freer R. (1981) Diffusion in silicate minerals and glasses: a data digest and guide to the literature. *Contrib. Mineral. Petrol.* **76**, 440–454.

Friedrich J. M., Wang M.-S. and Lipschutz M. E. (2003) Chemical studies of L chondrites. V: compositional patterns for 49 trace elements in 14 L4–6 and 7 LL4-6 falls. *Geochim. Cosmochim. Acta* **67**, 2467–2479.

Goodrich C. A., Wlotzka F., Ross D. K. and Bartoschewitz R. (2006) Northwest Africa 1500: plagioclase-bearing monomict ureilite or ungrouped achondrite? *Meteorit. Planet. Sci.* **41**, 925–952.

El Goresy A., Lin Y., Miyahara M., Gannoun A., Boyet M., Ohtani E., Gillet P., Trieloff M., Simionovici A., Feng L. and Lemelle L. (2017) Origin of EL3 chondrites: evidence for variable C/O ratios during their course of formation-A state of the art scrutiny. *Meteorit. Planet. Sci.* **52**, 781–806.

Grady M. M. and Pillinger C. T. (1986) Carbon isotope relationships in winonaites and forsterite chondrites. *Geochim. Cosmochim. Acta* **50**, 255–263.

Graham A. L., Easten A. J. and Hutchison R. (1977) Forsterite chondrites; the meteorites Kakangari, Mount Morris (Wisconsin), Pontlyfni, and Winona. *Mineral. Mag.* **41**, 201–210.

Gröning M. (2004) Chapter 40 – International Stable Isotope Reference Materials. In Handbook of Stable Isotope Analytical Techniques, pp. 874–906.

Grossman J. n. (1997) The Meteoritical Bulletin, No. 81, 1997 Jul.. *Meteorit. Planet. Sci.* **32**, A159–A166.

Grossman J. n. (1999) The Meteoritical Bulletin, No. 83, 1999 July. *Meteorit. Planet. Sci.* **34**, A169–A186.

Grossman J. N. (1994) The Meteoritical Bulletin, No. 76, 1994 January: The U.S. Antarctic Meteorite Collection*. *Meteoritics* **29**, 100–143.

Grossman J. N. (1998) The Meteoritical Bulletin, No. 82, 1998 July. *Meteorit. Planet. Sci.* **33**, A221–A239.

Grossman L., Beckett J. R., Fedkin A. V., Simon S. B. and Ciesla F. J. (2008) Redox conditions in the Solar Nebula: observational, experimental, and theoretical constraints. *Rev. Mineral. Geochem.* **68**, 93–140.

Hashizume K. and Sugiura N. (1998) Transportation of gaseous elements and isotopes in a thermally evolving chondritic planetesimal. *Meteorit. Planet. Sci.* **33**, 1181–1195.

Horstmann M., Humayun M. and Bischoff A. (2014) Clues to the origin of metal in Almahata Sitta EL and EH chondrites and implications for primitive E chondrite thermal histories. *Geochim. Cosmochim. Acta* **140**, 720–744.

Ieva S., Dotto E., Lazzaro D., Perna D., Fulvio D. and Fulchignoni M. (2016) Spectral characterization of V-type asteroids – II. A statistical analysis. *Mon. Not. R. Astron. Soc.* **455**, 2871–2888.

Irving A. J., Kuehner S. M., Ziegler K., Kuntz F. and Sipiera P. P. (2015) Northwest Africa 7135: An unusual reduced, unequilibrated chondrite containing oldhamite, daubreelite, schreibersite and djerfisherite, and with a unique oxygen isotopic composition. In 46th Lunar and Planetary Science Conference p. 2437.

Jarosewich E., Clarke C. R. S. and Barrows J. N. (1987) Allende meteorite reference sample. *Smithson. Contrib. to Earth Sci.* **27**, 1–49.

Kallemeyn G. W. and Wasson J. T. (1985) The compositional classification of chondrites: IV. Ungrouped chondritic meteorites and clasts. *Geochim. Cosmochim. Acta* **49**, 261–270.

Keil K. (2010) Enstatite achondrite meteorites (aubrites) and the histories of their asteroidal parent bodies. *Chem. Erde* **70**, 295–317.

Keil K. (1989) Enstatite meteorites and their parent bodies. *Meteoritics* **24**, 195–208.

Keil K. (2007) Occurrence and origin of keilite, $(Fe_{>0.5}, Mg_{<0.5})S$ in enstatite chondrite impact-melt rocks and impact-melt breccias. *Chem. Erde* **67**, 37–54.

Keil K. (1962) On the phase composition of meteorites. *J. Geophys. Res.* **67**, 4055–4061.

Keil K. and Fredriksson K. (1964) The iron, magnesium, and calcium distribution in coexisting olivines and rhombic pyroxenes of chondrites. *J. Geophys. Res.* **69**, 3487–3515.

Kimura M., Grossman J. N. and Weisberg M. K. (2008) Fe-Ni metal in primitive chondrites: Indicators of classification and metamorphic conditions for ordinary and CO chondrites. *Meteorit. Planet. Sci.* **43**, 1161–1177.

Koblitz J. (2005) MetBase – Meteorite Data Retrieval Software, version 7.1.

Krot A. N. (1994) Oxidized H, L, and LL chondrites. *Meteorit.* **29**, 486–487.

Kuehner S. M., Irving A. J., Ziegler K., Sanborn M. E. and Yin Q. (2015) F3/4 Chondrite Northwest Africa 7135: Further assessment of its relationship to clasts in the Cumberland Falls aubrite. In 78th Annual Meeting of the Meteoritical Society p. 5238.

Kuehner S. M., Wittke J. H., Ziegler K. and Irving A. J. (2016) Mineralogy and oxygen isotopic composition of exotic F6 chondrite clasts in the Cumberland Falls aubrite. In 47th Lunar and Planetary Science Conference p. 2304.

Larimer J. W. and Bartholomay M. (1979) The role of carbon and oxygen in cosmic gases: some applications to the chemistry and mineralogy of enstatite chondrites. *Geochim. Cosmochim. Acta* **43**, 1455–1466.

Lin Y. and Kimura M. (1998) Petrographic and mineralogical study of new EH melt rocks and a new enstatite chondrite grouplet. *Meteorit. Planet. Sci.* **33**, 501–511.

Lipschutz M. E., Verkouteren R. M., Sears D. W. G., Hasan F. A., Prinz M., Weisberg M. K., Nehru C. E., Delaney J. S., Grossman L. and Boily M. (1988) Cumberland Falls chondritic inclusions: III. Consortium study of relationship to inclusions in Allan Hills 78113 aubrite. *Geochim. Cosmochim. Acta* **52**, 1835–1848.

McCoy T. J., Keil K., Scott E. R. D., Benedix G. K., Ehlmann A. J., Mayeda T. K. and Clayton R. N. (1994) Low-FeO ordinary chondrites: A nebular origin and new chondrite parent body. In Lunar and Planetary Science XXV p. 865.

McDermott K. H., Greenwood R. C., Scott E. R. D., Franchi I. A. and Anand M. (2016) Oxygen isotope and petrological study of silicate inclusions in IIE iron meteorites and their relationship with H chondrites. *Geochim. Cosmochim. Acta* **173**, 97–113.

Miller M. F. (2002) Isotopic fractionation and the quantification of 17O anomalies in the oxygen three-isotope system: an appraisal and geochemical significance. *Geochim. Cosmochim. Acta* **66**, 1881–1889.

Moggi-Cecchi V., Pratesi G., Franchi I. A. and Greenwood R. C. (2009) Acfer 370: an anomalous chondrite related to the Cumberland Falls breccia. In 72nd Annual Meteoritical Society Meeting p. 5421.

Neal C. W. and Lipschutz M. E. (1981) Cumberland Falls chondritic inclusions: Mineralogy/petrology of a forsterite chondrite suite. *Geochim. Cosmochim. Acta* **45**, 2091–2107.

Nesvorný D., Roig F., Gladman B., Lazzaro D., Carruba V. and Mothé-Diniz T. (2008) Fugitives from the Vesta family. *Icarus* **193**, 85–95.

van Niekerk D. and Keil K. (2006) Classification of five new ordinary chondrites from North West Africa. *Chem. Erde* **66**, 153–158.

Osadchii V. O., Fedkin M. V. and Osadchii E. G. (2017) Determination of the equilibrium fO_2 in bulk samples of H, L, and LL ordinary chondrites by solid-state electrochemistry. *Meteorit. Planet. Sci.*. https://doi.org/10.1111/maps.12919.

Pourkhorsandi H., D'Orazio M., Rochette P., Valenzuela M., Gattacceca J., Mirnejad H., Sutter B., Hutzler A. and Aboulahris M. (2017) Modification of REE distribution of ordinary chondrites from Atacama (Chile) and Lut (Iran) hot deserts: Insights into the chemical weathering of meteorites. *Meteorit. Planet. Sci.* **52**, 1843–1858. https://doi.org/10.1111/maps.12894.

Rochette P., Sagnotti L., Bourot-Denise M., Consolmagno G., Folco L., Gattacceca J., Osete M. L. and Pesonen L. (2003) Magnetic classification of stony meteorites: 1. Ordinary chondrites. *Meteorit. Planet. Sci.* **38**, 251–268.

Van Roosbroek N., Debaille V., Pittarello L., Goderis S., Humayun M., Hecht L., Jourdan F., Spicuzza M. J., Vanhaecke F. and Claeys P. (2015) The formation of IIE iron meteorites investigated by the chondrule-bearing Mont Dieu meteorite. *Meteorit. Planet. Sci.* **50**, 1173–1196.

Rubin A. E. (2017) A pervasive reduction event on the L-chondrite parent asteroid. In Lunar and Planetary Science XLVIII p. 1151.

Rubin A. E. (2010a) Impact melting in the Cumberland Falls and Mayo Belwa aubrites. *Meteorit. Planet. Sci.* **45**, 265–275.

Rubin A. E. (1990) Kamacite and olivine in ordinary chondrites: intergroup and intragroup relationships. *Geochim. Cosmochim. Acta* **54**, 1217–1232.

Rubin A. E. (2010b) Physical properties of chondrules in different chondrite groups: implications for multiple melting events in dusty environments. *Geochim. Cosmochim. Acta* **74**, 4807–4828.

Rubin A. E. (1997) The Galim LL/EH polymict breccia: evidence for impact-induced exchange between reduced and oxidized meteoritic material. *Meteorit. Planet. Sci.* **32**, 489–492.

Rubin A. E., Breen J. P., Isa J. and Tutorow S. (2016) New nind of chondrite: a clast with carbonaceous, ordinary, and unique characteristics in the Northwest Africa 10214 LL3 breccia. In 47th Lunar and Planetary Science p. 1048.

Rubin A. E. and Wasson J. T. (2011) Shock effects in "EH6" enstatite chondrites and implications for collisional heating of

the EH and EL parent asteroids. *Geochim. Cosmochim. Acta* **75**, 3757–3780.

Rubin A. E. and Wasson J. T. (1995) Variations of chondrite properties with heliocentric distance. *Meteoritics* **30**, 569.

Russel S. S., McCoy T. J., Jarosewitch E. and Ash R. D. (1998) The Burnwell, Kentucky, low iron oxide chondrite fall: description, classification and origin. *Meteorit. Planet. Sci.* **33**, 853–856.

Ruzicka A., Grossman J., Bouvier A., Herd C. D. K. and Agee C. B. (2015) The Meteoritical Bulletin, No. 102. *Meteorit. Planet. Sci.* **50**, 1662-1662.

De Sanctis M. C., Ammannito E., Capria M. T., Tosi F., Capaccioni F., Zambon F., Carraro F., Fonte S., Frigeri A., Jaumann R., Magni G., Marchi S., McCord T. B., McFadden L. A., McSween H. Y., Mittlefehldt D. W., Nathues A., Palomba E., Pieters C. M., Raymond C. A., Russell C. T., Toplis M. J. and Turrini D. (2012) Spectroscopic characterization of mineralogy and its diversity across Vesta. *Science* **336**, 697–700.

Schrader D. L., McCoy T. J. and Gardner-Vandy K. (2017) Relict chondrules in primitive achondrites: remnants from their precursor parent bodies. *Geochim. Cosmochim. Acta* **205**, 295–312.

Scott E. R. D., Clayton R. N. and Mayeda T. K. (1985) Properties and genesis of two anomalous type 3 chondrites, Suwahib (buwah) and Willaroy. In Lunar and Planetary Science XVI pp. 749–750.

Stöffler D., Keil K. and Edward R. D. S. (1991) Shock metamorphism of ordinary chondrites. *Geochim. Cosmochim. Acta* **55**, 3845–3867.

Suavet C., Alexandre A., Franchi I. A., Gattacceca J., Sonzogni C., Greenwood R. C., Folco L. and Rochette P. (2010) Identification of the parent bodies of micrometeorites with high-precision oxygen isotope ratios. *Earth Planet. Sci. Lett.* **293**, 313–320.

Sugiura N., Arkani-Hamed J. and Strangway D. W. (1986) Possible transport of carbon in meteorite parent bodies. *Earth Planet. Sci. Lett.* **78**, 148–156.

Sugiura N., Arkani-Hamed J., Strangway D. W. and Matsui T. (1985) Thermal history and possible degassing of meteorite parent bodies. *Meteoritics* **20**, 767.

Sugiura N., Brar N. S., Strangway D. W. and Matsui T. (1984) Degassing of meteorite parent bodies. *J. Geophys. Res.* **89**, B641.

Tait A. W., Tomkins A. G., Godel B. M., Wilson S. A. and Hasalova P. (2014) Investigation of the H7 ordinary chondrite, Watson 012: implications for recognition and classification of type 7 meteorites. *Geochim. Cosmochim. Acta* **134**, 175–196.

Troiano J., Rumble D., Rivers M. L. and Friedrich J. M. (2011) Compositions of three low-FeO ordinary chondrites: indications of a common origin with the H chondrites. *Geochim. Cosmochim. Acta* **75**, 6511–6519.

Verkouteren R. M. and Lipschutz M. E. (1983) Cumberland Falls chondritic inclusions—II. Trace element contents of forsterite chondrites and meteorites of similar redox state. *Geochim. Cosmochim. Acta* **47**, 1625–1633.

Wasson J. T. and Kallemeyn G. W. (1988) Compositions of chondrites. *Philos. Trans. R. Soc. A Math. Phys. Eng. Sci.* **325**, 535–544.

Wasson J. T. and Kallemeyn G. W. (1984) Cumberland Falls (chondrite), Suwahib (Buwah) and other ordinary chondrites showing evidence of postaccretional reduction. In 47th Annual Meeting of the Meteoritical Society p. 105.

Wasson J. T., Rubin A. E. and Kallemeyn G. W. (1993) Reduction during metamorphism of four ordinary chondrites. *Geochim. Cosmochim. Acta* **57**, 1867–1878.

Weisberg M. K., Boesenberg J. S., Kozhushko G., Prinz M., Clayton R. N. and Mayeda T. K. (1995) EH3 and EL3 Chondrites: A petrologic-oxygen isotopic study. Abstr. Lunar Planet. Sci. Conf. vol. 26, page 1481, 26.

Weisberg M. K. and Kimura M. (2012) The unequilibrated enstatite chondrites. *Chem. Erde* **72**, 101–115.

Weisberg M. K., McCoy T. J. and Krot A. N. (2006) Systematics and evaluation of meteorite classification. Meteorites Early Sol. Syst. II, D. S. Lauretta H. Y. McSween Jr. (Eds.), Univ. Arizona Press. Tucson, 943 pp., p. 19–52, 19–52.

Weisberg M. K., Prinz M., Clayton R. N., Mayeda T. K., Grady M. M., Franchi I., Pillinger C. T. and Kallemeyn G. W. (1996) The K (Kakangari) chondrite grouplet. *Geochim. Cosmochim. Acta* **60**, 4253–4263.

Weisberg M. K., Prinz M. and Fogel R. A. (1994) The evolution of enstatite and chondrules in unequilibrated enstatite chondrites: evidence from iron-rich pyroxene. *Meteoritics* **29**, 362–373.

Weisberg M. K., Smith C., Herd C., Haack H., Yamaguchi A., Chennaoui Aoudjehane H., Welzenbach L. and Grossman J. N. (2010) The Meteoritical Bulletin, No. 98, September 2010. *Meteorit. Planet. Sci.* **45**, 1530–1551.

Whitlock R., Lewis C. F., Clark J. C. and Moore C. B. (1991) The Cerro los Calvos and La Banderia chondrites. *Meteoritics* **26**, 169–170.

Wlotzka F. (1993) A weathering scale for the ordinary chondrites. *Meteoritics* **28**, 460.

Yamaguchi A., Kimura M., Barrat J. A., Greenwood R. C. and Franchi I. A. (2015) Petrology, bulk chemical and oxygen isotopic composition of a low-FeO ordinary chondrite, Yamato 982717. In 46th Lunar and Planetary Science Conference, p. 1679.

Zanda B., Hewins R., Bourotdenise M., Bland P. and Albarede F. (2006) Formation of solar nebula reservoirs by mixing chondritic components. *Earth Planet. Sci. Lett.* **248**, 650–660.

Associate editor: Alexander N. Krot

Left blank intentionally.

Part III

Two Recent Meteorite Falls in Iran: Famenin and Moshampa

Chapter 7

Famenin Meteorite Fall

In-preparation for submission to the *Meteoritics & Planetary Science*

Title: THE FAMENIN METEORITE FALL: ANOTHER MEMBER OF A PROPOSED H^L CHONDRITE GROUPLET

Authors: Hamed Pourkhorsandi[1*], Jérôme Gattacceca[1], Pierre Rochette[1], Lydie Bonal[2], Massimo D'Orazio[3], Bertrand Devouard[1], Corinne Sonzogni[1]

[1]CNRS, Aix-Marseille Univ., IRD, Coll. France, CEREGE, Aix-en-Provence, France

[2]Institut de Planétologie et d'Astrophysique de Grenoble, Grenoble, France

[2]Dipartimento di Scienze della Terra, Università di Pisa, Pisa, Italy

[*]Corresponding author. *E-mail address*: pourkhorsandi@cerege.fr (H. Pourkhorsandi).

Abstract

The Famenin meteorite fell around 08:30 am local time (GMT+4.5) on 27 June 2015 on the roof an house in Famenin town, NW Iran. A single 640 grams stone was recovered, shattered into several pieces upon impact. The shape of the impact hole and the relative position of the recovered meteorites indicate a N-NW fall direction. Famenin is an ordinary chondrite with a well preserved chondrules composing different chondrules types, (Fe,Ni) metal, and troilite, phosphate, and chromite. The organic matter systematics and the olivine and low-Ca compositional distributions (percent mean deviations 17.8% and 31.2%, respectively) suggest it is a metamorphosed type 3 chondrite. Considering the average chemical compositions of olivine ($Fa_{17.5 \pm 4.7}$) and low-Ca pyroxene ($Fs_{16.8 \pm 7.5}$), and the grain density (3.88 gcc^{-1}), Famenin is an H chondrite. However, saturation magnetization is 26.0 Am^2/kg, indicates a bulk metal content similar to L chondrites. Similarly, the whole-rock Ni and Co contents (13073 and 540 μgg^{-1}, respectively) are closer to typical values for L chondrites than H chondrites. Average chondrule diameter (550 µm), average Co content of the kamacite (5.6 mgg^{-1}), (Fe,Ni) metal modal abundance (5 vol%), magnetic susceptibility, and whole-rock oxygen-isotopic composition indicate intermediate properties between H and L chondrites. Famenin, together with similar

intermediate meteorites, suggest the existence of a separate ordinary chondrite grouplet for which a different designation (H^L) is proposed.

Keywords: Iran, Fall, Chondrite, H/L

1. INTRODUCTION

Around 08:30 am local time (GMT+4.5) on 27 June 2015, a meteorite fell in Famenin town of Hamedan province (35° 7.12' N, 48°58.50' E) in Iran (Fig 1). R. Salimi a resident of the town heard the sound of an impacting object onto the roof of his house. He discovered that part of the roof was damaged and fragments of a stone were spread on the roof and in the yard. The impact had damaged the asphalt layer of the roof. Looking for the impactor, he found shattered fragments of the stone (meteorite) (Fig. 2). In addition, another sample (~ 10 grams) was found resting on the floor of the neighbor's house after breaking the window glass. The shape of the damaged roof and the relative position of the meteorite indicates a N-NW fall direction (Fig. 2a). News of the event propagated quickly via the local media. Despite additional searches by the locals, no additional samples were collected. No record of of probably related fireball sighting or atmospheric detonation sounds were reported.

Only two meteorite falls have been recorded in Iran before Famenin: Veramin (mesosiderite) (Graham and Hassanzadeh 1990; Ward 1901) and Naragh (H6 chondrite) (Adib and Liou 1979; Clarke 1975) fallen in 1880 and 1974, respectively.

The meteorite was classified in CEREGE (Aix-en-Provence) as H/L3 (i.e. an ordinary chondrite with intermediate properties between those of the H and L groups) and published in the Meteoritical Bulletin (Bouvier et al. 2017). Ordinary chondrites (OCs) with such an intermediate characteristic are rare and it has been suggested that they form an individual group of OCs (Kallemeyn et al. 1989; Trigo-Rodríguez et al. 2009; Wittmann et al. 2011). Studying these chondrites helps us to understand the relationship between different OC groups and broadens our knowledge on the diversity of the solar systems materials which themselves mirror the physico-chemical condition in the solar nebula.

Here, we investigate texture, mineral chemistry, whole-rock trace-element and oxygen-isotopic compositions, and physical properties (magnetic and grain density) of Famenin. We also compare Famenin with other intermediate H/L chondrites (Bremervörde, San Juan 041, and El Médano 195).

2. METHODOLOGY

Three polished thin and thick sections of Famenin and thick sections of San Juan (SJ) 041 and El Médano (EM) 195 were prepared for petrographic studies. Mineralogical and petrological studies were conducted with a Leica DM2500P optical microscope and a Hitachi S3000-N Scanning Electron Microscope (SEM) equipped with a Bruker X-ray Energy Dispersive Spectrometer (EDS) at CEREGE (Aix-en-Provence). Chemical compositions of the mineral phases were determined with CAMECA SX50 and SX100 electron microprobes at the CAMPARIS facility (Paris), using natural and synthetic standards, focused electron beam (~ 1 µm in diameter), an accelerating voltage of 15 kV and a beam current of 10 nA. To correct the deviation of Co content produced by the occurrence of an interference (form K_{BO}) between Co and Fe of the metal grains (Afiattalab and Wasson 1980), a correction for the Co content of by a factor equal to 0.0012 (Fe concentration) was applied.

Petrophysicial measurements were performed at CEREGE. Magnetic susceptibility was measured using a KLY2 instrument from Agico equipped with both a large (65cm^3) and a small (10cm^3) coil. Magnetic hysteresis properties were measured with a Princeton Micromag vibrating sample magnetometer (VSM) with a noise level of about 1 nAm2 and a maximum applied field of 1 T. Hysteresis loops allow the determination of coercivity (BC), saturation magnetization (MS), saturation remanent magnetization (MRS), high-field susceptibility (□HF, including both diamagnetic and paramagnetic contributions). Coercivity of remanence (BCR) was evaluated through DC back-field demagnetization of the saturation remanence.

An helium pycnometer was used for the grain density measurements. .

The whole-rock trace-elements content of Famenin was determined by Inductively Coupled Plasma - Mass Spectrometry (ICP-MS) using a Perkin-Elmer NexION® 300x spectrometer at the Pisa University's Dipartimento di Scienze della Terra. Allende carbonaceous chondrite reference

sample (USNM 3529, splite 20, position 22) was dissolved and analyzed along with Famenin to check the accuracy of the results. About 50-100 mg of each powder were dissolved in a mixture of HF and HNO_3 on a hot plate at ~120 °C inside screw-top perfluoroalkoxy (PFA) vessels. Then the sample solutions were diluted to 50 mL in polypropylene vials. In each step of sample preparation, Mill-Q® purified water (18.2 M cm), ultrapure HF and HNO_3 were used. The sample solutions were introduced into the plasma after online mixing with a solution containing 20 ng/mL each of Rh, Re and Bi as internal standards. The elements Li, Be, Ga, Rb, Sr, Y, Zr, Nb, Mo, Cs, Ba, REE, Hf, Ta, W, Pb, Th, U were determined in "standard mode", whereas the elements Sc, V, Cu were determined in "kinetic energy discrimination mode, KED" using a He flow of 3.7 mL/min. Analyses were done using an external calibration performed with a solution of the BE-N (alkaline basalt) geochemical reference sample. In Table 1 the results of the ICP-MS analyses of Allende along with the literature values are reported. The analytical precision is between 5 and 10% RSD for elements with concentrations > 0.5 µg/g and between 10 and 20% RSD for elements with concentrations < 0.5 µg/g.

Measurements of $\delta^{18}O$ and $\delta^{17}O$ of two Famenin 1.5 mg aliquot of silicates hand-picked from a powdered and acid-washed 200 mg bulk sample were carried out at the Stable Isotopes Laboratory of CEREGE. Laser fluorination coupled with isotope ratio mass spectrometry (IRMS) (Alexandre et al., 2006; Crespin et al., 2008) adapted for measurement of extraterrestrial materials (Suavet et al. 2010) was used for this purpose. The three oxygen isotopic compositions were measured with a dual-inlet mass spectrometer Thermo-Finnigan Delta Plus. In addition to Famenin, Ochansk (H), Homstead (L), and Bremervörde (H/L) were analyzed for comparison. The oxygen isotope results are expressed in ‰ versus the international reference standard V-SMOW: $\delta^{18}O = [(^{18}O/^{16}O)_{sample}/(^{18}O/^{16}O)_{V\text{-}SMOW}\text{-}1]\times1000$ and $\delta^{17}O = [(^{17}O/^{16}O)_{sample}/(^{17}O/^{16}O)_{V\text{-}SMOW}\text{-}1]\times1000$. The $\delta^{18}O$ and $\delta^{17}O$ values of the reference gas were calibrated with measurements of NBS28 standard ($\delta^{18}O$=9.60‰, Gröning, 2004). $\Delta^{17}O$ is computed as $\Delta^{17}O = \ln(1+\delta^{17}O) - \lambda\ln(1+\delta^{18}O)$ with λ=0.5247 (Miller 2002). The $\delta^{17}O$ value of the NBS28 standard ($\delta^{17}O$ =5.026‰) was computed so as to give $\Delta^{17}O$=0‰. The measurements were corrected on a daily basis using 1.5 mg quartz internal laboratory standard “Boulangé” (Alexandre et al. 2006; Suavet et al. 2010). During the analyzing period, the analytical uncertainties derived from repeated measurement (n= xx) of this internal laboratory standard are x‰, x‰, x‰ for $\delta^{17}O$, $\delta^{18}O$ and $\Delta^{17}O$, respectively.

Gamma spectroscopy of the two larger fragments (total ~23 g) were carried out from 16 to 24 July 2015 (683500 seconds) in LSCE (Gif-sur-Yvette).

The Raman experiments were performed at Laboratoire de Géologie de Lyon Terre, Planètes, Environnement (ENS Lyon) with a Labram spectrometer (Horiba-Jobin-Yvon) equipped with a Spectra Physics Argon ion laser and using 514.5 nm excitation. Carbonaceous matter is sensitive to laser-induced heating and can be locally altered. Moreover, the Raman bands of the polyaromatic carbonaceous matter are dispersive. Thus, to avoid any laser alteration of the carbonaceous matter and to have a meaningful comparison with reference meteorites from the literature, the same experimental and analytical conditions as in Bonal et al. (2016) were used. Raman spectra of the carbonaceous matter in Famenin were obtained both on isolated matrix grains. A raw piece of approximately 200 mg was gently crushed. Around 30 matrix grains (typical apparent diameter around 30 µm) were then manually selected according to color and texture under a binocular microscope. The selected matrix grains were pressed between two glass slides that were also used as substrate for the Raman analysis. This procedure allows working on ‘‘fresh” samples and helps enhance heat dissipation, thereby minimizing thermal damage.

3. RESULTS

3.1. Hand specimen description

Upon the impact, the meteorite fragmented into two large and eight small pieces. All the recovered mass is about 630 g in which two bigger pieces comprise 565 g and the rest are as small fragments with masses between 5 to 25 g (Fig 2). Famenin has weakly developed regmaglypts and the fusion crust has a black to dark-brown color with shiny patches of glassy material covering the fusion crust as an additional layer. The remnants of roofing asphalt material can be seen as black patches with sizes up to 5 cm.

In broken surface it has a light grey color. Fine-grained clasts lighter in color than the rest of the meteorite are present (Fig. 2b). (Fe,Ni) metal grains show no sign of weathering. Distinct chondrules, few fine-grain clasts with light lithology, (Fe,Ni) metal and troilite are easily discernible by naked eye.

3.2. Optical and electron microscopy

1905 3.2.1. Famenin

1906 The fusion crust shows a vesicular texture with magnetite grains in the outmost side and
1907 narrow troilite veinlets toward the interior of the meteorite formed by the melting and
1908 recrystallization of the primary troilite during atmospheric passage of the meteorite (Fig. 4a).

1909 Point counting under reflected light optical microscopy, with a step-size of 50 μm, yields the
1910 following proportions: 90 vol% silicates, 5 vol% (Fe,Ni) metal, and 5 vol% troilite (n = 584).
1911 Barred olivine, cryptocrystalline, porphyritic, and radial pyroxene chondrule types are present
1912 (Fig. 3, 4). Average apparent chondrule diameter is 550 ± 296 μm (n = 100), with a median,
1913 mode, and maximum diameters of 510, 360, and 1960 μm, respectively (Fig. 5).

1914 Backscattered electron (BSE) images of the Famenin chondrite are shown in Fig. 4b-g.
1915 Olivine and pyroxene are not completely equilibrated and some show normal zoning. Overall,
1916 olivine shows more homogeneity than the pyroxene. The matrix is clastic and comprises
1917 individual mineral and chondrule fragments of different types. (Fe,Ni) metal and troilite are not
1918 completely separated from each other. Compared to troilite, most of the (Fe,Ni) metal grains are
1919 relatively round. Opaque rims consisting mostly of troilite aggregated with (Fe,Ni) metal and
1920 (Fe,Mg) silicates surround some of the chondrules. Fig. 4-g shows a barred olivine chondrule
1921 with normal zoning containing dendritic grains crystallized out of the feldspathic glass.

1922 Olivine exhibits undulatory extinction and displays planar fractures with about 200 μm
1923 spacing. Troilite displays finely polycrystalline textures with domain size of about 10 μm (Fig.
1924 4h). Based on the olivine optical microscopy, and using the classification of Stöffler et al.
1925 (1991), Famenin is very weakly shocked and has a shock stage of S2.

1926 3.2.2. El Médano 195

1927 EM 195 is classified as H/L3 (Ruzicka et al. 2015) (Fig. 6). Point counting under reflected
1928 light optical microscopy, with a step-size of 80 μm, yields the following proportions: 79 vol%
1929 silicates, 9 vol% (Fe,Ni) metal, and 12 vol% troilite (n = 531). Majority of the (Fe,Ni) metal and
1930 troilite grains are in contact with each other. Troilite rims are preserved and few (Fe,Ni) metal
1931 globules are present. The terrestrial weathering effects on EM 195 are limited to thin rims of Fe
1932 oxides/oxyhydroxides around few (Fe,Ni) metal grains. Average apparent chondrule diameter is
1933 570 ± 331 μm (n = 84), with a median, mode, and maximum diameters of 480, 426, and 1970

μm, respectively (Fig. 5). Except some grain rims, the abundance of the weathering products is low and it is a has a weathering grade W1 (Wlotzka 1993).

3.2.3. San Juan 041

SJ 041 is classified as H/L6 (Garvie 2012). This process has led to the destruction of the chondrules and the separation of (Fe,Ni) metal and troilite from each other. Fig. EA1 shows a picture of this meteorite. Elongation of the (Fe,Ni) metal and troilite and the presence of melt pockets containing troilite droplets indicates that SJ 041 is heavily shocked. Point counting under reflected light optical microscopy, with a step-size of 80 μm, yields the following proportions: 84 vol% silicates, 7 vol% (Fe,Ni) metal, and 8 vol% troilite (n = 601). The majority of the (Fe,Ni) metal and troilite grains are in contact with each other. The (Fe,Ni) metal and troilite show terrestrial weathering effects in some parts. The meteorite has a weathering grade W2.

3.3. Mineral chemistry

The representative chemical compositions of olivine, low-Ca, and (Fe,Ni) metal are reported in Table 2, 3, and 4. Low-Ca pyroxene show wider composition range than the olivine (Fig. 7). The percent mean deviations (PMD) are 18% and 31% for olivine and low-Ca pyroxene, respectively. Average olivine (n = 71) and low-Ca pyroxene (n = 34) compositions are $Fa_{17.5\pm4.7}$ and $Fs_{16.8\pm7.5}$, respectively. Although silicates are not equilibrated, olivine compositions are dominantly in the xxx-xxx interval, in the range for H chondrites (Fig. 7). The average Co concentration (n = 8) of kamacite is 5.6 mg/g (Table 4). This value is intermediate between the concentrations reported for H and L chondrites (Rubin 1990).

Representative chemical compositions of olivine and low-Ca pyroxene are reported in Table 5. PMD for olivine and low-Ca pyroxene is 29% and 23%, respectively. Average olivine and low-Ca pyroxene compositions are $Fa_{16.9\pm6.0}$ (n = 13) and $Fs_{17.2\pm5.6}$ (n = 10), respectively and are in the range of H chondrites values (e.g., Brearley and Jones 1998).

Table 6 reports the representative olivine and low-Ca chemical compositions. In accordance with its equilibrated texture, mineral chemistry shows a narrow distribution. PMD for olivine and low-Ca pyroxene is 0.8% and 3.5%, respectively. Average olivine and low-Ca pyroxene

compositions are $Fa_{22.5\pm0.2}$ (n =4) and $Fs_{18.3\pm0.8}$ (n = 5), respectively. The values are near the lower limits of L chondrites, but still are outside the defined limits by Nomenclature Committee.

3.4. Magnetic properties

Magnetic susceptibility χ and saturation magnetization (*Ms*) are proxies of the bulk metal content and opaque mineralogy, and can be used for the classification of different meteorite groups (Gattacceca et al. 2014; Rochette et al. 2003a). The average magnetic susceptibility measured on four pieces with masses in the range 5-11 grams is $\log\chi = 5.07$ (with χ in $10^{-9}m^3kg^{-1}$), in agreement with susceptibilities of Tieschitz and Bremervörde H/L3 (Rochette et al. 2003a). Saturation magnetization measured on a 0.08 gram fragment is Ms = 24.9 Am^2kg^{-1}, in agreement with the values reported for L chondrites (xxx) (Gattacceca et al. 2014). Mrs/Ms and Bcr/Bc ratios for Famenin plots near the L and lower values of H chondrites (Fig 8). Similar to the magnetic properties, the grain density differs between different meteorite groups (e.g., Consolmagno et al. 2006). The average grain density measured on an 11.0 gram fragment is 3.88 ± 0.02 gcc^{-1}, near the upper limit for H chondrites (Fig. 9), making it one of the OCs with highest grain densities.

Because of its significant terrestrial weathering (W2 grade) the magnetic properties of SJ 041 cannot be interpreted robustlyin terms of original metal content.

For EM 195, the magnetic susceptibility is $\log\chi=4.99$ which is within L chondrites range. However, one has to take into account the susceptibility decrease due to weathering.

3.5. Trace-element bulk chemistry

The whole-rock trace-element composition of Famenin is reported in Table 1. The CI-normalized Masuda-Coryell diagrams of Famenin along with the mean values reported for H, L, and LL OCs (Wasson and Kallemeyn 1988) are shown in Fig. 10. The trace-element content of Famenin is chondritic and it follows the general trend of OCs. Having a Ni content of 13.1 mg/g compared to the average values of H (16.0 mg/g), L (12.0 mg/g), and LL (10.2 mg/g) chondrites, Famenin is intermediate between H and L, more closer to the L chondrite range. Its Co content is 540 µg/g which compared to the average values of H (810 µg/g), L (590 µg/g) and LL (490 µg/g) chondrites, lies in between L and LL chondrites.

3.6. Oxygen-isotopic composition

The whole-rock oxygen-isotopic composition analysis results for two aliquots of Famenin along with the data for Ochansk, Homstead, and Bremervörde are reported in the Table 7. Fig. 11 depicts the $\Delta^{17}O$ versus $\delta^{18}O$ values of Famenin along with the data for H, L, LL, and H/L (Tieschitz and Bremervörde) chondrites from (Clayton and Mayeda 1991). Considering the $\Delta^{17}O$ values of 1.00 and 1.03 (average 1.01, n = 2) and 1.00 for Famenin and Bremervörde, respectively, they are in the range of the L and H/L OCs values (Clayton and Mayeda 1991). However, they show slightly higher $\delta^{18}O$ values than the majority of the L chondrites and Bremervörde compared to the values reported in Clayton and Mayeda (1991). Our analysis on Bremervörde, puts it in the vicinity of Famenin and Homstead (analyzed in this work) as well as the Tieschitz and xxx (L) (analyzed by Clayton and Mayeda 1991).

3.7. Cosmogenic radionuclides

The data show the presence of ^{7}Be ($t_{1/2}$ = ~ 53 days; 477 keV), ^{54}Mn ($t_{1/2}$ = ~ 312 days; 834.8 keV), ^{22}Na ($t_{1/2}$ = ~ 2.6 years; 1274.5 keV) and ^{26}Al ($t_{1/2} = 7.17\times10^{5}$ years; 1808.65 keV). The detection of short-lived nuclides such as ^{7}Be and ^{54}Mn and the detailed reports in the media confirm the occurrence of this fall event.

3.8. Organic matter

Each individual Raman spectra obtained on matrix of Famenin exhibits the D- and G-bands, attesting the presence of polyaromatic carbonaceous matter. Spectral differences (e.g., shape, relative intensity…) are visible on the raw Raman spectra, reflecting variable structural order of the polyaromatic carbonaceous matter within Famenin. These differences are confirmed by the range of spectral parameters obtained through the analytical adjustment. Spectral parameters are dispersed but tend to be distributed among two main groups with the following mean values:

Famenin (A – 15 sp.): $FWHM_D$ (cm^{-1})= 151.8 ± 17.2 and I_D/I_G = 1.03 ± 0.06

Famenin (B – 15 sp.): $FWHM_D$ (cm^{-1})= 56.2 ± 13.6 and I_D/I_G = 1.13 ± 0.21

Spectra acquired on manually selected matrix grains are both of type “A” and “B”.

The observed spectral variability reflects variable thermal metamorphism experienced by Famenin: type “A” spectra reflect thermal metamorphism comparable to that experienced by a type 3.4 chondrite, while type “B” spectra reflect a higher thermal metamorphism (>3.7) (Fig. 12).

It has to be noted that the type "A" spectra are quite variable as well with spectral parameters of individual spectrum distributed over the range from Bishunpur (3.1) to Tieschitz (3.6).

4. DISCUSSION

3.1. Classification

Famenin is an OC, but it shares properties with both H and L chondrites, making its classification problematic.

Considering the average chemical compositions of olivine and low-Ca pyroxene, and the grain density, Famenin is an H chondrite. However, some other properties do not fit those observed in H chondrites. The whole-rock Ni and Co contents are closer to the values of L chondrites. Magnetic susceptibility (5.07) is intermediate between H (log $\chi = 5.32 \pm 0.10$, n = 145 falls) and L chondrites (log $\chi = 4.87 \pm 0.10$, n = 144 falls) (Rochette et al. 2003b). The modal (Fe,Ni) metal abundance is lower than the H chondrites values (5 vol% versus 8 vol%) (Weisberg et al. 2006). Saturation magnetization indicates a bulk metal content similar to L chondrites (Gattacceca et al. 2014). Average chondrule diameter in Famenin (550 μm) is intermediate between the H and L chondrites (Weisberg et al. 2006). The average Co content in kamacite in Famenin (5.6 mg/g) is intermediate between values measured in H and L chondrites, 4.4-5.1 and 7.0-0.95 mg/g, respectively (Rubin 1990) (Fig. 13). Oxygen-isotopic bulk composition of Famenin is different from values measured in H chondrites. Its $\Delta^{17}O$ is in the range of L chondrites; however, $\delta^{18}O$ is higher in Famenin and is closer to the field of Tieschitz and Bremervörde H/L chondrites.

In accordance with the analysis of the organic matter, the olivine and low-Ca pyroxene PMD values indicate a petrologic type 3 (ranging from 3.5 to 3.7) (Sears et al. 1982).

Considering these evidences, we classify Famenin as an H/L3 chondrite.

3.2. H/L Chondrites

Table 8 is a list extracted from the Meteoritical Bulletin showing the meteorites classified as H/L chondrites. This designation is ambiguous. The H/L designation as described by Kallemeyn et al. (1989) refers to the chondrites with properties intermediate between H and L chondrites.

2047 However, H/L is also often used to describe meteorites whose assignation to H or L group is
2048 unclear, with a meaning close to the H(L) or L(H) classification. While some well-described
2049 meteorites such as Bremervörde, Cali, LaPaz Icefield (LAP) 031047, and Tieschitz are classified
2050 as H/L chondrites based on their intermediate characteristics (Kallemeyn et al. 1989; Trigo-
2051 Rodríguez et al. 2009; Wittmann et al. 2011); the majority of meteorites classified as H/L are
2052 simply H or L chondrites that have not been classified thoroughly for one or several of the
2053 following reasons: unequilibrated mineral composition and low number of analyzed minerals and
2054 no measurement of chondrule size, lack of mineral chemistry data and high weathering grade
2055 which decreases the efficiency of magnetic classification. After filtering out these poorly
2056 classified meteorites, we are left with a population of truly intermediate chondrites that would
2057 deserve a specific classification nomenclature. We propose to call these latter H^L chondrites.
2058 Famenin, Bremervörde, Tieschitz and Cali, as falls, and SJ 041, EM 195, NWA 4726, SaU 301,
2059 JaH 113 and LAP 03147, as finds, are members of this grouplet.

2060 Considering the gradual oxygen fugacity changes between different regions in the Solar
2061 nebula (e.g., Rubin 1990), the occurrence of meteorites originating from parent bodies with
2062 intermediate compositions between H and L chondrites is reasonable (Kallemeyn et al. 1989;
2063 Trigo-Rodríguez et al. 2009; Wittmann et al. 2011). As in Famenin and some other H^L
2064 chondrites, their olivine and low-Ca pyroxene is not necessarily in between H and L chondrite
2065 chemical ranges. There are other characteristics, such as oxygen-isotopic composition,
2066 siderophile content, metal composition, and metal abundance, which suggest that they are H^L
2067 chondrites indeed. Considering the fact that meteorites are being classified mostly only based on
2068 their olivine and low-Ca compositions, it is possible that many unique samples (in this case H/L
2069 chondrites) are being overlooked and misclassified.

2070 We suggest that Famenin and H^L chondrites might originate from a parent body with
2071 intermediate composition between H and L chondrites and define an intermediate ordinary
2072 chondrite group (Trigo-Rodríguez et al. 2009; Wittmann et al. 2011). To characterize such a
2073 group, a systematic work on selected OCs to analyze their mineralogical, chemical and oxygen-
2074 isotopic compositions is required. Metal abundance would be a useful factor to choose the
2075 possible H^L meteorites for detailed studies. Based on magnetic properties (Rochette et al. 2003;
2076 Gattacceca et al. 2014), a significant number of OC falls classified as H or L are in the H/L

range. Pointing only type 3, the list is Bovedy (L3 with logχ =5.01), Dhajala (H3, 5.08) Sharps (H3, 4.99). Such studies would shed light on the intergroup and intragroup relationships between OCs.

5. CONCLUSIONS

Our detailed study of Famenin meteorite indicates it is a type 3 OC with characteristic intermediate between the H and L groups, as a number of other OCs. These chondrites might be members of another group originating from a different parent body for which we propose to use a new designation (H^L) rather than the ambiguous H/L designation that is also and mostly used for meteorites that could be either H or L chondrite. Works on OCs with intermediate properties will help to test this hypothesis.

Acknowledgments

Behzad Qiasvand and *Nojum* magazine are thanked for their efforts in obtaining the Famenin meteorite samples for scientific studies. We thank I. Lefèvre (LSCE) for gamma spectroscopy. The first author thanks M. Zadsaleh for the Fig. 1, and M. Djamali and D. Pourkhorsandi for their help for sample shipment. Cultural Office of the French Embassy in Tehran is acknowledged for providing Ph.D. grant for the first author. Support from the Gundishapur PHC program is also acknowledged.

References:

Adib D., and Liou J. G. 1979. The Naragh meteorite - A new olivine-bronzite chondrite fall. *Meteoritics* 14:257–272. http://adsabs.harvard.edu/abs/1979Metic..14..257A.

Afiattalab F., and Wasson J. T. 1980. Composition of the metal phases in ordinary chondrites: implications regarding classification and metamorphism. *Geochimica et Cosmochimica Acta* 44:431–446. http://www.sciencedirect.com/science/article/pii/0016703780900423 (Accessed August 11, 2015).

Alexandre A., Basile-Doelsch I., Sonzogni C., Sylvestre F., Parron C., Meunier J.-D., and Colin F. 2006. Oxygen isotope analyses of fine silica grains using laser-extraction technique: Comparison with oxygen isotope data obtained from ion microprobe analyses and application to quartzite and silcrete cement investigation. *Geochimica et Cosmochimica Acta* 70:2827–2835.

Bonal L., Quirico E., Flandinet L., and Montagnac G. 2016. Thermal history of type 3 chondrites from the antarctic meteorite collection determined by Raman spectroscopy of their polyaromatic carbonaceous matter. *Geochimica et Cosmochimica Acta*. http://linkinghub.elsevier.com/retrieve/pii/S0016703716303477.

Bouvier A., Gattacceca J., Agee C., Grossman J., and Metzler K. 2017. The Meteoritical Bulletin, No. 104. *Meteoritics & Planetary Science* 52:2284–2284. http://doi.wiley.com/10.1111/maps.12930.

Brearley A. J., and Jones R. H. 1998. Chondritic meteorites. *Reviews in Mineralogy and Geochemistry* 36.

Clarke R. S. 1975. The Meteoritical Bulletin. *Meteoritics* 10:133–158. http://doi.wiley.com/10.1111/j.1945-5100.1975.tb00018.x.

Clayton R., and Mayeda T. 1991. Oxygen isotope studies of ordinary chondrites. *Geochimica et Cosmochimica Acta* 55:2317–2337. http://www.sciencedirect.com/science/article/pii/001670379190107G.

Consolmagno G. J., Macke R. J., Rochette P., Britt D. T., and Gattacceca J. 2006. Density, magnetic susceptibility, and the characterization of ordinary chondrite falls and showers. *Meteoritics & Planetary Science* 41:331–342. http://doi.wiley.com/10.1111/j.1945-5100.2006.tb00466.x (Accessed January 19, 2016).

Crespin J., Alexandre A., Sylvestre F., Sonzogni C., Paillès C., and Garreta V. 2008. IR Laser Extraction Technique Applied to Oxygen Isotope Analysis of Small Biogenic Silica Samples.

Dauphas N., and Pourmand A. 2015. Thulium anomalies and rare earth element patterns in meteorites and Earth: Nebular fractionation and the nugget effect. *Geochimica et Cosmochimica Acta* 163:234–261. http://www.sciencedirect.com/science/article/pii/S0016703715001891 (Accessed June 19, 2015).

Friedrich J. M., Wang M.-S., and Lipschutz M. E. 2003. Chemical studies of L chondrites. V: compositional patterns for 49 trace elements in 14 L4-6 and 7 LL4-6 falls. *Geochimica et Cosmochimica Acta* 67:2467–2479. http://www.sciencedirect.com/science/article/pii/S0016703703000243 (Accessed June 24, 2015).

Garvie L. A. J. 2012. The Meteoritical Bulletin, No. 99, April 2012. *Meteoritics & Planetary Science* 47:E1–E52. http://doi.wiley.com/10.1111/maps.12026.

Gattacceca J., Suavet C., Rochette P., Weiss B. P., Winklhofer M., Uehara M., and Friedrich J. M. 2014. Metal phases in ordinary chondrites: Magnetic hysteresis properties and implications for thermal history. *Meteoritics & Planetary Science* 49:652–676. http://doi.wiley.com/10.1111/maps.12268 (Accessed October 9, 2015).

Graham A. L., and Hassanzadeh J. 1990. The Meteoritical Bulletin. *Meteoritics* 25:59–63. http://doi.wiley.com/10.1111/j.1945-5100.1990.tb00971.x.

Gröning M. 2004. Chapter 40 – International Stable Isotope Reference Materials. In *Handbook of Stable Isotope Analytical Techniques*. pp. 874–906.

Jarosewich E., Clarke C. R. S., and Barrows J. N. 1987. Allende Meteorite Reference Sample. *Smithsonian Contributions to the Earth Sciences* 1–49. https://repository.si.edu/handle/10088/813 (Accessed January 31, 2017).

Kallemeyn G. W., Rubin A. E., Wang D., and Wasson J. T. 1989. Ordinary chondrites: Bulk compositions, classification, lithophile-element fractionations and composition-petrographic type relationships. *Geochimica et Cosmochimica Acta* 53:2747–2767. http://www.sciencedirect.com/science/article/pii/0016703789901464 (Accessed October 4, 2015).

Miller M. F. 2002. Isotopic fractionation and the quantification of 17O anomalies in the oxygen three-isotope system: an appraisal and geochemical significance. *Geochimica et Cosmochimica Acta* 66:1881–1889.

Rochette P., Sagnotti L., Bourot-Denise M., Consolmagno G., Folco L., Gattacceca J., Osete M. L., and Pesonen L. 2003a. Magnetic classification of stony meteorites: 1. Ordinary chondrites. *Meteoritics & Planetary Science* 38:251–268. http://doi.wiley.com/10.1111/j.1945-

5100.2003.tb00263.x (Accessed October 4, 2015).

Rochette P., Sagnotti L., Bourot-Denise M., Consolmagno G., Folco L., Gattacceca J., Osete M. L., and Pesonen L. 2003b. Magnetic classification of stony meteorites: 1. Ordinary chondrites. *Meteoritics & Planetary Science* 38:251–268. http://doi.wiley.com/10.1111/j.1945-5100.2003.tb00263.x.

Rubin A. E. 1990. Kamacite and olivine in ordinary chondrites: Intergroup and intragroup relationships. *Geochimica et Cosmochimica Acta* 54:1217–1232. http://www.sciencedirect.com/science/article/pii/001670379090148E (Accessed October 4, 2015).

Ruzicka A., Grossman J., Bouvier A., Herd C. D. K., and Agee C. B. 2015. The Meteoritical Bulletin, No. 102. *Meteoritics & Planetary Science* 50:1662–1662. http://doi.wiley.com/10.1111/maps.12491.

Sears D. W., Grossman J. N., and Melcher C. L. 1982. Chemical and physical studies of type 3 chondrites—I: Metamorphism related studies of Antarctic and other type 3 ordinary chondrites. *Geochimica et Cosmochimica Acta* 46:2471–2481. http://www.sciencedirect.com/science/article/pii/0016703782903702 (Accessed October 4, 2015).

Stöffler D., Keil K., and Edward R.D S. 1991. Shock metamorphism of ordinary chondrites. *Geochimica et Cosmochimica Acta* 55:3845–3867.

Suavet C., Alexandre A., Franchi I. A., Gattacceca J., Sonzogni C., Greenwood R. C., Folco L., and Rochette P. 2010. *Identification of the parent bodies of micrometeorites with high-precision oxygen isotope ratios,*.

Trigo-Rodríguez J. M., Llorca J., Rubin A. E., Grossman J. N., Sears D. W. G., Naranjo M., Bretzius S., Tapja M., and Sepúlveda M. H. G. 2009. The Cali meteorite fall: A new H/L ordinary chondrite. *Meteoritics & Planetary Science* 44:211–220. http://doi.wiley.com/10.1111/j.1945-5100.2009.tb00729.x.

Ward H. A. 1901. Veramin Meteorite. *American Journal of Science* s4-12:453–459. http://www.ajsonline.org/cgi/doi/10.2475/ajs.s4-12.72.453.

Wasson J. T., and Kallemeyn G. W. 1988. Compositions of Chondrites. *Philosophical Transactions of the Royal Society A: Mathematical, Physical and Engineering Sciences* 325:535–544. http://rsta.royalsocietypublishing.org/content/325/1587/535 (Accessed July 3, 2015).

Weisberg M. K., McCoy T. J., and Krot A. N. 2006. Systematics and Evaluation of Meteorite Classification. *Meteorites and the Early Solar System II, D. S. Lauretta and H. Y. McSween Jr. (eds.), University of Arizona Press, Tucson, 943 pp., p.19-52* 19–52.

Wittmann A. et al. 2011. H/L chondrite LaPaz Icefield 031047 – A feather of Icarus? *Geochimica et Cosmochimica Acta* 75:6140–6159. http://www.sciencedirect.com/science/article/pii/S0016703711004352 (Accessed September 29, 2015).

Wlotzka F. 1993. A weathering scale for the ordinary chondrites. *Meteoritics* 28:460. http://articles.adsabs.harvard.edu/full/1993Metic..28Q.460W.

Figure captions:

Fig. 1: Famenin fall location.

Fig. 2: Picture showing the; a) Famenin fall place on the roof of an house. Note a N-NW fall direction. b-c) Different fragments of Famenin meteorite.

Fig. 3: Optical microscopic images of Famenin in transmitted (a) and reflected (b) light.

Fig. 4: Optical and electron microscope images of Famenin. g) In this figure, a type I chondrule, smaller in size with Mg-rich olivine grains and metal droplets can be seen. Small copper and chromite grains occur along with phosphate and metal grains.

Fig. 5: Size frequency distribution of the chondrule diameters in Famenin and El Médano 195. Horizontal axis values mark the upper limits of the size bins.

Fig. 6: Optical microscopic image of El Médano 195 in reflected light.

Fig. 7: Histograms showing the compositional distributions of randomly chosen a) olivine (n = 71) and b) low-Ca pyroxene (n = 35) grains in Famenin.

Fig. 8: Hysteresis properties for Famenin and other ordinary chondrites. Data source: Gattacceca et al. (2014).

Fig. 9: Plot showing the grain density vs. magnetic susceptibility for Famenin and other ordinary chondrites. Data source: Consolmagno et al. (2006).

Fig. 10: CI-normalized trace-element chemical composition of Famenin. Mean OCs data from Wasson and Kallemeyn (1988).

Fig. 11: $\Delta^{17}O$ versus $\delta^{18}O$ values of Famenin compared to type equilibrated H, L, and LL and 3-5 H^L. Ochansk, Homstead, and Bremervörde analyzed for comparison in this work. Data sources: LAP 031047 (Wittmann et al. 2011), other samples (Clayton and Mayeda 1991). $\Delta^{17}O$ values are calculated using a slope of 0.52.

Fig. 12: Spectral parameters of Raman bands of carbonaceous materials in Famenin and in reference chondrites: $FWHM_D$ vs. I_D/I_G. Averages (points) and standard deviations (bars) are plotted for reference samples (black symbols) and for Famenin (open symbols). Spectral parameters of individual spectrum are plotted for Famenin (small grey diamonds).

Fig. 13: a) Kamacite Co vs. Fa and b) Kamacite Co vs. kamacite Ni contents of Famenin and ordinary chondrite. Data source: Rubin (1990).

Electronic annex:

EA-1: Optical microscopic image of San Juan 041 in reflected light.

Table headings

Table 1: Trace-element (µg/g) determined by ICP-MS for Famenin and Allende as reference sample. Allende composition is reported from the literature for comparison.

Table 2: Representative olivine compositions (in wt%) from Famenin.

Table 3: Representative low-Ca pyroxene compositions (in wt%) from Famenin.

Table 4: (Fe,Ni) metal compositions (in wt%) from Famenin.

Table 5: Representative olivine and low-Ca pyroxene compositions (in wt%) from El Médano 195.

Table 6: Representative olivine and low-Ca pyroxene compositions (in wt%) from San Juan 041.

Table 7: Results of the whole-rock oxygen isotopes analyses.

Table 8: A list of meteorites classified with intermediate characteristics between H and L chondrites reported in the Meteoritical Bulletin.

Fig. 1:

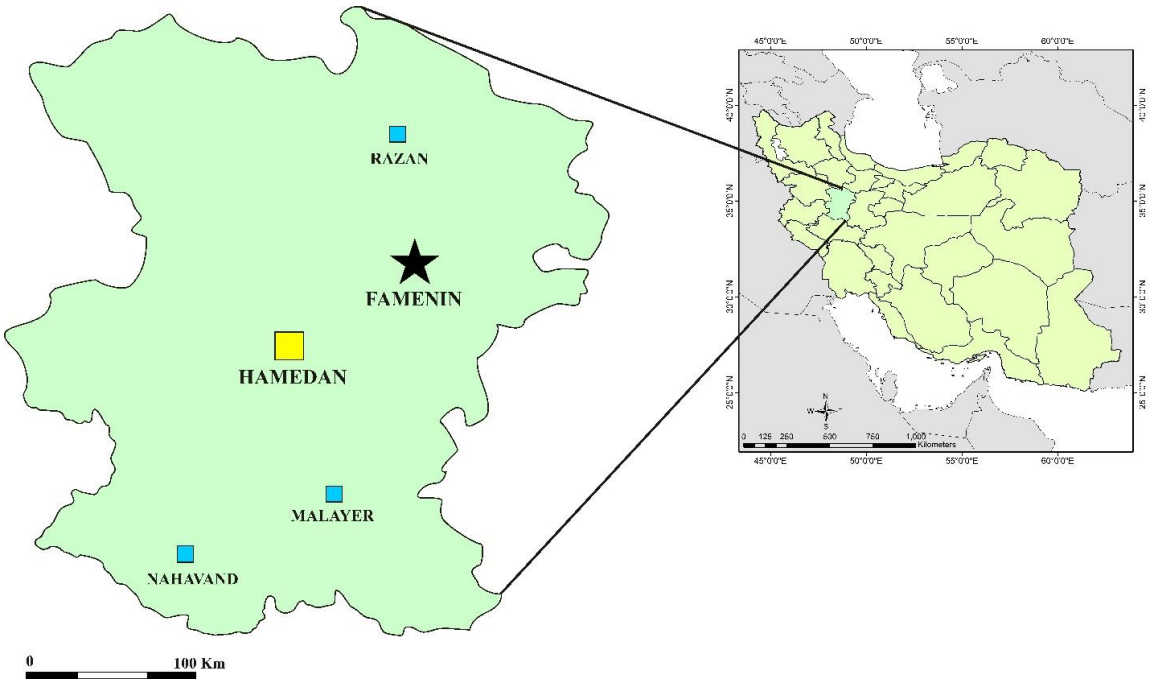

Fig. 2:

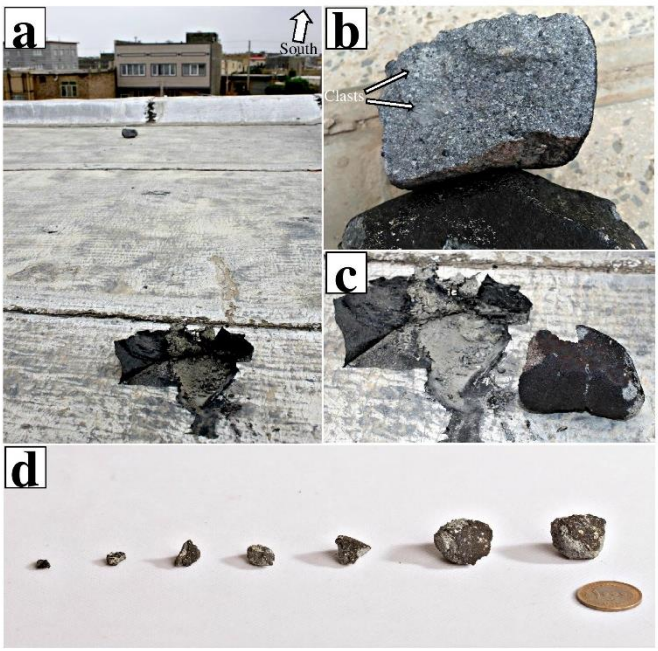

2270 **Fig. 3:**

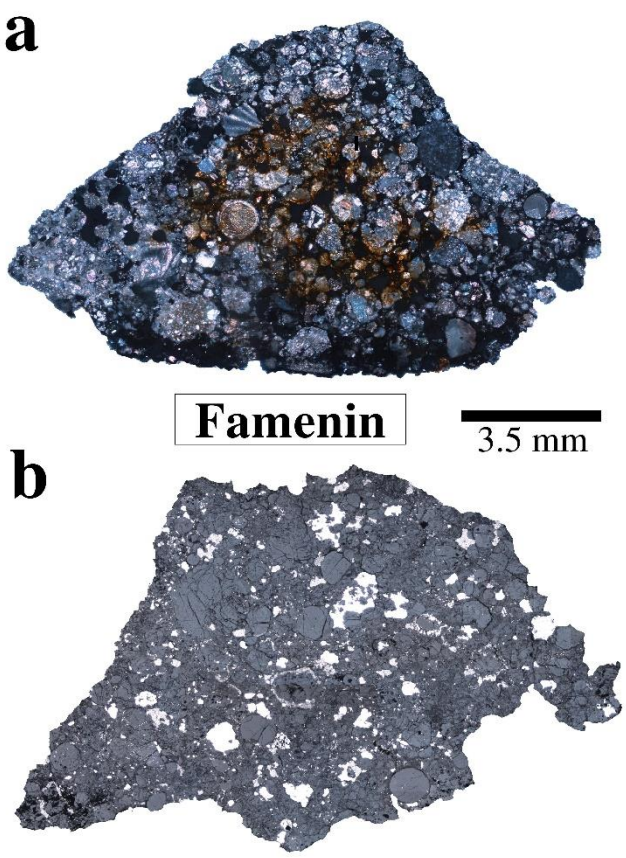

2271

2272

2273

2274

2275

2276

2277

2278

2279

2280 **Fig. 4:**

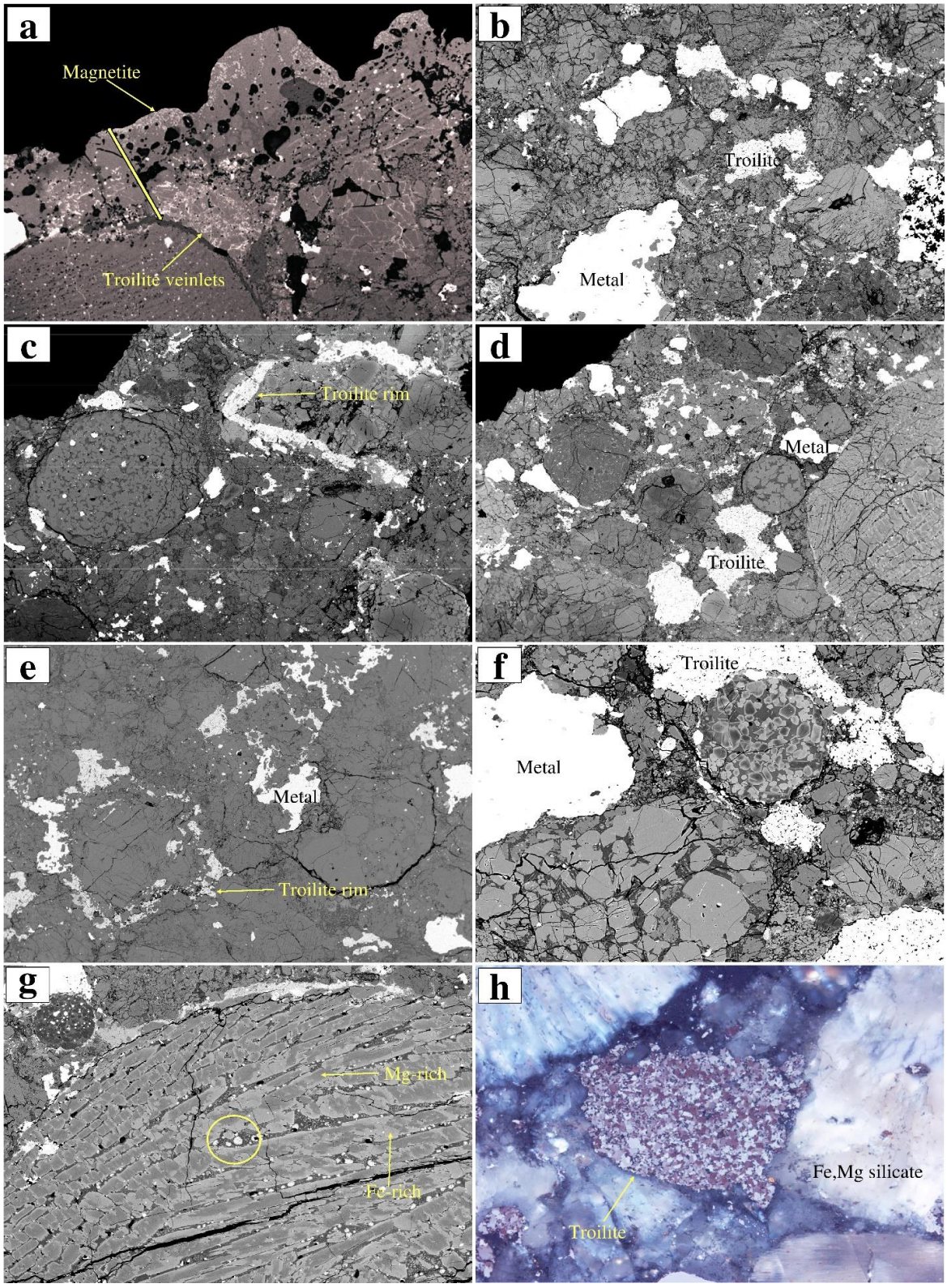

2281

Fig. 5:

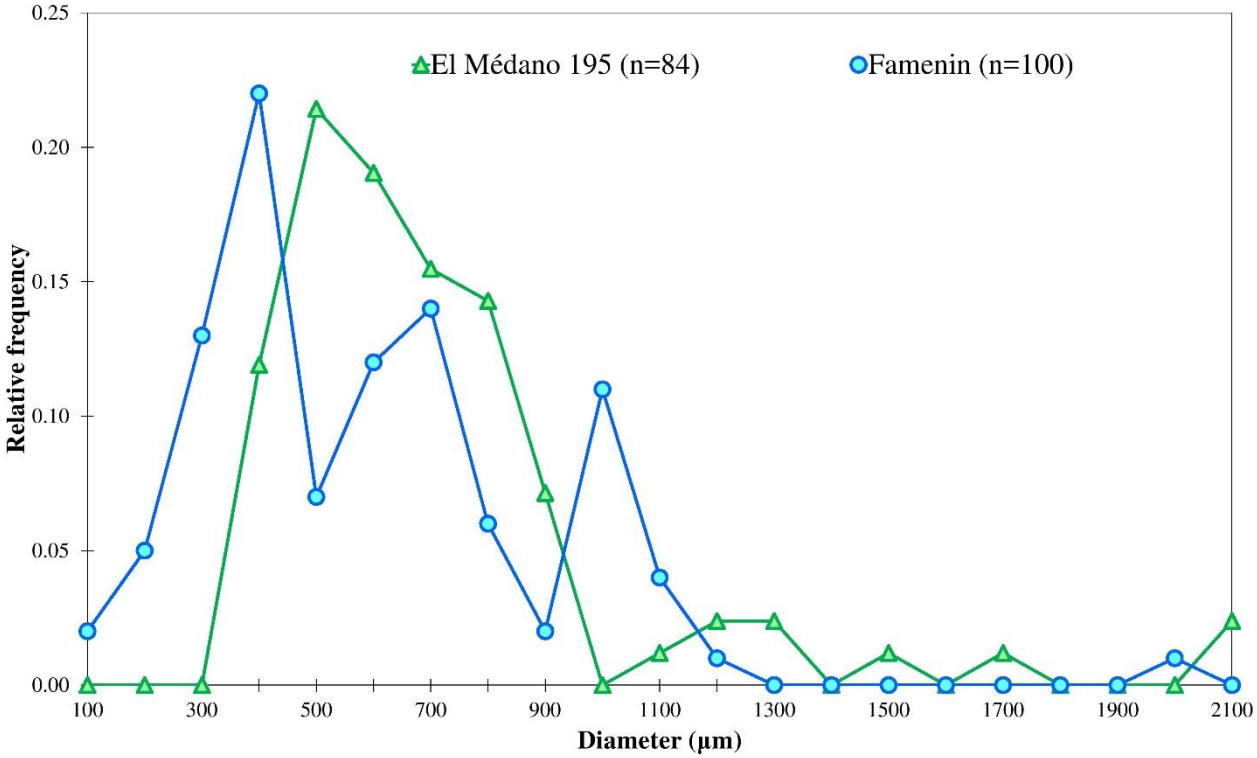
El Médano 195 (n=84)
Famenin (n=100)
Relative frequency
0.25
0.20
0.15
0.10
0.05
0.00
100
300
500
700
900
1100
1300
1500
1700
1900
2100
Diameter (µm)

Fig. 6:


EM 195
3 mm

2288 **Fig. 7:**

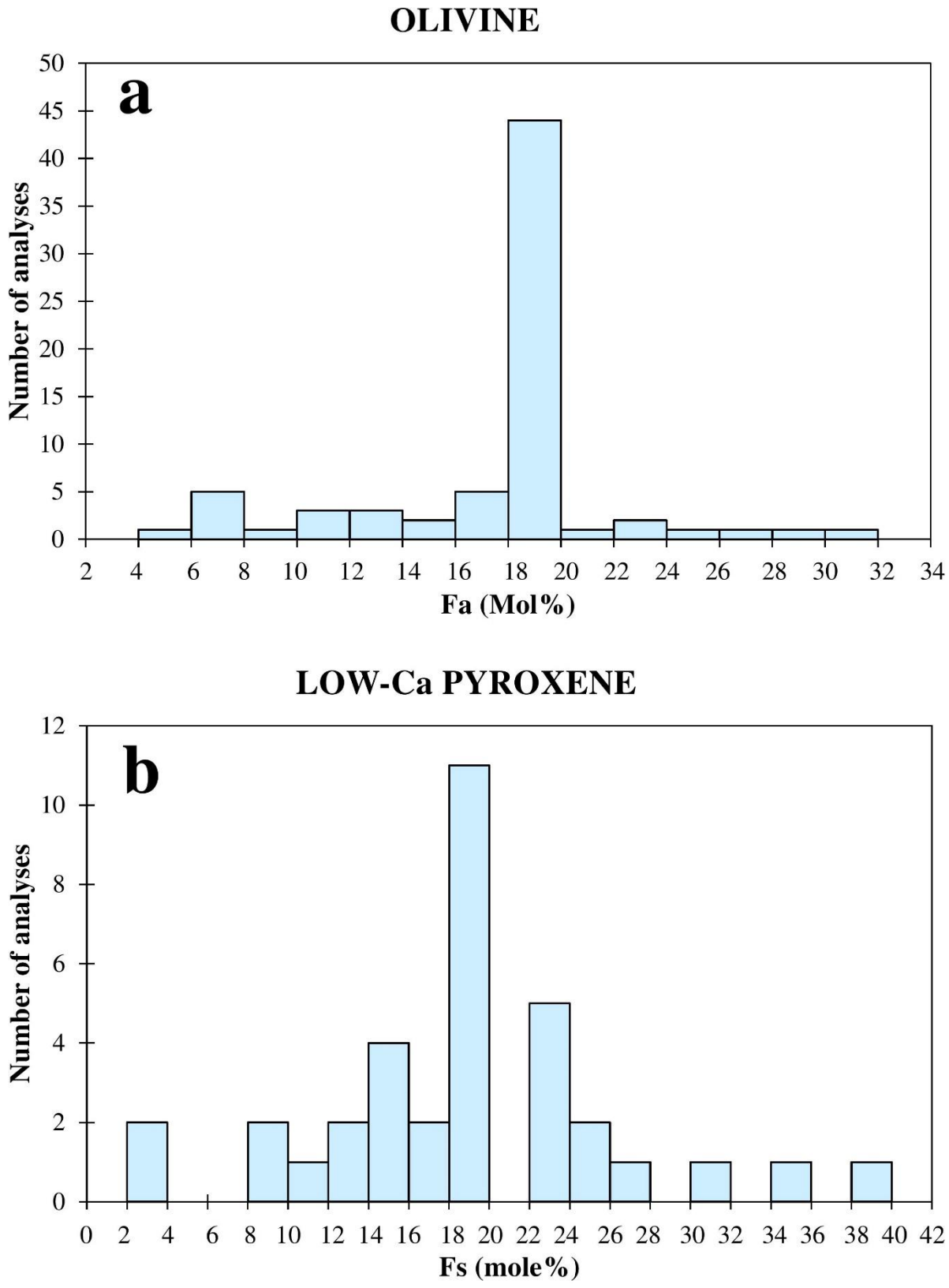

2289

Fig. 8:

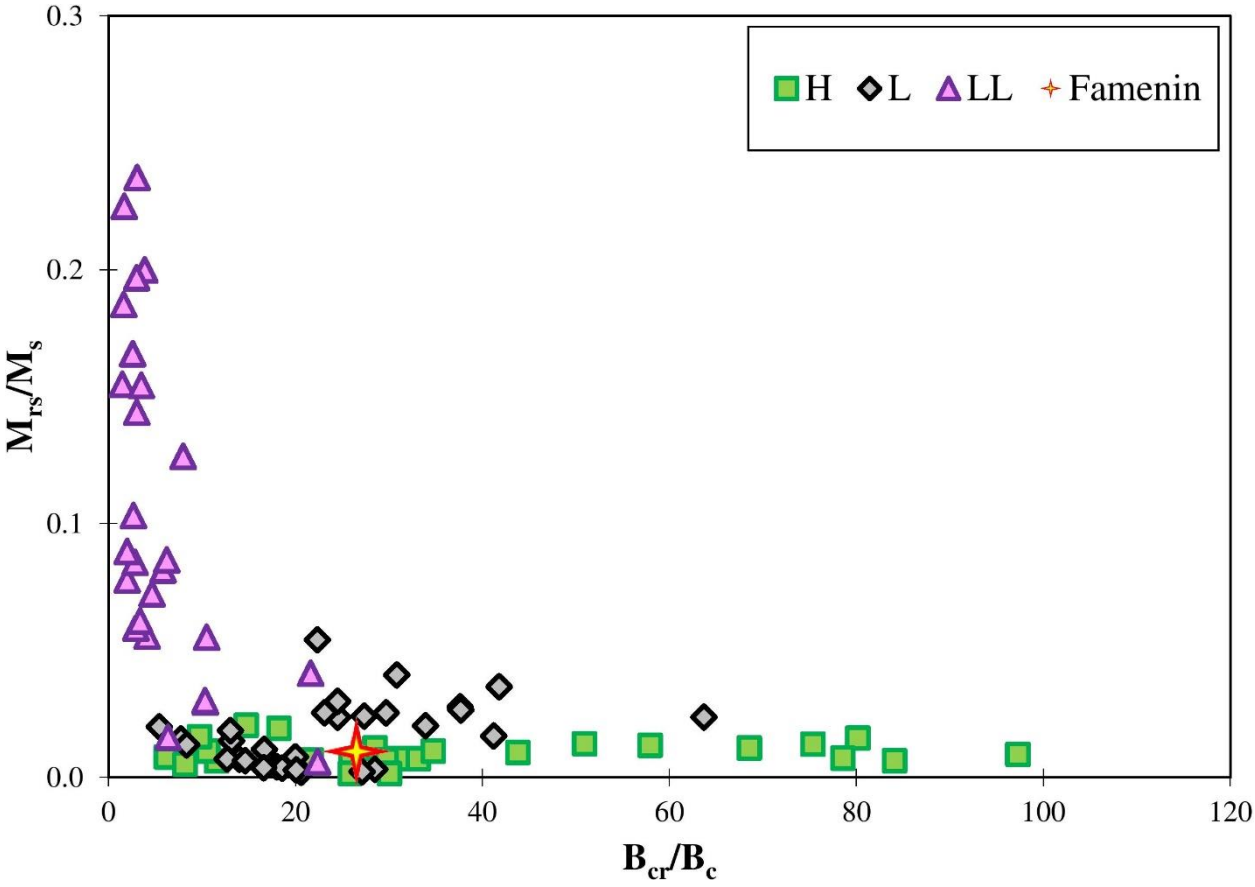

2302 **Fig.9:**

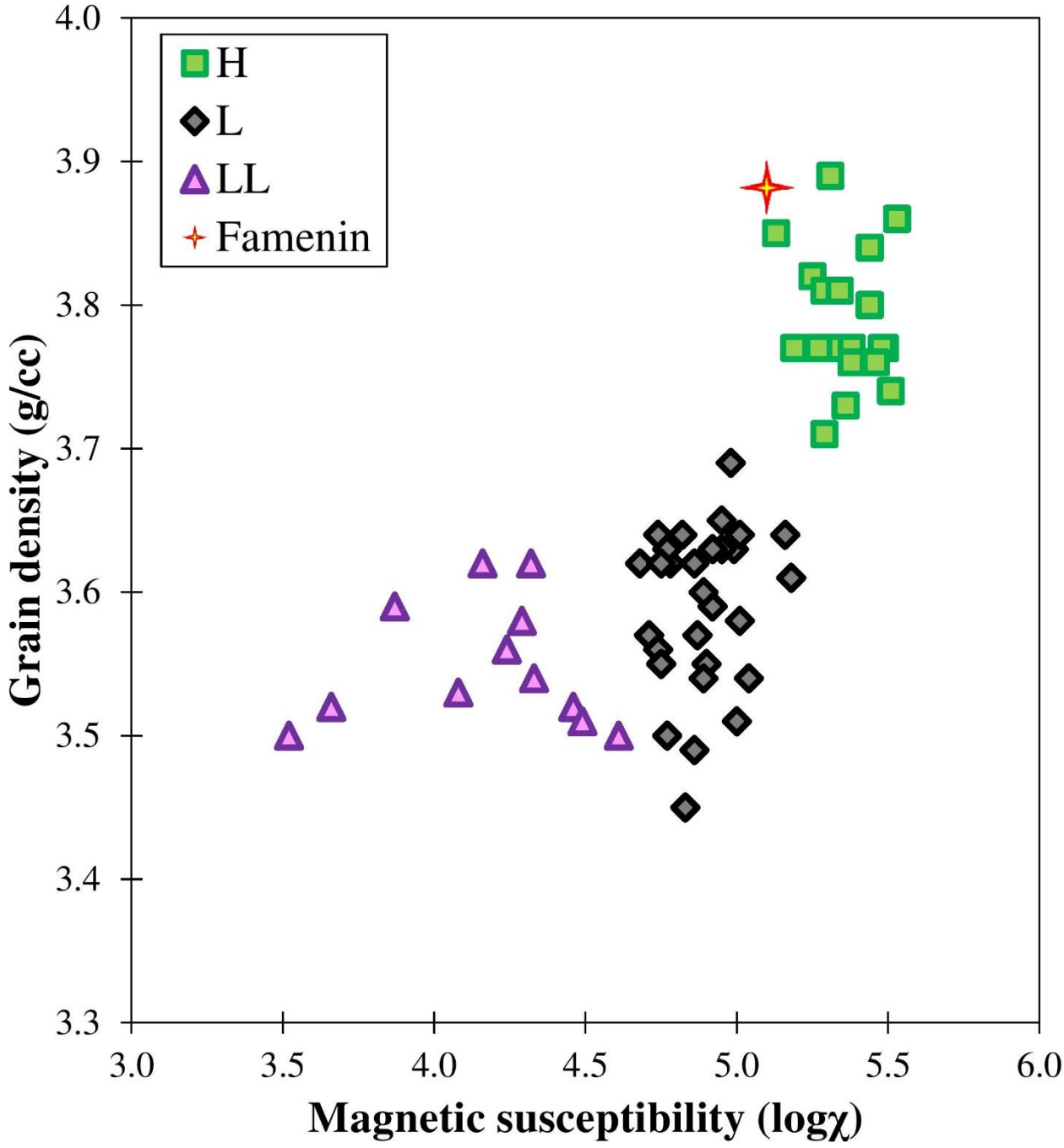

2303

2304

2305

2306

Fig. 10:

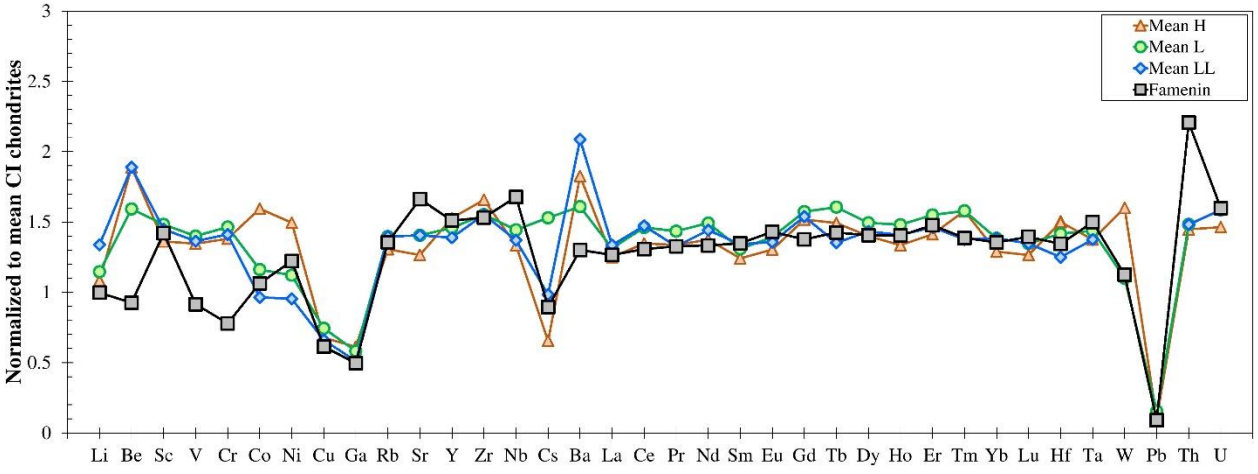
Mean H
Mean L
Mean LL
Famenin
Normalized to mean CI chondrites
0
0.5
1
1.5
2
2.5
3
Li Be Sc V Cr Co Ni Cu Ga Rb Sr Y Zr Nb Cs Ba La Ce Pr Nd Sm Eu Gd Tb Dy Ho Er Tm Yb Lu Hf Ta W Pb Th U

Fig. 11:

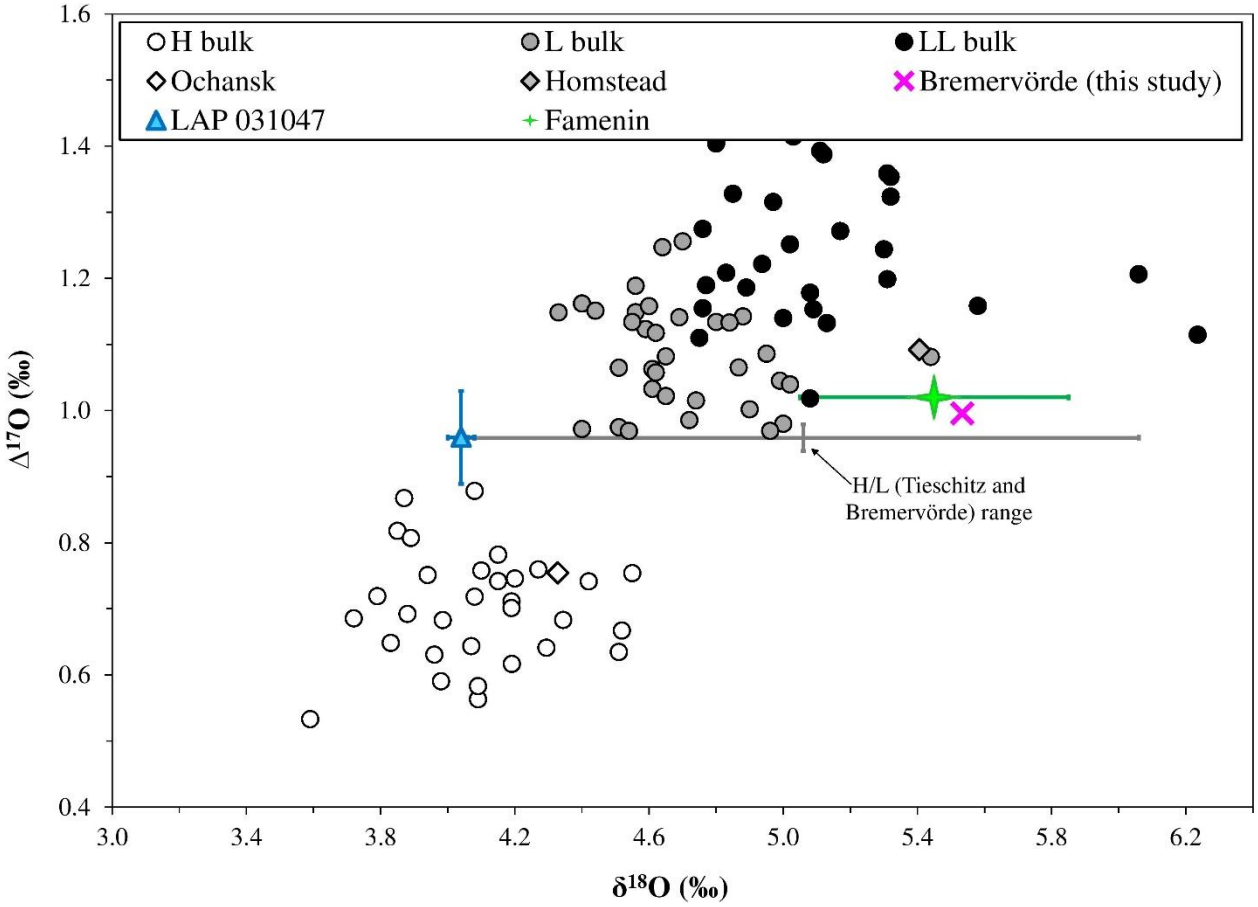
H bulk
L bulk
LL bulk
Ochansk
Homstead
Bremervörde (this study)
LAP 031047
Famenin
H/L (Tieschitz and Bremervörde) range
Δ17O (‰)
δ18O (‰)
0.4
0.6
0.8
1.0
1.2
1.4
1.6
3.0
3.4
3.8
4.2
4.6
5.0
5.4
5.8
6.2

Fig. 12:

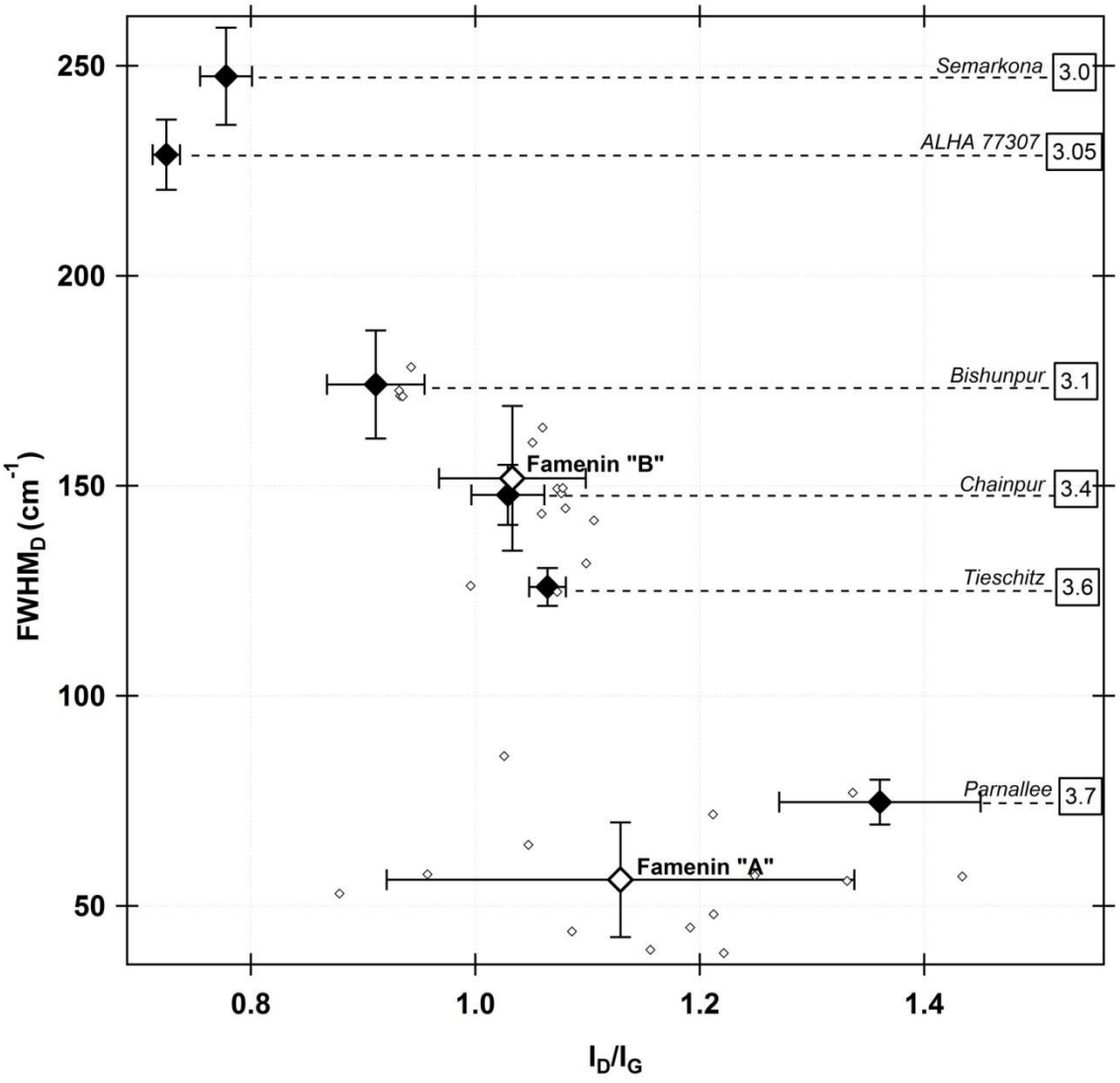
Semarkona
3.0
ALHA 77307
3.05
Bishunpur
3.1
Famenin "B"
Chainpur
3.4
Tieschitz
3.6
Parnallee
3.7
Famenin "A"
250
200
150
100
50
0.8
1.0
1.2
1.4
FWHM$_D$ (cm^{-1})
I_D/I_G

2322 **Fig. 13:**

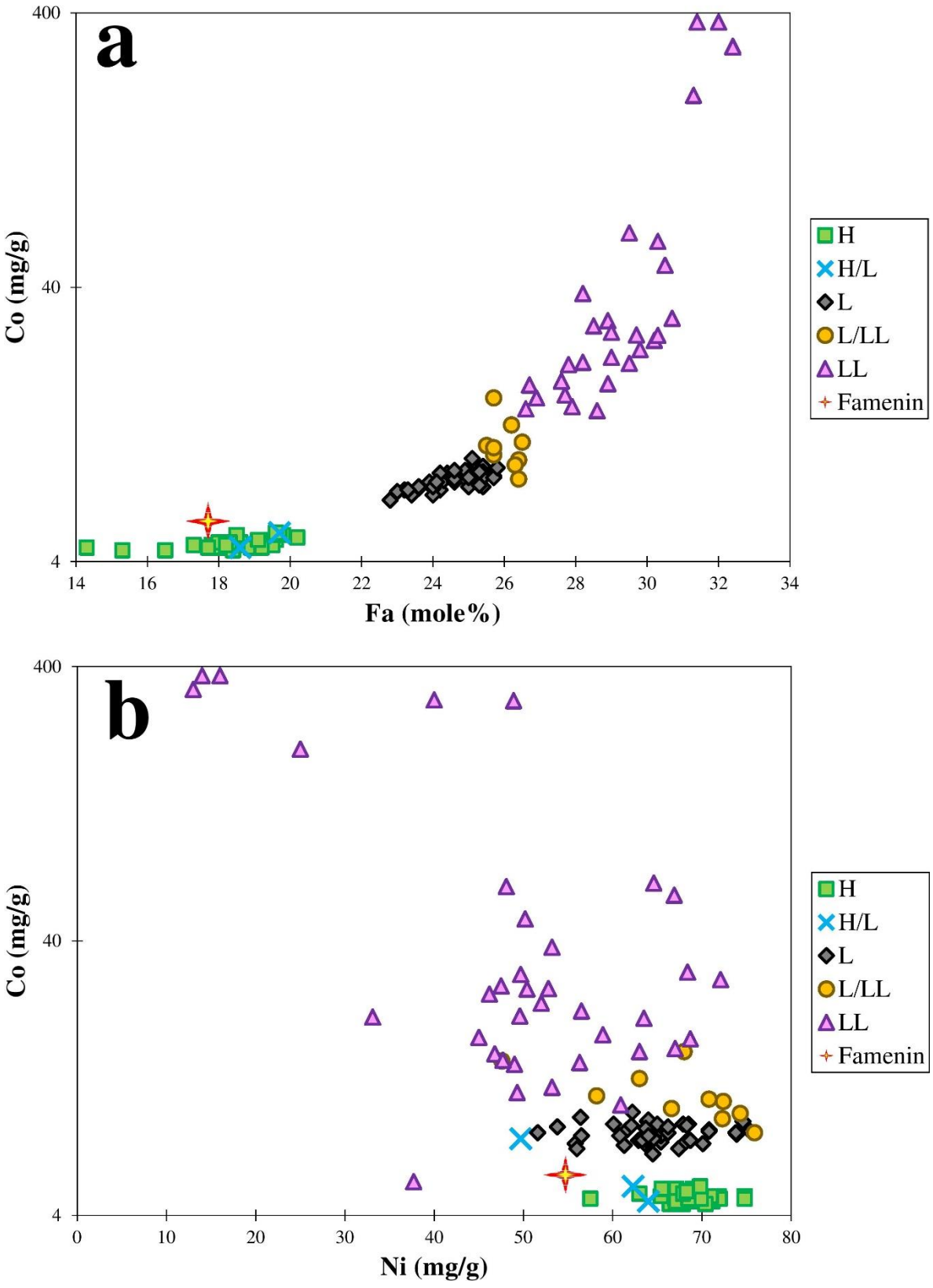

2323

Fig. EA-1:

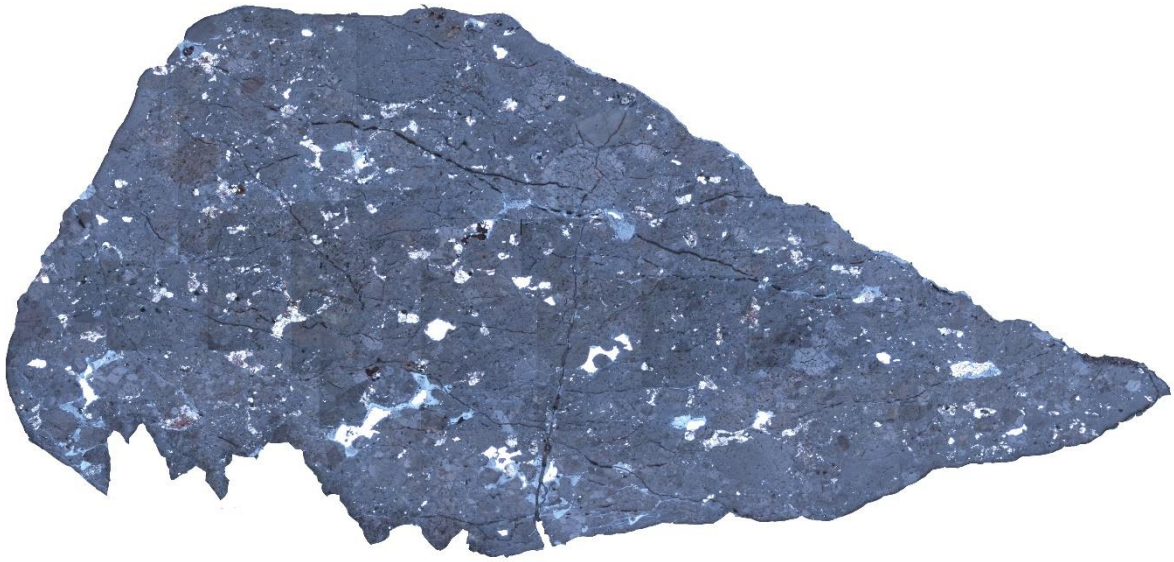

Tables:

Table 1:

	Famenin	Allende	Allende[a]	Allende[b]	Allende[c]
Li	1.57	1.58	-	1.5	-
Be	0.025	0.039	-	-	-
Ga	4.9	5.5	6 ± 1	6.15	-
Rb	3.01	1.17	1.2 ± 0.1	1.10	-
Sr	13.1	16.5	12 ± 3	-	-
Y	2.17	2.81	3.1 ± 0.1	3.10	-
Zr	5.8	7.1	9 ± 3	9.0	-
Nb	0.45	0.58	-	0.62	-
Cs	0.164	0.086	-	0.086	-
Ba	2.99	4.8	4 ± 1	4.00	-
La	0.30	0.51	0.52 ± 0.04	0.52	0.53
Ce	0.80	1.30	1.33 ± 0.08	1.33	1.38
Pr	0.12	0.20	0.21 ± 0.01	0.210	0.21

Nd	0.61	1.03	0.99 ± 0.03	0.99	1.07
Sm	0.20	0.32	0.34 ± 0.02	0.34	0.34
Eu	0.080	0.112	0.11 ± 0.01	0.11	0.12
Gd	0.27	0.40	0.42 ± 0.02	0.42	0.44
Tb	0.051	0.072	0.081 ± 0.010	0.081	0.08
Dy	0.34	0.48	0.42 ± 0.03	0.42	0.54
Ho	0.077	0.104	0.10 ± 0.01	0.10	0.11
Er	0.24	0.30	0.29 ± 0.01	0.29	0.31
Tm	0.034	0.054	-	0.0572	0.05
Yb	0.22	0.30	0.30 ± 0.02	0.30	0.33
Lu	0.034	0.046	0.052 ± 0.006	0.052	0.05
Hf	0.16	0.20	0.21 ± 0.01	0.21	-
Ta	0.024	0.040	-	-	-
W	0.11	0.17	-	0.167	-
Pb	0.22	1.27	1.39 ± 0.25		-
Th	0.12	0.20	-	0.065	-
U	0.013	0.017	-	0.016	-
Sc	8.2	11.2	11 ± 1	11.0	-
V	50	95	92 ± 6	92	-
Cr	2064	3664	3626 ± 140	-	-
Co	540	605	600 ± 100	612	-
Ni	13073	14800	14200 ± 200	-	-
Cu	74	104	119 ± 19	119	-
Zn	38	110	110 ± 5	117	-

The unit is µg/g.

[a]Jarosewich et al. 1987.

[b]Friedrich et al. 2003.

[c]Dauphas and Pourmand 2015.

Table 2:

SiO_2	41.90	47.44	49.78	41.59	40.79	40.04	39.81	39.31	39.43	39.86	39.95	39.75	39.39	39.75	39.43	39.52	39.18	40.13	39.05	39.36	40.17	39.06	38.16
Al_2O_3	-	7.06	6.97	1.55	-	-	-	-	-	-	-	-	-	-	-	-	-	-	-	-	0.25	-	-
FeO	6.11	4.85	7.99	12.27	14.40	15.45	15.63	16.69	16.90	17.04	17.06	17.09	17.04	17.21	17.25	17.37	17.28	17.20	17.34	17.62	17.38	18.11	22.53
Cr_2O_3	0.65	1.27	0.52	0.11	0.14	0.33	0.17	-	-	-	-	-	-	-	-	-	0.07	0.37	0.24	-	0.15	-	0.22
MnO	0.43	0.17	0.32	0.28	0.27	0.31	0.30	0.28	0.59	0.46	0.38	0.45	0.50	0.48	0.51	0.43	0.48	0.42	0.48	0.49	0.47	0.45	0.30
MgO	49.99	36.89	35.45	44.84	45.45	43.35	43.70	42.91	42.59	42.89	42.78	42.36	42.16	42.54	41.98	42.28	41.86	41.55	41.67	42.13	41.20	41.76	38.17
CaO	0.09	2.75	0.38	0.13	0.10	0.11	0.13	0.07	-	-	-	-	-	-	-	-	0.05	0.05	-	-	0.08	-	0.07
Total	99.25	100.57	101.55	100.78	101.18	99.53	99.79	99.35	99.60	100.39	100.22	99.71	99.12	100.03	99.23	99.68	99.04	99.79	98.90	99.64	99.74	99.37	99.54
Fa (mol%)	6.39	6.85	11.17	13.26	15.05	16.60	16.65	17.85	18.09	18.13	18.20	18.37	18.38	18.40	18.63	18.64	18.70	18.75	18.82	18.90	19.03	19.47	24.79

Detection limits (wt%) = Si (0.07), Al (0.06), Ti (0.13), Fe (0.16), Cr (0.07), Mn (0.14), Mg (0.07), Ca (0.05).

Table 3:

SiO_2	58.67	58.80	56.77	56.61	55.11	55.96
Al_2O_3	0.36	0.11	0.14	0.82	0.05	0.70
TiO_2	0.07	0.03	0.13	0.11	0.01	0.10
FeO	3.63	4.17	10.88	11.31	17.62	18.38
Cr_2O_3	1.11	0.31	0.12	0.98	0.59	0.67
MnO	0.58	0.29	0.52	0.29	0.66	0.77
MgO	34.16	36.36	30.99	29.69	25.44	21.60
CaO	1.97	0.26	0.68	0.97	0.29	1.96

Total	100.56	100.33	100.21	100.77	99.78	100.14
Fs (mol%)	6.27	6.41	16.90	17.71	28.67	32.21

Detection limits (wt%) = Si (0.07), Al (0.06), Ti (0.13), Fe (0.16), Cr (0.07), Mn (0.14), Mg (0.07), Ca (0.05).

Table 4:

Fe	96.79	95.52	94.99	94.88	94.36	91.90	93.16	93.86	75.40	72.80	72.38	67.73	67.93	66.13	65.98	65.01	64.00	
Co	0.58	0.70	0.75	0.34	0.49	0.59	0.48	0.56	0.19	0.22	b.d.l.	b.d.l.	b.d.l.	b.d.l.	b.d.l.	b.d.l.	b.d.l.	
Ni	3.22	4.64	5.21	5.42	6.07	6.11	6.40	6.70	25.27	27.81	27.97	31.73	32.47	33.43	33.85	34.10	35.37	
Total	100.58	100.87	100.95	100.65	100.92	98.60	100.04	101.11	100.86	100.82	100.36	99.46	100.40	99.69	99.56	99.11	99.37	

b.d.l. = below detection limit.

Detection limits (wt%) = Fe (0.21), Co (0.18), Ni (0.18).

Table 5:

SiO_2	38.62	38.84	39.02	40.81	40.07	40.15	40.39	55.29	56.65	58.06	57.00	53.83	57.89	55.42	57.28
TiO_2	b.d.l.	b.d.l.	b.d.l.	b.d.l.	b.d.l.	b.d.l.	b.d.l.	0.23	0.20	b.d.l.	0.19	b.d.l.	b.d.l.	b.d.l.	b.d.l.
FeO	20.62	18.27	17.02	11.40	17.48	17.37	15.40	11.26	10.46	6.64	10.91	18.47	5.69	14.75	10.63
MnO	0.46	0.39	0.42	0.03	0.53	0.45	0.50	0.50	0.50	0.34	0.56	0.57	0.37	0.48	0.56
MgO	38.62	40.41	41.60	46.60	41.10	40.87	41.72	30.12	30.55	33.35	30.48	24.64	34.28	26.52	29.96
CaO	b.d.l.	b.d.l.	b.d.l.	b.d.l.	b.d.l.	b.d.l.	b.d.l.	0.48	0.39	0.16	0.42	0.61	0.17	0.62	0.80
Total	98.31	97.90	98.06	98.84	99.18	98.84	98.01	97.87	98.75	98.54	99.56	98.12	98.39	97.80	99.23
Fa (mole%)	23.05	20.23	18.67	12.07	19.27	19.26	17.16	-	-	-	-	-	-	-	-
Fs (mole%)	-	-	-	-	-	-	-	17.17	15.99	10.02	16.59	29.24	8.49	23.48	16.34

Detection limits (wt%) = Si (0.07), Al (0.06), Ti (0.13), Fe (0.16), Cr (0.07), Mn (0.14), Mg (0.07), Ca (0.05).

Table 6:

SiO_2	38.73	38.69	39.65	38.45	55.59	55.57	55.66	56.53	55.60
FeO	20.46	20.42	20.84	20.88	12.35	12.03	12.81	11.48	12.57
Cr_2O_3	b.d.l.	b.d.l.	b.d.l.	b.d.l.	0.62	0.37	0.21	0.36	0.59
MnO	0.47	0.51	0.43	0.49	0.47	0.46	0.47	0.45	0.27
MgO	39.97	40.00	40.16	39.81	30.55	30.57	30.13	30.88	29.00
CaO	0.00	0.00	0.00	0.00	0.26	0.63	0.30	0.34	1.39
Total	99.62	99.62	101.08	99.63	99.84	99.62	99.58	100.04	99.41
Fa (mole%)	22.31	22.27	22.55	22.74	-	-	-	-	-
Fs (mole%)	-	-	-	-	18.39	17.88	19.15	17.15	19.03

Detection limits (wt%) = Si (0.07), Al (0.06), Ti (0.13), Fe (0.16), Cr (0.07), Mn (0.14), Mg (0.07), Ca (0.05).

Table 7:

Meteorite	**$\delta^{18}O$**	**$\delta^{17}O$**	**$\Delta^{17}O$**
Homstead	5.41	3.90	1.09
Bremervörde	5.53	3.87	1.00
Famenin	5.73	4.01	1.03
	5.17	3.69	1.00
Ochansk	4.33	3.01	0.75

Table 8:

Name	Class	Weathering grade	Fa (mol%)	Fs (mol%)	Magnetic Susceptibility
Bremervörde	H/L3.9	W0	18.6	-	4.97
Cali	H/L4	W0	22.8 ± 0.9	15.8 ± 6.9	5.11
DaG[a] 369	L(H)3	W3	16.8 (9.3-27.4)	9.1 (4.4-17.7)	-
DaG 378	H(L)3	W2	14.3 (0.9-26.6)	7.9 (2.1-25.2)	-
DaG 591	H(L)6	W3	20	17.4	-
Dhofar 428	H(L)5	W4	21.5	18.5	-
EM[b] 195	H/L3	W1	16.9 ± 6.0	17.2 ± 5.6	4.99
Famenin	H/L3	W0	17.4 ± 3.7	17.1 ± 9.0	5.09
JaH[c] 113	H/L4	W2	-	-	4.9
LAP[d] 031047	H/L	A	23	17	-
NWA[e] 1518	H/L3	W2	21	18.3	-
NWA 1534	H/L4	W2	20.5	17.6	-
NWA 1554	L/H4	W3	-	-	5
NWA 1955	H/L3-4	-	20.6	20.44	-
NWA 2001	H/L4	W0	22.0	19.3	5.21

NWA 2521	H/L3	W2	18.2 ± 7.3	14.3 ± 6.1	
NWA 2617	H/L4	W2	19.5 - 20.5	16.2 - 21.2	4.93
NWA 3330	H/L5	W3	21.8	18.8	-
NWA 3342	H/L4	W1	17 - 28	11.2 - 19.9	-
NWA 4089	H/L 4/5	W3	21.2	18.1	-
NWA 4097	H/L3	W2	7.9 - 24	4.7 - 18.8	-
NWA 4150	H/L6 Imc	W0/1	24.1	19.9	-
NWA 4152	H/L6	W2	20.4	20.4	-
NWA 4153	H/L6	W3	20.1	20.1	-
NWA 4154	H/L6	W4	20.6	20.6	-
NWA 4155	H/L6	W3	21.2	21.2	-
NWA 4156	H/L6	W3	19.9	19.9	-
NWA 4334	H/L3	W1	2.0 - 30.0	4.3 - 17.2	-
NWA 4357	H/L3	W1	3.7 - 31.1	2 - 24.3	-
NWA 4725	H/L3.6	W2	16.3 ± 9.1	5.17 ± 3.09	-
NWA 4726	L/H5	W2	24.67 ± 0.31	22.06 ± 1.33	4.98

NWA 5809	H/L5	W3	20.7	17.5 - 18.2	4.95
NWA 5945	H/L3	-	24.2 ± 2.0	14.5 ± 5.7	-
NWA 7327	H/L5	W3	20.5 ± 0.3	18.4 ± 1.5	-
NWA 10287	H/L5	W0/1	21.7 - 21.9	18.4 - 19.1	5.2
SJ[f] 041	H/L6	W2	22.5 ± 0.2	18.3 ± 0.8	4.59
SaU[g] 147	H/L4	W3	19.5	17.2	-
SaU 185	L/H4-5	W2	19.4 - 24.5	17.2 - 20.6	-
SaU 301	H/L4	W1	19.0 - 20.0	16.6 - 19.2	4.99
SaU 324	H/L6	W3/4	20.3	17.6	-
Tieschitz	H/L3.6	W0	-	-	4.98
Y[h]-983336	H/L5	B	21	19.2	-
Y-983388	H/L6	C	21.1	18.3	-
Y-983430	H/L5	A/B	20.9	18.4	-
Y-983551	H/L6	C	21.5	18.5	-
Y-983629	H/L6	A/B	20.9	18.5	-
Y-983931	H/L4	A/B	21.3	13.2	-

Y-000746	H/L4-5	B/C	20.3	14.6	-
Y-000782	H/L4	B/C	21.0	18.5	-

[a]Dar al Gani, [b]El Médano, [c]Jiddat al Harasis, [d]LaPaz Icefield, [e] Northwest Africa, [f]San Juan, [g]Sayh al Uhaymir, [h] Yamato.

Data source: Meteoritical Bulletin. Mineral chemistry and magnetic susceptibility data for Bremervörde from Rubin (1990) and Rochette et al. (2003), respectively. Same data for Cali from: Trigo-Rodríguez et al. (2009).

Left blank intentionally.

Chapter 8

Moshampa Meteorite Fall

Title: MOSHAMPA METEORITE FALL

1. INTRODUCTION AND THE FALL EVENT

On Thursday, 2015 July 30, between 20:10 and 20:15 local time (+04:30 GMT), a very bright fireball appeared in the evening sky of N and NW Iran (Fig. 1). Thousands of observational reports in the north to north-west of the country spread immediately in the local and international media. Very loud sonic booms were heard in Zanjan province. Later analysis by Gitterman et al. (2016) shows the infrasound signals produced by the bolide's explosions were observed by acoustic sensors in Israel from a distance of 1200-1350 km. With the help of the local media, we launched a questionnaire to receive the details of the event from the population. More than two hundred observational reports were received from different provinces. A preliminary speculation suggested NW of Zanjan city (around Moshampa village) to be the fall area (Fig. 2) (Pourkhorsandi 2015). The following news confirmed this suggestion. Ghadir Mohammadi, a farmer from Moshampa village was working in his rice field near the Moshampa village, close to the Qezel Ozan river when he heard four loud booms (the last one the being much louder) and saw a zig-zag shaped cloud in the sky. He heard the sound of an object falling into the wet soil about 5-10 m away from him (coordinates: 36° 57' 57"N, 47° 41' 28"E). Worried it might be unexploded military ordnance, he went back to the village. He then heard about the fireball reports and realized that the army and police were looking for the object. The day after, he went back to the fall place and found a 1554 g stone buried about 20 cm deep in a hole and informed the media about his finding. Ten additional fragments, with a total weight of ~700 g, were found two weeks later by Shahram Mohammadi near the location of the main mass. Fig. 3 shows the main mass and some other fragments of Moshampa. We visited the fall place on November 2015. During this visit, we examined the main mass in the finder's house and searched for about two hours in the eastern part of the fall area. Searching in this mountainous area did not lead to any meteorite find.

We classified this meteorite as an LL5 with the official name Moshampa. Moshampa meteorite fall just happened 33 days after Famenin (H/L3) meteorite fall in the adjacent province

(Hamedan). Two other meteorite falls in Iran date back to 1880 Veramin mesosiderite (Graham and Hassanzadeh 1990; Ward 1901) and 1974 Naragh H6 (Adib and Liou 1979; Clarke 1975).

In this work, we report the textural, mineral chemistry, magnetic susceptibility, and whole-rock trace element chemistry of the meteorite. Based on these data we discuss the classification of this meteorite.

2. METHODOLOGY

The analytical methods used in this study are similar to the ones applied to the Famenin meteorite (previous chapter). In order to avoid repetition, we do not mention them here.

3. RESULTS

3.1. Hand specimen description

We examined the main mass in the fall place (Moshampa village). In addition, for classification and the further studies, we had received two pieces of the meteorite weighting 16.36 and 7.36 g which were separated from the main mass about two months after the event.

The main mass is roughly pyramidal with an approximate size 15×10×7 cm (Fig. 3). Except the broken part, the surface is composed of regmaglypts, melt droplets and polygonal cracks. The fusion crust has a dull black and brown color, the latter occurring on the “apex” of the sample. The soil burial and subsequent washing with water by the finder has introduced soil material to the cavities and cracks of the fusion crust. The atmospheric broken surface is light brown in color with patches of oxidized material which can be due to the effect of washing (Fig. 3a,b). The sampling broken surface shows a light gray interior with a typical chondritic texture. Large chondrules (up to 2.5 mm), troilite/Fe-Ni metal grains and shock darkened clasts can be spotted by naked eye (Fig. 3c). The separation of the chondrules from the rest of the sample while broking has exhibited half-spherical cavities. A fine-grained clast with a lighter color than the rest of the meteorite and size of 5×6 mm occur in the broken surface (Fig. 3c).

3.2. Optical and electron microscopy

Fig. 4 shows the mosaic images of the meteorite in reflected and transmitted optical light. The prepared sections cover parts of the fusion crust in which it shows a heterogeneous layering composed of outer and inner areas. A mixture of vesicles, magnetite grains and troilite veinlets, is a typical ordinary chondrite fusion crust (Fig. 5a,b). Referring to Genge and Grady (1999) nomenclature, the melted crust (outer region) is composed of quench phases of magnetite and olivine and pyroxene crystals in galss. Excluding some euhedral grains, dendritic magnetite crystals are the dominant shape of this mineral and occur in the matrix of the porphyritic texture of the ferromagnesian silicates (Fig. 5b). Rapid solidification of the melted crust has led to the formation of chondrule-like assemblages (Fig. 5b). Magnetite crystals and its assemblages are relatively bigger adjacent to the vesicles; this can be related to the accessibility of the atmospheric oxygen to form bigger grains. Vesicles are mostly concentrated at the base of melted crust. In general, they are round and in some cases occur as elongated structures parallel to the melted crust baseline. The ferromagnesian minerals of the melted crust are generally smaller than their counterparts in the interior and show darker shades in reflected polarized light. In addition a melted crust is also present (Fig. 5a). It is composed of two layers; a layer of silicate glass and relic ferromagnesian crystals adjacent to the melted crust and a lower layer with interconnected troilite veinlets and troilite/(Fe,Ni) metal quenched assemblage.

A low magnification survey of the sections shows a fractured texture (breccia) with different types of chondrules and clasts in a clastic matrix (Fig. 4). An oxidation rim has been developed around a (Fe,Ni) metal grain which shows the effect of terrestrial environment even a short time after the fall. Fig. 5c shows a fine-grained clast composed of olivine, pyroxene and plagioclase. The abundance and size of (Fe,Ni) metal grains in this clast is lower than the rest of the meteorite. A one mm clast comprising bigger plagioclase grains (up to 100 μm) than the rest of the meteorite and different troilite/(Fe,Ni) metal assemblage is present (Fig. 5d). This clast has a petrologic type 6. Modal analysis on a mosaic photo performed by *ImageJ* software shows 4.3 vol% troilite, 1.3 vol% (Fe,Ni) metal and the rest as silicates and voids. Troilite, the dominant opaque mineral, is fractured (Fig. 5d) and in some regions with domain sizes 50-100 μm is polycrystalline (Fig. 5e). Relatively large barred olivine, porphyritic, granular and cryptocrystalline are the main observed chondrules types (Fig. 4). Olivine shows undulatory extinction and planar fractures. Inside the (Fe,Ni) metal grains of this clast and adjacent to a troilite inclusion, an elongated copper grain is present (~ 20 μm) (Fig. 5f). The average

plagioclase size is less than 50 µm. Based on the troilite texture, presence of copper, and olivine optical characteristics and using the criteria of Bennett and McSween (1996), Rubin (1994), and Stöffler et al. (1991), Moshampa has a S3 (weakly shocked) shock stage.

Based on the shape of the opaque mineral, chondrule shape and abundance, and the plagioclase size (Van Schmus and Wood 1967), Moshampa is a petrologic type 5 breccia containing type 6 clasts.

3.3. Mineral chemistry

Representative compositions of olivine and low-Ca pyroxene are shown in Table 1. The analysis of olivine and low-Ca pyroxene grains, in the host and the fine-grained and type 6 clasts, show that they are chemically similar and the minerals are equilibrated. However, type 6 clast has a bit more oxidized composition which can be the result of higher thermal metamorphism (McSween and Labotka 1993). The average olivine and low-Ca compostions are $Fa_{29.1\pm0.2}$ (n = 10), $Fs_{23.8\pm0.3}$ (n=3), respectively. These values are in the range of the values reported for LL chondrites (e.g., Brearley and Jones 1998).

3.4. Trace element composition

The whole rocks trace element composition of Moshampa is reported in Table 2. CI-normalized trace element composition of Moshampa shows a pattern similar to the mean ordinary chondrites (Fig. 6). Rare earth elements (REE) content is lower than the mean values but it shows a general undifferentiated pattern. Europium positive anomaly would form in the presence of plagioclase.

3.5. Magnetic properties and densitometry

Magnetic susceptibility $\log\chi$ ($\times 10^{-9}$ m^3/kg) measured on a 23.8 g fragment is 3.80. This is in the range of the values reported for LL chondrites (4.10±0.30, Rochette et al. 2003).

The average grain density measured on a 4.68 g fragment is 3.53±0.03 (n = 6) g/cm^3. This is in the range of the values reported for LL and some L chondrites (Consolmagno et al. 2006).

3. DISCUSSION

All our observations show that Moshampa is a brecciated LL ordinary chondrite. The metal abundance (represented by modal abundance and magnetic susceptibility), grain density, and mineral chemistry all point to this classification.

Considering the similar mineral composition (chemistry) and different petrologic type, Moshampa is a genomict breccia (Biscoff et al. 2006).

Based on the petrographic observation and the mineral chemical distribution, Moshampa is a petrologic type 5 (Van Schmus and Wood 1967).

Based on the presented evidence, Moshampa meteorite is classified as a brecciated LL5 chondrite.

4. CONCLUSIONS AND PERSPECTIVES

We conducted a multimethod study on a meteorite fallen on 30 July 2015 in the NW of Iran near Moshampa village (Zanjan province). The responsible fireball was observed by thousands of people after in the sunset. Our analysis showed that Moshampa meteorite is an ordinary chondrite, a member of LL group with a petrologic type 5. Moshampa is genomict breccia and the clasts both show fine-grained and type 6 texture. Detailed magnetic study on Moshampa at CEREGE (not reported here) has shown its peculiar magnetic mineralogy. The related publication will appear using the data presented here along those magnetic data in the near future.

Acknowledgments

Kazem Kookaram, Mohsen Ranjabaran, and Amir Hassanzadeh are thanked for their helps during communications with the locals. The first author thanks M. Zadsaleh for the Fig. 2. Cultural Office of the French Embassy in Tehran is acknowledged for providing Ph.D. grant for the first author and for supporting the visit by the French team.

References

Adib D., and Liou J. G. 1979. The Naragh meteorite - A new olivine-bronzite chondrite fall. *Meteoritics* 14:257–272. http://adsabs.harvard.edu/abs/1979Metic..14..257A.

Bennett M. E., and McSween H. Y. 1996. Shock features in iron-nickel metal and troilite of L-group ordinary chondrites. *Meteoritics & Planetary Science* 31:255–264. http://doi.wiley.com/10.1111/j.1945-5100.1996.tb02021.x (Accessed September 30, 2015).

Biscoff A., Scott E. R. D., Metzler K., and Goodrich C. A. 2006. Nature and origins of meteoritic breccias. In *Meteorites and the early solar system II*, edited by Lauretta D. S., and Mcsween H. Y. Tuscan: The University of Arizona Press. pp. 679–712.

Brearley A. J., and Jones R. H. 1998. Chondritic meteorites. *Reviews in Mineralogy and Geochemistry* 36.

Clarke R. S. 1975. The Meteoritical Bulletin. *Meteoritics* 10:133–158. http://doi.wiley.com/10.1111/j.1945-5100.1975.tb00018.x.

Consolmagno G. J., Macke R. J., Rochette P., Britt D. T., and Gattacceca J. 2006. Density, magnetic susceptibility, and the characterization of ordinary chondrite falls and showers. *Meteoritics & Planetary Science* 41:331–342. http://doi.wiley.com/10.1111/j.1945-5100.2006.tb00466.x (Accessed January 19, 2016).

Genge M. J., and Grady M. M. 1999. The fusion crusts of stony meteorites: Implications for the atmospheric reprocessing of extraterrestrial materials. *Meteoritics & Planetary Science* 34:341–356. http://doi.wiley.com/10.1111/j.1945-5100.1999.tb01344.x.

Gitterman Y., Pinsky V., Mazur M., and Ataev G. 2016. Estimating parameters of unusual regional explosions from seismo-acoustic observations in Israel. In *35th General Assembly of the European Seismological Commission*. p. 168.

Graham A. L., and Hassanzadeh J. 1990. The Meteoritical Bulletin. *Meteoritics* 25:59–63. http://doi.wiley.com/10.1111/j.1945-5100.1990.tb00971.x.

McSween H. Y., and Labotka T. C. 1993. Oxidation during metamorphism of the ordinary chondrites. *Geochimica et Cosmochimica Acta* 57:1105–1114. http://www.sciencedirect.com/science/article/pii/001670379390044W (Accessed October 4, 2015).

Pourkhorsandi H. 2015. Where is the Zanjan meteorite? *Nojum* 250:12–15.

Rubin A. E. 1994. Metallic copper in ordinary chondrites. *Meteoritics* 29:93–98. http://onlinelibrary.wiley.com/doi/10.1111/j.1945-5100.1994.tb00659.x/abstract (Accessed September 30, 2015).

Van Schmus W. R., and Wood J. A. 1967. A chemical-petrologic classification for the chondritic meteorites. *Geochimica et Cosmochimica Acta* 31:747–765. http://www.sciencedirect.com/science/article/pii/S0016703767800309 (Accessed July 1, 2015).

Stöffler D., Keil K., and Edward R.D S. 1991. Shock metamorphism of ordinary chondrites. *Geochimica et Cosmochimica Acta* 55:3845–3867.

Ward H. A. 1901. Veramin Meteorite. *American Journal of Science* s4-12:453–459. http://www.ajsonline.org/cgi/doi/10.2475/ajs.s4-12.72.453.

Wasson J. T., and Kallemeyn G. W. 1988. Compositions of Chondrites. *Philosophical Transactions of the Royal Society A: Mathematical, Physical and Engineering Sciences* 325:535–544. http://rsta.royalsocietypublishing.org/content/325/1587/535 (Accessed July 3, 2015).

Figure captions:

Fig. 1: Image sequence showing the fireball of Moshampa meteorite fall. The video recorded from Langarud (37°11′49″N 50°09′13″E) in Gilan province shows ~ 5 seconds of appearance in the sky. Credit: Ali Ezzati. Link to the video: https://youtu.be/L9ogyu6LeEU

Fig. 2: Moshampa meteorite fall location.

Fig. 3: Moshampa meteorite fragments. a,b) The main mass of the meteorite. Credits: M. Ranjbaran and A. Hassanzade, respectively. c) One of the fragments of the type specimen. d) Fusion crusts showing cracks during thermal fluctuations during atmospheric entry. e) Some other fragments of the Moshampa meteorite. Credit: Sh. Mohammadi. f) The main mass showing the regmaglypts.

Fig. 4: Optical images of Moshampa in reflected (a) and transmitted (b) light.

Fig. 5: Optical microscope images of Moshampa. a) Fusion crust and its two main parts (melted crusts and substrate). b) Magnetite crystals and aggregates in the fusion crust. c) Fine-grained clast showing silicates and smaller (Fe,Ni) metal grains. d) A fractured troilite grain. The type 6 clast can be seen in the upper right. e) A polycrystalline troilite grain. f) A copper grain crystallized around a troilite inside the (Fe,Ni) metal.

Fig. 6: CI-normalized chemical composition of Moshampa and mean ordinary chondrites. Mean ordinary chondrites data from Wasson and Kallemeyn (1988).

Table headings:

Table 1: Representative olivine and low-Ca pyroxene compositions (in wt%) in Moshampa.

Table 2: Trace element concentrations (µg/g) determined by ICP-MS for Moshampa.

Figures:

Fig. 1:

Fig. 2:

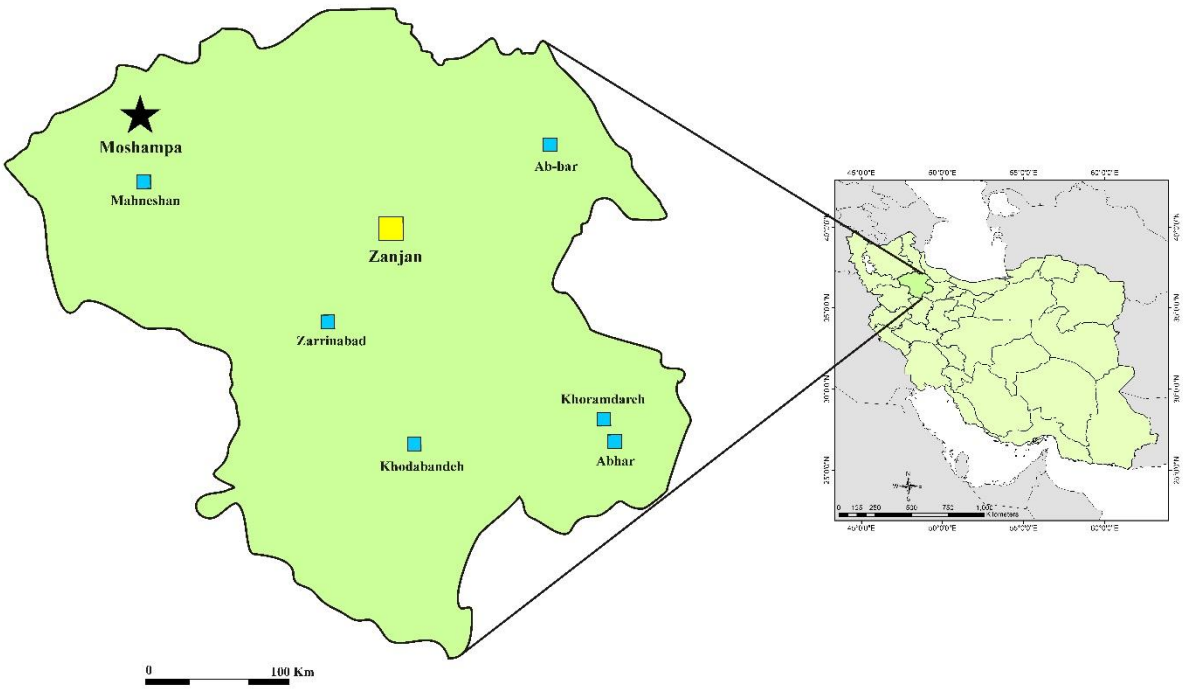
Moshampa
Mahneshan
Ab-bar
Zanjan
Zarrinabad
Khoramdarch
Khodabandeh
Abhar
0
100 Km

Fig. 3:

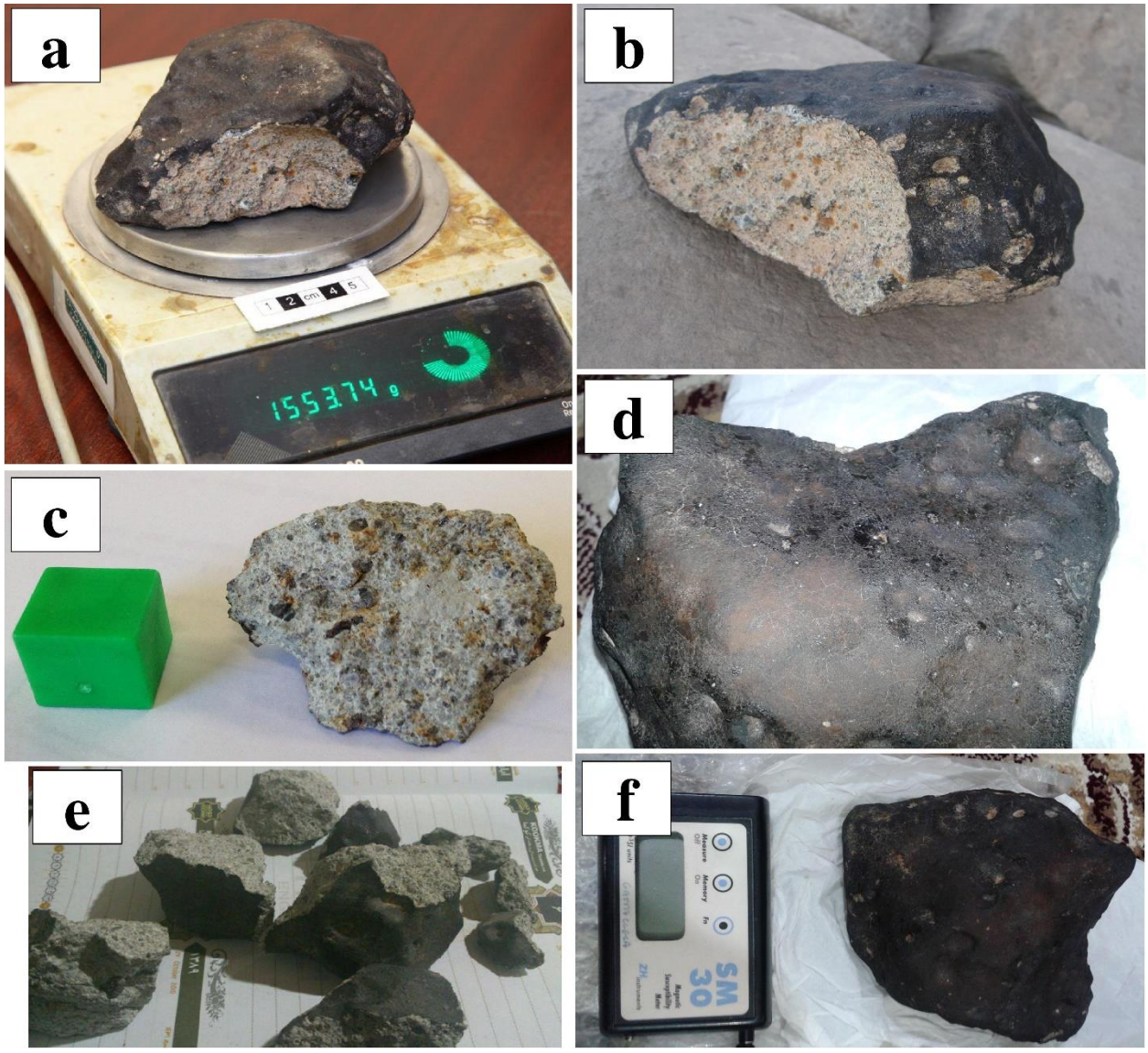

2621 **Fig. 4:**

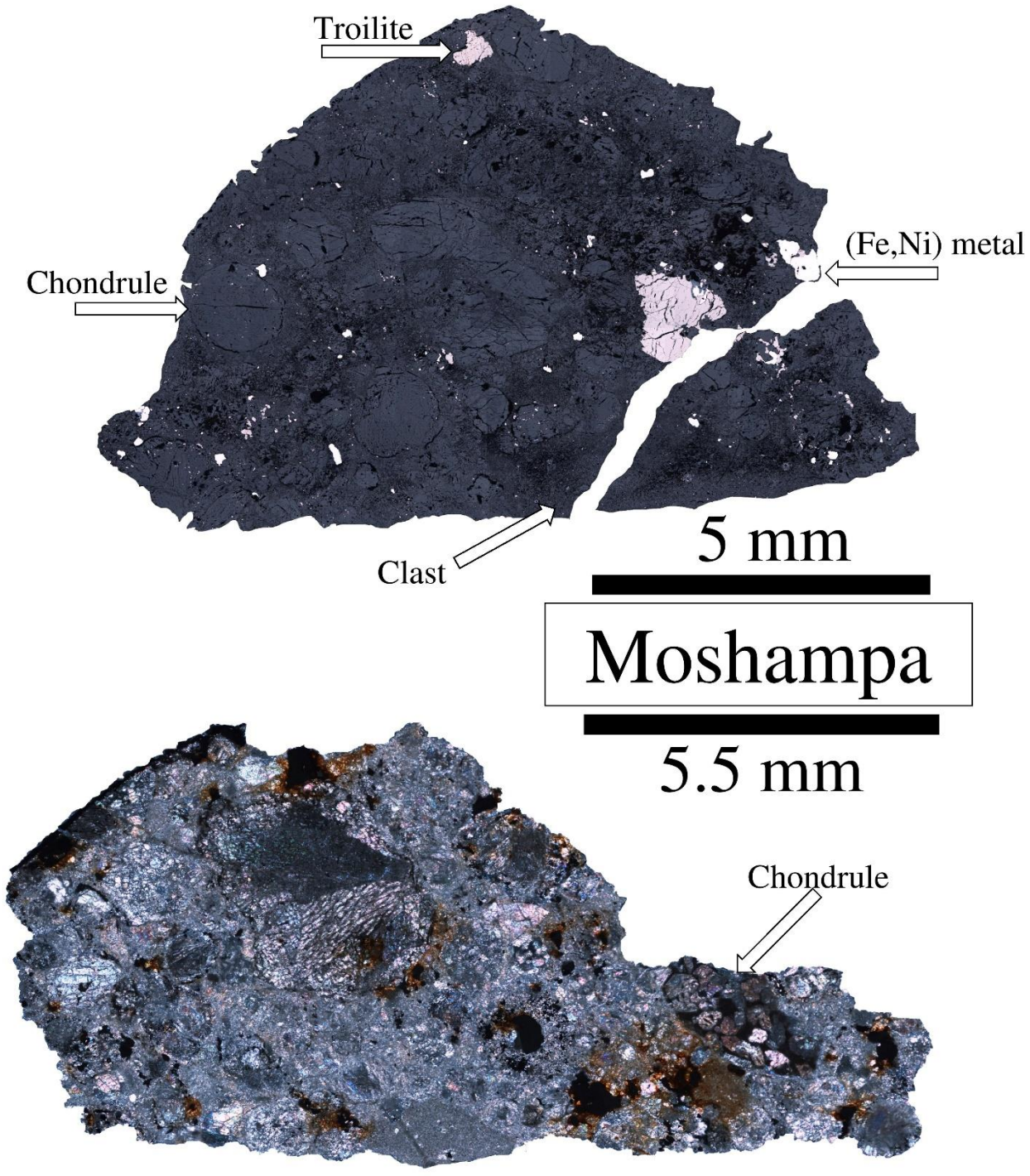

2622

2623

2624

Fig. 5:

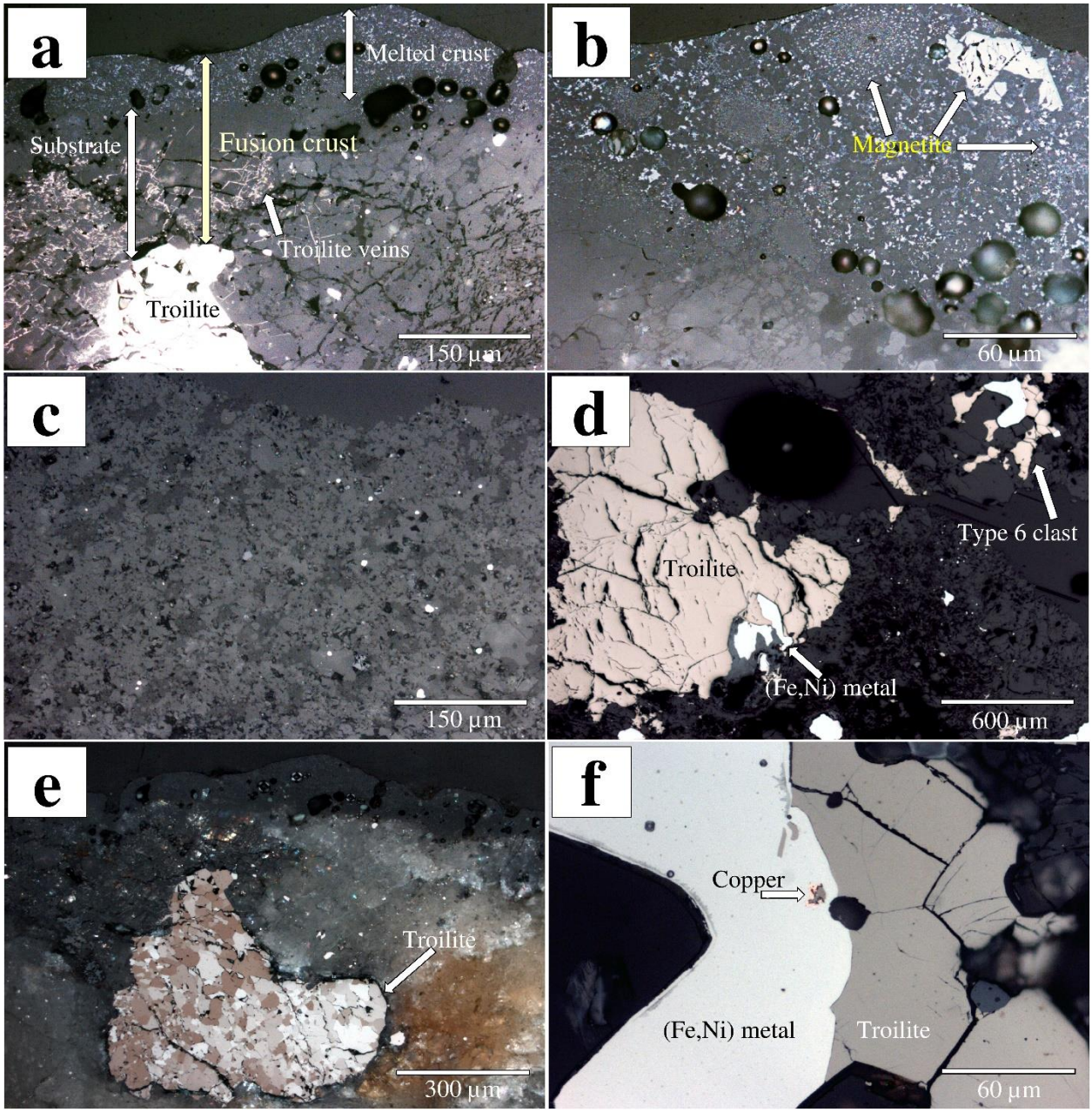
a
Melted crust
Substrate
Fusion crust
Troilite veins
Troilite
150 µm
b
Magnetite
60 µm
c
150 µm
d
Type 6 clast
Troilite
(Fe,Ni) metal
600 µm
e
Troilite
300 µm
f
Copper
(Fe,Ni) metal
Troilite
60 µm

Fig. 6:

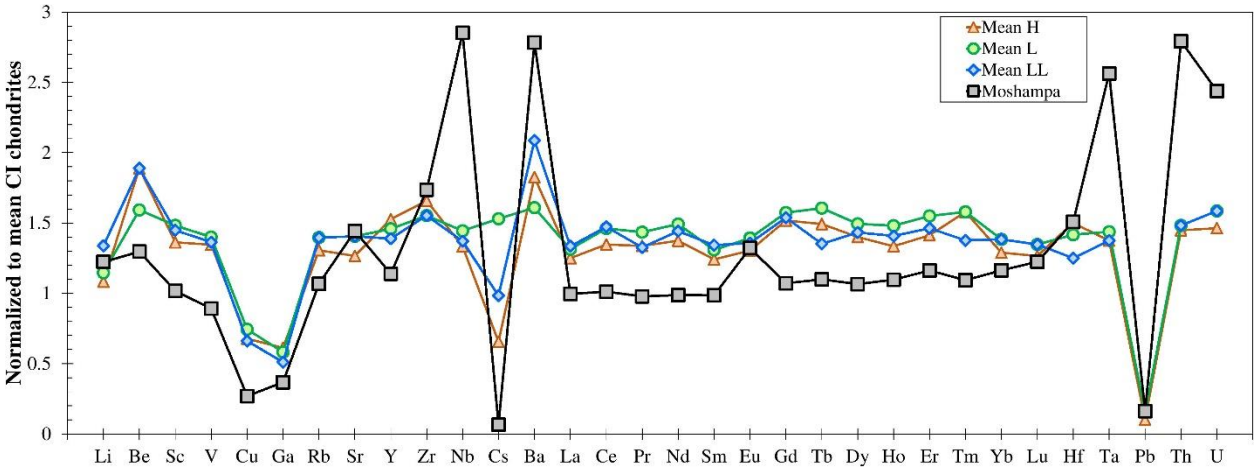
Normalized to mean CI chondrites
3
2.5
2
1.5
1
0.5
0
Mean H
Mean L
Mean LL
Moshampa
Li Be Sc V Cu Ga Rb Sr Y Zr Nb Cs Ba La Ce Pr Nd Sm Eu Gd Tb Dy Ho Er Tm Yb Lu Hf Ta Pb Th U

Tables:

Table 1:

	Host	Host	Host	Host	Host	Host	Host	Fine-grained[1]	Fine-grained	Fine-grained	Fine-grained	[2]Type 6	Type 6
SiO2	37.92	38.53	38.32	38.74	38.92	55.77	56.31	38.56	38.47	37.97	38.51	38.85	54.88
FeO	26.39	26.41	26.47	26.24	26.62	15.85	15.59	26.61	26.42	25.98	26.14	26.54	15.56
MnO	0.48	0.46	0.37	0.42	0.50	0.49	0.37	0.39	0.36	0.37	0.58	0.41	0.47
MgO	36.47	36.35	36.37	35.95	36.44	27.41	27.79	36.11	36.07	35.45	35.50	35.16	27.28
CaO	-	-	-	-	-	0.93	0.97	-	-	-	-	-	0.98
Total	**101.25**	**101.75**	**101.52**	**101.34**	**102.49**	**100.45**	**101.03**	**101.67**	**101.32**	**99.77**	**100.73**	**98.96**	**99.17**
Fa (mole%)	28.87	28.96	28.00	29.05	29.08	-	-	29.25	29.12	29.14	29.24	29.75	-
Fs (mole%)	-	-	-	-	-	24.05	23.49	-	-	-	-	-	23.78
Wol. (mole%)	-	-	-	-	-	1.80	1.87	-	-	-	-	-	1.92

[1]Fine-grained clast. [2]Type 6 clast.

Table 2

	Li	Be	Sc	V	Cu	Ga	Rb	Sr	Y	Zr	Nb	Mo	Cs	Ba	La	Ce	Pr	Nd	Sm	Eu	Gd	Tb	Dy	Ho	Er	Tm	Yb	Lu	Hf	Ta	Pb	Th	U
Mosham pa	1.92	0.035	5.9	49	32.6	3.6	2.37	11.4	1.64	6.6	0.77	1.30	0.012	6.4	0.235	0.623	0.090	0.451	0.147	0.074	0.211	0.039	0.261	0.060	0.186	0.027	0.185	0.030	0.181	0.041	0.39	0.081	0.020

2663

Left blank intentionally

Chapter 9

Conclusions and Perspectives

Title: CONCLUSIONS AND PERSPECTIVES

1. CONCLUSIONS

In this thesis, main parts of the works conducted during the author's doctoral studies since January 2015 were presented. This work is dedicated to the study of meteorites from Iran (falls and finds) and hot deserts (finds). Part of these meteorites were recovered in expeditions which I participated (in Chile, Iran, and Western Sahara). Classification and weathering of these samples were the main subjects of focus. The conclusions of different parts of this study are listed as followings:

Among 694 classified meteorites collected from different regions of the planet (Fig. 1), 95% are ordinary chondrites, particularly H5 and L6 chondrites. Meteorites from Chile (n = 373; 53%) and Iran (n = 219; 31%) were the major sources of the study. Comparison of the magnetic susceptibility with weathering grade data shows different weathering behavior in meteorites from different hot deserts, resulting in formation of different secondary products which itself is mainly governed by the climate.

In accordance with previous suggestions, the Lut Desert, where the majority of Iranian finds were recovered (Fig.2) is a suitable place for meteorite conservation, accumulation, and searching. Amongst the classified samples from the Lut Desert (n=219), 191 of them are H5 chondrites. H5 and L5 chondrites are the most abundant collected meteorites from the Lut Desert. Our data indicate that these meteorites belong to two main strewnfields located in Kalut. H5 chondrites show higher weathering grades than the L5 samples. Comparison of the macroscopic and microscopic data of the L5 and H5 fragments, indicate a lower terrestrial weathering and lower terrestrial age for the L5. Terrestrial ages of three selected samples from different regions of Lut Desert show a range of 10-30 kyr. This is in the range of the values reported for meteorites from other hot deserts.

Alteration of troilite to pyrite or marcasite is a ubiquitous and unique characteristic of meteorites from Lut, especially the Kalut H5 fragments. Troilite weathering in the Lut occurs in at least in two steps. First, it turns into pyrite or marcasite, indicating the presence of extra sulfur

and sulfuric acid, and later to Fe oxides/oxyhydroxides. A decrease in the magnetic susceptibility compared to the average values for fresh and fall samples of each meteorite group is evident in the Lut meteorites. The XRD data shows the presence of hematite, maghemite, goethite, akaganéite, and magnetite, produced during terrestrial weathering. The weathering products in Lut and San Juan DCA in the Atacama Desert meteorites are different from each other. Lut meteorites show higher oxides abundance and higher terrestrial alteration than those from San Juan. This is in agreement with the much wetter present day and past climate (over the Holocene) in Lut compared to the Atacama Desert. Maghemite, goethite, and hematite are the dominant weathering phases in Lut samples, however, goethite is the dominant phase in the San Juan samples and hematite is absent. Sequential combustions shows the presence of carbonates in majority of the Lut meteorites. Comparison of the total carbon (TC), total organic carbon (TOC), $CaCO_3$ contents show that the Lut samples are richer in this compounds than those from the Atacama and Sahara deserts. We observe an increase in the carbon contents (TC and TOC) of the Lut meteorites during terrestrial weathering due to formation of $CaCO_3$.

Desert weathering has changed the chemical composition of the Lut meteorites. Elements with higher abundance in the soil and relatively mobile behavior like Li, Sr, Mo, Ba, LREE, Tl, Th, and U are enriched in the meteorites. REE, Sr, Ba contents are different between meteorites from different hot deserts. This can be used to track the finding places of the meteorites. The highly weathered meteorites from Lut desert have lower ΣREE contents than those of the moderately weathered meteorite from Atacama. This is interpreted as the higher interaction of Atacama meteorites with the terrestrial environment than Lut samples, because of low weathering rate in the Atacama and more time available for this process to happen.

El Médano 301 a meteorite found in Atacama is an ungrouped chondrite with overall texture and trace-element distribution similar to those of ordinary chondrites, but with silicate (olivine and low-Ca pyroxene) compositions that are more reduced than those in ordinary chondrites, with average olivine and low-Ca pyroxene of $Fa_{3.9\pm0.3}$ and $Fs_{12.8\pm4.9}$, respectively. It shows similarities with chondritic clasts in Cumberland Falls aubrite, and with Northwest Africa 7135 and Acfer 370 ungrouped chondrites. Our observations suggest the formation of El Médano 301 in a nebular region compositionally similar to ordinary chondrites but with a different redox state, with oxygen fugacity ($fO2$) in this region lower than that of ordinary and higher than that

of enstatite chondrites condensation region. A second, possibly nebular, phase of reduction by the production of reducing gas phases (e.g., C-rich) could be responsible for the subsequent reduction of the primary material and the occurrence of reverse zoning in the low-Ca pyroxene and lower average Fa/Fs ratio. Based on the IR spectra of El Médano 301, we suggest the possibility that the parent body of this chondrite was a V-type asteroid.

Famenin meteorite fallen on 27 June 2015 on the roof an house in Famenin town, NW Iran, is a type 3 ordinary chondrite intermediate between H and L chondrites. Famenin, together with similar intermediate meteorites, suggest the existence of a separate ordinary chondrite grouplet for which a different designation (H^L) is proposed.

Moshampa meteorite fallen on 30 July 2015 near Moshampa village, NW Iran, is a brecciated LL5 chondrite.

2. PERSPECTIVES

- Classification of even “ordinary-looking” meteorites is useful, since rare samples like El Médano 301 can be discovered among them.
- This works is considered as the beginning of studies on meteorites from Iran, regarding the high potential of the country, more works on different deserts should continue.
- Meteorite search in the other regions of the Lut desert (besides Kalut) would be fruitful.
- The two meteorite strewnfields in the Kalut (particularly their terrestrial ages) and possible impact craters related to them should be thoroughly investigated.
- Studying the geomorphological evolution and palaeoclimatic conditions of Lut desert, with focusing on the surface dating, sedimentology of Kalut, and studying the sediment cores (extracted from the central Lut extracted during one of the missions of the author).
- Studying troilite weathering in Lut meteorites by using different mineralogical and geochemical methods. Preliminarily data on this topic already have been obtained with SEM and Raman Spectroscopy.
- Studying the effects of terrestrial weathering on isotopic composition of hot desert meteorites using data already obtained during this thesis.
- Collecting meteorites from the Antarctica and comparing their terrestrial weathering with those from hot deserts. A publication based on the data obtained on Antarctica and hot desert

meteorites is planned in the near future. In addition, a trip to the Antarctica is expected for the author during his post-doc work in the coming year.

- A national network of cameras to observe fireballs would be useful to track the falling meteorites in Iran.

Figure captions:

Fig. 1: Number of meteorites classified and co-classified by the author during this work. Raw map source: photos8.com

Fig. 2: a) Meteorites from Iran (total number: 246), and b) central Lut Desert, in the Meteoritical Bulletin. Diamonds and circles represents falls and finds, respectively. Red and white colors indicate meteorites classified during this study and other studies, respectively. Satellite image source: Google Earth.

Figures:

Fig. 1:

Fig. 2:

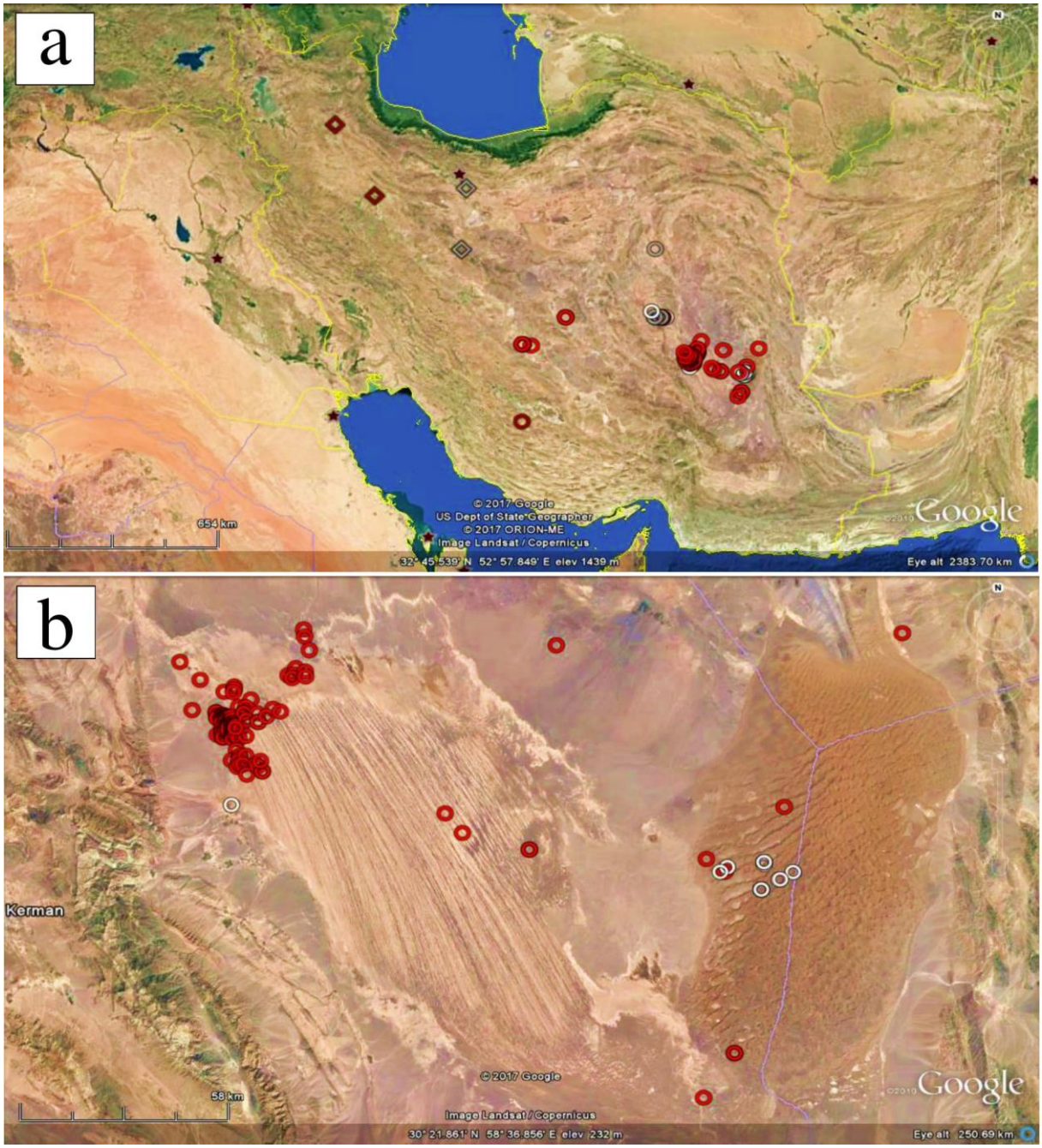
a
654 km
© 2017 Google
US Dept of State Geographer
© 2017 ORION-ME
Image Landsat / Copernicus
32° 45' 539" N 52° 57' 849" E elev 1439 m
Eye alt 2383.70 km
Google
b
Kerman
58 km
© 2017 Google
Image Landsat / Copernicus
30° 21' 861" N 58° 36' 856" E elev 232 m
Eye alt 250.69 km
Google